STUDIES IN PHOTOIONIZATION

A Thesis Submitted For The Degree

Of

Doctor of Philosophy

in

The University of Oxford

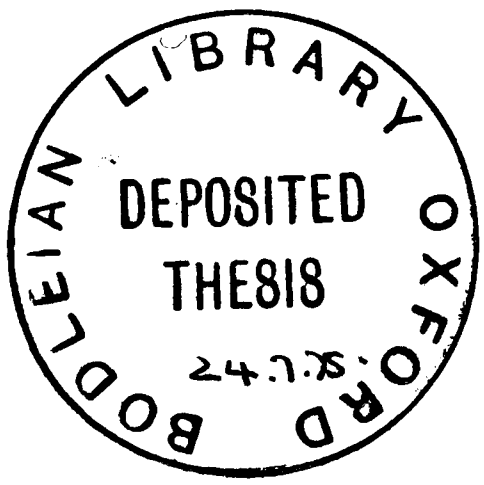

by

J. R. Crellin, Worcester College

Physical Chemistry Laboratory,

Oxford.

Hilary Term

1975

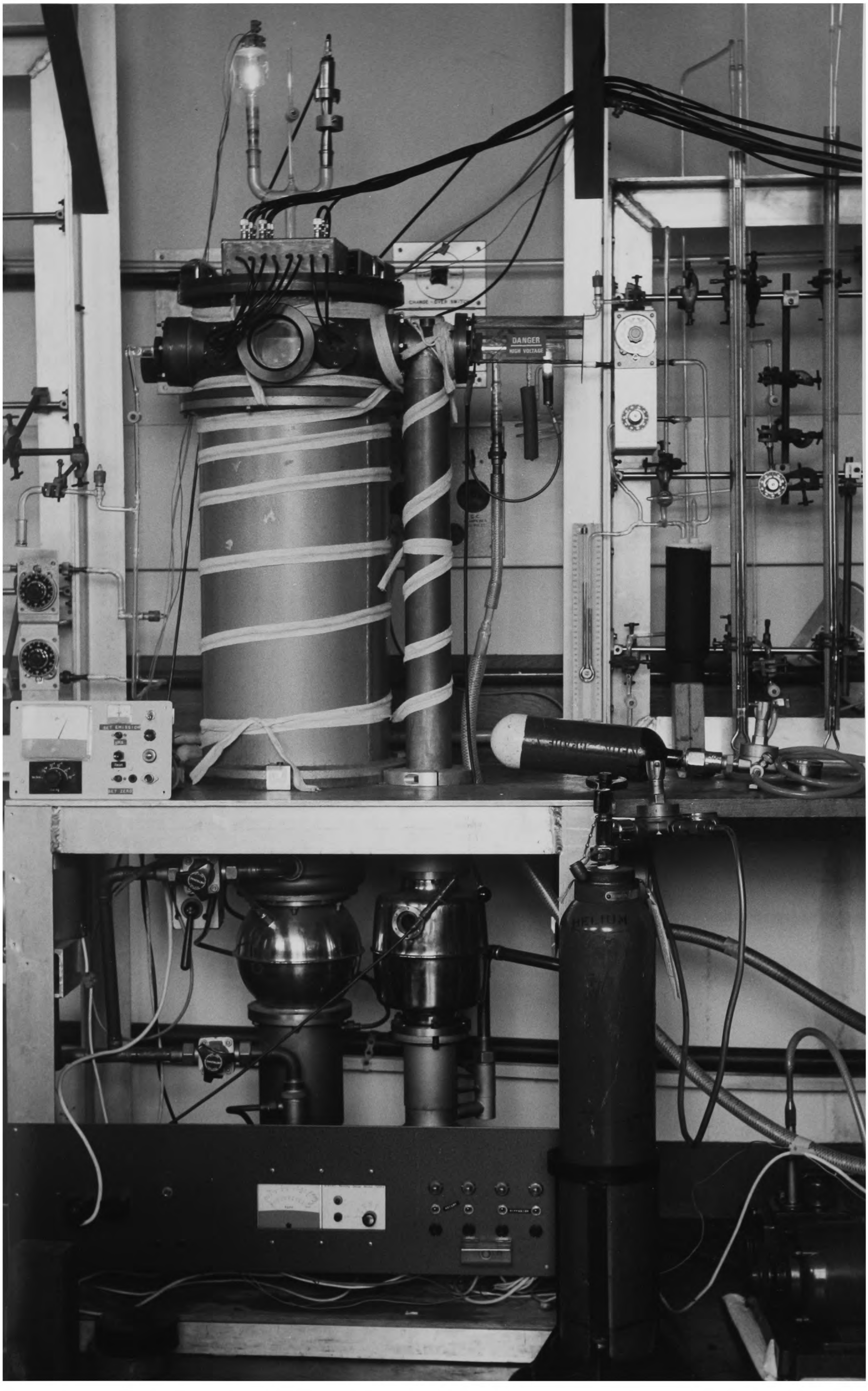
DANGER
HIGH VOLTAGE
SET EMISSION
SET ZERO
HELIUM

ACKNOWLEDGEMENTS

The author wishes to thank his supervisor, Dr. C. J. Danby, for his unfailing and valuable assistance throughout this work. He is also greatly indebted to I. G. Simm and J. H. D. Eland for helpful comments and stimulating discussions. The help given by J. P. Whitworth is a little harder to define but demands acknowledgement.

It would be wrong to give no mention of the members of the technical staff who have helped in many ways. Particular thanks are extended to I. March for assistance with the constructional side, J. Jessup for much sound advice in electronics and K. Calkin for some expert glassblowing. For perhaps the most difficult job of all, typing from my manuscript, I thank Mrs. J. Ling for a very efficient and professional job.

J.R.C.

CONTENTS

Chapter 1 - Introduction

CHAPTER ONE

A. INTRODUCTION

This thesis is concerned with the study of fragmentations of ions in the gas phase. Two experimental techniques have been used, the established one of photoelectron spectroscopy (PES) and a newer technique of fragment ion kinetic energy analysis. The two types of experiment are carried out using the same basic hardware and are complementary in the sense that one, PES, provides information about the electronic and vibrational states of the ion and the other shows how parent ions produced in these states decompose.

The fundamental process under investigation is one of photoionization and the theory of this is discussed in chapter 1B. The theory of photoelectron spectroscopy is covered in chapter 1C and the theory of ionic fragmentation in chapter 1D. A discussion of some general practical considerations is given in chapter 1E.

Chapter 2 is concerned with a description of the equipment and its development to a state suitable for the experiments envisaged. Chapter 3 presents the methods used to derive useful information from the experimental results. It includes a study of the fragmentation of the ion O_2^+ where many of the results derived can be compared with those calculated from other types of experiment.

An experimental investigation of the fragmentation of ions derived from a group of halogen compounds is presented in chapter 4 and a study of the triatomic compound nitrogen dioxide is presented in chapter 5.

B. PHOTON MOLECULE INTERACTIONS

When an atom or molecule absorbs a photon there are many ways in which the quantum energy may be distributed. The atom or molecule may be transferred from an initial low lying state to an excited state; the absorption lines from a given initial state forming a spectral series. The wavelength difference between successive members of such a series decreases as shorter wavelengths are approached and the series converges on a series limit beyond which lies a region of continuous absorption. This corresponds to photoionization of the atom or molecule and is continuous because any excess of energy can be removed as kinetic energy of the separating electron and ion:-

$$h\nu = (V_i + E_k)e$$

where V_i is the "ionization potential" of the species concerned and E_k is the sum of the kinetic energies of the electron and positive ion. As the ion will be at least several thousand times heavier than the electron nearly all the kinetic energy must be taken by the electron in order to conserve momentum. It is usual therefore to neglect the kinetic energy imparted to the positive ion.

In the visible and near ultra-violet regions the absorption spectrum of an atom or molecule corresponds generally to the more loosely bound valence electrons. It is possible however to excite electrons other than the valence electrons and in the X-ray region this is the dominant form of excitation and of ionization. Excitation of inner electrons can also occur in optical spectra and as is to be expected photon energies are higher than is

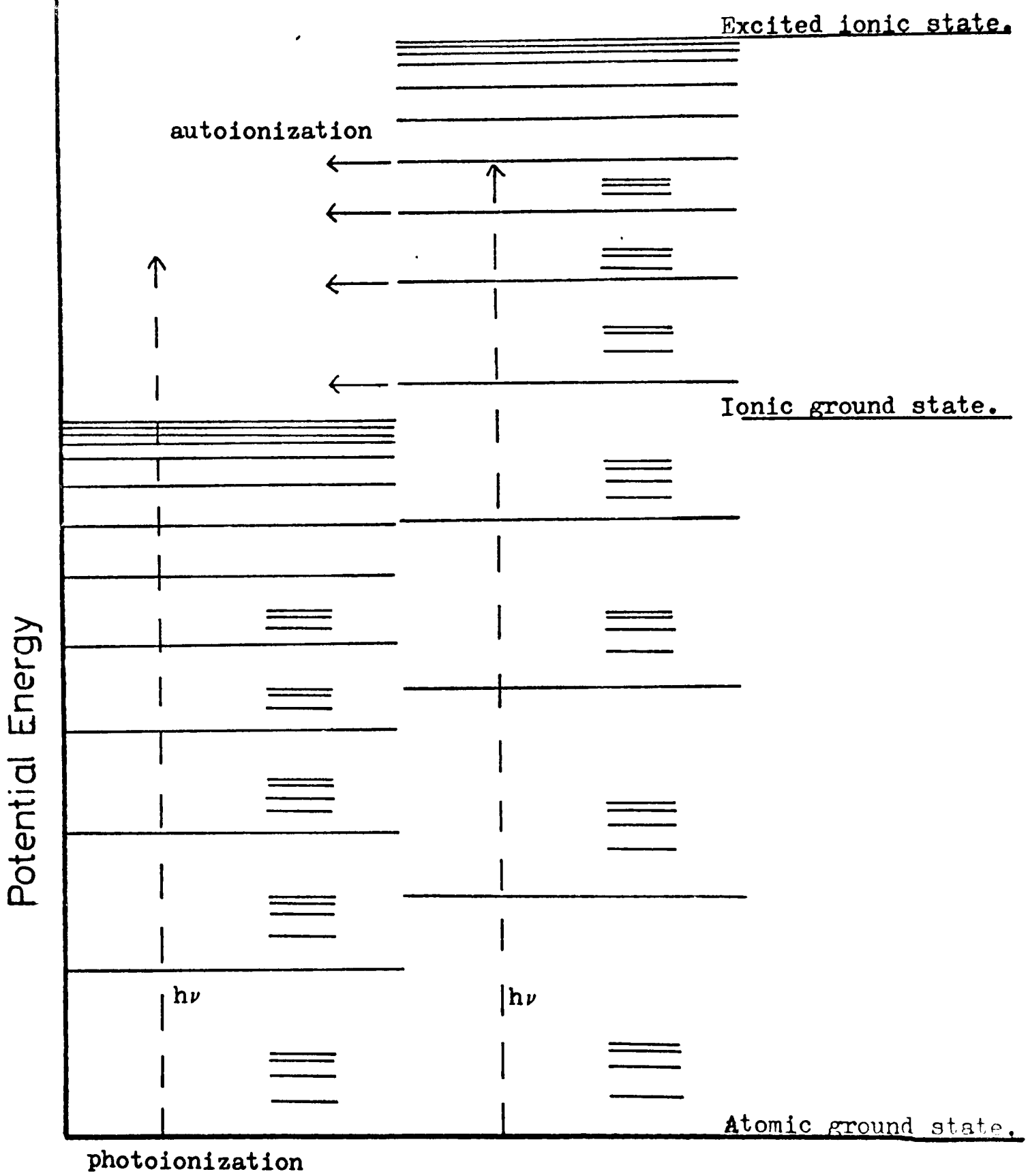
Excited ionic state.
autoionization
Ionic ground state.
Potential Energy
hν
hν
Atomic ground state.
photoionization

Figure 1.1

normally the case for outer electron transitions. These absorption lines are to be found in the vacuum ultra-violet region (wavelengths below about 2000Å) converging to series limits which correspond to excited ionic states. An example is afforded by thallium, the ground state outer shell configuration of which is $6s^2 6p$. As well as "normal" spectra corresponding to excitation to $6s^2$ ns or $6s^2$ nd states, transitions are also observed in which the excited states are 6s6p np configurations corresponding to excitation of an inner 6s electron.

Part or all of such inner electron series may overlap with the "normal" photoionization continuum as indicated in figure 1.1. In such cases absorption of a photon of energy higher than the first ionization potential of the species but not above the series limit for the inner transition can result in one of two processes. Either it excites the outer electron and photoionization occurs or it can excite the inner electron yielding a "superexcited" state. In the latter case the sequence of events is governed by the relation between the discrete and continuum states of the same energy. If they correspond to states of the same angular momentum, there is a finite probability of a radiationless transition from the discrete superexcited state into the corresponding state of the ion plus an electron with kinetic energy. This process is known as autoionization.

In a molecule the possibility exists of a transition to an unstable state or a stable state above its dissociation limit resulting in the process known as predissociation. This may occur from an ionic state to

another ionic state; from a molecular state to another molecular state or even from a superexcited molecular state to an ionic state which would constitute a dissociative autoionization.

The first experimental evidence for the existence of excited states capable of autoionization came from observations of multiple electron emissions upon X-ray absorbtion by Auger[1] in which only one electron has an energy that varies with that of the X-radiation used; the others having energies characterized by the atom involved. This Auger effect is a particular case of the general phenomenon of autoionization which has since been observed extensively in optical spectroscopy.

Selection rules for autoionization in atoms were first formulated by Shenstone[2] by analogy with those governing molecular predissociation. The ability to exhibit autoionization properties is limited to those levels above the lowest ionization threshold which encounter a continuum with the same parity and total angular momentum as themselves, and for L - S coupling the same L and S values. This will of course only be true to the extent to which L - S coupling holds.

Similarly there is a finite probability of a radiationless transition in a molecule only if there is a mixing of the eigenfunctions of the states concerned. Selection rules for such radiationless transitions have been formulated[3] and are the same whether the result is autoionization or predissociation.

They state that[4]:-

i) Both states must have the same total angular momentum J; i.e. $\Delta J = 0$.

ii) Both states must have the same multiplicity; $\Delta S = 0$.

iii) The Λ values of the two states may differ by 0 or $\pm$ 1; i.e. $\Delta\Lambda = 0$ or $\pm$ 1.

iv) Both states must be positive or both must be negative.

v) For identical nuclei both states must have the same symmetry in the nuclei; i.e. s $\leftrightarrow$ a.

The first, fourth and fifth rules are rigorous. The second holds only approximately as indeed is the case with radiative transitions. The third holds only insofar as Λ is defined. Detailed examples illustrating these selection rules are given by Herzberg[5], an invaluable source of information on these matters.

Photoionization experiments to date have in the main been concerned with the following studies;

a) Determination of energy thresholds, e.g. ionization potentials for the removal of various electrons (including vibrational spacings of particular electronic states).

b) Determination of the variation of transition probability with the energy of incident photons above the threshold and the relative probabilities for transitions to different ion-electronic states from the molecular ground state.

c) Determination of the products of the photoionization and possibly the energy distributions of the products.

Measurement of photoionization cross-sections as a function of wavelength provides a superior method to that of electron impact for measuring ionization potentials. The wave function for the final continuum state in a photoionization event is an attractive Coulomb wave, distorted at small

distances by screening effects due to the inactive electrons, Thus the matrix element:-

$$\int \Psi_i^* r \Psi_f dr$$

(where Ψ_i is the wave function for the bound state and Ψ_f that for the "free" state) is finite and hence the cross section is finite at the threshold.

To a first approximation the threshold laws apply as follows:-

Photon impact excitation has a resonance threshold law.

Photoionization obeys a step function threshold law.

Electron impact excitation obeys a step function law.

Electron impact ionization has a threshold law represented by a linear function of the excess energy.

These crude approximations will only hold, if at all, at and just above the threshold. For photoionization it is fairly true; except where autoionization occurs as for example in the case of carbon dioxide where the cross section decreases rapidly with energy.

A number of methods are available which can provide more detailed information about the mechanisms of photo-ionization processes. If vibrationally and/or electronically excited states of the residual ion are populated observation of fluorescent decay to the ground state can be used to monitor the population of these excited states. The radiation is weak however and difficult to measure. Carbon dioxide has been studied in this way[6], the resolution being sufficient to resolve vibrational structure of the $^2\Pi u \rightarrow {}^2\Pi g$ system of CO_2^+.

The ionic products of photoionization may be studied

by mass spectrometry. This technique has the advantage that energy determination of the photon beam is easier and more precise than for an electron beam, and that the form of threshold law makes for more accurate threshold energy determination. Also the ionizing beam is uncharged, allowing more efficient drawout from the ionization region, and the ionization region may be kept at room temperature. Photoionization mass spectrometry has been reviewed by Reid[7].

C. PHOTOELECTRON SPECTROSCOPY

C(i) Introduction

Photoelectron spectroscopy involves the kinetic energy analysis of electrons ejected from an atomic or molecular system after the absorbtion of a photon of sufficient energy. Two techniques have been extensively developed; working in different bands of photon energy:

i) In the technique characterized as "Electron Spectroscopy for Chemical Analysis" (ESCA)[8] X-rays in the range $\sim 12\mathring{A}$ to $\sim 0.6\mathring{A}$ are used. These have sufficient energy to photoeject core as well as valence electrons of the target material. "Chemical shifts" of core electron levels have been correlated with the bonding environment of the atom concerned. Solid samples are used normally although some work with gases and vapours has been carried out.

ii) In the technique developed by Turner[9] ultraviolet photons in the range $\sim 300\mathring{A}$ to $\sim 3000\mathring{A}$ are used; these will only eject outer electrons from the valence shells of atoms or molecules and the sample is introduced as a gas or vapour. The use of solid samples at these energies would introduce large uncertainties in the electron energy due to the energy lost in overcoming the work function of the solid.

Whereas the observation of photoion current as a function of wavelength (the photoion yield curve) may show many peaks associated with autoionizing states of the neutral parent, as well as steps associated with the ion states, each peak in the photoelectron spectrum will correspond to a state of the ion (usually but not inevitably a directly populated one).

The energy of the photoelectron is given by:-

$$E_n = h\nu - I_n - \Delta E_{vib} - \Delta E_{rot} - E(R)$$

where E_n is the energy of an electron corresponding to the n'th ionization potential, I_n; ΔE_{vib} and ΔE_{rot} are the changes in vibrational and rotational energy during ionization and E(R) is the recoil energy of the ion. E(R) and E_n are of course related by the requirement of momentum conservation and for the case of ejection of an electron by a molecule E(R) will always be insignificant and smaller than the resolution of the technique as determined by other factors.

PES has the following applications:-

i) Determination of molecular ionization potentials. The spectra are a ready source of first and higher ionization potentials and the method is the best available except in very simple systems where Rydberg series are easily observable in the ultraviolet. In many cases a ready distinction is provided between adiabatic and vertical ionization potentials, although in the absence of clear vibrational structure precise values of the two parameters may be difficult to assign. It must be borne in mind that if the electron is photoejected from a strongly bonding orbital the (0,0) transition may be so weak as to be undetectable and the apparent adiabatic ionization potential will not be the true one.

ii) The determination of photoionization cross sections at specific frequencies.

iii) The determination of Franck - Condon factors. Only the retarding field energy analyzer can give this information directly since it is equally sensitive to electrons of all

energies. However for other energy analyzers an "instrument function" may be determined as has been done for the parallel plate analyzer by Chilton[10].

iv) The investigation of angular distributions of photoelectrons, the fundamental theory of which is well established[11]. This will give information on the symmetry type of the molecular orbital from which the electron arises.

v) The determination and characterization of electronic states of the molecular ion. It is this application with which we are concerned here as it gives information of fundamental interest to the investigation of ionic dissociation under the same ionization conditions.

In practice PES is of great value for increasing our understanding of molecular electronic structure because of the simple relationship between the spectrum and the configuration of the molecule being investigated. This arises from the theorem of Koopmans[109] and two approximate but useful rules.

Koopmans' theorem states that each ionization potential in a direct ionization process is equal in magnitude to an orbital energy. It is of course an approximation; but a very valuable one which applies well except in cases where orbital energies are nearly degenerate.

The two further rules are:-

i) Each band in a PE spectrum corresponds to ionization from a single molecular orbital.

ii) Each occupied molecular orbital of binding energy less than that of the ionizing radiation will give rise to a single band in the spectrum.

If these rules applied totally a PE spectrum would

be a direct reflection of the molecular orbital diagram of the parent molecule. They are simplifications however and more bands than there are orbitals may appear in the spectrum due to two electron processes (very rare); degeneracies that are not reflected in the ionic states (e.g. due to the Jahn-Teller effect) or in cases such as oxygen, with unpaired spin in the ground state, where Koopmans' theorem and the simple rules do not apply.

A discussion of apparatus design principles in PES has appeared recently[12] which discusses the factors determining resolution and sensitivity and reviews the types of spectrometer in use.

C(ii) Autoionization Effects in PES

Autoionization processes which give rise to sharp maxima (or sometimes minima) in the total ionization cross section curve for both atoms and molecules provide, at the wavelength of the maxima, an alternative pathway for ionization which may be several orders of magnitude more probable than direct ionization. Therefore when the excited state which autoionizes has a lifetime comparable with a vibrational period it can no longer be assumed that the electron is lost from an entity of the same geometry as the original molecule. The probability for production of the various ionic vibrational levels will reflect therefore the Franck Condon factors connecting them to the autoionizing excited state rather than to the ground state. Several examples of this effect have been found[13]; oxygen[14] shows a marked difference in the vibrational envelope of the photoelectron band for the $^2\Pi_g$ ionic state when neon resonance photons ($h\nu$ = 16.8eV) are

used rather than the more usual helium resonance photons ($h\nu$ = 21.22eV). In fact 20 distinct vibrational states are observed in the band with neon radiation as compared to 4 with helium radiation and a new broad maximum is superposed on the normal intensity distribution. This is explained as being due to resonance absorbtion by a Rydberg state of oxygen at the energy of neon 736Å radiation, which preionizes to $O_2^+ X^2\Pi g$ producing a broad distribution of vibrationally excited O_2^+ ions.

Smith[15] has pointed out that if a molecule has an inner ionization potential less than about 2eV above the photon energy, E, being used there may well be Rydberg states of the molecule in the vicinity of E which, when excited, will autoionize if permitted by the selection rules.

Autoionization effects in helium resonance PES would therefore be expected in molecules with orbitals at energies of about 21 - 24eV. This is, in general, unusual but cannot entirely be ruled out. For neon resonance radiation which is used extensively in the work presented here auto-ionization must be considered as a strong possibility.

C(iii) Multiple Photoelectron Processes

Since the interaction of a molecule and a photon is described by a one-electron operator; only states which, in the simple MO description, are characterised by an electronic configuration differing from that of the neutral molecule by one molecular orbital will normally be observed in photo-ionization experiments. If however the simple Hartree-Fock model breaks down and there is strong correlation between pairs of electrons multiple electron transitions become

possible.

Lorquet and Cadet[16] have examined the validity of the selection rule which in photoionization and photoelectron experiments forbids any transition to ionic states for which the electron configuration differs from the ground state of the neutral molecule by more than one molecular orbital.

This is shown to be a first approximation only. If configuration interaction is taken into account weak transitions to doubly orthogonal states may become allowed. Cases have been found where multiple photoionization has quite a high probability[17], only however at higher photon energies than 21.22eV; the highest used in the present work.

C(iv) Ionic Dissociation in Photoelectron Spectroscopy

If absorbtion of a photon leads to the population of an excited stable molecular state from which there is a probability of a radiationless transition to an unstable state, to a stable state above its dissociation limit or indeed directly to an unstable state, then photofragmentation will occur. In the case of predissociation this will manifest itself in the PE spectrum as a broadening of vibrational levels if the lifetime of the state first populated in the ionization event is short compared to a vibrational period. If the lifetime is very short or direct photoionization to a dissociative state is occurring the PE spectrum may be lost in the background noise. It is important to consider this possibility when investigating photoion-fragmentations.

D. IONIC FRAGMENTATION

D(i) Introduction

The study of dissociative states of molecules is of fundamental interest as a means of achieving greater understanding of the kinetics and mechanisms of chemical reactions. It is of the most direct relevance of course to unimolecular reactions; being indeed a way of studying such reactions with the complication of intermolecular energy exchange removed. A molecule is, ideally, studied as an isolated entity whose dissociation characteristics will be determined solely by intramolecular effects. Thus studies of photodissociation reactions can yield information about partitioning of available internal energy amongst the degrees of freedom of the products and hence test the theories of unimolecular decay. Busch and Wilson have studied the photodissociation of triatomic molecules by laser light and measured the kinetic energies of the recoiling fragments thereby obtaining a picture of the distribution of excess energy in the products[18].

Experimentally however it is easier to make such investigations on ions. There is no fundamental reason to expect the dynamics of ionic decay to differ appreciably from those of decay of neutrals. Thus the Quasi-Equilibrium theory of mass spectra, first put forward in 1952[19], is equivalent to a contemporary formulation of the kinetics of thermal unimolecular decompositions[20].

Many experimental techniques have been developed for study of ionic decomposition including:

i) The investigation of "metastable" ions in mass spectrometry. Information is gained on the nature of

fragmentations occurring within a particular time after ionization. The exact time scale varies with the experimental parameters but in general the range of ion lifetimes from 10^{-8} to 10^{-5} seconds may be covered. Beynon[21], using specialized instruments, has shown that it is possible to observe events having lifetimes from 10^{-9} to 10^{-3} seconds. The shape of a metastable peak will give information about the energy released in the decomposition.

ii) Fragment ion kinetic energy measurement in a mass spectrometer by retardation or deflection methods. In retardation methods[22] a field is applied in a direction opposite to that of beam travel and the kinetic energy is derived from a plot of peak height against retarding potential. In deflection methods[23] a field is applied perpendicular to the ion beam thus bringing ions with velocities perpendicular to the beam back on axis. Kinetic energies can also be derived from an analysis of the peak shape in single focussing mass spectrometers. These methods will, of course, provide information about fragmentations occurring within the source residence time of a mass spectrometer ($<10^{-8}$ seconds).

iii) The decomposition of ions formed with a known internal energy by charge exchange with simple monatomic or diatomic ions may be studied[24]. Dissociation lifetimes of the ions produced or the kinetic energy released may be measured. Using this technique the uncertainty of initial excitation energy usually present with electron impact ionization is removed. However the interaction leading to ionization may take place over a time scale comparable to the time for dissociation; hence complicating the problem. Photoionization and electron impact ionization are essentially instantaneous as far as even fast decompositions are concerned

and the dissociation can therefore be discussed in terms of the internal energy of the ion without regard to how the energy was acquired. By choosing a range of different ions and states thereof for the exchanging species a breakdown curve may be constructed; giving the abundance of various fragments as a function of excitation energy.

iv) Ion fragment kinetic energies can be directly measured by an energy analyzer - with or without mass analysis[21,25,26]. This is naturally a more direct method and the kinetic energy distribution observed is easier to interpret and capable of greater resolution in principle than in the mass spectrometric methods of ion kinetic energy analysis. As in mass spectrometry, photoionization or electron impact ionization may be used but photoionization is favoured as direct information about the ionic states involved is available via the parallel technique of photoelectron spectroscopy. In the present work a spectrometer is described that has been developed to be usable both for measuring ion kinetic energies and photoelectron spectra.

v) Yields of fragment ions may be measured as a function of photoionization wavelength either with mass analysis or simply as total ion yield (the photoionization cross section)[27,28]. Apart from its provision of direct information, such as appearance potentials, this work is of great value for comparison with theoretical models of photoionization and fragmentation. Many compounds have now been investigated in this way[27,28].

vi) By combining the techniques of photoelectron and mass spectroscopy one may study ions produced from a precisely defined ionic state. In this technique ions are studied in coincidence with kinetic energy analysis of the

electron lost in their formation[29,30]. The technique can be used either to construct a breakdown curve (only for initial internal energies corresponding to reasonable intensity in the photoelectron spectrum) or to study kinetic energy release as a function of initial internal energy. This technique has been used to observe directly an isolated state in the ion $C_2F_6^+$ [31] as well as in investigations of the fragmentations of many triatomic molecules[32,33,34] and to construct a breakdown diagram for acetone[35].

D(ii) The Fragmentation of Simple Ions

For a monatomic or diatomic species one can write an expression for the transition probability from the ground state of the species to each of the states of the ion. Probabilities can be determined as a function of excitation energy with sufficient precision in the simplest cases to suggest that the problem is well understood.

Even for triatomic and simple, highly symmetric molecules such as cyanogen enough may be known about ionic states for a fairly direct interpretation of fragmentation of the ions. If the ionizing transition is to a repulsive state of the ion the dissociation will be essentially immediate and the kinetic energy of the products will be simply related to the shape of the repulsive potential energy surface and the geometry of the parent molecule (assuming a Franck-Condon transition). For transitions to bound ionic states crossings to repulsive states or to bound states above their dissociation limits have to be considered.

However, even for diatomic molecules quantum

mechanical calculations are at present only possible for certain states of the simpler systems and even then are only approximate. The validity of the approximations is however well understood.

Oxygen is a case of a diatomic molecule for which the ionic states, unbound and bound, are well characterized[36]. However although most of the characteristics of the photo-fragmentation of O_2^+ are easily explained the formation of O^+ ions with a small translational kinetic energy release was not so easily explained at first[25]. The energetic O^+ ion component is completely explained in terms of predissociation of the $^2\Sigma_g^-$ state of O_2^+ to give $O\,^3P$ and $O^+\,^4S$ via an unbound state. Computation of the expected energy distribution from thermodynamic and spectroscopic data gives very good agreement with the experimental result as is shown in chapter 3.

The analysis of the dissociations of triatomic ions in terms of well characterized ionic states and thermodynamic data is not so easy but in favourable cases much information may be gained as has been in the cases of N_2O^+, COS^+, CO_2^+ [32]. Attempts have been made to compare results obtained for other triatomic ions with statistical predictions as for example with SO_2^+ [33]. It is not however very relevant to apply statistical theories to such small molecules where the selection rules must play an important role. However it is to be hoped that information may be gained that will lend insight into the sort of processes which will be occurring in larger molecules and therefore give some idea as to which assumptions in any statistical model of dissociation may be valid. It has been found, for

example, that CS_2^+ fragments via rapid internal conversion to lower lying states of the ion than those originally excited; demonstrating the validity of a common assumption made in statistical theories for even such a small molecule (see section D(v)).

Thus triatomic ions, although rather attractive as subjects of experiment, tend to fall somewhere between the postulated theories of direct and statistical dissociation.

Three possible mechanisms are useful as models of real dissociations; direct dissociation, predissociation and internal conversion followed by predissociation.

True direct dissociation can only occur if the electron removed in the ionization process is strongly bonding and it seems reasonable to expect that, in such cases, a correlation between the character of the orbital from which the electron was lost and the products formed will exist. In such cases of direct dissociation of a particular ionic state there cannot be any vibrational structure in the corresponding band of the photoelectron spectrum; any state that has such structure yet is known to be dissociating must be doing so via some type of radiationless transition to a dissociative state or to a bound state above its dissociation limit.

Herzberg[5] has described three idealized cases of such predissociation:

a) predissociation via a non-radiative transition from the bound state to a continuous state.

b) predissociation on a single electronic energy surface by rearrangement of vibrational energy.

c) predissociation as a result of the rotational energy which a molecule possesses in excess of the dissociation limit.

Internal conversions followed by vibrational predissociation represents a sub-class of predissociation, but a very important one in this work as it is the postulated mechanism upon which the Quasi Equilibrium theory is based. According to this theory all excited molecular ions relax rapidly by conversion of their electronic excess excitation energy into vibrational energy of the ionic ground state followed by a vibrational predissociation. The internal conversion process is strictly controlled by selection rules in small molecules but is thought to reach completion in $\sim 10^{-11}$ sec. in large molecules. The Quasi Equilibrium theory is described in detail in the next section.

D(iii) Statistical Theories of Ionic Fragmentation - the Quasi Equilibrium Theory

The first attempt to explain ion decomposition kinetics was the Quasi Equilibrium theory of Rosenstock et al.[19]. The theory has since been reformulated many times and has been the subject of several reviews,[37,38,39,40,41,42,43].

The earliest applications of the QET were in calculations of mass spectrometer cracking patterns. In order to do the calculations it was necessary to guess at the internal energy distributions of the molecular ions formed by electron impact. To fit the experiments even approximately very broad distributions were required. These required distributions were in fact demonstrated to be unreasonable[44].

The problem was traced to poor arithmetical approximations for densities of states and other required parameters. This problem did however serve to emphasise the dependence of the theory on reliable values of internal energy

distributions. New, but imposing, methods of evaluating densities of states and sums of degeneracies were developed. However, the fact is that the calculation of mass spectral patterns does not pose a very stringent test of the theory. The necessary averaging over an assumed, or even well known, internal energy distribution renders less convincing whatever success that may be achieved.

Now, however, three distinct techniques exist for studying ions with a reasonably well defined internal energy. These are the charge exchange; monoenergetic electron attachment and photoelectron-photoion coincidence methods. Between them these three techniques have already provided a large amount of largely unassimilated data on ionic fragmentation. Also a simple and accurate method of evaluating densities of states[45] has appeared and helped to dispel some of the remoteness associated with actual calculations.

QET is essentially equivalent to the statistical theory of unimolecular reactions. It is however important to emphasize the differences:

Gas phase unimolecular reactions only display first order kinetic behaviour as long as the gas pressure is such that energy transfer for both activation and deactivation of molecules is fast relative to the rate of dissociation. An ionic decomposition however, in the low pressure conditions of a typical experiment, is truly unimolecular in that each ion is an isolated system.

The starting point for any theory of ionic fragmentation must be a collection of ions with a distribution of energies and hence also an internal distribution over vibrational and quite possibly vibronic levels.

QET makes the following assumptions:

1) The time for dissociation is long compared to the time of the interaction leading to the production of the ion.

2) The rate of dissociation of the ion is slow relative to the rate of internal equilibration.

3) Each dissociation process may be described as a motion along a "reaction coordinate" separable from all other internal coordinates.

The first two assumptions allow one to discuss the dissociation in terms of the internal energy of the parent but without regard to the mode of acquisition of the energy. The first assumption holds true for electron impact ionization and photoionization and probably holds for simple charge exchange. For field ionization however it does not necessarily hold[39].

The second and third assumptions are analogous to and in the spirit of the assumptions of the absolute rate theory of Eyring et al[46] as reformulated by Marcus and Rice[20].

The idea that a statistical theory of ionic fragmentation should have some validity is suggested by the well known strong dependence of mass spectral fragmentation pattern on structure and the usual non-dependence on the orbital from which ionization occurred.

This implies that dissociation does not immediately follow on ionization; the assumption of a diatomic model, with immediate dissociation, if possible, is not in general correct and intermediate models are hopelessly complex. An obvious alternative assumption takes the opposite extreme; that is complete randomization of ion energy before dissociation.

In formulating a statistical theory it is necessary to choose some method of describing the dissociation process. This leads to the, generally adopted, concept of a reaction coordinate, which may be defined as follows:

The reaction coordinate is a generalized internal coordinate, involving nuclear motions only, which is selected for each reaction such that its variation takes the equilibrium configuration corresponding to the separated products via the lowest energy route between the reactant and product configurations[38].

Since each dissociation is assumed to be relatively slow the Born-Oppenheimer approximation should hold for the separation. As in absolute rate theory the change in potential energy at the saddle point is assumed to be sufficiently small for motion of the system along the coordinate to be taken as translation. The remaining assumption that is required is that the total number of energy states form what is essentially a continuum (described by a density of states function $\rho(E)$). The validity of this assumption is discussed in section D(v) of this chapter.

It is now relatively easy to derive an expression for the rate of reaction as a function of internal energy E. Taking an ensemble of systems with energy between E and $E + \delta E$; the number of states available to members of the ensemble is $\rho(E)\delta E$. Of these some will correspond to the system being in an activated complex configuration with potential energy ϵ_o in the reaction coordinate.

There must be some kinetic energy of translation ϵ_t in the reaction coordinate if the reaction is to proceed, and an associated density of translational states $\rho_t(\epsilon_t)$ is

defined. The activated complex has energy $E - \epsilon_i$ in other degrees of freedom. (Writing $\epsilon_o + \epsilon_t$ as ϵ_i - the activation energy of the reaction).

Therefore the number of states corresponding to an activated complex configuration is

$$\rho^{\ddagger} (E - \epsilon_i)\ \rho_t(\epsilon_t)\ \delta E.$$

The fraction with energy ϵ_t is:

$$\frac{\rho^{\ddagger} (E - \epsilon_i)\ \rho_t(\epsilon_t)}{\rho(E)}$$

One needs therefore to determine $\rho_t(\epsilon_t)$ and the relationship between the rate of dissociation and ϵ_t. By considering the energy levels of a particle in a one dimensional box of length l and the classical frequency of crossing at the saddle point as in transition state theory we get:

$$\rho_t(\epsilon_i) = \frac{1}{h}$$

A system with total energy E may dissociate with ϵ_t having any value from zero up to the maximum available in the activated complex configuration, E.

Therefore the final expression for the rate constant of dissociation is:

$$k = \frac{1}{h} \sum_{\epsilon_t = 0}^{\epsilon_t = E} \frac{\rho(E - \epsilon_i)}{\rho(E)} \qquad [1]$$

The approximation that dissociation is slow implies that the activated complex states are a small fraction of the total and hence:

$$\rho^{\ddagger} (E - \epsilon_i)\ \rho_t(\epsilon_t) \ll \rho(E)$$

No quantitative comparison of general theory, as described above, and experiment is at present possible. If W(E) is defined as the number of states of a system having energy less than or equal to E, then $\rho(E) = \frac{dW(E)}{dE}$ and equation [1] can be written

$$k = \frac{1}{h} \frac{W^{\ddagger}(E)}{dW(E)/dE} \qquad [2]$$

There is a simple, if not direct, relationship between ϵ_o and $\Delta H^{\ddagger}$ and between $W^{\ddagger}/W$ and $\Delta S^{\ddagger}$ where $\Delta H^{\ddagger}$ and $\Delta S^{\ddagger}$ have their usual significance for a reaction at a given temperature.

Setting aside the question of how the approximate frequencies are to be selected one can easily evaluate the rate expression [1] for an arbitrary collection of N harmonic oscillators by using the Dirichtlet integral and seemingly suitable boundary conditions. The Dirichtlet approximation requires $N \ll K$ where K is the number of quanta in a collection of oscillators and hence at low energies the derived equation can be greatly in error. Better methods have been suggested for determining densities of states. Rabinovitch et al.[47] use an empirical modification of the semiclassical equation,

$$W(E) = (N!)^{-1}[(E + aE_z)/h\bar{\nu}]^N$$

where E_z is the vibrational zero point energy and $\bar{\nu}$ is the geometric mean of oscillator frequencies at moderate and high energies, coupled with direct counting of states at lower energies.

D(iv) The Calculation of Parameters in Statistical Theories

Several methods for calculating the number and density of energy levels for systems of harmonic oscillators or harmonic oscillators and free rotors have been developed[45,48,49,50]. Many of these formulae have been compared to exact counting of states for artificial models by Forst and Prasil[52] who concluded that the techniques of the Laplace transform and steepest descents[45,48] yield the best all round approximation while a semiclassical type of formula[47] requires least computational effort and still gives excellent results in most cases.

The fact that in a real system states may be disallowed if they are unbound or if they are excluded by angular momentum conservation requirements has been considered by Forst and Prasil[53] using their formulation of the method of steepest descents. They found that the effects on density of state calculation of excluding vibrationally dissociated states and including effects due to anharmonic vibration tend to cancel; justifying the more usual neglect of these considerations. This is readily understood in that a real molecule not only dissociates at a certain level of vibrational excitation but is also anharmonic, that is, vibrational energy level spacing decreases with increasing energy. Consequently anharmonicity tends to increase the sum or density of states and when anharmonicity and the exclusion of dissociated states are considered together the net effect on the density of states is not too appreciable. The computed unimolecular rate constant is similarly unaffected.

The effect of considering a more realistic model

for the interatomic potential, such as the Morse oscillator representation, compared to the use of the harmonic oscillator model is moderate at almost all energies so that non-thermal systems with high excitation energies are not likely to be any worse, or better, represented by the harmonic oscillator model than are thermal systems at lower energies.

The consideration of different assumptions regarding the activity of rotations by Forst and Prasil[53] led to great differences in the way that the unimolecular decay constant depended on initial rotational energy. An experimental test of this effect does not at present seem possible; it would be necessary to prepare a molecule with a known rotational quantum number, then give it sufficient internal excitation energy and measure its unimolecular decomposition rate.

The QET is often approached by determining rate constants from assumed properties of the activated complex corresponding to a particular reaction path. Klots[54] has reformulated the QET by considering the reverse process of bimolecular ion-molecule association and the principle of microscopic reversibility. This allows explicit consideration of angular momentum conservation and permits the use of the properties of the separated products rather than those of the activated complex.

The formulation of this approach is:

$$k(E + E_o) = \frac{1}{h} \frac{\sum_{x=0}^{x=E} g_i \frac{\sigma_i}{\pi\lambda^2}}{\rho(E + E_o)} \qquad [3]$$

where $\rho(E + E_o)$ is the density of states of the parent species g_i is the degeneracy factor of the separated states of internal energy x, and σ_i is the cross section for their

association. λ is the de Broglie wavelength associated with the relative velocity of the products. The degeneracy factors can be evaluated subject to additional constraints such as conservation of angular momentum. In order to use this description cross sections must be supplied for the bimolecular association. The simplest model, and the one adopted in the first instance by Klots is the Langevin picture of spiralling collisions dominated by the long range potential. Using this model simple expressions for fragmentation rate constants are obtained[55]. There are however instances where the Langevin model is clearly inadequate as in the case of the loss of a hydrogen atom by benzene studied by Andlauer and Ottinger[24] in which it is apparent that the reverse reaction is very much slower than is predicted by the Langevin model. The model shows that rotational energy should play an important part in effecting unimolecular decomposition with one small exception: in the neighbourhood of the fragmentation threshold molecular rotation will give rise to a centrifugal barrier to decomposition. Tunnelling through this barrier can occur and will give an anomalous mass dependence if it does[56]; this seems to account for the observed intensities of metastable ions in methane and its isotopic variants[57].

The Langevin model also predicts that rate constants should go through a maximum as a function of energy. This is not likely to be observable as they are predicted at quite high energies where anharmonicities and dissociated vibrational states obscure the issue.

Another reformulation of QET has been given by Levine[58] in which free energies are used to indicate the stability of excited molecules and a set of non-interacting

activated states is considered.

D(v) Tests of the Statistical Theories

It is a fundamental assumption of QET; as of the RRKM and Absolute Rate theories, that energy randomization in the decomposing atom or molecule is rapid compared to the rate of dissociation. It is therefore of great fundamental importance to test this hypothesis experimentally.

Some interesting results have been obtained by Rynbrandt and Rabinovitch[59]. They studied the system:

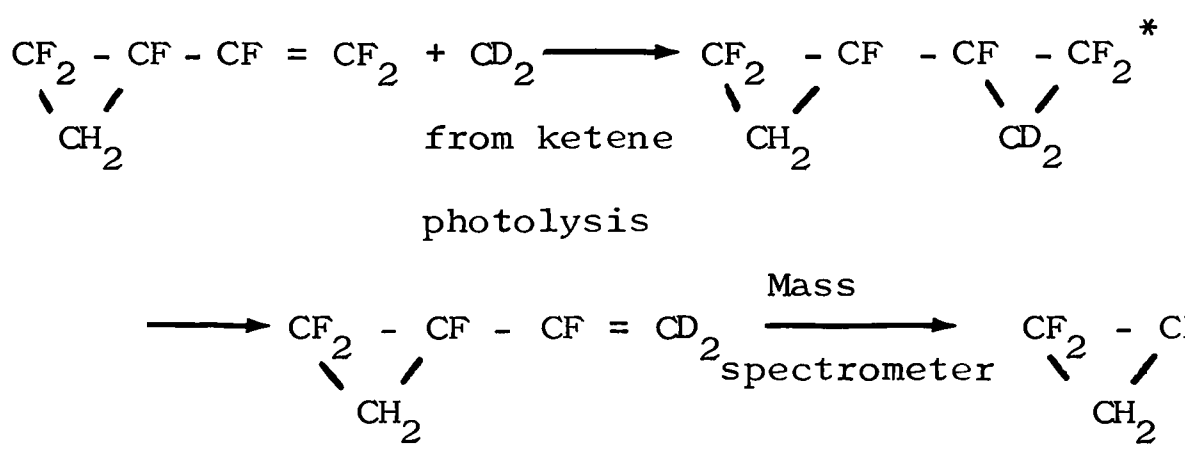

or

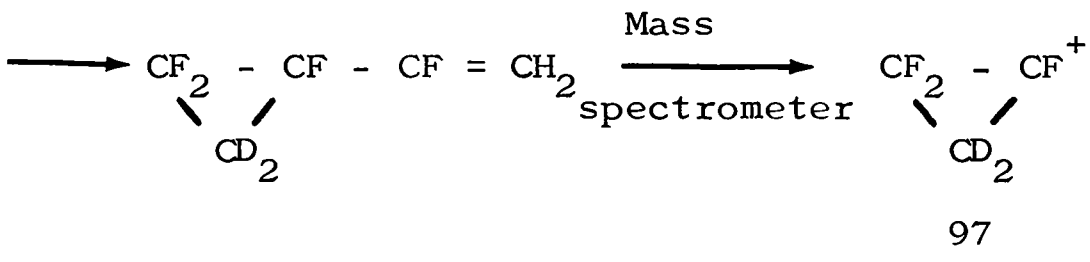

in which the ratio of mass 95 to 97 peaks in the mass spectrum of the product will be a measure of the proportion of reaction occurring on the "activated" (*) end of the molecule. To eliminate kinetic isotope effects they also studied the symmetrical reaction:

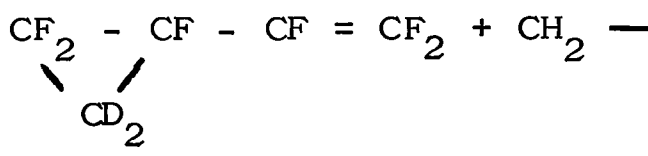

By studying the reaction at pressures up to four atmospheres the effective rate of intramolecular randomization

was derived as ~1.1 x 10^{12} $sec.^{-1}$. They considered that their results demonstrated a failure of complete randomization; albeit a slight one. The rate of equilibration found is in fact enough to suggest that the equilibrium hypothesis has at least a useful region of validity. There is also evidence from kinetic energy release in certain fragmentations that energy is not completely equilibrated in activated complexes[60]. The value of this evidence is however uncertain due to the spread of ionizing electron energies used and the assumptions used in the treatment.

Another important consideration is the question of the interconversion of electronic and vibrational energy before dissociation. As first formulated the QET assumed that all dissociations occur from the ground state of the ion and that any excited states decay first by radiationless transitions to the ground state. There is no reason why processes occurring directly from excited states of the ion should not still be described by a formulation of QET, indeed many such processes have now been observed. Rosenstock et al.[61] found that two pairs of competing reactions of $C_6H_6^+$; one pair leading to $C_6H_5^+$ and $C_6H_4^+$; the other pair to $C_4H_4^+$ and $C_3H_3^+$, were independent; with the second pair occurring from the first excited state of $C_6H_6^+$. Simm[31] has shown directly by a photoelectron - photoion coincidence technique that ions in the first excited state of $C_2F_6^+$ decompose directly to $C_2F_5^+$ without prior internal conversion to the ground state.

It is important to know what the probability of internal conversion in a given system will be and hopefully more experimental work on this problem will be carried out. Photoelectron spectroscopy has demonstrated that for a large number of compounds there are considerable "gaps" between

electronic states of an ion; nevertheless many mass spectra can be interpreted successfully in terms of decomposition from the ground state.

A theoretical formulation of radiationless processes has been given by Jortner, Rice et al.[62]; their key observation being that a system undergoing such transitions is in a compound state. They consider a division of the system into two or more sets of states which are allowed to interact to generate the exact eigenstates of the system. Supposing the least dense set to consist of a finite number of discrete energy levels and the others to have a continuous spectrum; they consider a relaxation process to occur when a compound state of the system consisting of some superposition of discrete and continuous states decomposes into the continuum.

This may not occur for small molecules when the density of vibrational levels in the ground electronic state is relatively low, unless the levels are broadened in some way (e.g. by collisions). Rates are obviously reduced by large energy gaps between states.

Calculations by Bixon and Jortner[63] suggest that radiationless transition lifetimes lie in the range $\sim 10^{-12}$ sec. to $\sim 10^{-5}$ sec; the first time being that for an allowed transition in naphthalene; the second being the time for a spin forbidden relaxation in benzene.

For a dissociation observed in conventional mass spectrometry rates of radiationless transitions not less than 10^{9} sec^{-1} will be required if all decompositions are to occur from the ground state of the ion. If conditions for ions are similar to those for molecules then it is apparent from calculations that radiationless transitions will play an important role for fragmentations of large molecules. In

other studies of ionic fragmentations such as those presented here fragmentations occurring at lower rates may be observed, for which radiationless transitions are even more likely to be important. It is not however clear that the assumption of complete prior internal conversion to the ground state will apply to "smaller" molecules and for these species one must expect to see dissociation from excited ionic states.

Many studies have shown agreements of varying degree between experimental measurements and QET predictions. Vestal[64] has calculated breakdown diagrams for various compounds and found good agreement with experimental observations[66].

Andlauer and Ottinger[24], in an elegant charge exchange experiment, have measured dissociation rate constants as a function of internal energy for benzonitrile, benzene and thiophene. They have found good agreement with statistical predictions assuming that in the case of benzene some of the observed processes occur from isolated ionic states. Reports of reasonable agreement with predictions have appeared for abundances of metastables[65] and their kinetic energy releases[66].

An important case of non-agreement with QET predictions was found by Lifshitz and Long[67] in their studies on appearance potentials in photoionization of perfluoroethane and perfluoropropane.

It was quickly found in early work on paraffinic hydrocarbons that the breaking of a C-H bond is a comparatively low yield process when compared to the breaking of a C-C bond[68]. This has been rationalized in the terms of the QET by assuming a rather rigid activated complex for C-H fission and a relatively non rigid one for C-C breakage. This is achieved by reducing vibrational frequencies for the C-C

bond and perhaps assuming free internal rotations.

However Lifshitz and Long found that "unacceptably extreme" assumptions had to be made about the activated complex to account for differences in appearance potentials and relative yield for C-F and C-C breakage in perfluorocarbons. They conclude that these reactions probably involve direct decomposition from repulsive electronic states.

D(vi) Other Theories of Ionic Decomposition

Other approaches to the problem have been formulated but only QET has been at all generally applied to experimental findings.

A quantum mechanical theory for unimolecular reactions not involving the assumptions of absolute rate theory but using instead the theory of resonance scattering was developed by Mies and Krauss [69]. A resonance state, synonymous with the activated complex of unimolecular kinetics, is associated with a set of widths which measure the coupling to various dissociation continuum channels. If the widths are small compared to spacings between neighbouring states coupled to the same continuum, then an ensemble of molecules prepared in a given activated state will decay exponentially with time (as does a radiating state). However Mies and Krauss consider that unimolecular decay is a problem in overlapping resonances which they consider using Fano's[70] overlap treatment. The interesting result of this is that under certain circumstances there would be considerable deviations from the expected exponential decay.

A theory of the cross sections of gas phase reactions which proceed without activation energy has been developed

by Light[71]: the "Phase Space" theory. This is based on the hypothesis that the decompositions of a complex are governed by the phase space available to each product under conservation of angular momentum and energy. Thus as with Klots' reformulation of QET more account is taken of the properties of products or at least of the dissociating complex on the back of the dissociation curve.

A quantum mechanical approach to the harmonic oscillation approximation has been formulated by Knewstubb[72] based on the work of Mies and Krauss. In this paper he develops in detail the further assumptions necessary for QET to be valid. In an earlier paper[73] Knewstubb describes a ballistic model and examines the relevance of the theory of classical trajectories to ion fragmentation and to the calculation of rate coefficients for such processes. Klots[55] has pointed out the equivalence of this approach and his reformulation of QET. Indeed Knewstubb also predicts maxima in rate constants as a function of energy.

Gilbert, Rice and Freed[74] have used the language of Stochastic processes and consider the events leading to dissociation to constitute a Markov chain. Their description is not easily correlated with the physical parameters of a real molecule but it does include explicitly the concept of competing reaction pathways and makes no assumptions regarding energy randomization.

Paraffin fragmentations have been given a Slater type of treatment[75] but the model calculations given are of doubtful applicability since a linear chain is assumed with completely different normal vibrational modes to those of a real paraffin.

Lindholm has found many new Rydberg series in the UV spectra of a number of molecules and has correlated these with the results of PES and MO calculations[76].

He assumes that mass spectral data may be used in correlating an ionization occurring primarily from a particular bond with a corresponding cleavage of that bond. In studies of sym-triazine[76] Lindholm et al rationalize the fragmentation to give HCN and a mass 54 ion which is associated with ionization of a π electron of only weak bonding properties in this way:-

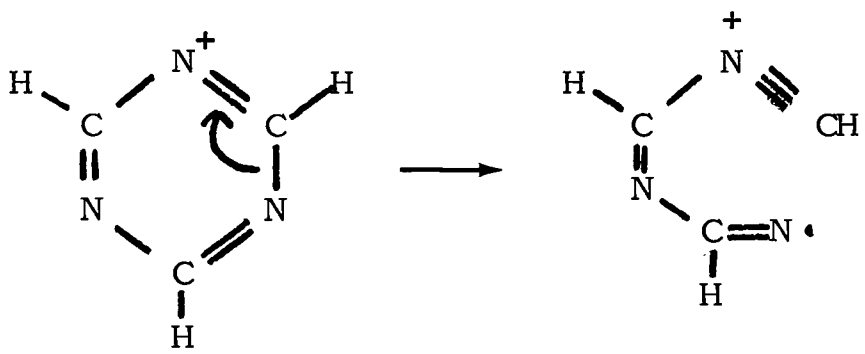

Such explicit description of fragmentation processes is of little value predictively and it is noteworthy that they refrain from discussing the subsequent split to give HCN and $C_2N_2H_2^+$ and cannot explain the formation of ions of mass 28 at higher energies.

The change in calculated electron density on vertical ionization is not necessarily related to relative bond strengths in the ion which are in fact determined by changes occurring in the electronic structure as one bond is stretched and others are adjusted for minimum potential energy.

This latter problem has been considered in detail by Lorquet et al[77] for the classic case of the mass spectrum of ethylamine in which one possible fragmentation process;

$$CH_3\ CH_2\ NH_2^+ \longrightarrow CH_2\ NH_2^+ + CH_3$$

is extremely important with respect to other possibilities such as

$$CH_3\ CH_2\ NH_2^+ \longrightarrow CH_3\ CH_2^+ + NH_2$$

Leclerc and Lorquet[78] show that the density of states of the ion is large and therefore assume most of the fragmentations to occur from the ionic ground state.

They calculated the potential energy surface of the ground state as a function of C-C and C-N bond lengths and showed that less energy is required to break the former than the latter. The wave function used in the early calculations was however a poor one. In further calculations[77] they used wave functions calculated by the CNDO/2 method;(which describes bond extensions poorly and gives poor dissociation energies) and also wave functions calculated by a derived method, due to Fischer and Kollman, which give satisfactory bond lengths and dissociation energies but poor charge distributions. The methods agreed reasonably on the charge distribution suggesting that the derived method gives useful wave functions. Rather than calculate the energy as a function of C-C and C-N bond lengths with an otherwise "frozen" geometry which is only valid near the energy minimum they allowed other atoms to adopt equilibrium positions at larger specific C-C and C-N extensions, thus introducing an important energy correction. Such calculations are difficult however and could only be done for a few points leading to a calculated graph of potential energy along the reaction coordinate. Surprisingly both curves (from C-C and C-N extension) are similar showing poor agreement with the experimental

dissociation energy of a C-C bond. The results of these more extended calculations are therefore inconclusive although they do point in the right direction.

Hirota et al.[80] assume that the probability of fragmentation can be calculated from the change distribution of the highest occupied molecular orbital in the neutral molecule, disregarding bonding or antibonding properties of all other valence electrons. If these other electrons <u>are</u> taken into account it is found that C-C and C-N bonds have nearly equal force constants.

Dewar[81] has stated that "if a perturbation treatment is carried out properly one finds the contributions of frontier orbitals are by no means dominant" when discussing the validity of the Frontier Orbital theory for the explanation of organic reactions. There is no reason to believe it will work better for unimolecular fragmentation of ions.

A third method of explaining the ethylamine case is the notorious "Mechanistic" interpretation of mass spectroscopy[82]. The molecule is supposed to be ionized in such a way that an electron is removed from a nitrogen atom, inducing a shift:-

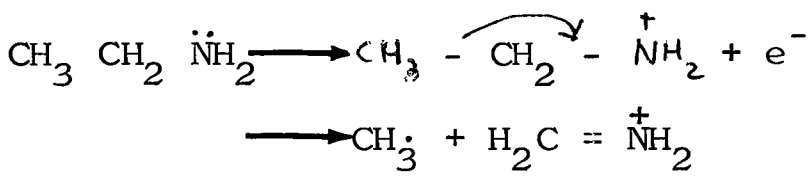

However this suffers from the fault that it depends on the concept of localized charge on an atom in a molecule which is known to be almost meaningless from theoretical calculations. In view also of the known independence of fragmentation upon the electron initially ionized in molecules such as these the mechanistic approach can be seen to be of no more value than as a mnemonic. Several authors have

expressed concern at the approach[83].

Any really satisfactory explanation would have to consider the energies of possible products of such reactions since activation energies are generally very low for ion-molecule reactions. Since $NH_2 = CH_2^+$ is very stable the potential surface must reflect the fact that as a C-C bond is stretched the electron distribution will change as the C-N bond assumes double bond character. The work of Lorquet et al. should achieve this if refined far enough.

D(vii) Kinetic Energy Release in Fragmentation

It has been recognized for some time that the use of electron impact mass spectroscopic appearance potentials to derive thermodynamic data can be very unreliable[55]. The minimum potential needed to cause an ionic fragmentation in any real system can only provide an upper limit to the thermodynamic energy requirement. There are two reasons why the appearance energy of a dissociation process will only give an upper bound to the heats of formation of the products. The first is that an activation energy may exist for the reverse reaction and the second is that if the process is to occur at all it must occur irreversibly. For the reaction to occur within the time scale of the experiment, some kinetic energy must be imparted to the products, indeed in the limit of no kinetic energy release at all the products would not separate and no reaction would occur. For a reaction occurring on a time scale of 10^{-11} seconds (a not uncommon figure), a kinetic energy of 0.01 eV is required if the products are to separate to a distance of 10Å in the available time.

This additional energy, which is neglected in appearance energy measurements, has come to be known as the "kinetic shift". It is interesting to note that on this basis the appearance energies of metastable ions in mass spectra should give closer estimates of thermodynamic limits. Distinct differences between metastable and "normal" appearance potentials have been noted[153] and this difference has been called the "measurable part of the kinetic shift"[154].

The excess energy imparted to products in a decomposition will, except in the case of fragmentation of a diatomic ion, be partitioned between translational, vibrational and rotational energies of product fragments. Several attempts have been made to account theoretically for the way in which this partitioning will occur[155,156,157].

The Quasi Equilibrium theory can only predict the distribution of kinetic energy in the "reaction coordinate" upon passing through the activated complex. The extension of this to the kinetic energy of the separated fragments will involve a further assumption connecting this reaction energy and the relative translational energy of products. The simplest assumption is expressed as the relation

$$\epsilon_k = \epsilon_t + E_r$$

where ϵ_t is the kinetic energy in the reaction coordinate and E_r is the activation energy of the reverse process. ϵ_t is therefore equated with the translational part of the kinetic shift. This assumption is presented in diagramatic form in figure 1.2.

Figure 1.2

A simple model of ionic dissociation.

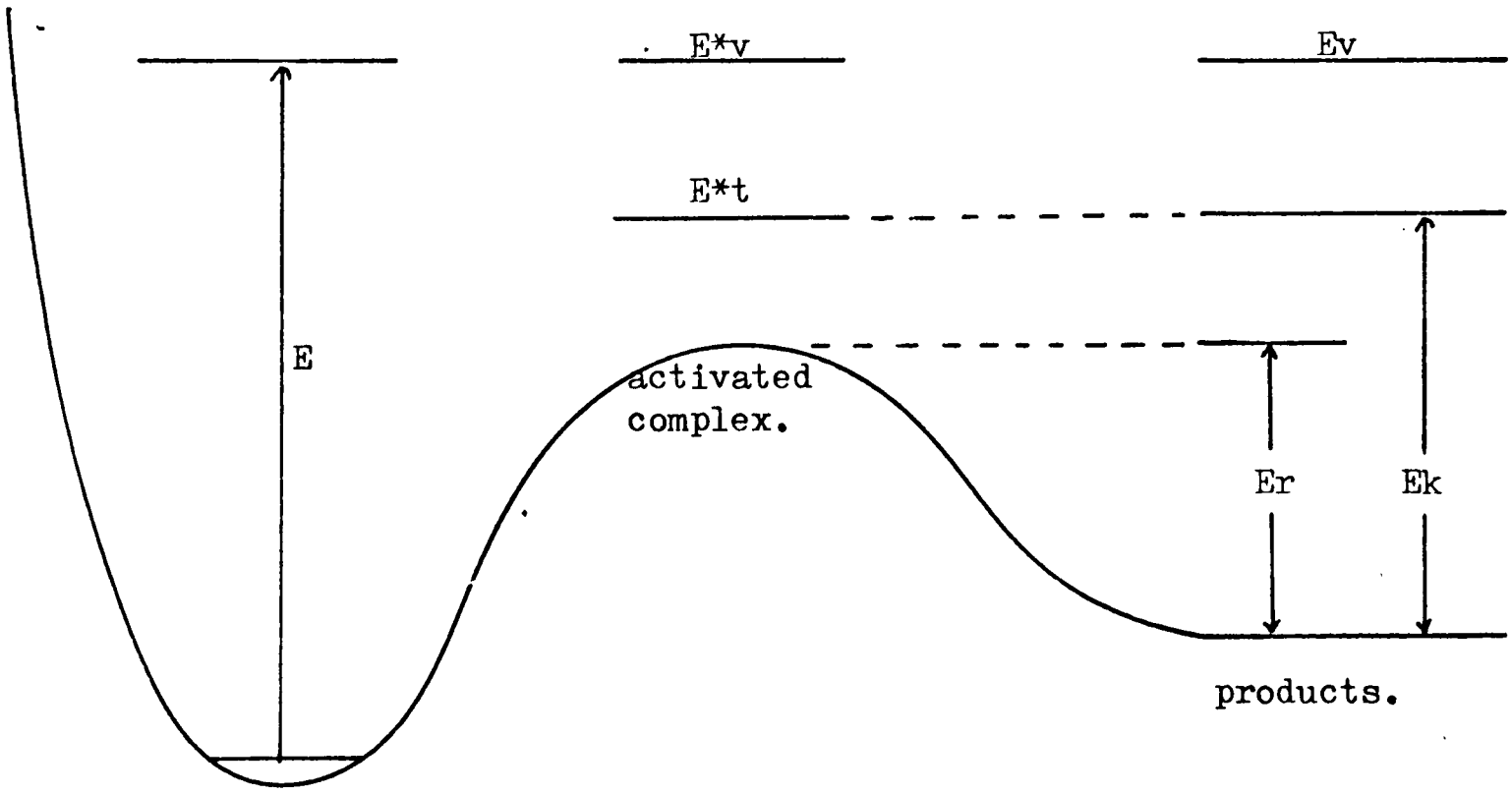

E excitation energy of dissociating state.

Ev vibrational energy of products.

Et kinetic energy in the reaction coordinate.

Ek kinetic energy of products.

Er activation energy of reverse reaction.

Such a model implies that internal energy of the separating fragments does not contribute to overcoming the energy barrier for the reverse reaction and conversely that the products of a fragmentation will be vibrationally cooler than expected.

Several attempts have been made to reconcile experimentally measured kinetic energies of the products of fragmentation reactions with theory[157,158]. Where agreement has been found between classical theory and experiment it has usually been found necessary to assume an activated complex with less than N-1 degrees of vibrational freedom (N is the number of oscillators in the parent ion). This reduction in the effective number of oscillators has been effected in various ways, the simplest being the treatment of Franklin[157] who assumed that a proportion α of the available oscillators would be "active" ones and hence $\epsilon_t = \frac{E^*}{\alpha N}$ where E* is the excess energy of the complex. He derived a value of 0.44 for α from experimental observations on a group of reactions. However the general applicability of this formula is doubtful[159].

Klots[55] has, by use of QET and Langevin collision theory, derived a simple relation between excess energy and kinetic energy release upon fragmentation. In the more common (rotational) "barrier negligible" case this is formulated as

$$E^* = (S + 1)\, kT^* + \sum_i \epsilon_i [\exp(\epsilon_i / kT^*) - 1]^{-1} \quad \ldots 4$$

where $\bar{\epsilon}_t = kT^*$. The parameter S is related to the number of rotational degrees of freedom R in the reaction products. ϵ_i are the quantum energies of the oscillators describing the vibrational degrees of freedom of the products. The

derived parameter $\frac{dE^*}{d\bar{\epsilon}_t}$ can be viewed as a measure of the effective number of degrees of freedom among which excess energy is partitioned. This parameter is now susceptible to measurement by photoelectron-photoion coincidence spectroscopy[29]. Indications have already appeared that in certain cases the effective number of degrees of freedom may attain magnitudes greater than the physical number present[156].

The distribution of kinetic energies predicted by Klots' formulation of QET is very nearly that of a two-dimensional Boltzmann gas[95]; the average energy being the kT* of equation 4. As was discussed above it was not expected that a distribution of kinetic energies of fragmentation would have its maximum value at zero energy as this formulation would predict. It seems necessary therefore to modify the result at least to the extent of disallowing zero kinetic energy release. This leads to the rather difficult question as to what constitutes an effectively zero kinetic energy release. The consideration in the first paragraph of this section perhaps provides a clue.

Theoretical treatments of the dynamics of decay of long-lived collision complexes found in bimolecular collisions in molecular beams have been derived[160] and related to experiments. This provides a useful alternative technique for observing what are essentially the same reactions with which we are concerned in the study of ionic fragmentation.

E. SOME EXPERIMENTAL CONSIDERATIONS

E(i) Photon Sources

The photon source used depends on the type of photoionization study being carried out. Continuous sources in conjunction with a vacuum UV monochromator offer distinct advantages over line sources in searching for autoionizing processes and in determining relative transition probabilities where it is desirable to follow the change in photoionization cross section with the wavelength of incident photons. Resonance line sources offer greater intensity with better resolution than a monochromator will normally provide. A detailed discussion of UV line and continuous sources is given by Samson[108]. In studies of dissociative ionic states use of a variable wavelength photon source would be desirable; however in practical terms an experiment such as the one described herein would be impossible to perform using such a source owing to the low intensities obtained. Where synchrotron radiation is available of course the possibilit of high intensities even after use of a monochromator would make the idea more attractive. Work is being carried out in this field[85]. In all cases where dispersed radiation from a continuous source has been used it has been necessary to monitor the photon flux with a photo-multiplier sensitized to UV radiation. The most common undispersed source used is the direct current, windowless, helium discharge lamp in which approximately 2 kV is applied across helium at around 1 torr pressure in a capillary tube. The bulk of the radiation is in the 584 Å (21.22 eV) line due to the $2\,^1P_1 \longrightarrow 1\,^1S_0$ transition. The next emission to longer wavelength is at

about 3000Å (4 eV) arising from the $^3P \longrightarrow {}^3S$ series and since few substances have ionization potentials below 5 eV this does not interfere. It has been found in this investigation and elsewhere[86] that the 584Å lines of the $^1P \longrightarrow {}^1S$ series account for at least 98% of the emission in this spectral region; most of the remaining radiation is accounted for by the $3^1P_1 \longrightarrow 1^1S_o$ transition at 23.1 eV. Small amounts of impurities will very easily degrade the purity of the radiation. Traces of hydrogen cause emission of the Lyman α line at 1215Å (10.20 eV). Fortunately it is not too difficult to purify the gas stream using a cooled molecular sieve. Out-gassing of the lamp structure may be a problem that is usually overcome by allowing the lamp to become thoroughly hot before making measurements. The state of the discharge is readily assessed by examining the lamp output, in the visible region, with a small direct vision spectroscope. The lines of the hydrogen Balmer series and oxygen and nitrogen emission lines should all be absent.

It has been found possible to use resonance lines of gases other than helium by adding a small proportion of the gas to the helium flow. Available lines are:

neon	(16.85 eV
	(16.67 eV
argon	(11.84 eV
	(11.62 eV
hydrogen	(12.0872 eV
	(10.198 eV

None of these sources have the virtually single line purity of the helium discharge however.

By the use of a much higher current density and lower helium pressure one can obtain significant amounts of

radiation from ionized helium at 303Å [86]. The 584Å line is still dominant however and the ionization energy range between about 30 eV and 40.8 eV is usually obscured in PES by overlying bands arising from 21.22 eV ionization. Special care must be taken to avoid hydrogen impurity together with both water cooling and fast differential pumping of the helium lamp to help dissipate the large input power. Such HeII radiation has been of use in detecting energy levels that lie above 21.22 eV in nitrogen, oxygen and other molecular ions[88].

E(ii) Energy Analysers

Many varied types of analyser have been described for energy resolution of electron or ion beams. Energy analysers have been reviewed by Klemperer[89]; those of particular use in PES have been reviewed by Turner[90] and two more general reviews have appeared recently[12,91]. There are fundamentally three ways of measuring the energy of charged particle beams:

a) by using retarding fields so that only particles of sufficiently high energy can pass to the collector;

b) by deflection in electric or magnetic fields so that particles of different velocities are deflected to varying degrees and can be separated by slit systems;

c) by time of flight methods.

For ion beams the retarding and the deflection types of analyser are the most straightforward and useful.

The resolving power of any energy analyser is defined as the ratio of the energy of the beam, E, to the energy spread after analysis, ΔE, i.e. $E/\Delta E$. ΔE needs to

Figure 1,3

The concentric grid retarding field energy analyzer.

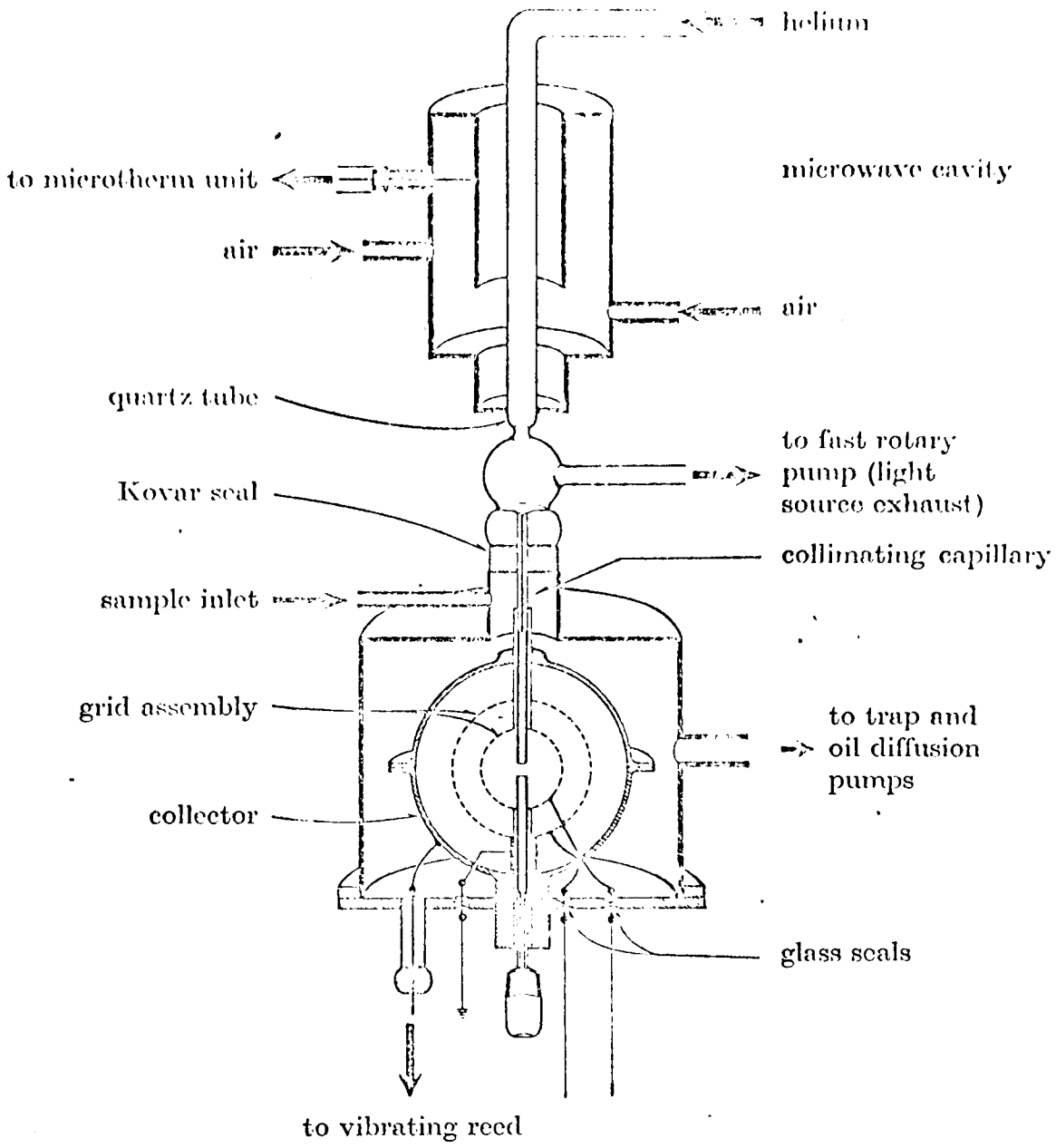

Taken from reference 93.

be defined in relation to the peak shape of the analysed beam; it is usual to use the "FWHM" - the full width at half maximum. In a well designed analyser $\Delta E \simeq \frac{1}{2} \Delta Ef$ where ΔEf is the base width of the energy spread.

The oldest method for determining the kinetic energy of a stream of charged particles is to arrange a retarding electrostatic field at the collector. The energy is deduced from the height of the potential barrier that they can just surmount. In his review of retarding methods Simpson[92] has pointed out that the height of this barrier is not actually a measure of the total kinetic energy, but of the momentum perpendicular to the equipotential lines.

The response yields the integral:

$$I(E_o) = \int_E^{\infty} N(E)dE$$
$$o$$

rather than the actual energy distribution which can be obtained by differentiating.

The simplest retarding field analyser is based on parallel plates; for PES the method has been developed to the form of the concentric grid analyser described by Frost et al.[93].

In this design, depicted in figure 1,3, the disadvantages of earlier retarding field designs are to a large extent removed. A fairly large region of ionization may be used without sacrificing resolving power which is limited by other factors in any case. The sensitivity in terms of electron flux is therefore very large - especially so as all photo-electrons formed are analysed. However an electron multiplier cannot, of course, be used and the

necessity of differentiating the spectrum results in quite poor observed signal to noise ratios. This form of spectrometer is however ideal for measuring transition probabilities as collection of electrons is isotropic. In practical terms the resolving power of such a machine is limited to about 100 and for better resolving powers a more sophisticated analyser has to be used. Various types of electrostatic filter lens have been described[91] in which particles above a critical energy are transmitted but these have not been used in general for PES or ion kinetic energy work.

An electrostatic lens was used as an energy filter by Frost for the energy analysis of an ion beam from a radio frequency source and in ion beam inert gas scattering experiments[94]. The use of an energy filter lens in low energy electron diffraction experiments is described by Zeeman et al.[95].

The retarding potential difference method is capable of electron energy resolutions of 0.008 meV[96] and has been extensively used in electron-atom scattering experiments.

The type of analyser most used in PES or ion kinetic energy analysis is the deflection type. In general these analysers only accept a beam of very restricted divergence but the consequent loss of particle flux is compensated by the capability of using an electron multiplier as the detector.

In all such systems the field configuration causes the particles to follow a trajectory which is some function of their energy. From consideration of this trajectory through the analyser one may derive expressions for the energy dispersion, the source dimensions and collector

Figures 1.4, 1.5 and 1.6

Energy analyzers.

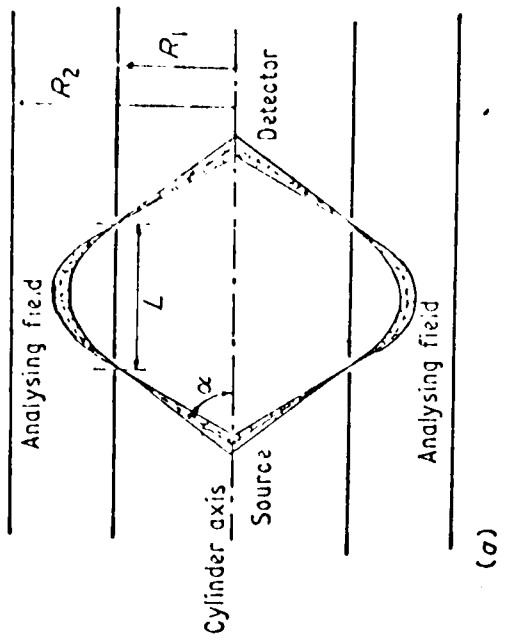

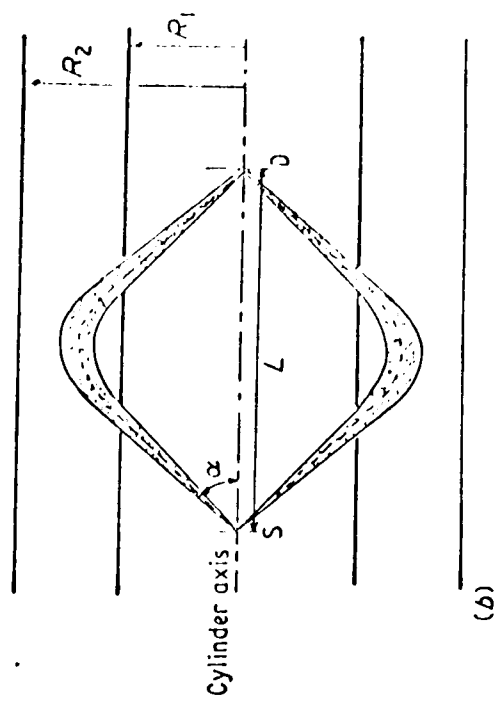

1,6

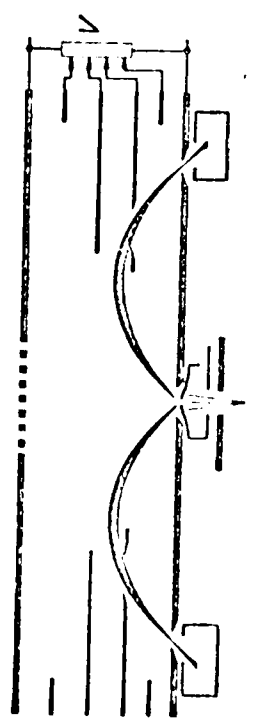

1,5

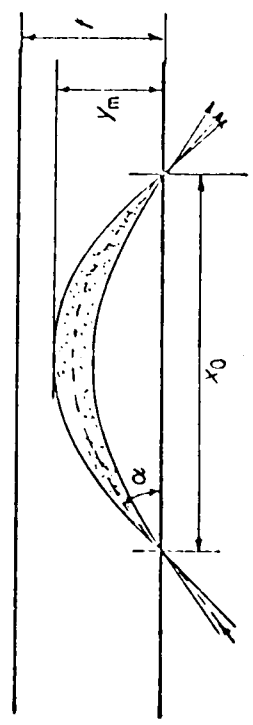

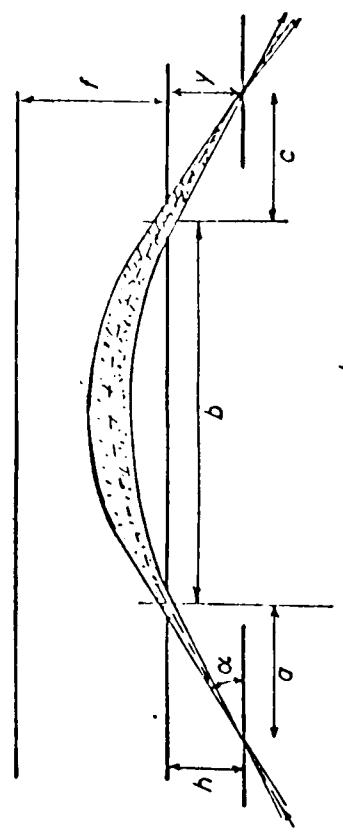

1,4

geometry effects, as well as the effect on transmission and resolving power of angular aberrations.

Perhaps the simplest type of deflection analyser is the parallel plate (figure 1,4a) devised by Yarnold and Bolton[97] for analysis of ion beams and by Harrower[98] for electron beams. Its use in PES is described by Eland and Danby[99]. This type of analyser has the advantages of ease of construction and freedom from fringing field problems as entrance and exit slits are at earth potential, however the focussing is weak and small entrance angles have to be used, (see Appendix A). Green and Proca[100] showed that by the use of a 30^{o} entrance angle double focussing could be obtained; in this case the source and image focus points are outside the front plate in the field free region (figure 1,4b) unlike in the 45^{o} entrance angle case where the focus points are on the earth plane.

By rotating the parallel plate about the y axis the "fountain" spectrometer is obtained (figure 1,5). Schmitz and Mehlhorn[101] considered the 30^{o} entrance angle version of this which they consider to have the best transmission/resolving power ratio of any design of analyser. However the ring shaped collector precludes the use of an electron multiplier.

Rotation of the parallel plate around the x axis creates the cylindrical mirror analyser (figure 1,6a). Again second order focussing is obtainable; now for $\alpha = 42.3^{o}$ [102] (figure 1,6b). Figure 1,6a shows the first order focussing case; equivalent to the 45^{o} parallel plate analyser. Various calculations have been performed showing that the efficiency of this type of analyser can be very high[91]. It has been

Figures 1.7, 1.8 and 1.9

Energy analyzers.

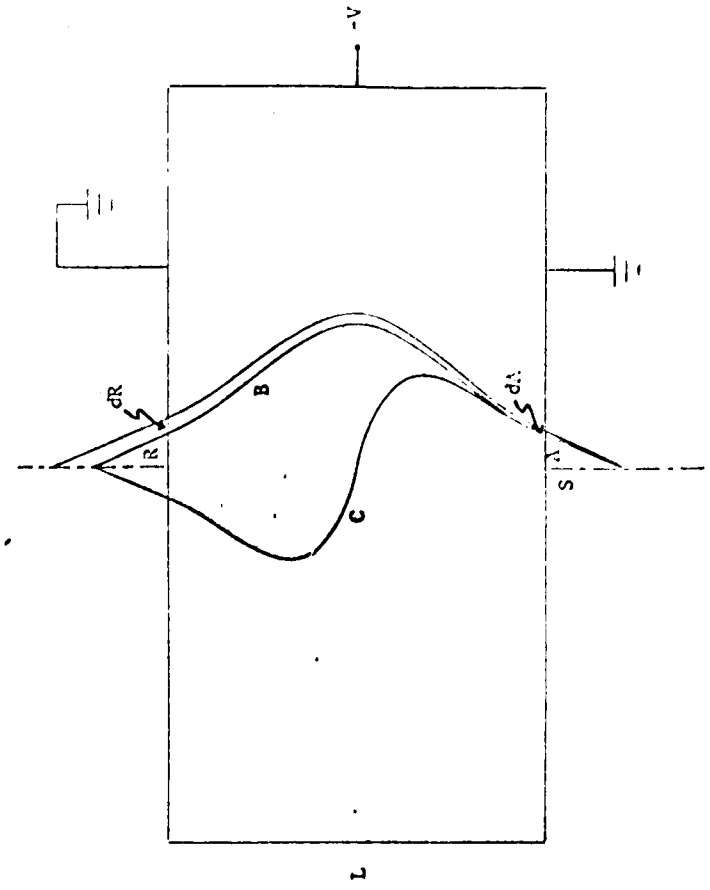

1,9

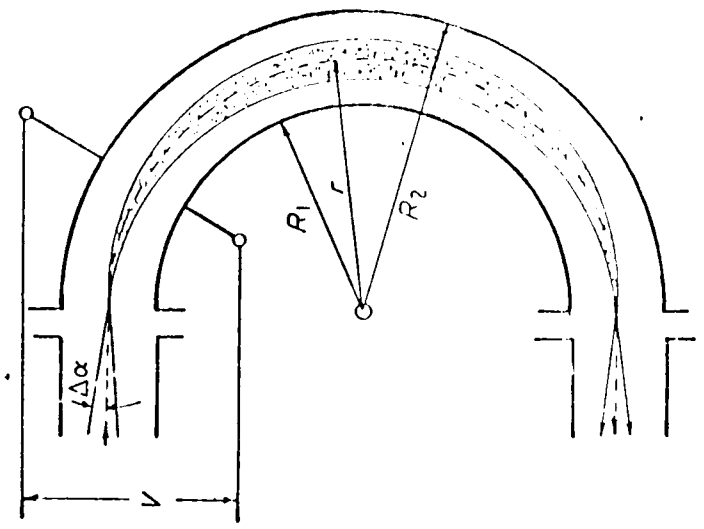

1,8

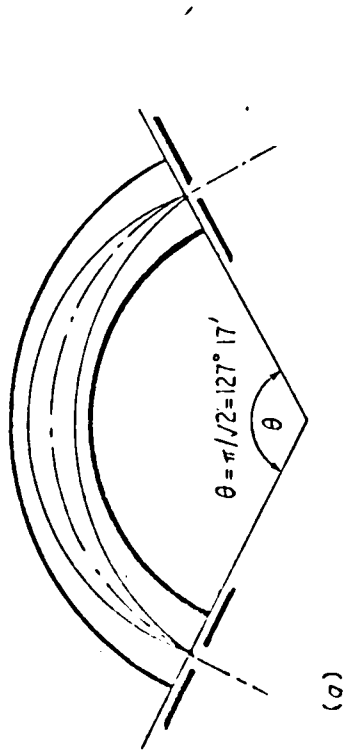

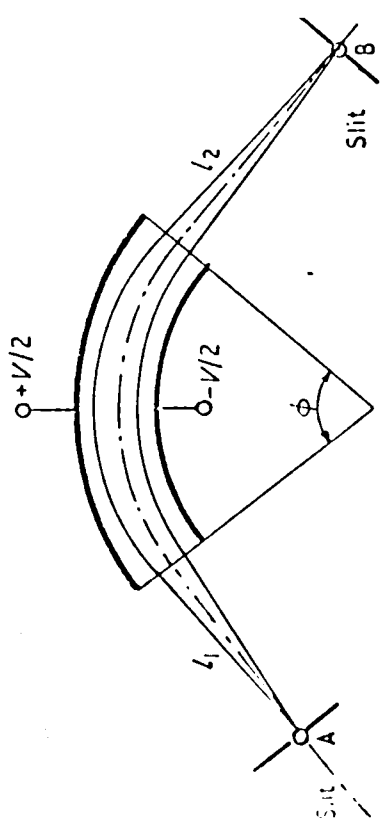

1,7

used in Auger electron studies and in studies of secondary electrons[91].

Perhaps the most commonly used analyser in PES is the 127° cylindrical sector field analyser. This is a specific case of the general sector field analyser for which the foci are the field boundaries. Figure 1,7a shows the 127° analyser, 1,7b the general case. This type of kinetic energy analyser is much used in the double focussing mass spectrometer and was first described for use in photoelectron spectroscopy by Turner[86] with a claimed ultimate resolving power of 1000. It has strong first order focussing in one direction and is suited to a line source of electrons. Fringing fields at the slits are a problem.

The 180° spherical condenser analyser (figure 1,8) has the advantage of a focussing effect in two dimensions but construction is difficult. The problem of fringing field correction at the slit points has been elegantly solved[110] by using electron lenses to produce images of physically distant slits at the geometrically correct points. Focussing is first order but has been shown to be perfect for a 360° analyser[91]. A 180° low energy electron spectrometer was used by Simpson[92].

The performance of a given analyser can be assessed from the product $\omega x \; E/\Delta E$, known as the collecting power, where ω is the solid angle from which particles may be collected. This is, however, only relevant for relatively compact sources. For this reason the product of source area and collecting power has been used as a criterion of analyser performance and is known as the "luminosity". This is a

relevant consideration in the study of vapours since at pressures low enough for ion-molecule or electron-molecule collisions to be improbable the light absorbtion is also small and a large source size is preferable. For this reason the cylindrical mirror type of analyser is probably less useful in this sort of work than might appear at first as it is only well suited to nearly point sources.

Many other analyser types have been described. These include saddle point field analysers in which separation is due to the chromatic dependence of a lens distortion at its external zones, quadrupole filters and many types using magnetic field or crossed electric and magnetic fields. A recent suggestion is that of the "pill box" analyser (figure 1,9)[103] which has many claimed advantages but is as yet untried in practice. These claimed advantages are small size, ease of construction and strong focussing permitting a high particle flux at good resolution.

Chapter 2 - Instrumental Section

Figure 2.1

The Energy Analyser

This is constructed of brass which is coated with graphite on all surfaces exposed to the ion or electron path. The analyser is mounted in the vacuum vessel on two knife edges set along the top slit axis and a pillar mounted on the back plate. The source region is enclosed and connected to the lamp and sample ports by flexible copper pipes. Connections to the multiplier are made via two flexible copper tubes containing wires insulated by short lengths of glass tubing. Other connections to the analyser and source plates are made via wires similarly insulated by glass tubes.

Figure 2.1

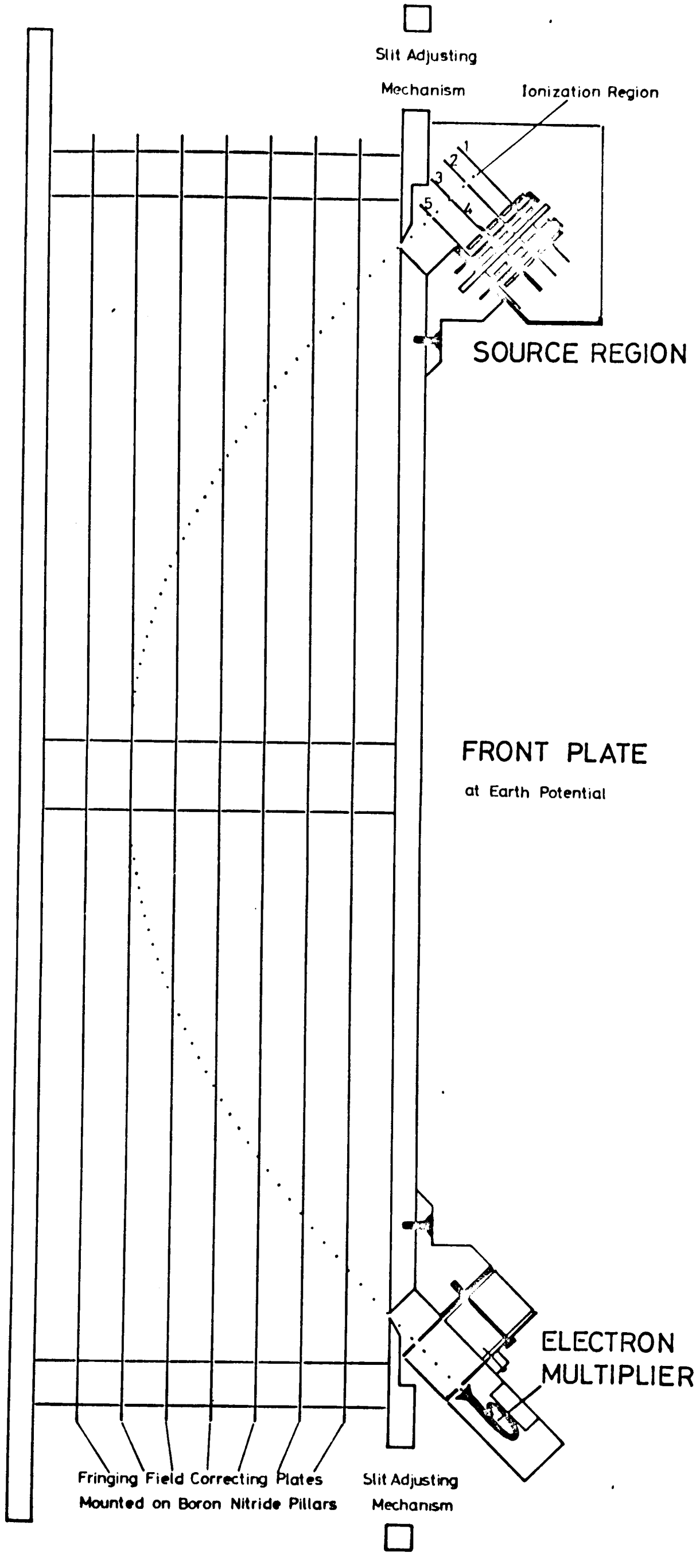
Slit Adjusting
Mechanism
Ionization Region
1
2
3
5
SOURCE REGION
BACK PLATE
FRONT PLATE
at Earth Potential
ELECTRON
MULTIPLIER
Fringing Field Correcting Plates
Mounted on Boron Nitride Pillars
Slit Adjusting
Mechanism

CHAPTER TWO

A. THE SPECTROMETER

The spectrometer used in the present investigation was originally used purely as a photoelectron spectrometer and was developed as such into an instrument capable of a resolving power ($E/\Delta E$) of 500[105,25]. A resolution of 12 meV was obtained for the argon $^2P_{\frac{1}{2}}$ peak and in the $^2\pi_g$ band of oxygen the spin orbit splitting of 23 meV was observed. This resolution represented a value close to the theoretical one for the slit widths used. In practice it was found that a resolving power of the order of 250 could be obtained with larger slit widths at much higher count rates and for most investigations this method of working was adopted.

The spectrometer consists of a parallel plate analyzer similar to but larger than the one described by Eland and Danby[99] mounted in a large brass vessel evacuated by an oil diffusion pump backed by a two stage rotary pump. Fixed ports are provided for the light source and sample inlet. The analyser can easily be adjusted to align with the light beam as it is mounted on knife edges pivoting on the axis of the entrance slit. This adjustment may be effected while the spectrometer is evacuated.

The further adjustments of the analyzer to bring it parallel to and at the correct distance from the light beam are carried out by screws inside the vacuum chamber. This alignment is performed with the aid of an aligning rod passed through the lamp capillaries to define the light path. After initial alignment while at atmospheric pressure the

Figure 2.2

Connections to the analyser

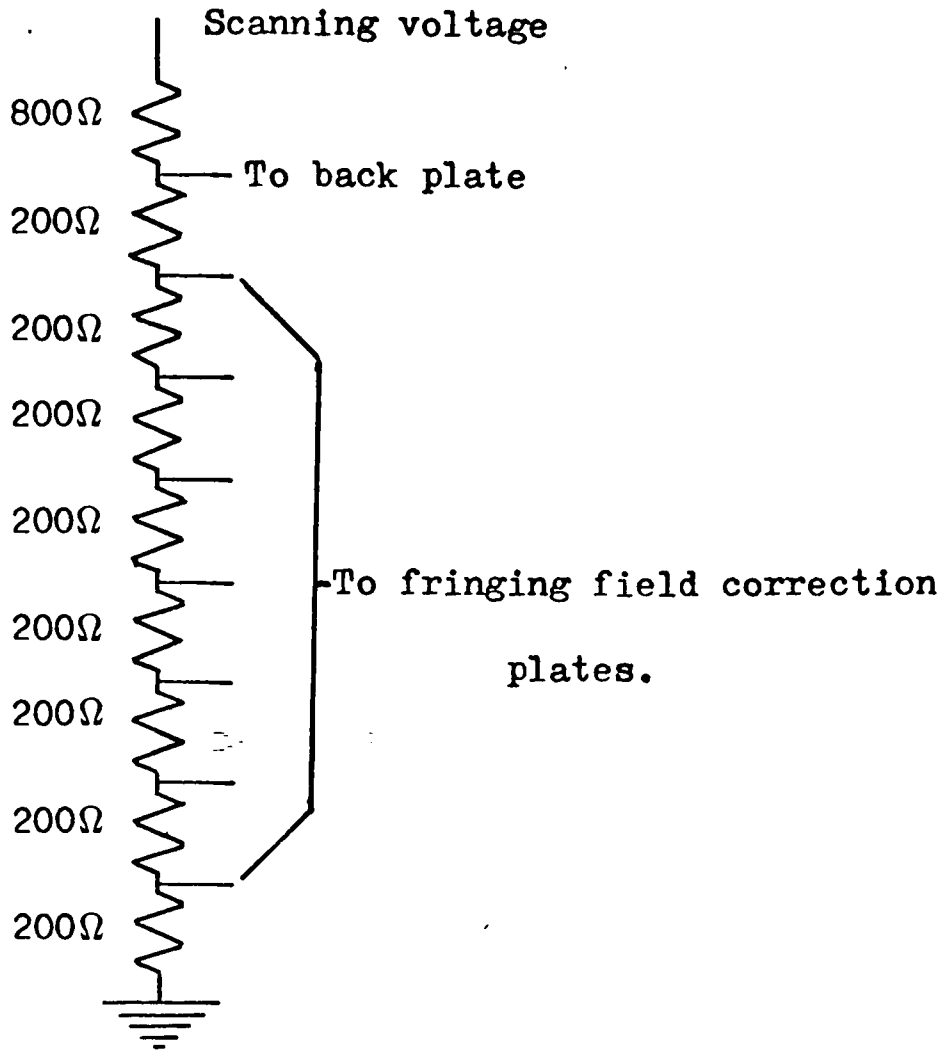

"rocking motion" is adjusted for optimum count rate under vacuum conditions.

A sectional diagram of the analyser and associated equipment is shown in figure 2.1. A detailed discussion of the analyser dimensions and their implications is given in Appendix B. The field at the edges of the analyser is controlled by seven fringing field correction plates. These are spaced evenly between the front and back plates and are held at voltages appropriate to their position by a resistor chain connected between the back plate and earth (the front plate potential). By including another resistor between the back plate and the scanning voltage an experimentally convenient coincidence of control voltage and the actual transmission energy in eV. of the analyser is obtained (see figure 2.2). The plate separation of the analyser is one third of the slit separation. For this case the voltage on the back plate is 2/3 of the transmission energy in electron volts. The whole of the metal surfaces of the analyser are

covered in graphite to minimize reflection of off focus electrons or ions and reduce any surface potential effects that might occur on an imperfectly clean brass surface.

Brass blocks are mounted at 45° on the front plate to carry the entrance and exit collimating plates. The ionization region is enclosed in a brass box mounted on the upper brass block. Communication between this box and the inlet and lamp ports is achieved via corrugated copper pipes. A three inch brass sidearm connects with the enclosed ionization region via the lamp inlet port and is evacuated by a diffusion pump backed by another two stage rotary pump. In this way the immediate ionization region is differentially pumped and higher sample inlet rates can be tolerated with only a small rise in the pressure in the main vessel. This is of great value if corrosive or otherwise objectionable samples are run as it protects the analyser and multiplier from being exposed to the sample to too great an extent.

Originally for PES work a cylindrical platinum source tube with a 0.5 mm exit slit was used to enclose the ionization region. Samples were let into this tube diffusively from the opposite end of the tube to the lamp. There is no doubt that for PES work this arrangement was best - the high resolutions quoted were obtained using it. However for the ion kinetic energy investigations carried out more recently it is necessary to have a small electric field acting across the ionization region. To this end a source was designed and fitted in which the ionization region was flanked by flat plates. The development of this source configuration for optimum performance with ions is described in part B of this chapter. However it may be mentioned here that the

construction of the source region is such that modifications are readily and speedily carried out. The various plates are mounted on three rods, separated by boron nitride washers. Two 1/8 inch aligning rods are firmly pushed into holes in the brass mounting block and hold the plates in accurate alignment until the nuts on the three mounting rods are fully tightened. They have, of course, to be removed once the source is assembled to avoid shorting the plates to one another. Electrical connections to the source, analyser and mutliplier are taken through three ports containing glass-metal seals.

The electrons or ions leaving the exit slit of the analyser are detected by a channel electron multiplier housed in a small brass box mounted on the lower brass block. Two plates at earth potential are placed between the multiplier and the exit slit of the analyser. Slits in these plates allow ions or electrons to pass that leave the analyser at about 45^{o}. This collimation of the beam leaving the analyser was found to be necessary to cut out reflected electrons leaving the analyser at odd angles[105].

The widths of the entrance and exit slits to the analyser are varied simultaneously by a control operating via a Wilson seal. The interior of the vacuum chamber is lined with mu-metal to reduce stray magnetic fields. For high resolution PES work another mu-metal screen may be erected around the whole spectrometer but this is not found to be necessary for the ion kinetic energy work. The effect of field correcting coils on the performance of the spectrometer even for high resolution PES was found to be negligible[25] provided that all screens were in place and the various

Figure 2.3

The Discharge Lamp

This is constructed of pyrex glass. Three aligned capillaries define the light path; the first is the discharge capillary; the second a throttling capillary to maintain the pressure in the first; and the third is a differential pumping "window" connecting to the spectrometer. The volume between the second and third capillaries is evacuated by a two stage rotary pump.

Figure 2.3

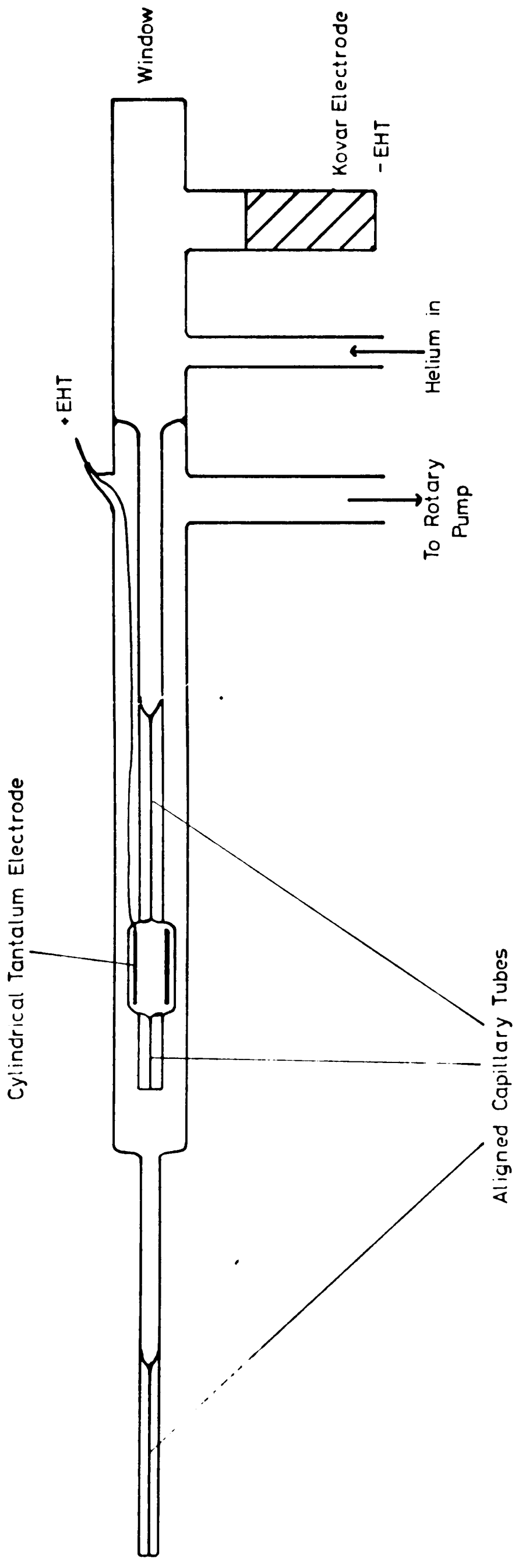
Window
Kovar Electrode
-EHT
Helium in
+EHT
To Rotary Pump
Cylindrical Tantalum Electrode
Aligned Capillary Tubes

Figure 2.4

The Lamp Gas Supply

Helium and neon at slightly above atmospheric pressure (in case of any leaks in the tubes from the cylinders) are mixed via needle valves A and B into the intermediate pressure region where they pass through a molecular sieve cooled in liquid nitrogen. Pure gas at the intermediate pressure is reduced in pressure to a few torr by needle valve C and enters the lamp.

Figure 2.4

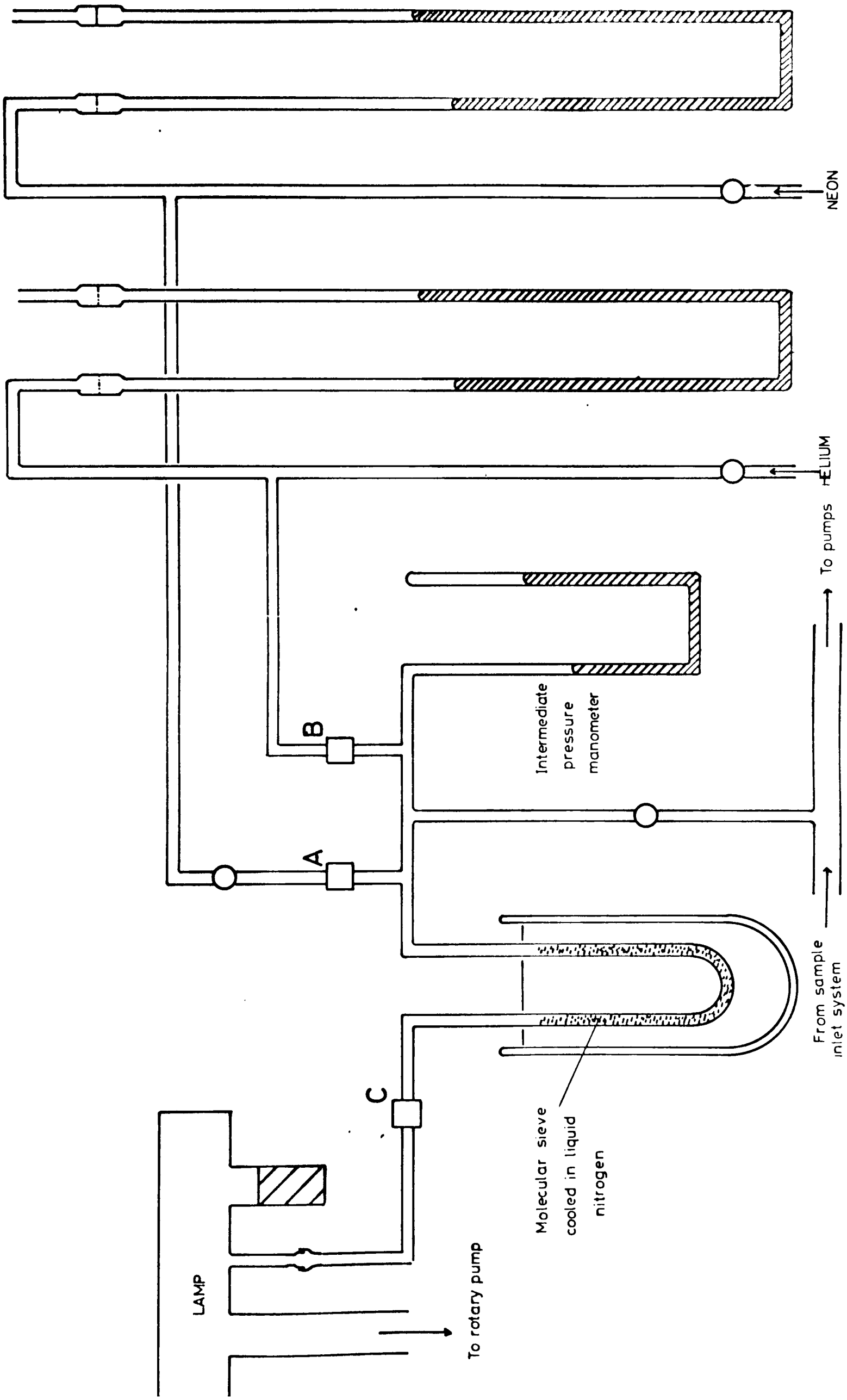
NEON
HELIUM
To pumps
Intermediate pressure manometer
B
A
C
From sample inlet system
Molecular sieve cooled in liquid nitrogen
LAMP
To rotary pump

plates of the source region were scrupulously degreased and coated with a smooth film of colloidal graphite. The pumps and their associated circuitry are magnetically screened and cutout devices are fitted in case electricity or water supplies fail. With no gas in the discharge lamp a pressure of 3×10^{-7} torr is attained. With the present lamp running under normal experimental conditions however the pressure reads as 2×10^{-6} torr on the ionization gauge - it must be borne in mind however that ionization gauges are rather insensitive to helium or neon.

The lamp design finally adopted for use in this spectrometer is shown in figure 2.3. The development of this design is described in detail in section C of this chapter. The end of the lamp fits into a brass collar close to the ionization region and the main body of the lamp is sealed at the lamp port by a compressed O-ring. The lamp is thus held in position quite rigidly and alignment of the analyser with respect to the light beam is carried out as described above.

Gases for the discharge are metered by the system depicted in figure 2.4. In the present investigations helium and neon were the only gases used. A molecular sieve cooled in liquid nitrogen is used to purify the helium or neon as it is let into the lamp via two needle valves. The gases can be mixed via the two valves A and B into the low pressure region whence needle valve C meters the gas at about 50 torr down to a few torr in the lamp discharge capillary. Gas is pumped away from the lamp by a two stage rotary pump. A discharge is maintained in the lamp by a

Figure 2.5

The Sample Inlet System

The system is completely free of grease as greaseless taps and joints are used. Gaseous samples are stored in globes 1 and 2. Samples with low vapour pressures are evaporated directly into the spectrometer via the direct inlet.

Figure 2.5

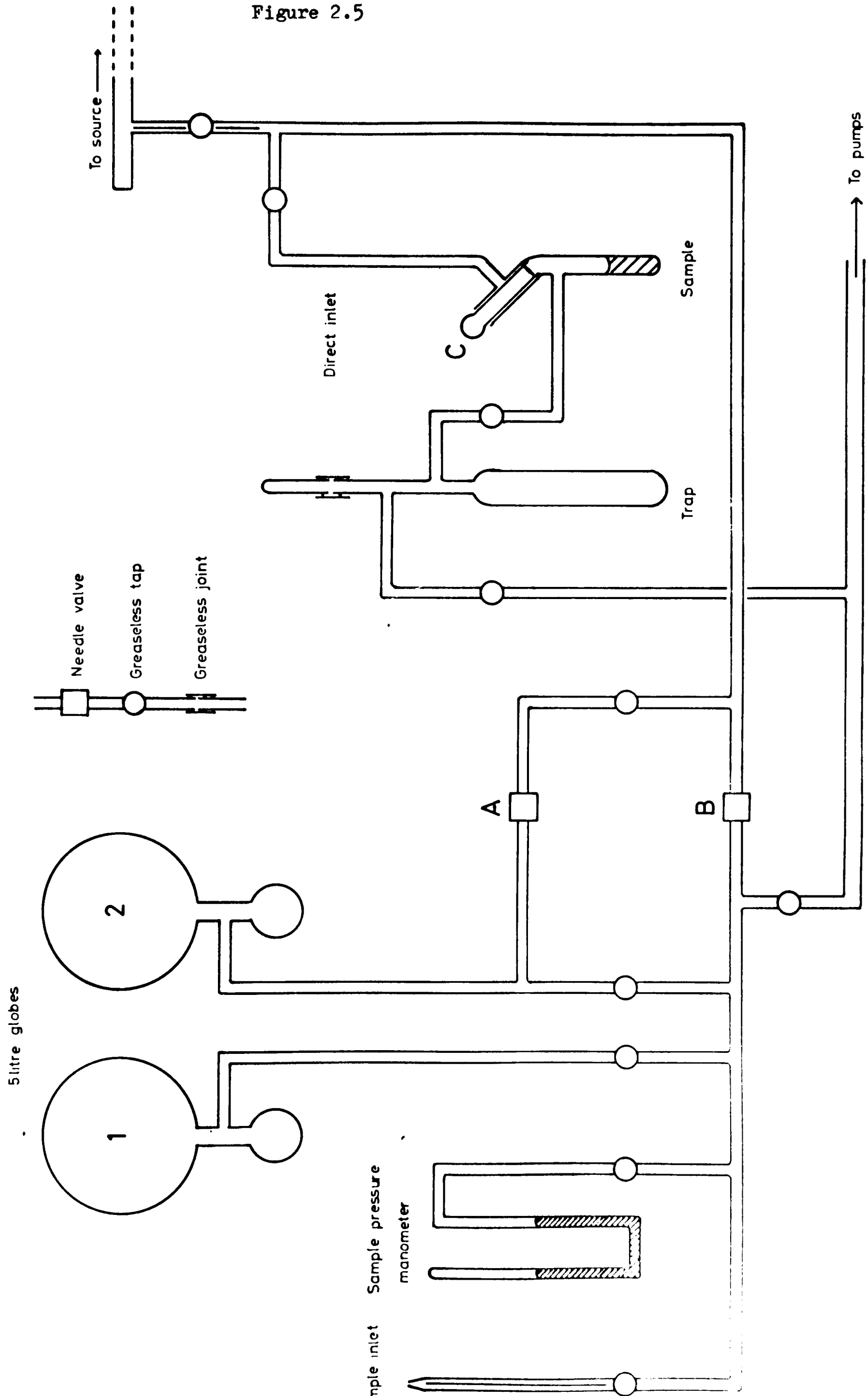
To source
To pumps
Direct inlet
Sample
C
Trap
Needle valve
Greaseless tap
Greaseless joint
A
B
5 litre globes
1
2
Sample pressure manometer
Sample inlet

DC supply of 2 kilovolts; currents of typically 30mA are used. The outer electrode of the lamp is made negative as it gets hotter than the positive electrode due to ion bombardment and is more effectively cooled by the atmosphere than the inner electrode which is in a virtual vacuum.

It is particularly important that no traces of impurity should enter the lamp. Hydrogen for example, usually present as water, will produce Lyman α radiation at 1215Å (10.2eV) under the operating conditions and both oxygen and nitrogen have many lines above 10eV which would cause serious interference. Spectral purity of the discharge may be checked by the use of a direct vision spectroscope to look for visible hydrogen, oxygen and nitrogen lines through the window at the back of the lamp. After the spectrometer has been let up to atmospheric pressure for any reason the lamp has to be run for a few hours to degas all such impurities. When running correctly the helium discharge is peach coloured; the neon discharge is brilliant red.

The sample inlet system is shown in figure 2.5. Gaseous samples or liquids with vapour pressures higher than about 1 cm of mercury are stored in one of the 5-litre globes at a pressure of up to about 10 cm of mercury and let into the spectrometer via the needle valve B. The other globe may contain a calibrant. For PES work this will typically be argon or methyl iodide which may be mixed with the sample gas stream via needle valve A. The importance of an internal calibrant was demonstrated by the work on hydrogen peroxide and hydrazine performed with this machine[25]. With hydrazine in particular a shift of 0.2eV in apparent electron energy occurred when the sample was introduced

presumably due to build up of hydrazine on surfaces. This shift was reflected in the position of methyl iodide and argon calibrant peaks.

For ion kinetic energy work a calibrant may again be important in cases where no parent ion is given by the sample. Typically argon is used unless its mass clashes with that of one of the sample fragments in which case nitrogen or krypton may be used. The calibrant in this case establishes the distribution for zero kinetic energy release in the centre of mass upon ionization.

For samples of low vapour pressure the "direct" inlet system is used. This system communicates directly with the source region of the spectrometer and the rate of influx of sample can only be controlled by varying the vapour pressure of the sample; this is achieved by cooling. This system is also used in cases where the sample would decompose on the metal in the needle valves, an example of this use was the PES investigation of hydrazine[25].

For the recording of photoelectron spectra the analyser voltage is scanned by a digital voltage scanner providing steps of 1,2,4,10,20,40 and 100mV at intervals of 1,4,10,40 or 100 seconds. The count rate is derived by a ratemeter with a time constant variable from 0.3 to 30 seconds. The spectrum is plotted on an X - Y recorder, a simple resistor - capacitor circuit being used to smooth the voltage steps. Accelerating potentials may be applied using the source plates in order to record low energy photoelectrons for which the analyser does not have a good transmission coefficient.

B. THE DEVELOPMENT OF THE SPECTROMETER IN THE COURSE OF THIS INVESTIGATION

This section describes the evolution of the spectrometer as it was developed to investigate fragment ion kinetic energies.

In principle a parallel plate energy analyser can be used to measure ion kinetic energies simply by reversing the potential applied to it. However in general the kinetic energy of a fragment ion will be less than 1ev; often very much less. Thus a constant acceleration has to be given to the ions in question and the precise way in which this acceleration is applied is one of the major subjects of this investigation.

The experiment envisaged above will provide a measure of the distribution of kinetic energies of ions leaving the source region after photoionization. However as yet there is no way to relate this distribution to a particular fragment. This information <u>is</u> available however as the flight time of an ion in the spectrometer will be related to its mass and energy.

$$t = C \frac{M^{\frac{1}{2}}}{E} \qquad \text{(see Appendix B)}$$

It has already been stated that the ion energy will be small and if the acceleration applied is substantially greater than the maximum ion energy the flight time will become simply a function of $M^{\frac{1}{2}}$. In fact it was decided early in this investigation to scan the ion energies by varying the accelerating field and keeping the analyser voltage constant; resulting in the virtual non-dependence of ion flight time in the analyser upon the initial ion energy.

In order to separate ions according to their flight time it is necessary to gate the entry of ions to the analyser in some way. At first this was achieved by pulsing the light output from the lamp[25]. A brief discussion of the results of investigations of this technique are now given; full details have been given elsewhere[25].

A resolving power of about 10 was obtained. An investigation of the factors affecting the spread of ion arrival times yielded the following results.

a) The lamp pulse width could not be reduced substantially below 4 μsec. As the ion flight time for an ion mass of 40 and 5eV of kinetic energy is about 100 μsec it can be seen that a shorter lamp pulse width would be preferable. A spread of 4 μsec places an upper limit on the resolving power of $t/2\Delta t = 12$. This is not the only factor limiting the resolution however. The spread of initial velocities of ions in the source causes a spread of flight times for two reasons.

i) The ions take varying times to accelerate from their initial velocities under the influence of the source field. This broadening was shown to be given approximately for thermal initial velocities by:

$$\delta t = 0.66 \frac{M^{\frac{1}{2}}}{V_s} \mu sec \qquad V_s \text{ is the source field.}$$

For an ion of mass 40 and V_s = 1.5 volts/cm. this is about 4μsec. Lower source fields are now used making the effect more important. Obviously ions with a broad distribution of kinetic energy release will have their spread of arrival times broadened by this effect although above a certain energy (half the actual source voltage) backward flying ions will not be observed and the effect is lessened.

It can be seen that to reduce this effect a high source field should be used; however this will degrade the energy resolution.

ii) Ions will have varying velocities after acceleration due to their thermal intiial velocities. This will only apply to the extent that the analyser will allow a small distribution of different ion energies to pass and it was found that a broadening of less than 0.5 μsec is to be expected from this effect.

iii) The finite width of the ionization region means that the total acceleration potential experienced by an ion will vary according to the exact point at which it is formed.

For an ion of mass 40 accelerated by 5 volts including a source potential of one volt this was calculated to contribute a broadening of 0.7 μsec: an unimportant amount. However it is this effect that is responsible for the degradation of energy resolution mentioned above. At a source potential of one volt this degradation is serious and from this point of view much lower source potentials are desirable.

It was realized in fact that the requirements of good mass and energy resolution were mutually incompatible with this method of working.

Difficulties in controlling the pulse width of the lamp or obtaining high pulse repetition rates also suggested that the technique should be changed. For cases where only a few fragments of widely varying mass are formed it would be advantageous to be able to use longer ion pulses in order to obtain higher count rates. The various lamp pulsing methods that were tried would not allow this.

The first source configuration used for ion kinetic

Figure 2.6

The original design of source region for ion kinetic energy studies.

Figure 2.7

The block mounted between plates A and B of the original source.

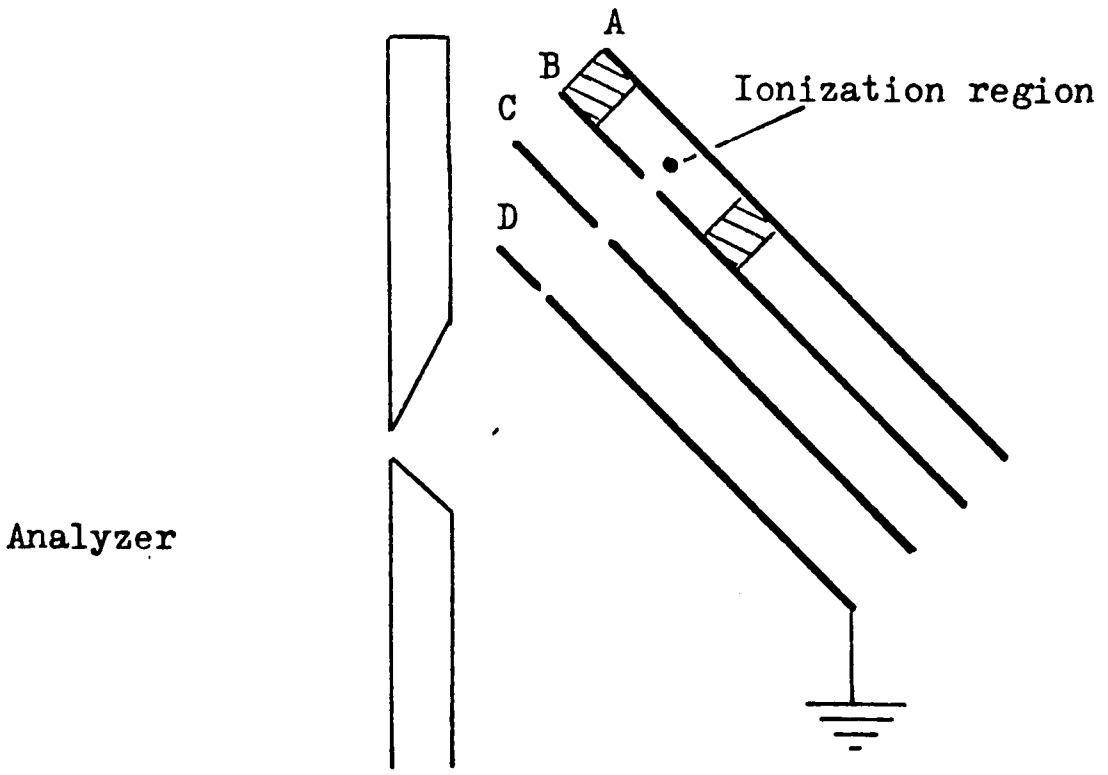

Figure 2.6

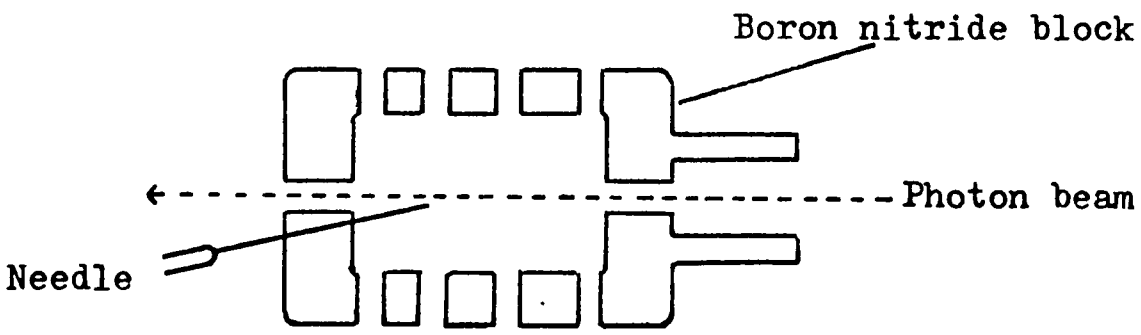

Figure 2.7

energy analysis was as roughly depicted in figure 2.6. The plates were made of $^{1}/_{16}$ inch thick brass and slits were 2 mm wide. The ionization region was fully enclosed (except of course for the exit slit and sample and photon beam ports); this being achieved by placing a hollow boron nitride block between the source plates A and B. As in PES work the sample was let diffusively into this region, creating a local high pressure of sample vapour between plates A and B. For ion work it was found that collisions in the source were of much greater importance than in PES and lower sample pressures had to be used. Because of this and also because of the desire to lessen thermal time of flight broadenings it was decided to experiment with the introduction of sample vapour via a hypodermic needle with its nozzle placed as near as practicable to the photon beam. The idea for this came from other work in this laboratory on a photoion-photoelectron coincidence spectrometer in which this method of sample introduction has been found to give a useful lowering of the apparent temperature of the sample vapour. (An apparent temperature of about 100^{o} K is found.) In the first instance the idea was tried by drilling an oblique hole in the boron nitride block to take a hypodermic needle. A number of $^{1}/_{8}$ inch holes were also drilled in the block to "open up" the source area. Figure 2.7 shows the arrangement used. The hypodermic needle was held at a potential appropriate to its position in the source by two resistors connected in series across the source plates.

Results with this arrangement were certainly encouraging although not in the way expected. No apparent lowering of sample temperature could be found (this would be expected to cause a narrowing of the observed distribution

of kinetic energies). However much higher sample influx rates could be tolerated without collision effects. The presence of ion-molecule collisions is detected if a high source field is used when a tail will appear to the low energy side of an experimental ion kinetic energy spectrum. This improvement is readily understood as the needle will provide a high concentration of sample in the photon beam yet the sample may escape quickly via the opened source and is differentially pumped away by the source region pump. That essentially no lowering of sample temperature occurs is also readily explained. In the photoion-photoelectron coincidence machine the hypodermic is at right angles to the photon beam and as close as possible to it. Thus ions do not travel at all far from the jet to the ionization region. With the grazing incidence of hypodermic and photon beam used in this experiment ions necessarily travel much further before reaching the ionization region and will undergo enough collisions to restore their three dimensional temperature distribution. However the value of this method of sample introduction was demonstrated; higher ion count rates could be obtained with no apparent collisional effects. It may be mentioned at this point that no absolute guide to the value of the sample pressure at the point of ionization is provided in this spectrometer. In practice the pressure in the main vacuum chamber is used as an indication but the meaning of any particular reading can only be determined empirically. For PES work pressures up to about 10^{-4} torr were used. For studies with ions pressures of up to 3×10^{-5} torr could be used without apparent collisional effects, using the original sample introduction procedure. Pressures in excess of 10^{-4}

Figure 2.8

The Final Source Region Design

The stainless steel plates are mounted on three bolts tapped into a block mounted at 45^{o} on the analyser front plate. The plates are separated by boron nitride pillars or mica sheets. The two alignment rods are kept in position during dismantling and reconstruction. Plates 3 and 4 form the upper and lower edges of a slit as shown. Plate 5 is at earth potential and is immediately above plates 6 and 7 which are really two half plates providing a capability of steering in the direction perpendicular to the paper. The sample needle is mounted in a boron nitride block between plates 1 and 2.

SECTION THROUGH SOURCE

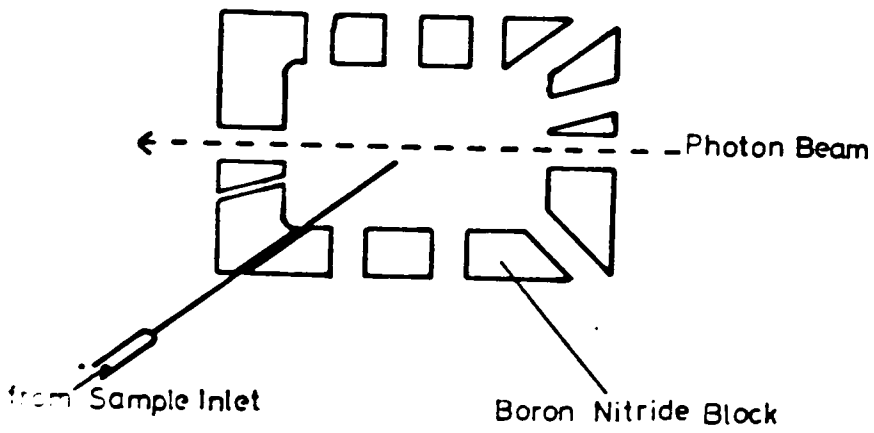

PLATES 3 & 4

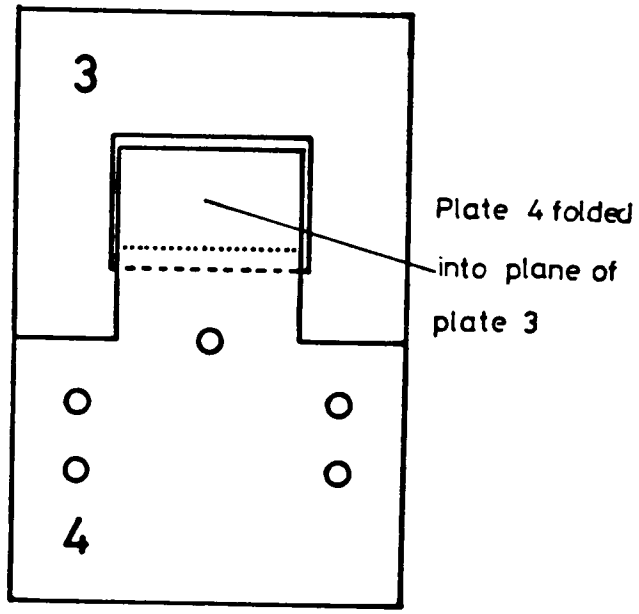

Plates separated by a mica insulator

THE SOURCE REGION

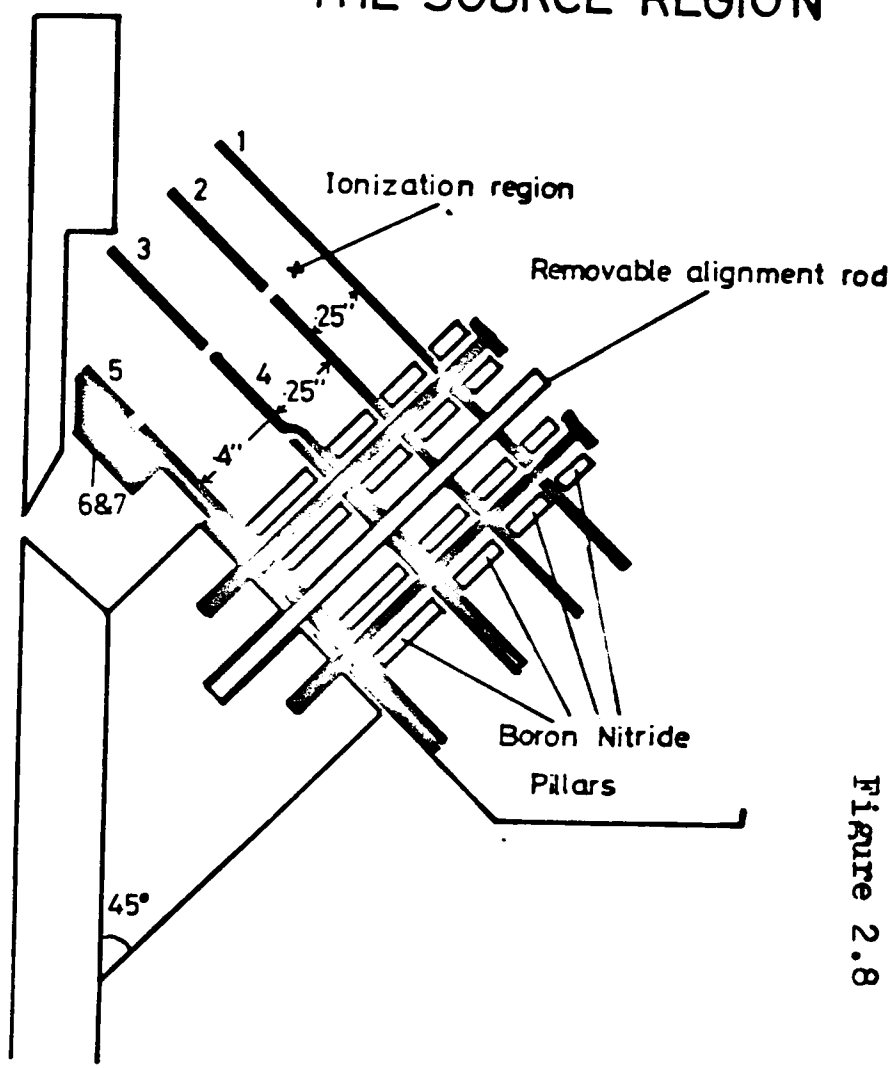

Figure 2.8

torr could be tolerated when the hypodermic was used but in practice lower pressures have always been used in order to be sure that collisions are not affecting results. It is a good idea to carry out any particular investigation at a few different sample introduction rates. Any significant collisional effects will then be shown up by pressure dependent variations in the observed distribution.

Many disadvantages with the construction of the source were by this time apparent - hardly surprisingly as it was essentially the product of extended modification of the original PES design. For this reason a new set of source plates were designed bearing in mind the following considerations.

a) The plates should be thinner - a $\frac{1}{16}$ inch thick slit will have an appreciable penetrating field when a potential difference is applied relative to the next plate which may well be causing the ion beam to spread unnecessarily.

b) The ability to apply "steering" fields across slits is desirable - to compensate for small misalignments of the source and also the compensate for any bulk relative motion of ions caused by the sample inlet procedure.

c) The source region should be completely open with the hypodermic needle at as acute an angle with a perpendicular to the ion beam as possible.

Accordingly a new source was constructed which was in all but one respect as depicted in figure 2.8. Plates 1 and 2 surround the ionization region and the source potential is applied between them. Split plate 3 and 4 is the first acceleration plate and also can provide a vertical steering field. Plate 5 is at earth potential and two small

plates 6 and 7 immediately behind it can provide a horizontal steering field. The hypodermic was mounted in a small boron nitride block in turn mounted on plate 2 but this arrangement gave consistently poor count rates. By swapping between this design and various old designs it was found empirically that the first method of mounting the hypodermic needle gave the best results and hence a boron nitride block was constructed as in figure 2.8 to provide a "semi-open" source region. A power supply was constructed capable of supplying suitable stable but variable voltages to all the new source plates.

The source was dismantled and reconstructed many times while trying to find the optimum conditions. Tests were performed after each reconstruction using argon ions without mass analysis. Eventually after the (stainless steel) source plates had been thoroughly cleaned, degreased and reblacked several times, the analyser alignment optimized and the positioning of the needle perfected it was found possible to obtain at very low source fields a kinetic energy distribution for argon ions as in figure 2.19. This represents a great improvement on the results obtained two years ago in which peak widths of 100 meV were obtained with argon ions. It is felt that this does show a reduction in the effective sample temperature although it is difficult to decide what actual temperature it represents. This problem is discussed further in section D of this chapter. It is very difficult to say to what extent the distribution is experimentally broadened. With the same source PES results with resolving powers in the 250 region are obtained which represents a broadening of about 10-12 meV at the energy of

the argon $2P_{\frac{1}{2}}$ peak. However it has been found consistently in this investigation that photoelectron results are, as expected, much more sensitive to such effects as stray magnetic fields than photoion results and such a large broadening may not be operating in the ion kinetic energy measurements. The spectrometer in its present form is indeed extremely suitable for the measurement of photoelectron spectra even though it is now optimized for ions. Resolutions of about 40 meV (at the argon $2P_{\frac{1}{2}}$ peak) are quite satisfactory for routine PES and are easily obtained.

Ion kinetic energy spectra are normally measured with the analyser slits wide open in which case the argon ion kinetic energy peak is broadened to about 35 meV, however count rates are much higher and it is not felt that much information will in fact be lost under these conditions.

The effect of the steering potentials was extensively investigated; it being found that a small potential across plates 3 and 4 (usually about 50-200 mV) increased the count rate dramatically. The effect of plates 5 and 6 is negligible at ion energies above about 4 eV although below this they do have a profound effect. This suggests that below this energy a small concerted motion of ions in the horizontal direction may be enough to cause ions to miss the multiplier. These facts suggested a new method of time gating the ions for mass analysis. If the potential across plates 3 and 4 is reversed it is found that a small value (again about 50-200 mV) will completely shut off the ion beam.

By applying a brief pulse to one of the plates of such a magnitude as to bring the potential back to the "pass" value it was found that a brief burst of ions could be let through the analyser. This idea was investigated further

Figure 2.9

A Block Diagram of the Ion Kinetic Energy Experiment

The analyser potential is fixed and the spectrum is scanned by varying the voltage on plate 2 of the source. The source voltage supply is designed so that the voltage between plates 1 and 2 (the source field) stays constant and the mean of the voltages on plates 3 and 4 is always a fixed proportion of the voltage on plate 2.

The pulses on plates 3 and 4 cause their relative voltage to reverse as shown in the inset plot of voltage versus time for the two plates.

Figure 2.9

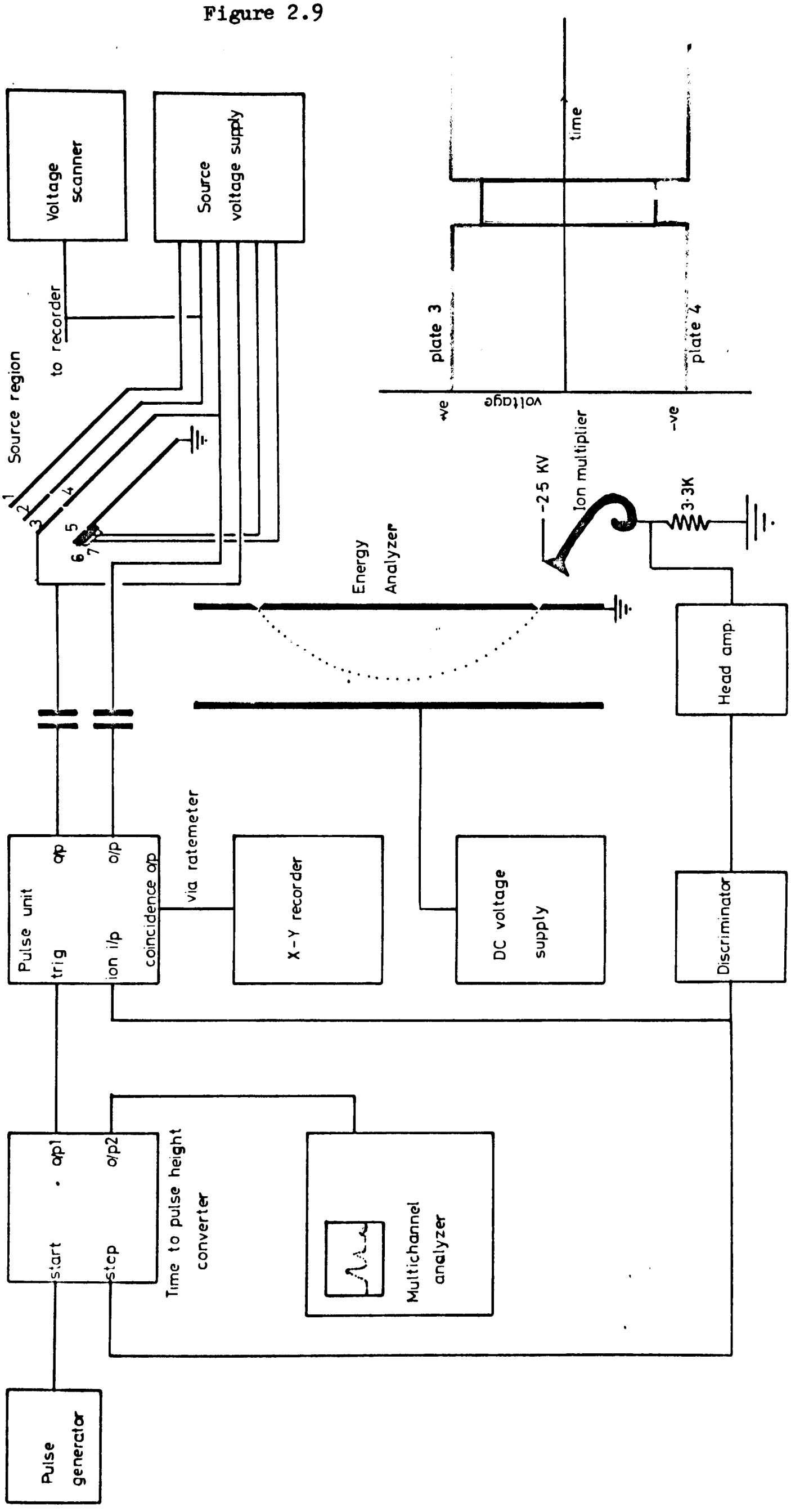
Voltage scanner
Source voltage supply
to recorder
Source region
1
2
3
4
5
6
7
time
plate 3
plate 4
voltage
+ve
-ve
-2·5 KV
Ion multiplier
3·3K
Energy Analyzer
Head amp.
Discriminator
Pulse unit
trig
ion i/p
coincidence o/p
via ratemeter
X-Y recorder
DC voltage supply
start
stop
o/p1
o/p2
Time to pulse height converter
Multichannel analyzer
Pulse generator

Figure 2.10

The Pulser and Coincidence Unit

Pulses of length 1 - 50 μsec are produced in opposite phase at two outputs (marked O/P) upon receipt of a trigger pulse at the input. These pulses are applied to plates 3 and 4 in the source. The trigger input also starts a delay circuit, consisting of two monostables in series, which after a variable delay of 10 - 1100 μsec will open a gate for a period set by the resolution control (0.5 - 20 μsec) allowing pulses applied at the "Ion I/P" to pass to the "Coincidence O/P".

Figure 2.10

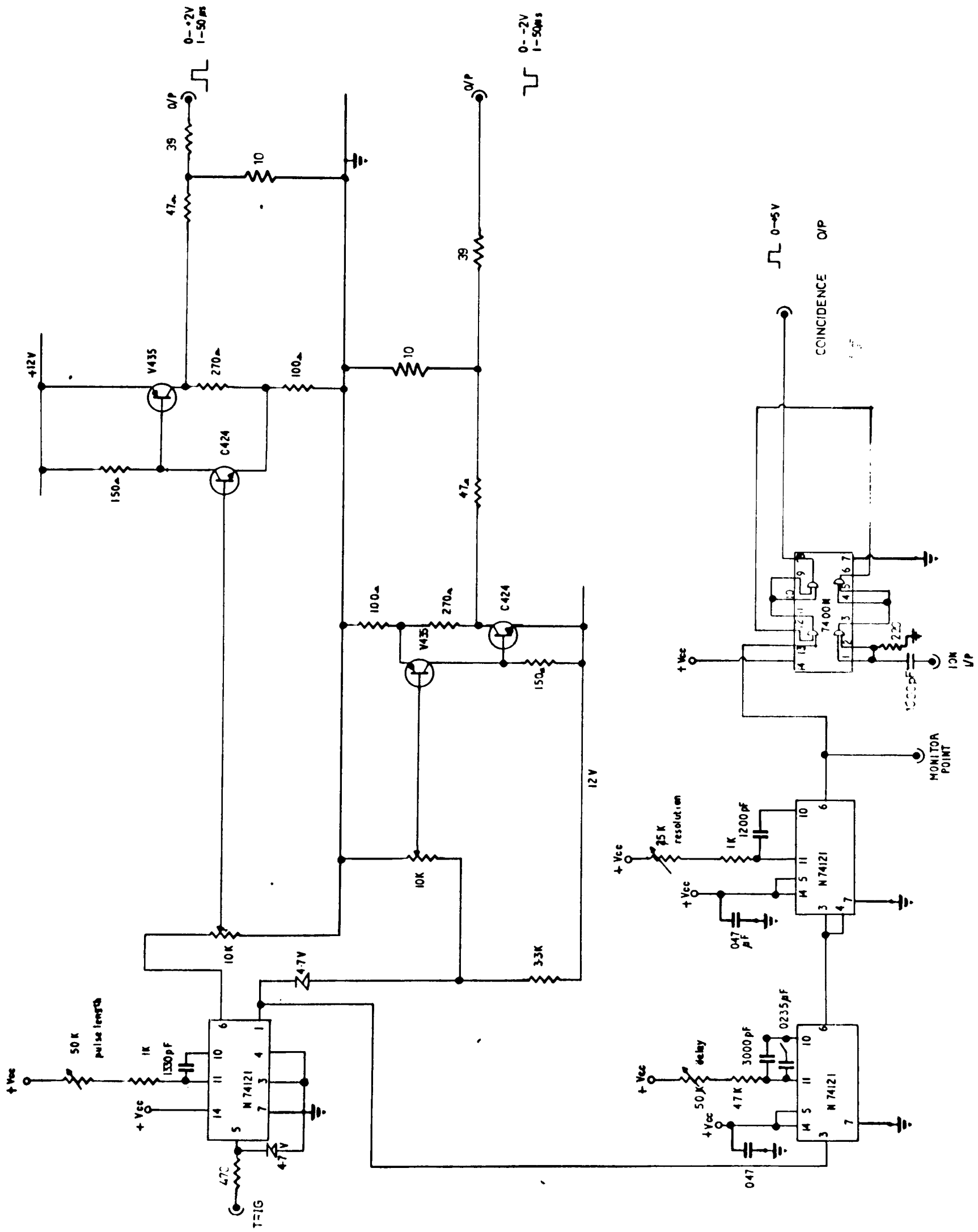
+12V
V435
C424
270Ω
100Ω
150Ω
47Ω
39
10
O/P
0-+2V
1-50ns
0--2V
1-50ns
12V
10K
4·7V
33K
50 K
pulse length
1K
1330pF
+Vcc
N 74121
T=IG
47Ω
0235μF
3000pF
delay
50K
47K
047
μF
25 K
resolution
1K
1200pF
7400N
COINCIDENCE
0-+5 V
MONITOR
POINT
10K

and immediately the advantage was apparent that, as the gating of the ions was performed outside the source region, arrival time spread, due to varying source residence times, would be eliminated. Thus one was free to use the low source fields necessary for good kinetic energy resolution without degrading the possible mass resolution.

A major question, however, was: what effect would the pulsing have itself on the kinetic energy resolution? The problem did not seem to be one susceptible to theoretical analysis but it was reasoned that to minimize any possible effect:

i) The plates should be symmetrically pulsed as depicted in figure 2.9 (the block diagram of the experiment).

ii) The pulse voltage used should be the minimum consistent with good gating and absolute voltages relative to the mean voltage on plate 3/4 should be minimized. This is achieved, as shown on the graph in figure 2.9, by arranging for the pulse voltages to "cross over" one another. In this way perturbations of the average voltage on plate 3/4 were minimized. A unit able to provide the required pulses and also a delayed coincidence gate to count ions arriving in particular time intervals was constructed by the laboratory electronic workshop. Its circuit diagram is shown in figure 2.10.

It was of course necessary to verify that ion kinetic energy peaks are not affected by this procedure. This was done using argon ions and recording kinetic energy distributions for ions gated by pulses varying from 2 to 20 μsec in length and with pulsing voltages up to a volt (in practise only about 200-400 mV is needed). Even in the worst case of a

Figure 2.11

The Kinetic Energy Distribution of Ions from CCl_2F_2

This shows the kinetic energy distribution of ions from CCl_2F_2, as plotted on the X-Y recorder, with the optimum steering potential on plates 3 and 4. On the same scale a distribution obtained with the steering potential removed, but under otherwise identical conditions, is replotted normalized to the same height.

Conditions of experiment

Analyser energy setting	5 volts
Source field	0.1 volts

One fifth of the accelerating field between plates 2 and 3/4.

Figure 2.11

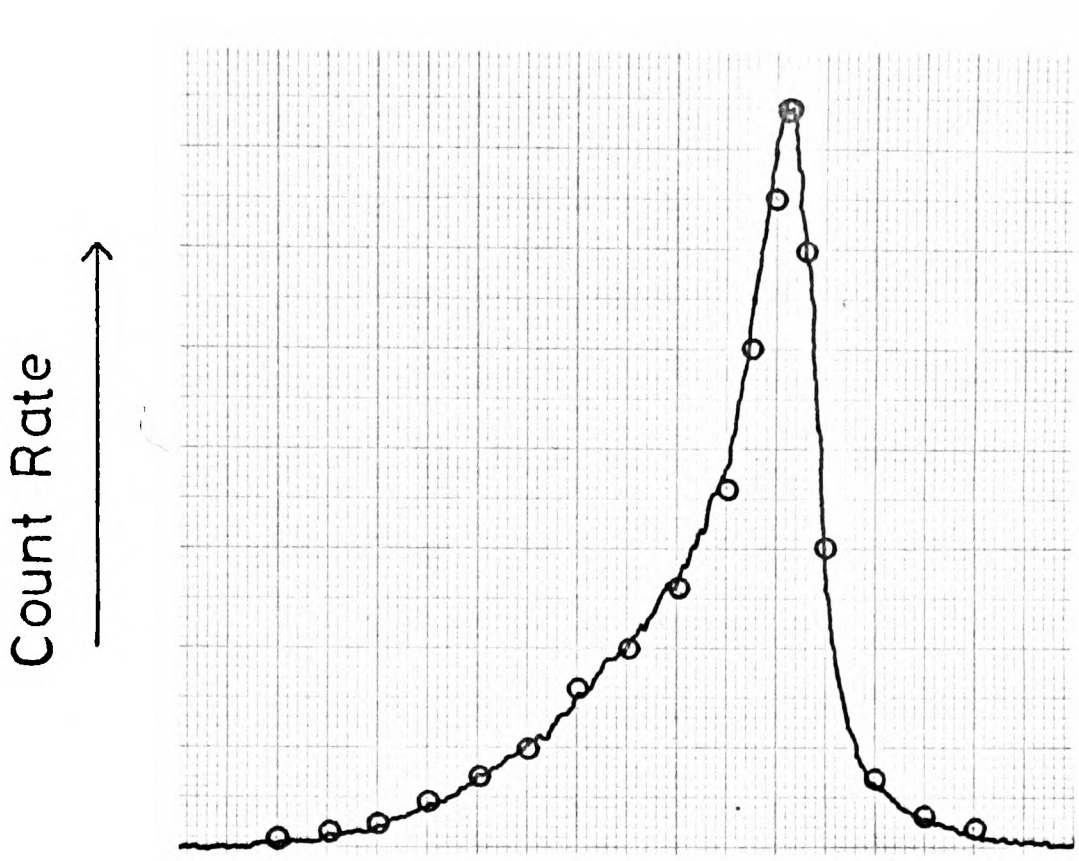

2 μsec one volt pulse no appreciable effect on the kinetic energy peak was seen.

Another possible disadvantage of the use of a steering potential is that it might affect ions of different energies by different amounts. It was felt necessary to investigate this possibility. If such an effect was present but only to a small extent it could be allowed for. If it was a large effect this method of working might have to be discontinued. Accordingly a kinetic energy distribution was recorded for CCl_2F_2 without mass analysis, first with and secondly without the optimum steering potential applied across plate 3/4. The distribution using no steering potential was replotted normalized to the same height as the other and compared with it. Figure 2.11 shows the result and as can be seen any such effect is slight. The same experiment was performed for the O^+ ions from O_2^+ which have higher kinetic energies and again no substantial difference was found.

The method was therefore adopted: the next problem was to optimize the acceleration potential and its mode of application.

As the resolution in mV of the analyser is proportional to the transmission energy of the analyser ($\Delta V/V$ is constant) it is desirable to use the lowest accelerating potential consistent with a useable count rate. Also due to the finite ionization region width it is best to use as small a source field as possible. In fact it is found that below about 150 mV across the source the width of the kinetic energy peak does not change (see figure 2.18). Eventually by trying many different permutations an acceleration

Table 2.1

Sample - argon. Pressure in spectrometer due to sample - 10^{-5} torr.

	Count rate	Source voltage (V)	Acceleration (V)	Voltage between plates 2 and 3/4 (V)	Analyser slit setting	Width of peak (mV)
A	3,000	0.1	5	1	open	40
B	1,200	0.1	5	1	½ open	30
C	1,500	0.1	5	2.5	½ open	30
D	1,100	0.2	5	1	½ open	45
E	2,000	0.4	5	1	½ open	60
F	500	0.1	5	0.5	½ open	35
G	1,200	0.1	10	1	½ open	50
H	6,000	0.2	10	1	½ open	45
I	6,000	0.2	10	1	open	70
J	6,000	0.2	10	5	open	95
K	10,000	0.4	10	5	open	90

The settings for experiment B were chosen because the voltage required across plate 3/4 to shut off the ion beam was much lower than it was in experiment C.

potential of 5 volts was adopted together with a source potential of 100 mV. These conditions represent a good compromise in terms of high count rate and low instrumental broadenings. The acceleration is applied as one volt between plates 2 and 3/4, the rest being applied between plate 3/4 and earth. In fact the mean potential of plate 3/4 is defined by a potentiometer connected between the plate 2 potential and earth. The plate 2 potential is scanned in order to obtain a kinetic energy spectrum.

Some typical results showing the effect of changes of the various experimental parameters are given in table 2.1. The mass spectrum of the sample is obtained by scanning the delay of the coincidence gate provided by the pulse unit (fig. 2.10) and plotting the coincidence output count rate against the delay time. A kinetic energy spectrum of a particular fragment is obtained by setting the coincidence gate to span the arrival times of the fragments concerned. The width of the ion gate pulse is set as wide as is consistent with the requirement of separating the fragment ions formed in order to obtain the highest possible count rates. The pulse unit is triggered by an oscillator set to such a frequency that the next ion pulse is formed after the arrival of the heaviest ion.

Recently a better method of data collection has become available. This involves the use of a multichannel analyser having 144 channels to record a complete time of flight spectrum at a particular kinetic energy setting. In this way the total peak for each fragment ion may be integrated and the procedure repeated for various energy values, thereby building up a plot of each fragment intensity

Figures 2.12, 2.13 and 2.14

The Time to Pulse Height Converter

Figure 2.12 shows the complete circuit diagram of the unit, which is reduced to block form in figure 2.12. Start pulses initiate the discharge of the timing capacitor and after a delay of 8 μsec (to allow for complete discharge) switch the bistable to the timing mode and simultaneously output a "true start" pulse. The bistable switches a charging current from a constant current source to charge the timing capacitor in a linear fashion. The voltage on the timing capacitor is monitored by a high input impedance DC emitter follower. Receipt of a stop pulse resets the bistable, thus stopping the timing ramp, and initiates the output sequence. Two monostables apply a 2 μsec gate pulse to an analogue gate placed after the emitter follower, 6 μsec after the ramp has stopped. This delay is to allow the voltage on the timing capacitor to stabilize. This gate allows a pulse 2 μsec wide and of magnitude equal to the timing capacitor voltage through to the inverting AC coupled output amplifier, which has a gain of 3.5 to provide a signal suitable for the multichannel analyser. Further stop pulses are inhibited as is the output of a pulse during the capacitor discharge period. If no stop pulse is received the next start pulse resets the bistable. Ranges are selected by varying the current supplied by the constant current source. Figure 2.14 shows a diagram of voltage versus time at various points marked in the block diagram for typical sequences of stop and start pulses.

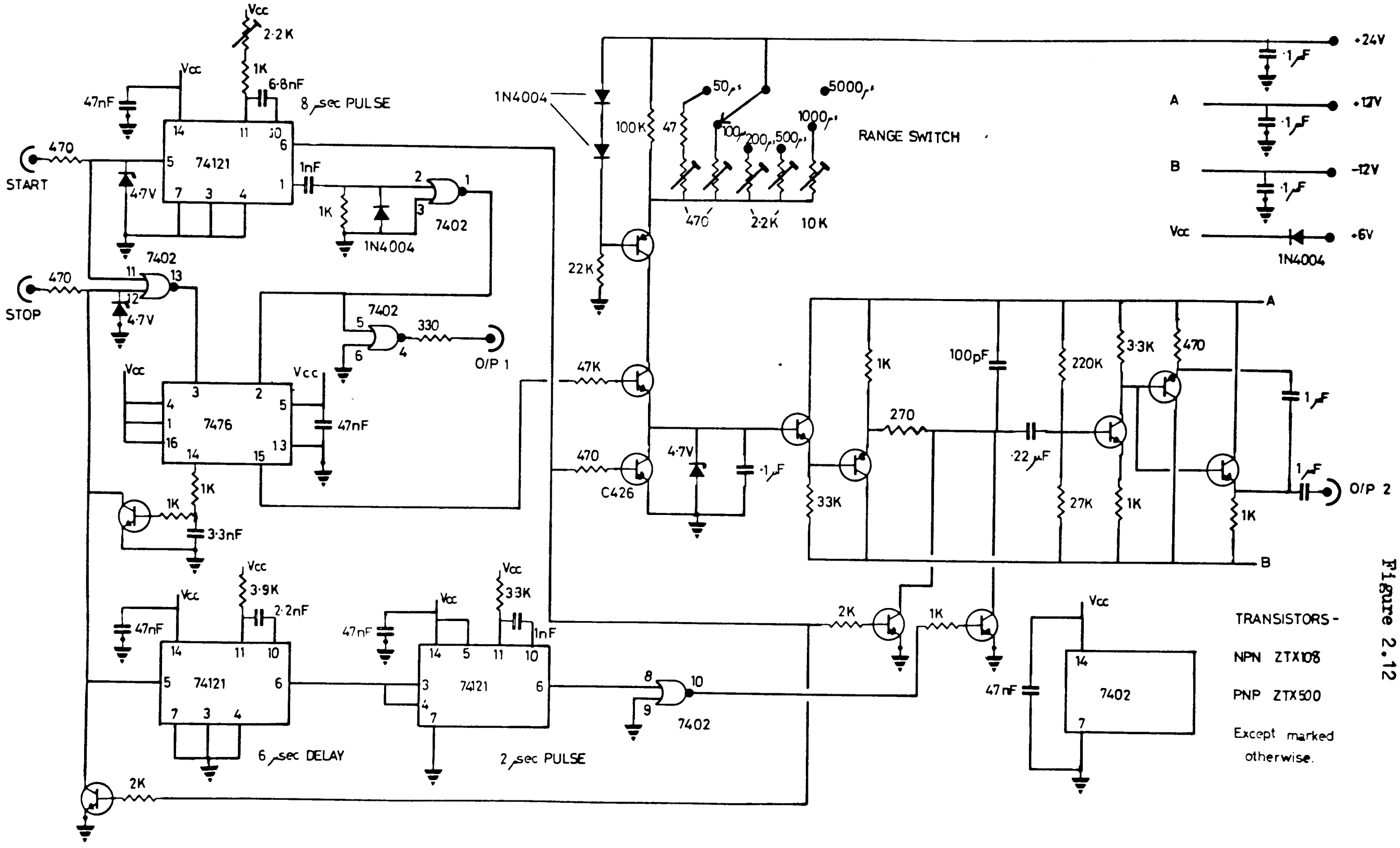
Vcc
2·2K
1K
6·8nF
8 μsec PULSE
47nF
Vcc
74121
470
START
4·7V
1nF
1K
7402
1N4004
7402
470
STOP
4·7V
7402
330
O/P 1
Vcc
Vcc
7476
47nF
1K
1K
3·3nF
Vcc
3·9K
2·2nF
47nF
74121
6 μsec DELAY
Vcc
33K
1nF
47nF
74121
2 μsec PULSE
8
10
9
7402
2K
1N4004
100K
47
50p
100p
200p
500p
1000p
5000p
RANGE SWITCH
470
2·2K
10K
22K
47K
470
C426
4·7V
·1μF
+24V
·1μF
A
+12V
·1μF
B
-12V
·1μF
Vcc
+6V
1N4004
A
1K
100pF
220K
3·3K
470
270
·22μF
33K
27K
1K
1K
1μF
1μF
O/P 2
B
2K
1K
Vcc
47nF
7402
7
TRANSISTORS -
NPN ZTX108
PNP ZTX500
Except marked otherwise.

Figure 2.12

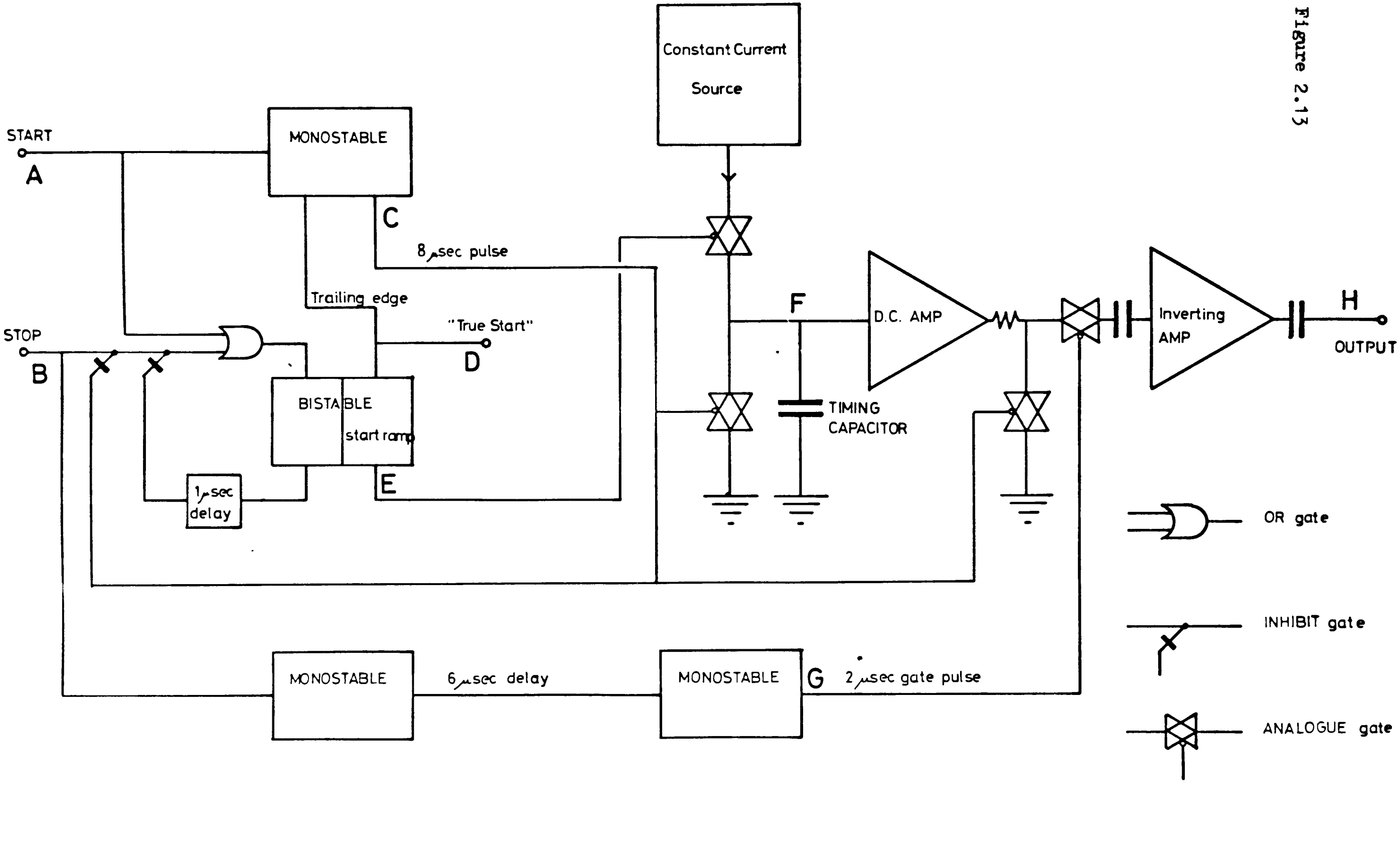
Constant Current Source
START
A
MONOSTABLE
C
8 μsec pulse
Trailing edge
"True Start"
D
STOP
B
BISTABLE
start ramp
E
1 μsec delay
F
D.C. AMP
TIMING CAPACITOR
Inverting AMP
H
OUTPUT
MONOSTABLE
6 μsec delay
MONOSTABLE
G
2 μsec gate pulse
OR gate
INHIBIT gate
ANALOGUE gate

Figure 2.13

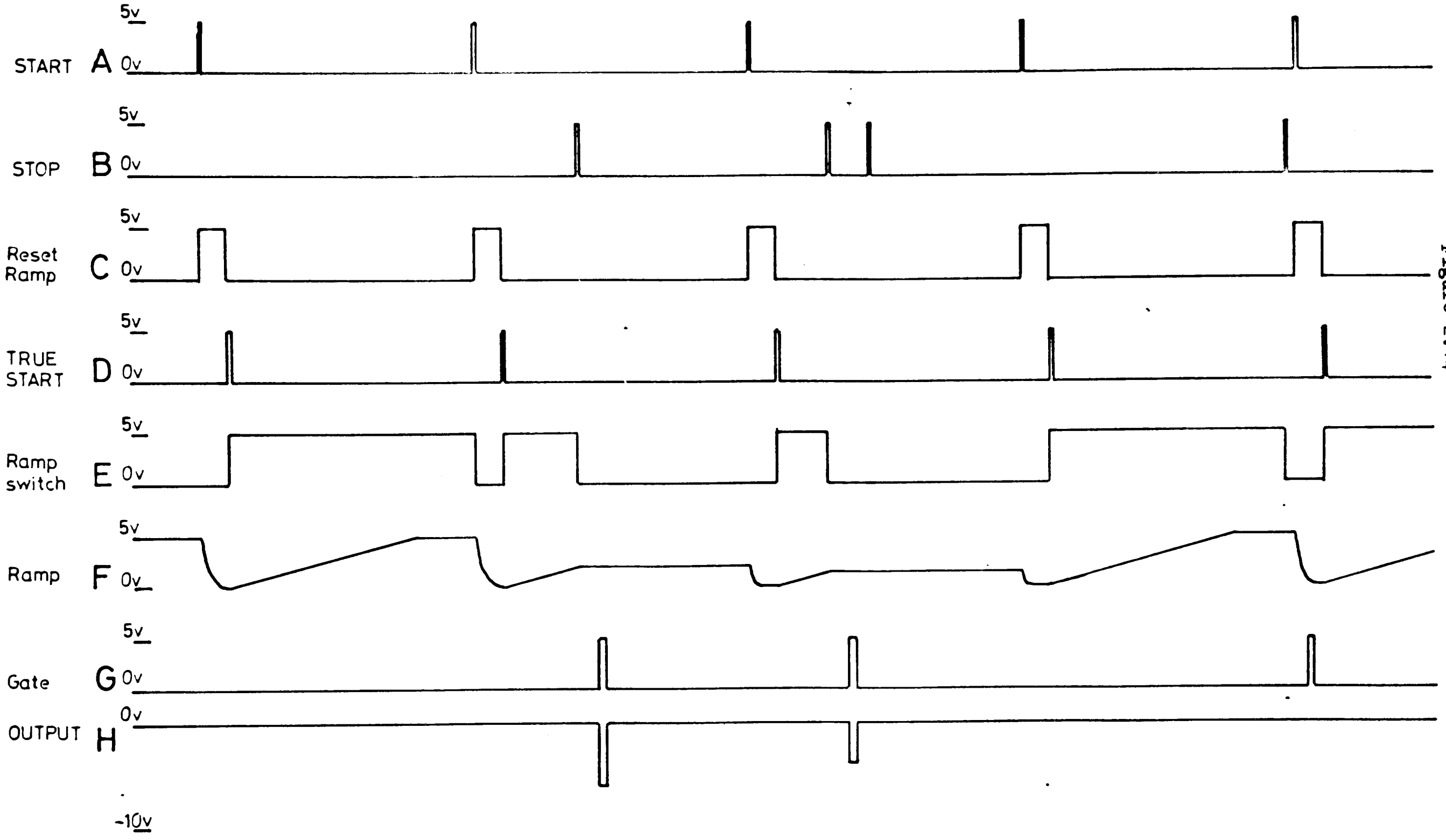
5v
START A 0v
5v
STOP B 0v
5v
Reset Ramp C 0v
5v
TRUE START D 0v
5v
Ramp switch E 0v
5v
Ramp F 0v
5v
Gate G 0v
0v
OUTPUT H
-10v
20μs

Figure 2.14

Figure 2.15

A Calibration Curve for the Time to Pulse Height Converter

The curve for the nominally 200 μsec range is shown. As can be seen the 140th channel (the last addressable channel) of the multichannel analyser is in fact accessed by a stop - true start time difference of 190 μsec.

Figure 2.15

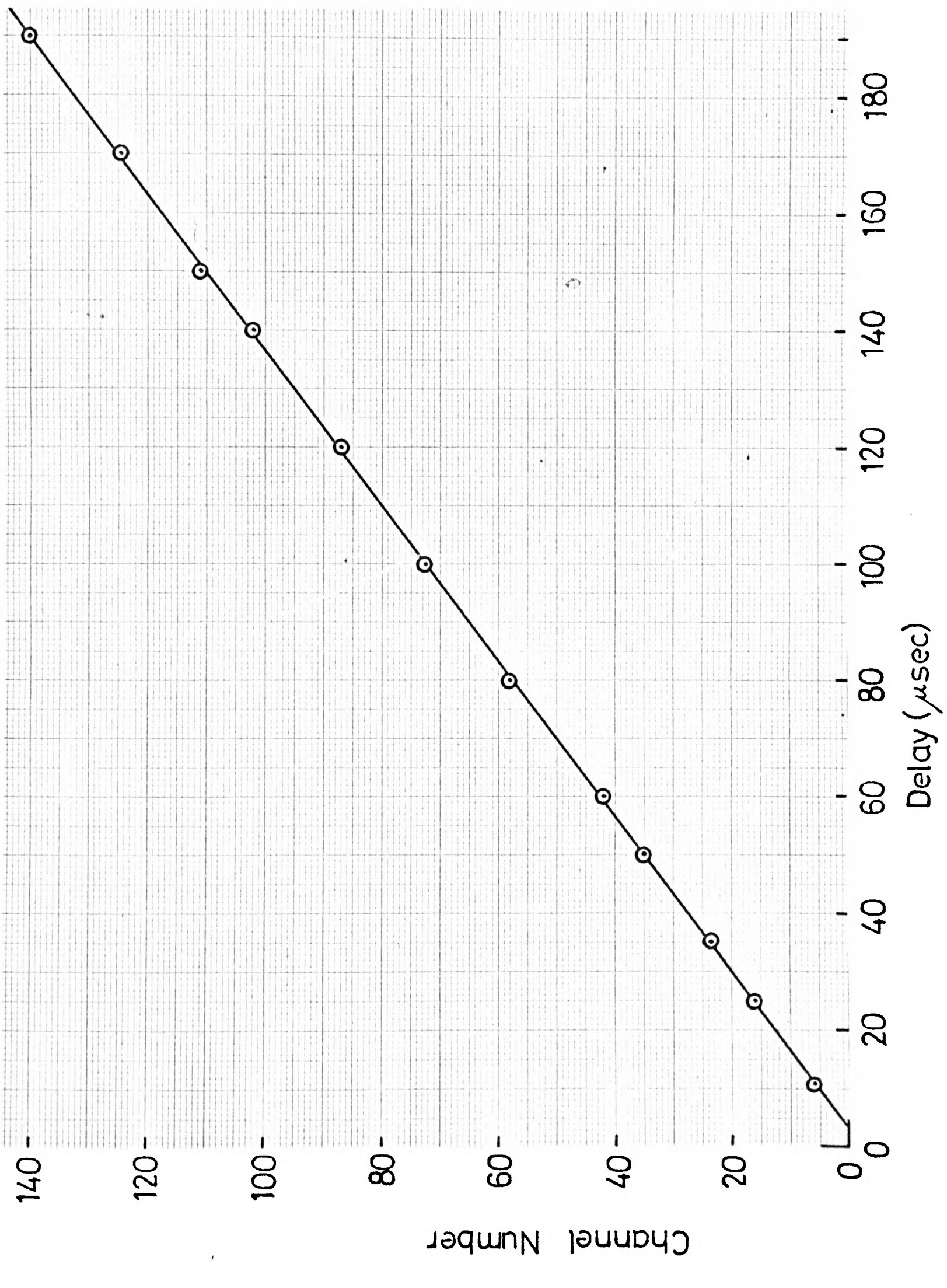
Channel Number
0
20
40
60
80
100
120
140
0
20
40
60
80
100
120
140
160
180
Delay (μsec)

Figure 2.16

The time of flight mass spectrum of $CClF_3$ as recorded on the multichannel analyzer. A weak peak due to parent ions can be seen above the $CClF_2^+$ peak.

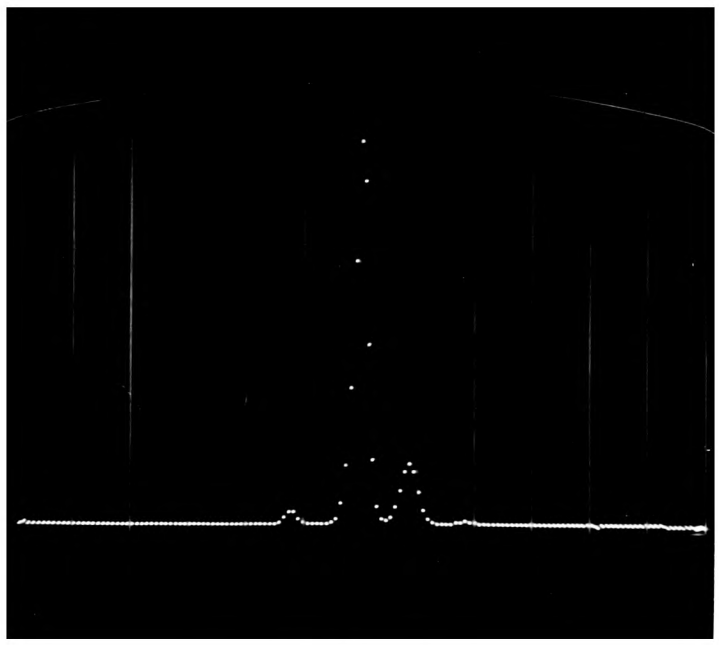

versus its kinetic energy.

As the multichannel analyser that was available accesses its channels according to the magnitude of an input pulse it was necessary to provide a means of converting the time of arrival of a pulse to a peak height of an electrical pulse. Commercial time to pulse height converters are

(a) very expensive;

(b) usually designed to deal with shorter time intervals than are used in this work;

(c) will accept random "start" pulses.

(a) is, of course, consequent on (b) and (c).

As this experiment requires a time-resolution only of the order of 1 μsec. and the start time for the time measurement is regularly repeated, it was decided to design a time to pulse height converter especially for the experiment. For such a time resolution it is perfectly allowable to use the, now very cheap, TTL logic integrated circuits. The circuit diagram of the unit is shown in figure 2.12. A block diagram making its mode of operation clearer is shown in figure 2.13. Ranges of 50, 100, 200, 500 and 1000 μsec. are provided - each for a nominal output of -7 volts, which is compatible with the multichannel analyser. Only one stop pulse per cycle is allowed (any more produce no output) but in practise as the count rate is always much lower than the pulse repetition frequency this is no disadvantage. The unit has a dead time of 8 μsec. per stop pulse coupled with another dead time of about 8 μsec. after "start" triggering. The unit is, in fact, substantially linear up to output voltages of -10 volts. A calibration curve for the 200 μsec. range is given in figure 2.15. A typical time of flight mass spectrum

as recorded by the multichannel analyser is shown in figure 2.16.

C. THE DISCHARGE LAMP

The original lamp used on this machine was of a simple design[25] with differential pumping provided only by the pump connected to the source region. This resulted in pressure readings of 1.5×10^{-5} torr while the lamp was running suggesting that a lot of helium was escaping into the main vacuum chamber. While this was satisfactory for PES it was felt to be less so for ion kinetic energy studies where collisions in the analyser are more likely. A new lamp was accordingly designed with three new features.

(a) A separate differential pumping connection is provided for evacuating the region between the discharge capillary and the second capillary.

(b) A "throttling" capillary is added after the second electrode but before the differentially pumped region in order to maintain the pressure in the discharge capillary. This becomes necessary with the more efficient differential pumping provided.

(c) A tantalum inner electrode was used to reduce the sputtering that had been observed with earlier lamps. This electrode was made quite large to reduce cooling problems (an earlier version of this lamp melted).

The design used is given in fig. 2.3.

The lamp has been found satisfactory in use and as mentioned earlier a pressure of 2×10^{-6} torr is reached in the main vacuum chamber with it running. It was, of course, necessary to find the optimum running conditions for this lamp; for the two discharge gases used in the present investigation a setting of needle valve C to $2\frac{1}{2}$ turns was

found to be suitable for neon or helium. When running with pure helium an intermediate pressure of 5 cms. of mercury was used - this pressure gives the highest count rates. A current of 40 mA in the lamp is used; this current representing the point of onset of saturation where the count rate versus current curve levels off.

For pure neon a pressure of 1.5 cms. Hg was used; this in fact represents a point just below the peak of the count rate versus pressure curve but neon is expensive and the loss of count rate for a quite high drop in flow rate of neon is small. Again, and for the same reasons, a current of 40 mA was used.

It was decided for the present experiment not to mix helium although this is suggested in the literature[86] as ion kinetic energy spectra provide no intrinsic check that the discharge being used is spectrally pure. Any helium I line mixed in with neon radiation would populate higher lying states of the ion and render the results valueless. At least with a photoelectron spectrum one would probably see clues that helium as well as neon resonance radiation was being produced.

The spectral purity of the discharges were investigated by running photoelectron spectra of argon and methyl iodide at high sensitivity.

For the helium discharge the only other significant ionizing energy found was that due to the Helium β line at an intensity 0.35 that of the α line. The γ line was just detected. No He II radiation was observed to be present and, providing the lamp had been run for long enough, no Hydrogen Lyman α ionization was detected.

For neon the picture is less good but adequate. The main neon lines were found to be in the ratio 3.3:1 with the 16.85 eV line being the most intense. After a good degassing period the following radiation was also detected:

H Lyman α 0.14 the intensity of the 16.85 eV line

H Lyman β 0.04 the intensity of the 16.85 eV line.

A few other lines in the 10 eV region were apparent, all of intensities less than 1/40 that of the 16.85 eV line. These could not be assigned to the expected N,O or Argon lines. No Helium resonance radiation at all was found, which is the most important requirement. For ion kinetic energy work the presence of Lyman α radiation will not in general matter although the possibility of an autoionizing resonance between this radiation and a state of the molecule under investigation should not be forgotten in interpreting results.

The use of argon in the lamp was investigated with a view to possible use of its quoted 13.84 eV line[5]. No detectable excitation of this line could be achieved however; the only radiation found being:

Lyman α at 10.198 eV

Lyman β at 12.0872 eV

and the argon lines at 11.84 eV and 11.62 eV.

D. THE MASS RESOLUTION OBTAINED IN THE ION KINETIC ENERGY TECHNIQUE

In previous work with a pulsed lamp the best mass resolving power attained was of the order of 10^{25}. This allowed, for example, the oxygen and nitrogen components of air to be separated. An improvement on this value would be very desirable however, it would be useful to be able to separate fragments differing from each other by only the mass of a hydrogen atom.

The new method of ion gating was expected to show an improvement over the older pulsed lamp technique for the following reasons.

(i) The spread of ion flight times between ionization and leaving the source slit is removed because gating occurs after the source. This was thought to be the main broadening effect with the pulsed lamp technique[25].

(ii) Pulses of down to 1 μsec. may be used to gate the ions - this compares favourably with the minimum lamp pulse length of 4 μsec. obtained earlier[25].

It is expected that the main broadening effect will now be the spread of ion flight times in the analyser. This is calculated in appendix B and is expected to be of the order of 3.5 μsec. for an ion of mass 40 and 5 eV energy with the analyser slits fully opened.

Experimentally it was found that this broadening was about 2 μsec. for the case of argon under the optimum acceleration and source field conditions decided upon from earlier investigations. The experimental dependence of the half height width of the peak obtained on the multichannel

Figure 2.17

The Time Width of Ion Arrival Times as a Function of Initiating Pulse Width

This shows the widths of peaks obtained for argon ions on the mutlichannel analyser as the width of the pulses on plates 3 and 4 was varied.

Ion acceleration	5 volts (1 volt between plates 2 and 3/4)
Source voltage	0.1 volts

Figure 2.17

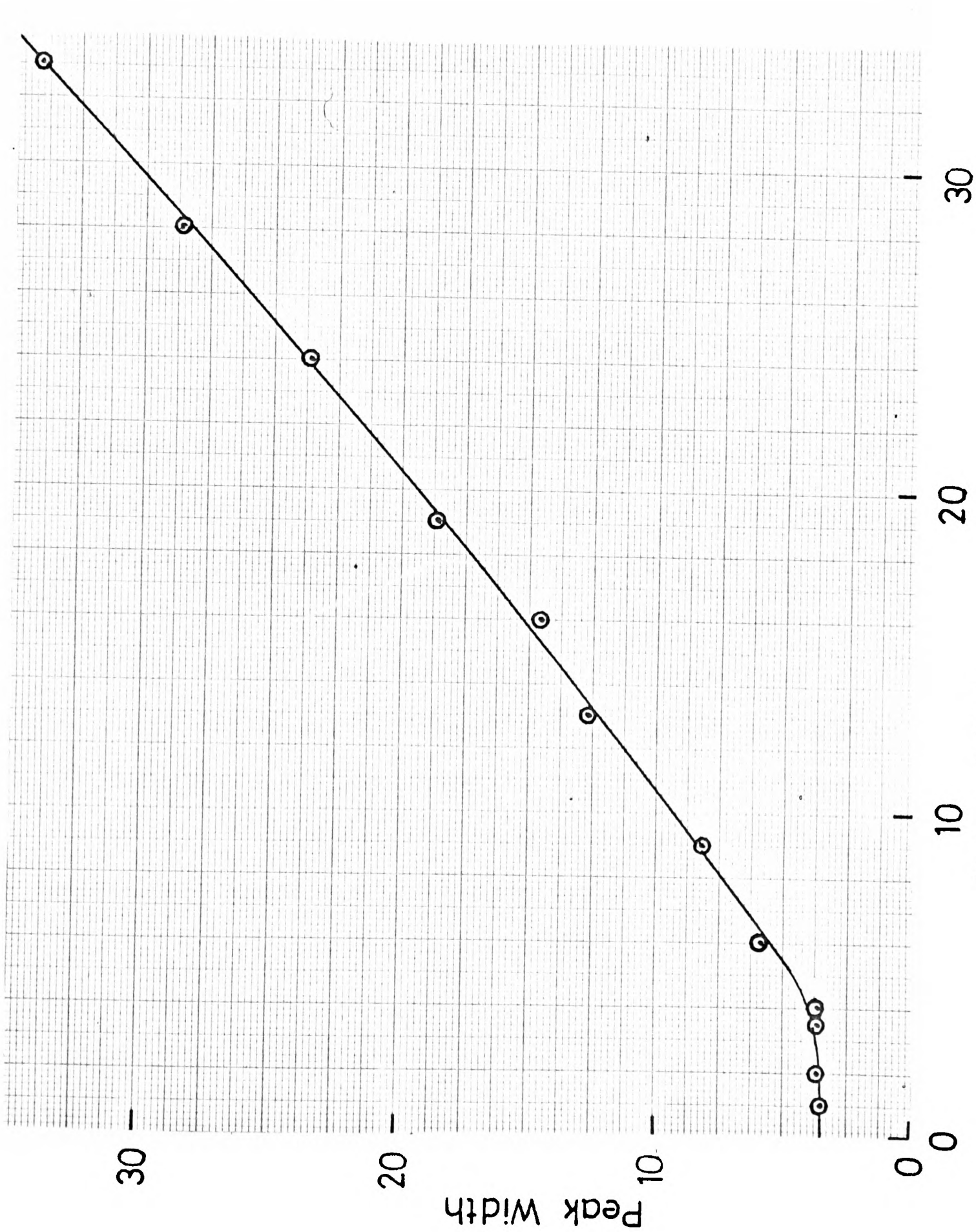

analyser upon the width of the ion gate pulse is given in fig. 2.17. It can be seen that the minimum peak width attainable is 3.6 μsec. and this is a constant for pulse widths between 1 μsec. and 4 μsec. The count rate falls off very rapidly at pulse widths below about 3 μsec. and above this value the count rate is nearly a linear function of pulse width. It is seen therefore that for these accelerations and pulsing conditions a pulse width of 4 μsec. is best in order to obtain the highest resolution at a good count rate. The resolving power for argon under these conditions is about 17-18; an improvement on the earlier value.

It was not found to be possible to effect a substantial improvement on this figure by using higher accelerations or different pulsing conditions. It would be expected that an improvement could be obtained by using narrower analyser slit width settings. It was found possible to achieve a minimum peak width of 3 μsec. for argon with the analyser slits reduced in width. This improvement is slight however and involves a much poorer count rate.

Processes yielding fragments differing in mass by two mass units or less cannot be investigated by this technique. This means that many of the simple organic compounds cannot be studied completely.

The resolving power is not found to improve for higher masses; for krypton it is about 15. In practice higher pulse widths are often used if this does not cause the overlap of fragment time of flight peaks. Obviously it is best to use the longest pulses consistent with this requirement.

Figure 2.18

Kinetic energy distribution half height width plotted against the source voltage for argon ions.

Analyser energy setting 5 volts

One fifth of the accelerating field between plates 2 and 3/4.

Figure 2.18

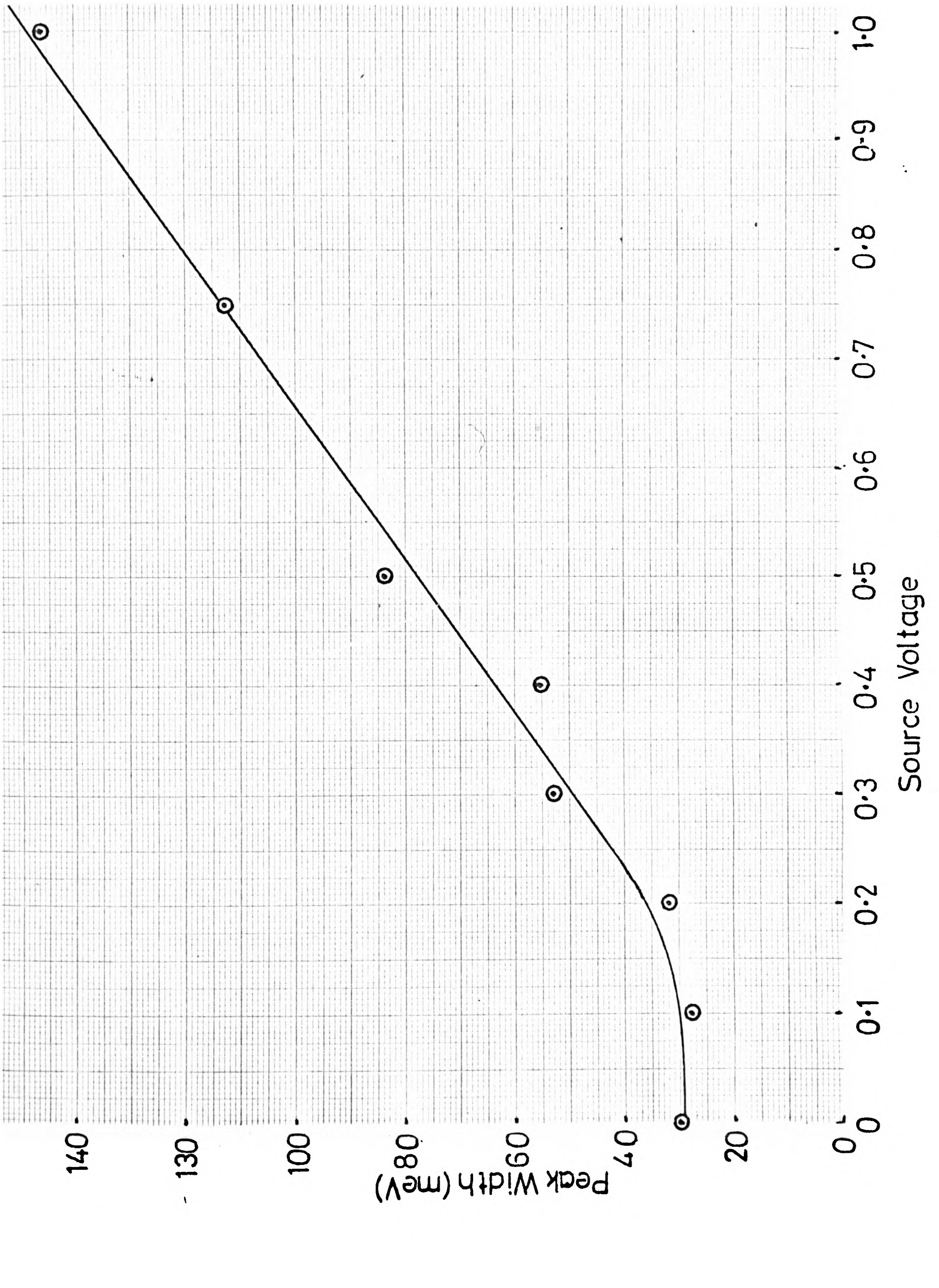
Peak Width (meV)
140
130
100
80
60
40
20
0
0
0·1
0·2
0·3
0·4
0·5
Source Voltage
0·6
0·7
0·8
0·9
1·0

E. THE ENERGY RESOLUTION OF THE TECHNIQUE

As has been mentioned earlier, the changes made to the spectrometer have vastly improved the narrowness of the energy distribution obtained for argon ions. Thus with the narrowest slit settings a peak of half height width of 28 meV is obtained at a source voltage of 0.1 volt.

The effect of the source field will be considered before moving on to the major problem of reconciling the observed peak shape with theoretical expectations.

It is found, as would be expected, that the observed peak width is a strong function of the source field. Above source voltages of about 0.2 volts this function is substantially linear. This suggests that the following simple treatment may be valid.

If the peak width is assumed to be made up of a basic width w and an added width Vsx where Vs is the source field and x is the actual width of the ionization region.

$$\therefore W_{\frac{1}{2}} = w + \frac{V_s x}{.635}$$

(0.635 cm. is the source plate separation.)

The slope of the plot of half height width versus source voltage should therefore give a value for the ionization region width. Fig. 2.18 gives this plot for a typical set of data using an acceleration of 5 volts and yields a value for the ionization region width of 1 mm. This would be expected from knowledge of the design of lamp used. If a narrower photon beam could be obtained then it would be possible to use higher source fields without degrading the energy resolution. An end cap has been fitted to the photoion-photoelectron coincidence spectrometer in this laboratory[29] with some success in achieving a narrower

Figure 2.19

Kinetic Energy Distributions for Argon Ions at Different Analyser Slit Widths

Ion acceleration 5 volts (1 volt between plates 2 and 3/4)

Source voltage 0.1 volts

A slit width 2.2 mm

B slit width 1.2 mm

C slit width 0.8 mm

The abscissa scale is 0.02 eV per cm. The ordinate scales are arbitrary.

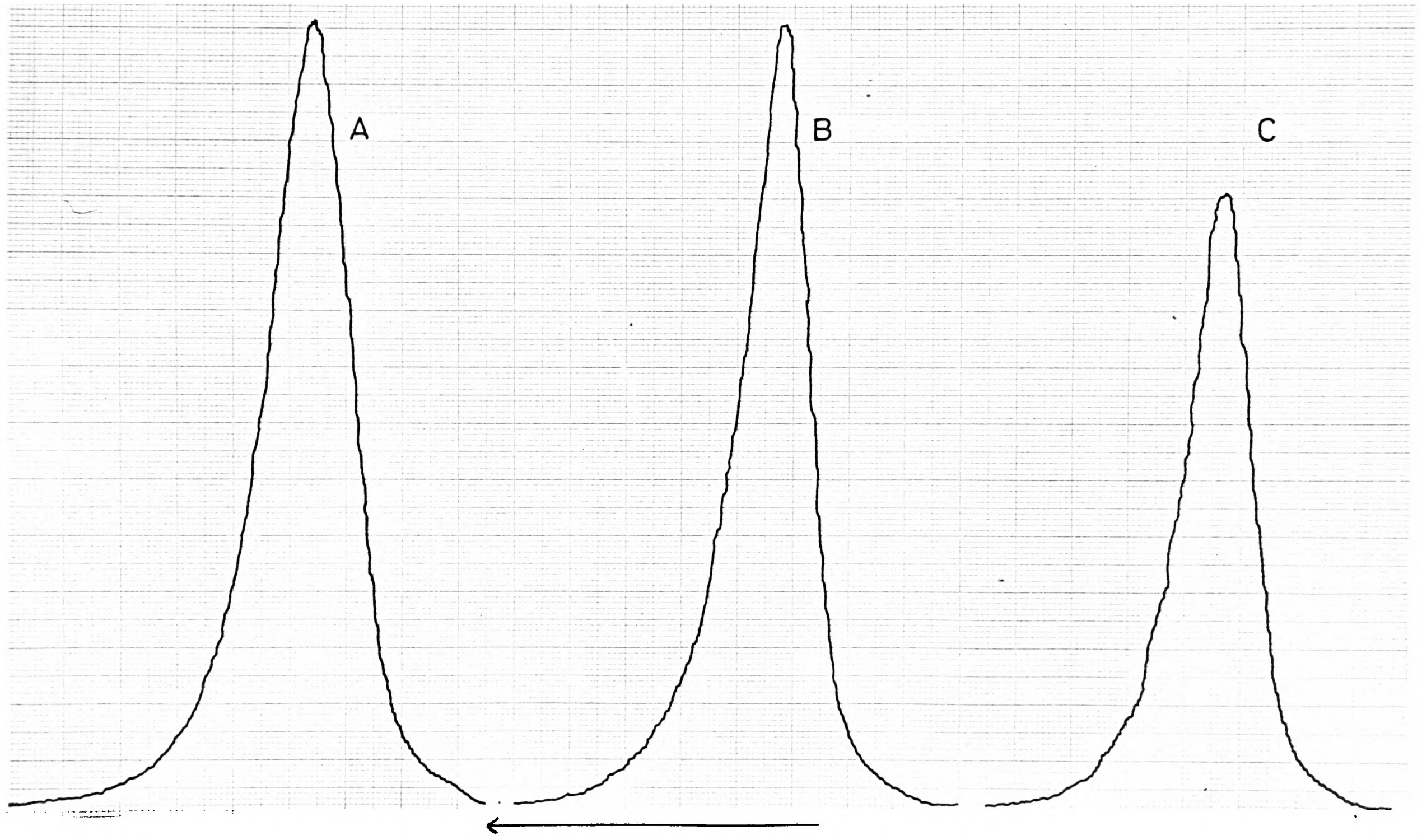

Figure 2.19

ionization region width. The beam intensity is cut however which would be a grave disadvantage if the same idea were applied to this spectrometer.

A set of argon ion kinetic energy distributions obtained at various analyser slit widths is shown in Fig. 2.19. The width of 28 meV is apparently incompatible with a source temperature of 300^{o} K for which a width of 46 meV would be expected. The problem of fitting a theoretical distribution to the observed one is however, not straightforward. This is because of uncertainty over the exact form of the function describing the angles of initial motion from which an ion will be collected. (See appendix A for a discussion of this function.)

A computer program was developed which would evaluate theoretical distribution functions taking this angular acceptance function into account. The mode of application of the function could be varied in many ways - including ignoring it completely. The results of many computations for various temperatures and maximum angles of acceptance led to the following deductions.

(i) It is possible to fit the observed peak <u>width</u> in many ways, including using a temperature of 300^{o} K and taking full account of the angular acceptance function for forward and backward flying ions.

(ii) Only for temperatures in the region of 180^{o} K however could the general <u>shape</u> of the high kinetic energy part of the experimental distribution be fitted by the theoretical curves. At this temperature many different forms of angular acceptance function would still allow a good fit on the high energy side.

Figures 2.20a, b and c

Experimental Kinetic Energy Distributions for Argon Ions with Computed Distributions Superimposed

20a. Open circles show the calculated distribution for 300° K. Black circles show the calculated distribution for 300° K with the full angular dependence function incorporated.

20b. Black circles show the calculated distribution for 180° K with no angular dependence function. Open circles show the calculated distribution for 180° K with the forward flying angular dependence function incorporated.

20c. Open circles show the calculated distribution for 180° K with the full angular dependence function incorporated but restricted to 90° total angle. Black circles show the same calculation for 200° K.

Figure 2.20a

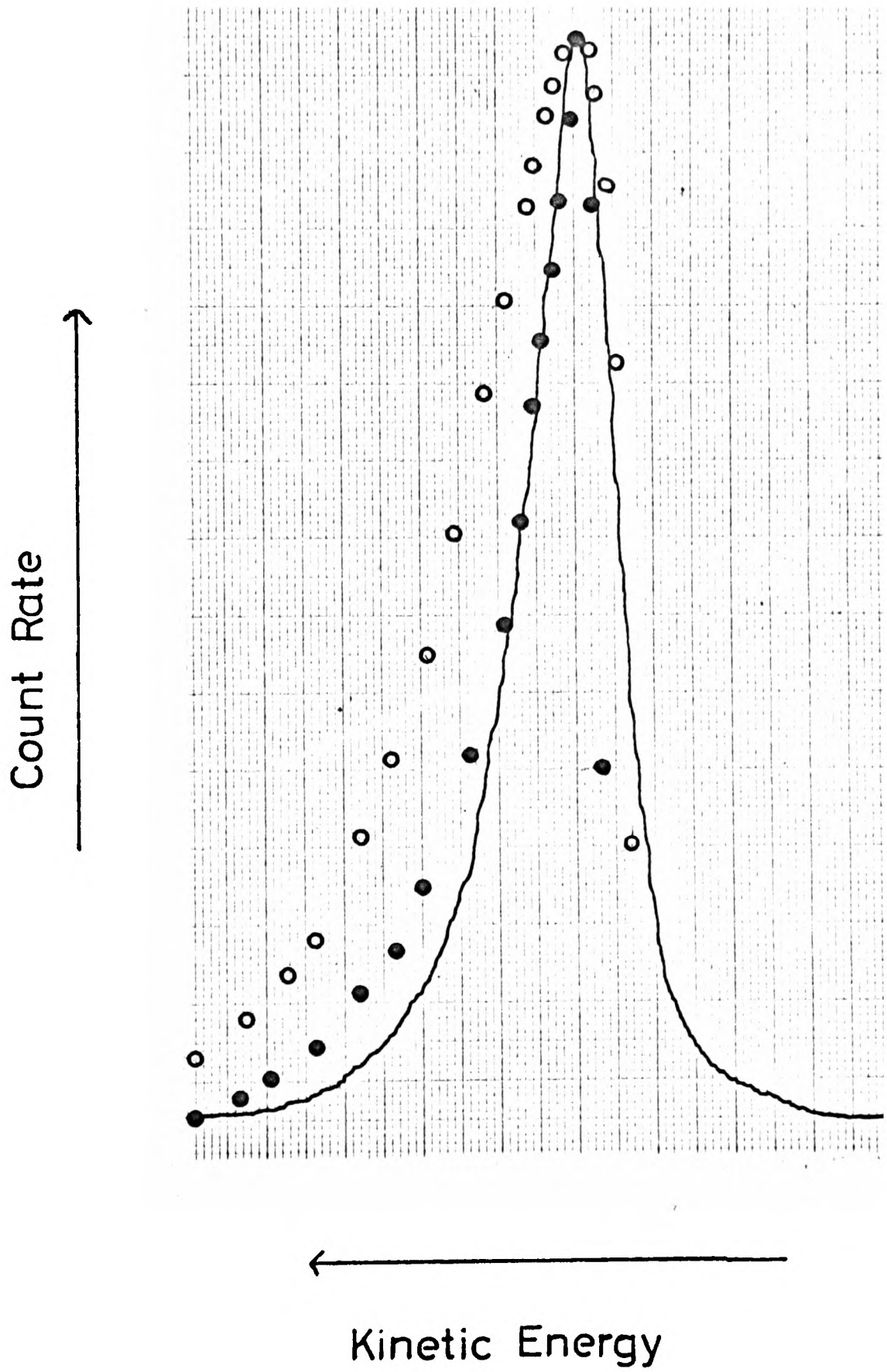

Figure 2.20b

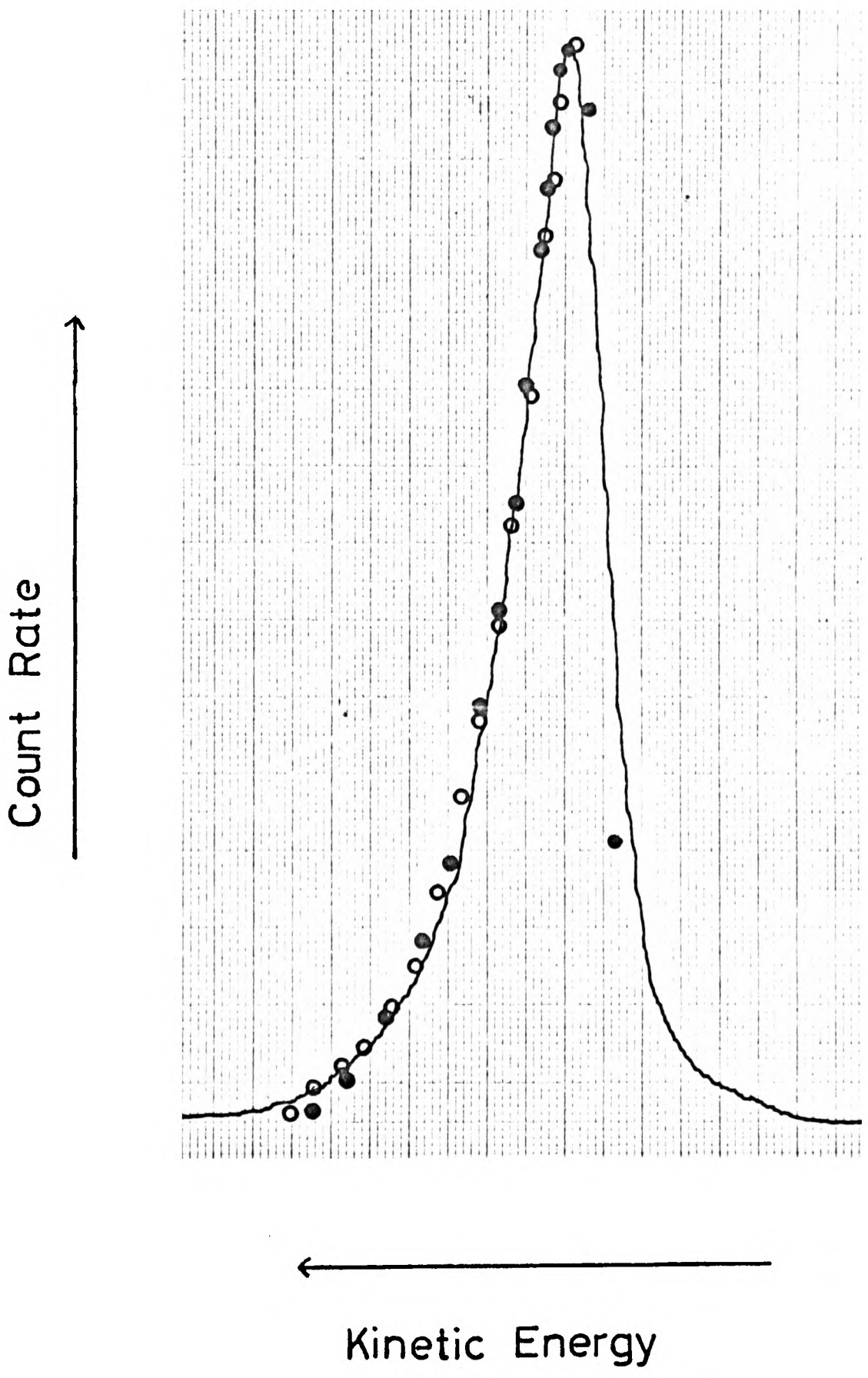

Figure 2.20c

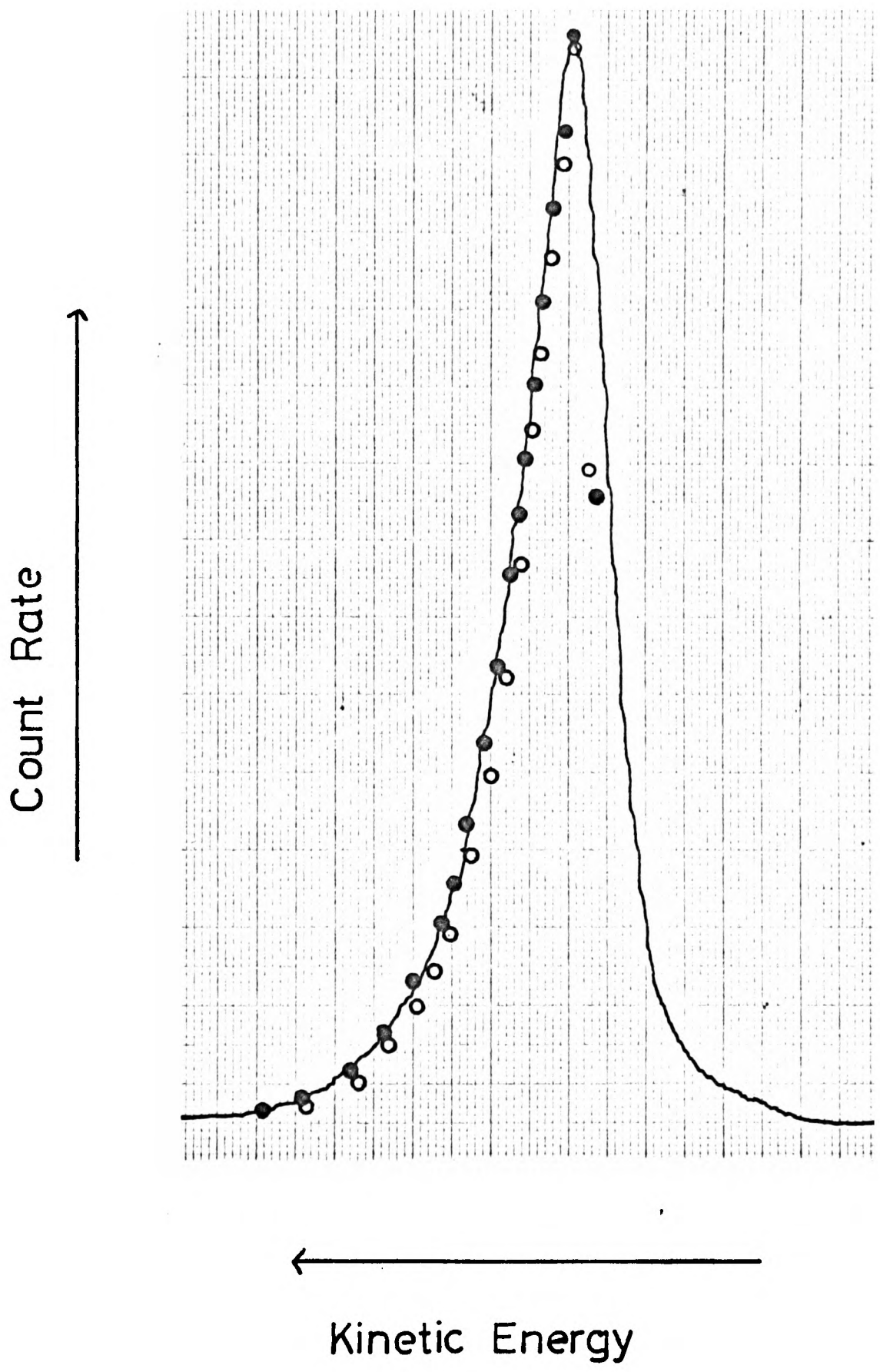

(iii) No theoretical function could reproduce the observed slope of the low energy side of the experimental distribution - they are all too steep. This is hardly surprising; a certain amount of instrumental broadening must be present and this will be most noticeable on the sharp low energy side of the distribution.

It was considered unlikely by the writer that the angular acceptance function as derived in appendix A, will apply in full. Ions with initial velocities at large angles to the analyser direction will surely have an almost nil chance of being collected even at very low energies. It was felt therefore that a distribution calculated with the total angle of acceptance limited to a maximum value probably represents a good approximation to the true situation. The best fit of the observed distribution that could be obtained considering all the above was found for a temperature of 180^{o} K and a maximum total acceptance angle of 90^{o}. Figures 2.20 (a, b and c) show the experimental peak together with various calculated distributions including the one chosen. This chosen distribution gives a fit a little on the "inside" of the experimental curve. This is because of the expected instrumental broadening mentioned earlier. A slightly higher temperature (200^{o} K) would fit the high energy side perfectly. It is thought safe to say, bearing in mind all the above, that the source temperature of this experiment is of the order of 180^{o} K and that the best angular acceptance function to use in computing theoretical distributions to compare with experiment is that given in appendix A limited to a maximum angle of 90^{o}.

Chapter 3 - The Interpretation of the Experimentally Measured Ion Kinetic Energy Distributions

CHAPTER THREE

THE INTERPRETATION OF THE EXPERIMENTALLY MEASURED ION KINETIC ENERGY DISTRIBUTIONS

A. INTRODUCTION

Although the technique described in chapter 2 provides a more direct way of measuring ion fragment energies than most alternative techniques, it does not give the distribution of the energy release in the frame of reference of the dissociating ion, the so-called CM (centre of mass) coordinates. The observed (LAB) distribution function will have been modified by two effects; (1) the initial thermal velocity of the parent ion and (2) the influence of the ion energy on the ion collection efficiency. These two effects are now to be discussed.

(1) The initial thermal velocities of the parent ion will be passed on to the fragments. The fraction of the thermal energy passed on will therefore depend on the mass of the fragment observed. It is thus a fundamental feature of the experiment that lighter fragment ions carry the more easy to interpret information. This is because they take more of the energy released in the fragmentation and less of the thermal energy of the parent than would a heavy fragment ion.

Thus in the investigation of NO_2^+ presented here the fragmentation to give $O^+ + NO$ gives the more easily understood kinetic energy distribution although the less favourable case of fragmentation to $NO^+ + O$ is by no means obscured by thermal effects. In $C_2F_6^+$ similarly, of the two

major fragmentations, the process giving CF_3^+ is expected to give a clearer energy release distribution. In fact in the other case of fluorine loss to give $C_2F_5^+$, despite the unfavourable weight ratio, much information may still be gained as the energy release is large in the decomposition. Less favourable is the case of ICN^+ which only fragments to give I^+ + CN at 21.22 eV ionizing energy. This compound was studied but the unfavourable mass ratio of the fragments coupled with a low release of kinetic energy rendered the results of doubtful value.

(2) The observed kinetic energy distribution will be distorted from the true one by any variation of the ion collection efficiency of the analyser with energy. This is not a fundamental effect but is inherent in any experiment in which the ions which are analysed and collected are travelling in one particular direction only. Putting it simply, the chance of collecting an ion which leaves the ionization region in a direction other than that exactly along the axis of the analyser entrance slit will depend upon its initial velocity and direction, as these factors determine whether or not it will be stopped by one of the slit edges. These two problems and their resolution are described in the next section.

B. THE FORM OF THE OBSERVED ENERGY DISTRIBUTION

In general the observed (LAB) kinetic energy distribution function will be the result of a combination of the distribution function, W(E), for the kinetic energy released in the centre of mass (CM) coordinates for the reaction and the thermal kinetic energy distribution of the parent ion.

If the kinetic energy released in CM coordinates is E_o then for the fragmentation

$$m_1^+ \longrightarrow m_2^+ + m_3 + E_o$$

the fraction of the kinetic energy carried by the ionized product is

$$E = \frac{m_3}{m_1} E_o$$

If the parent molecules have a Maxwellian distribution of thermal velocities before ionization, it can be shown[104] by vector addition of velocities that the kinetic energy distribution for m_2^+ observed in LAB coordinates has the form:

$$PE = \frac{m_1}{\pi kT m_1 (m_1 - m_2) E_o}^{\frac{1}{2}} \exp\left(-\frac{m_1 E + E_o(m_1 - m_2)}{m_2 kT}\right) \times \sinh\left(\frac{2\left\{m_1(m_2 - m_1)E_o E\right\}^{\frac{1}{2}}}{m_2 kT}\right) \qquad [1]$$

A derivation of this equation is given in appendix A for a single valued energy release E_o.

Thus the single valued energy release is broadened to an extent proportional to $E^{\frac{1}{2}}$. This is readily understood

by the following considerations. The kinetic energy of the ion m_2^+

$$E_2 = \tfrac{1}{2} m_2 v_2^2$$

so $$\frac{dE_2}{dv_2} = m_2 v_2 = (2E_2 m_2)^{\frac{1}{2}}.$$

Thermal energy of the parent ion has the effect of providing a constant velocity spread δv_2 and thus an energy spread proportional to $E_o^{\frac{1}{2}}$.

The half height width of the observed distribution can be approximated by [23]

$$w_{\frac{1}{2}} = 3.1 \times 10^{-2} \left(\frac{T E_o m_2 m_3}{m_1^2} \right)^{\frac{1}{2}} \qquad (w_{\frac{1}{2}} \text{ and } E_o \text{ in eV})$$

which is valid as long as E_o is greater than or equal to kT.

The LAB distribution of energies for a distribution of CM energy releases is not in general available analytically. An exception is the case of a Maxwellian kinetic energy release distribution.

A good approximation to the expected LAB distribution may however be obtained by building up a CM release distribution as a sum of discrete energy releases calculated by equation [1].

A further modification to the observed energy distribution is expected as a consequence of the varying probability of detection of an ion as a function of its initial energy and its initial angle of travel relative to the analyser direction.

This effect depends primarily on the geometry of the source region and the source field used and to a lesser extent on the accelerating potential applied after the source region. It is found that the application of a small

source field is desirable because without it the probability of collection of very low energy ions is not reproducible. For the conditions of the present experiment a function defining the initial angle of travel within which an ion will pass the source exit slit has been derived. The derivation is given in appendix A and a discussion of its application appears in chapter 2.E. Ions which leave the ionization region within an angle defined by:

$$\sin \frac{\theta}{2} = \left| \left(\frac{d^2(Vl + 2El \pm |(4E^2l^2 + 2VEl^2 - V^2d^2)^{\frac{1}{2}}|)}{4El(l^2 + d^2)} \right)^{\frac{1}{2}} \right|$$

will pass through the source exit slit.

Where d is half the slit width

l is half the source region width

V is half the source voltage

and E is the initial energy of the ion in eV.

The angle defined with a positive value of the inner square root term is the forward flying ion acceptance angle. This angle decreases with increasing energy to a minimum value given by

$$\sin \frac{\theta}{2} = \left| \left(\frac{ld^2}{l^2 + d^2} \right)^{\frac{1}{2}} \right|$$

as E tends to infinity.

The angle defined with a negative value of the inner square root term is the backward flying ion acceptance angle and decreases to zero at high values of E. It must be remembered however that in the practical experiment backward flying ions with energies above a value half that of the source voltage will strike the rear of the source and so not be collected. A plot of this acceptance angle function

Figure 3.1

The computed angular acceptance functions for the spectrometer.

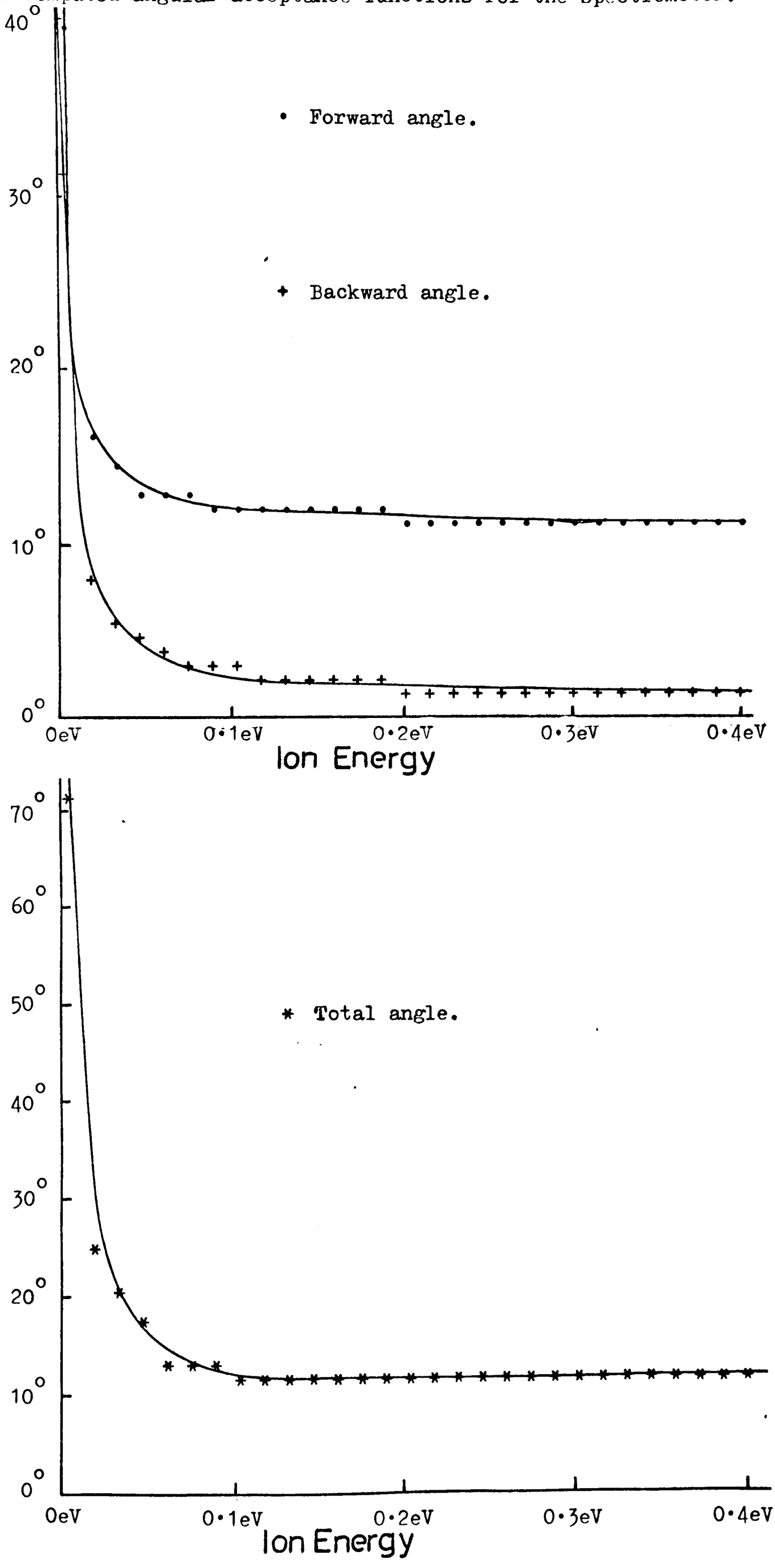

is given in figure 3.1 with parameter values chosen to approximate to the conditions of the actual experiment.

A computer program was developed to calculate and plot expected observed distribution functions for a weighted sum of discrete energy releases in the centre of mass coordinate. The use of this program is discussed in chapter 2 section E and the program is given in appendix C.

C. THE PROCESSING OF EXPERIMENTAL DATA

Experimental kinetic energy distributions were obtained in two forms. The first was as a plot on an X-Y recorder of count rate versus ion acceleration energy. In later experiments distributions were obtained in the form of a count of the total number of ions of a particular mass arriving in a defined time interval for various discrete values of acceleration energy. This was achieved by integrating peaks from time of flight mass spectra built up on the multichannel analyser. Normally measurements were made at intervals of about 20 meV energy and each mass spectrum allowed to accumulate for 100 or 400 seconds depending upon the count rate obtained for the compound in question. One major advantage of this method of collecting data is that drift of the voltage on the analyser will only affect the energy scale calibration but not the relative positions of the parent (or inert gas) peak and the various fragment energy distributions. In the original method parent or inert gas distributions had to be recorded before or after the fragment distribution with a small consequent danger of peak drift. It must be emphasized that the power supplies used were, in fact, very stable and any such effect would hopefully be very small.

The results from experiments using the multichannel analyser were treated in one or both of two ways. They can be plotted, with error bars equal in length to a two standard deviations, as number of counts against energy. Alternatively, they can be fitted to a mathematical function in order to produce a smoothed analytical version of the energy distribution

curve. The function chosen was:-

$$T(E) = C1e^{(x^2)} + C2e^{(x^4)} + C3e^{(|x|)} + C4\frac{x}{PQ + x^2} + C5\frac{x}{PQ + x^4}$$

where PQ is an empirically determined factor to improve the fit and two other empirical parameters "Peak" and "W" define x thus:

$$x = \frac{E - Peak}{W}$$

By the use of the computer a good fit of this function to the experimental results can normally be obtained in about five minutes. The program used is given in appendix C. The procedure does not work very well when the number of counts per point is very low as is the case for some minor fragments; this is to be expected where the statistical uncertainty of the points to be fitted is high. The procedure is very useful, where it is applicable, as it provides a good estimate of the exact position of the peak of the distribution and also simplifies subsequent processing.

Unfortunately it is not possible directly to unfold the LAB distribution function to give the CM release function. If peaks are seen in the observed distribution they will correspond to maxima in the CM release distribution but in the usual case where a smooth distribution function is found no simple interpretation is available. The procedure adopted therefore was to calculate energy distributions for various weighted sums of discrete CM energy release using the functions described in section B of this chapter. By repeated calculations and comparisons of calculations with experiment it is possible to arrive at a set of discrete energy releases that would give

Figure 3.2

The experimental energy distribution of $CClF_2^+$ ions is plotted using error bars and the line drawn through these points to represent the experimental curve. The black dots show points on the derived fit function found by the computer.

Figure 3.2

The experimental distribution of energies of $CClF_2^+$ ions formed from $CClF_3$ upon photoionization together with a plot of the derived function fit.

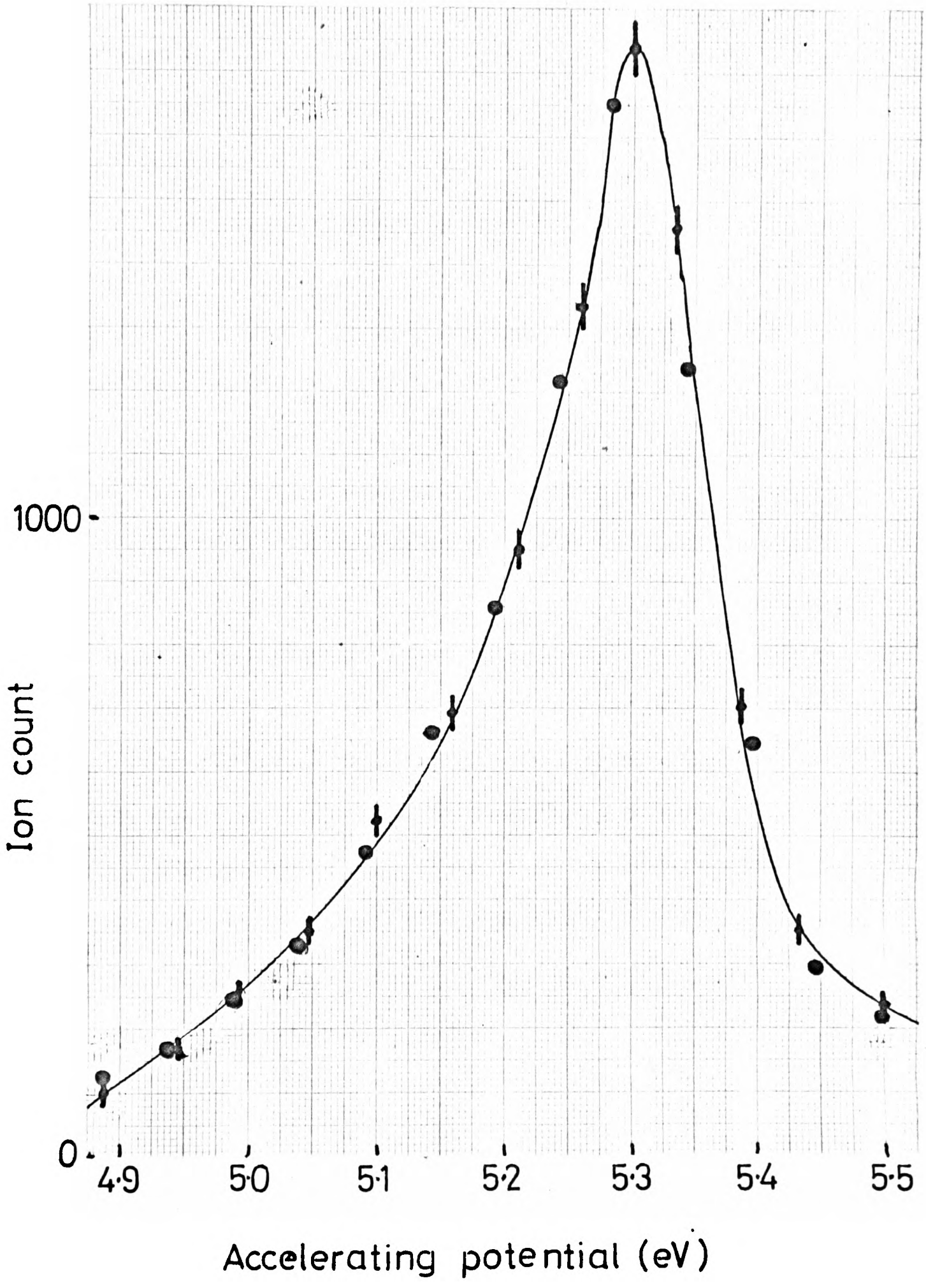

the observed experimental distribution. However this is not to say that the discrete energy release values decided upon have any meaning as such; indeed this is thought to be unlikely. They should however give a good idea of the shape of a continuous energy release distribution. For most of the molecules investigated, essentially continuous energy release distributions are expected in terms of the energy resolution of the technique used.

To obtain a plot of the energy release distribution represented by a particular set of discrete energy releases the weighting used for each energy value is divided by the energy band width it covers.

The fitting of empirical discrete release values to the experimental curve was performed using a computer program written for the purpose and given in appendix C.

The validity of the idea of fitting experimental points to an analytical function was extensively investigated as described in appendix C. The computer program used to obtain the fit also computed the root mean square error of the fit function points. The resulting function was only used if the RMS error was lower than the statistical uncertainty of the results. Figure 3.2 shows a plot of the experimental energy distribution of $CClF_2^+$ ions formed from $CClF_3$ together with the derived function fit.

Figure 3.3

The observed kinetic energy distribution of O^+ ions formed from O_2^+ upon photoionization at 21·22 eV.

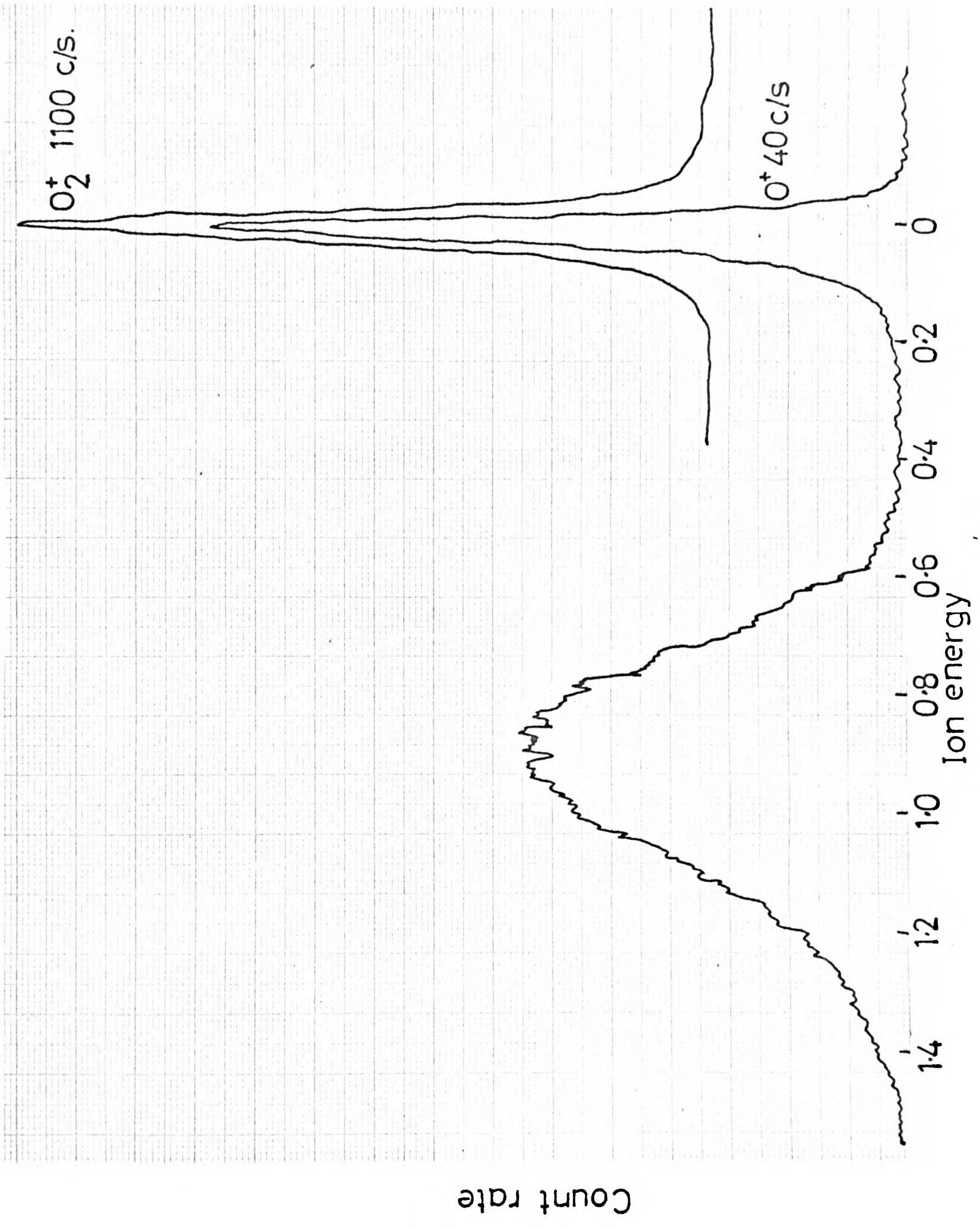

Figure 3.4

Potential energy curves for O_2 and O_2^+.

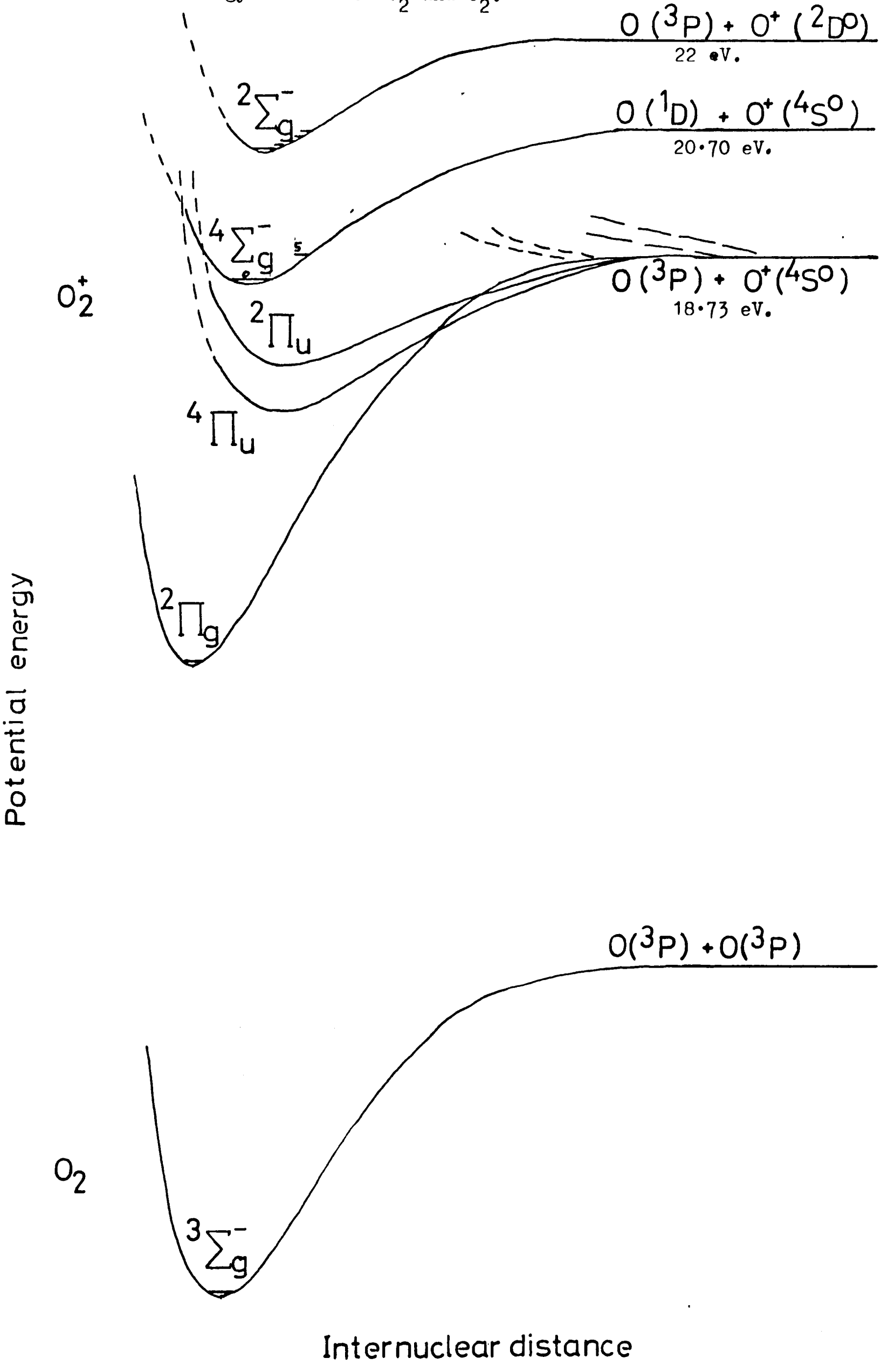

D. THE KINETIC ENERGY DISTRIBUTION OF O^+ IONS FORMED FROM THE FRAGMENTATION OF O_2^+

The fragmentation of O_2^+ ions produced by photo ionization at 21.22 eV is of particular interest in the appraisal of the technique described here, because it is effectively the only fragmentation for which the form of the CM release of energy is almost completely known from other experimental data. The O_2^+ fragmentation has been investigated previously by other techniques[25,26,116,29,119].

The experimentally observed distribution of O^+ kinetic energies is shown in figure 3.3 together with the distribution of energies of the parent ions. Two distributions of energy are apparent; one of very low kinetic energy and another broad distribution centred on a release of 0.9 eV. A simplified diagram of the potential energy curves of oxygen and the O_2^+ ion is given in figure 3.4. This is based on the curves given by Gilmore[117]. Dissociation limits corresponding to formation of O^+ and O in various electronic states are shown.

The high kinetic energy O^+ ions have already been shown to arise from predissociation of ions in the $^2\Sigma_g^-$ state to the lower dissociation limit corresponding to $O(^3P)$ and $O^+(^4S^o)$[25,119]. Evidence for this mechanism is provided by the fact that radiation due to the allowed transition

$$^2\Sigma_g^- \longrightarrow {}^2\Pi_u$$

has not been observed[119]. The time scale of the predissociation can therefore be set somewhere between a vibrational period of about 10^{-13} sec. and the radiation lifetime of about 10^{-8} sec.

Figures 3.5 and 3.6

These show the experimental kinetic energy distribution of O^+ ions formed from O_2 upon photoionization at 21.22 eV, together with calculated distributions.

The ~~first,~~ figure 3.5, shows the distribution calculated for complete predissociation of the $^2\Sigma_g^-$ state of O_2^+. The energy releases in centre of mass are:

Energy (eV)	Weight (Franck Condon factor)	Vibrational level of $^2\Sigma_g^-$
1.56	0.18	0
1.69	0.24	1
1.82	0.22	2
1.94	0.16	3
2.05	0.12	4
2.15	0.04	5
2.23	0:03	6

Figure 3.6 shows the calculated distribution for the above energy releases together with the following energy releases:

Energy	Weight
0.0	0.1
0.13	0.03

This corresponds to the expected energy releases assuming complete predissociation of the $v = 4$ and $v = 5$ levels of the $^4\Sigma_g^-$ state.

Figure 3.5

The O^+ kinetic energy distribution together with a calculated distribution assuming the complete predissociation of the $^2\Sigma_g^-$ state.

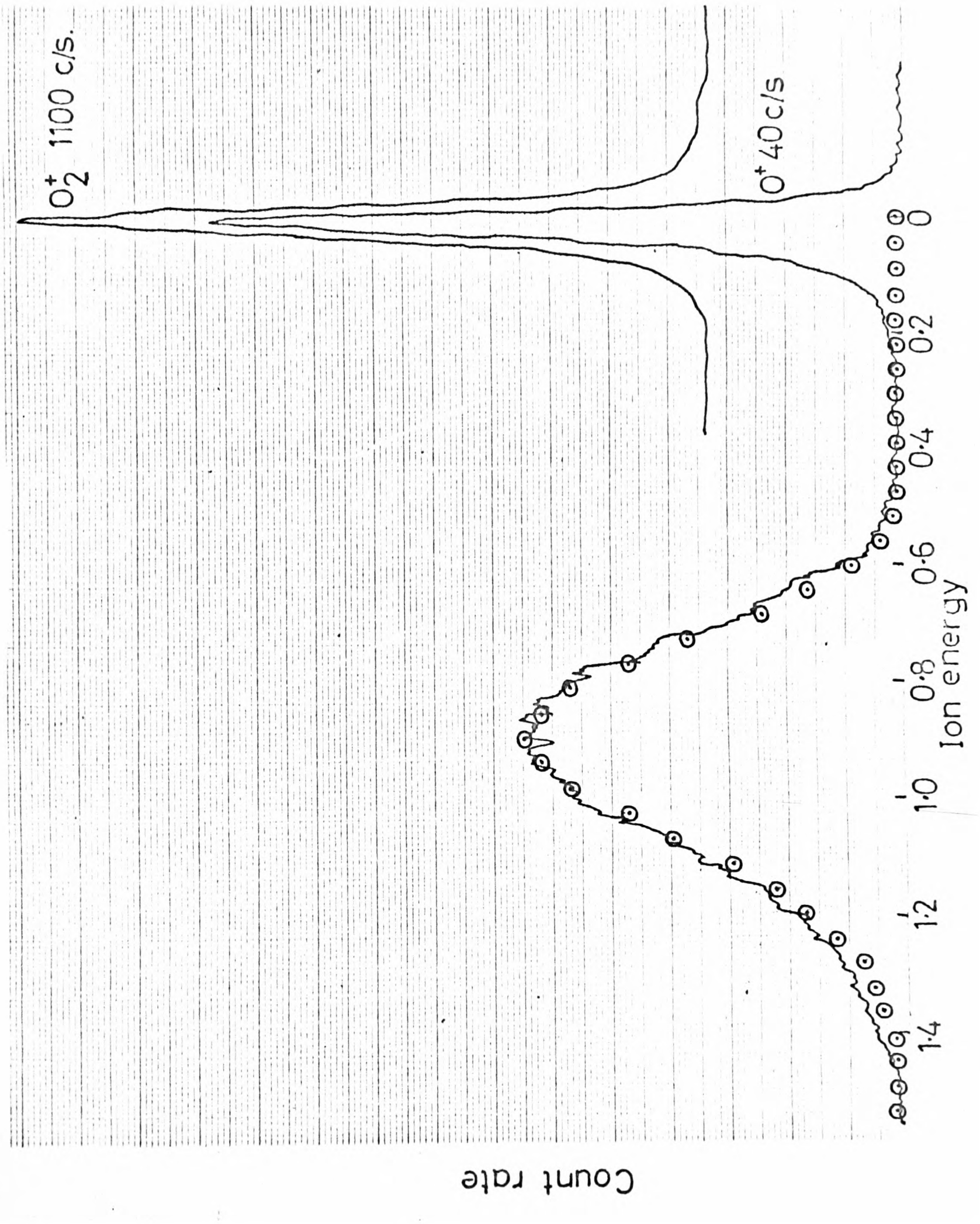

Figure 3.6

The O^+ kinetic energy distribution together with the complete calculated distribution.

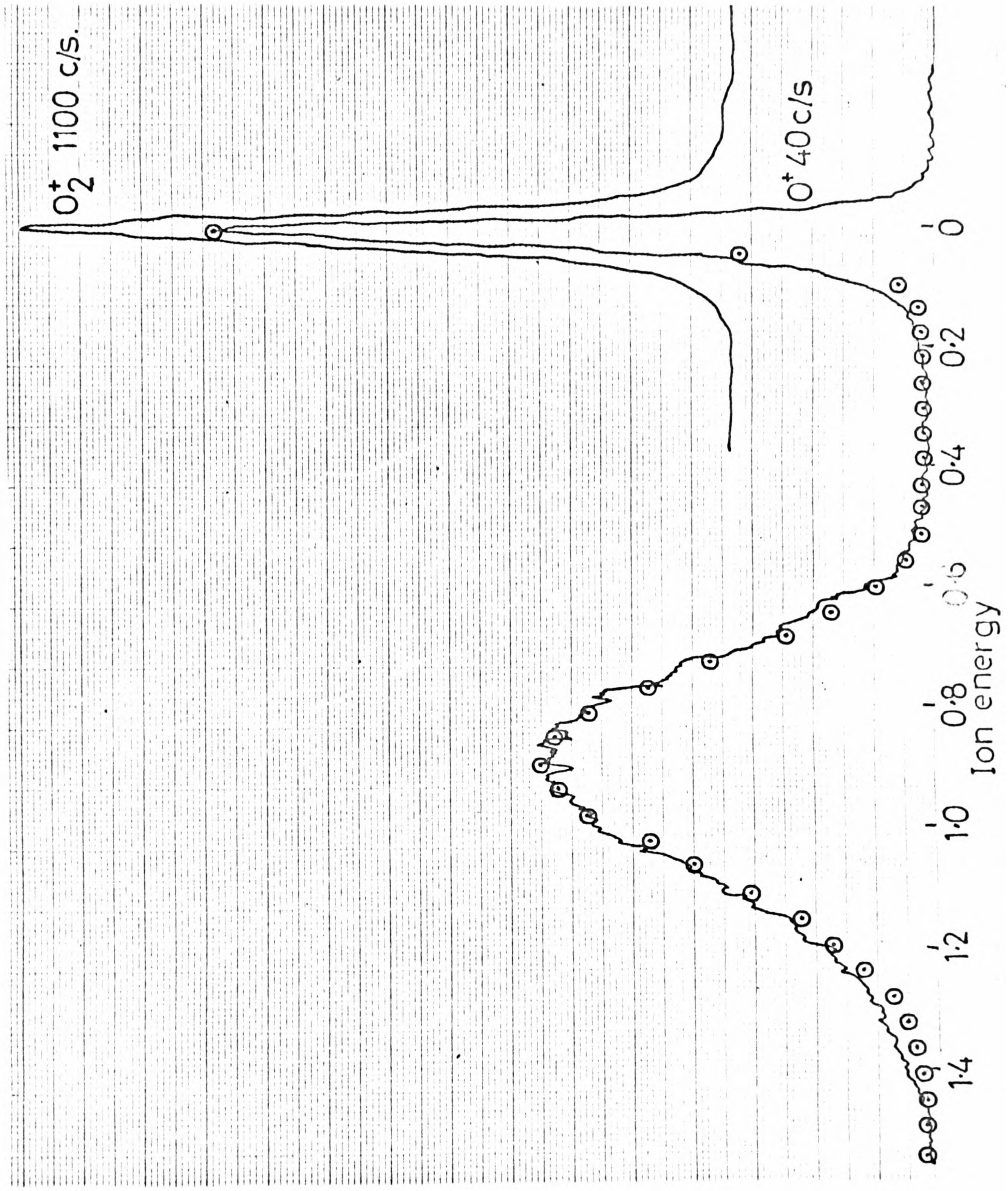

Table 3.1

Energy levels of the O_2^+ ion and dissociation limits.

State of ion or products		Energy eV	Reference
$O_2^+ \ ^2\Sigma_g^-$	$v = 6$	20.96	118
	$v = 5$	20.88	
	$v = 4$	20.78	
	$v = 3$	20.67	
	$v = 2$	20.55	
	$v = 1$	20.42	
	$v = 0$	20.29	
$O^+(^4S^o) + O(^1D)$		20.70 eV	119,117
$O^+(^4D^o) + O^-(^2P^o)$		20.60 eV	
$O_2^+ \ ^4\Sigma_g^-$	$v = 5$	18.84	118
	$v = 4$	18.71	
	$v = 3$	18.58	
$O^+(^4S^o) + O(^3P)$		18.73 eV	119,117

The dissociation limit values are based on the figures

$$D(O_2) = 5.115 \text{ eV}$$

$$IP(O) = 13.614 \text{ eV}$$

and excitation potentials for O given by C. E. Moore[120].

The energies of the vibrational states of $^2\Sigma_g^-$ and their Franck-Condon factors in He I photoionization are well known from photoelectron spectroscopy[118] and the energy of the dissociation limit is known from spectroscopic data [117,119]. The expected energy distribution for complete predissociation of the $^2\Sigma_g^-$ state may therefore be calculated exactly and a comparison of calculation and experiment is shown in figure 3.5. It can be seen that the agreement is good providing a satisfactory demonstration of the validity of the energy distribution calculations. The explanation for the occurrence of very low energy ions is less simple. They could arise from loss of energy in collisions in the source. This possibility is easily dismissed for two reasons. Firstly the relative intensity of low kinetic energy ions does not vary with pressure and secondly if this mechanism were occurring one would expect to see ions having kinetic energies between those of the two distributions. This effect can only been seen at very high sample pressures.

Two mechanisms for production of low energy ions have been proposed [86,116]. Either some higher vibrational levels of the $^2\Sigma_g^-$ state are predissociating to produce the electronically excited products $O(^1D) + O^+(^4S^o)$ or the highest levels of the $^4\Sigma_g^-$ state are dissociating to $O(^3P) + O^+(^4S^o)$. Table 3.1 gives the energy levels involved. The vibrational peaks of the $^2\Sigma_g^-$ state above the upper dissociation limit have been said to be broadened in the photoelectron spectrum of O_2 [86]. This is uncertain however as the electron energy is very low for these peaks and experimental aberrations at these low energies could well be broadening the peaks. Photoelectron spectra of oxygen recorded on the

spectrometer used in this investigation with an acceleration applied to the electrons do not show any appreciable broadening. The fact that the lines are not broadened does not rule out predissociation of these higher vibrational levels of the $^2\Sigma\bar{g}$ state to give $O(^1D) + O^+(^4S^o)$; it does however render the possibility less likely, as it would have to be occurring faster than the competing predissociation to give $O(^3P) + O^+(^4S^o)$. This consideration in itself suggests that the proposed mechanism is unlikely. There are many dissociative states leading to the $O^3P + O^+(^4S^o)$ dissociation limit that probably cross with the $^2\Sigma\bar{g}$ state. Predissociation of higher vibrational levels of $^2\Sigma\bar{g}$ to the higher dissociation limit would require the presence of very shallow dissociative states. Such states quite possibly do exist but predissociation via them should be slower than the alternative energetic predissociation. The alternative possibility of a crossing of a bound state on the left hand part of the $^2\Sigma\bar{g}$ potential curve is ruled out by the known shape of the only bound potential curve leading to the upper dissociation limit; the $^4\Sigma\bar{g}$ state.

In the alternative case of predissociation of upper vibrational levels of the $^4\Sigma\bar{g}$ state this mechanism is more likely - both the $^2\Pi u$ and the $^4\Pi u$ state leading to the lower dissociation limit probably cross with the $^4\Sigma\bar{g}$ state on the steeply repulsive part of the curve. According to the figures in Table 3.1 however, only the level corresponding to the $v = 5 \leftarrow 0$ transition of the $^4\Sigma\bar{g}$ state is higher than the dissociation limit and this is a very weak peak in the photoelectron spectrum. The energy of the $v = 4 \leftarrow 0$ transition is very close indeed to the computed value of the

dissociation limit however and a small error in either figure is possible.

At this point it is helpful to inspect the observed kinetic energy distribution again. If predissociation of the v = 5 level of the $^4\Sigma_g^-$ state of O_2^+ was responsible for the low energy band of O^+ ions a kinetic energy release of 0.11 eV would be expected. This is clearly not the case. The low energy O^+ peak is of much the same shape as the O_2^+ parent peak and not displaced at all from the zero energy point. It must appear therefore that the v = 4 level is marginally above the dissociation limit and is responsible for most of the low energy O^+ ions observed in the experiment.

To test this hypothesis then an attempt was made to fit the total observed distribution using energy releases computed from the known levels of the $^2\Sigma_g^-$ state as before and the two energy release values of 0.11 eV and OeV in the ratio of the observed peak heights of the v = 5 and v = 4 levels of the $^4\Sigma_g^-$ state in the photoelectron spectrum of O_2^+. A good fit was found for a relative weighting of the two groups of kinetic energy release of 1:7. This is in good agreement with the relative peak height of the relevant peaks in the photoelectron spectrum. The fit is shown in figure 3.6. Measurement of the photoelectron spectrum of oxygen using a spherical grid retarding field analyser has shown that 20% of photoionization of O_2 leads to the $^2\Sigma_g^-$ state of O_2^+ [121]. If this state is completely predissociated it would be expected that the abundance of energetic O^+ ions would be 20% of the total ion count. This ratio is not observed experimentally because of the discrimination of the spectrometer against energetic ions. But by comparison of

the observed abundance of low and high kinetic energy ions a test can be made of the allowance for this energy discrimination effect used in the theoretical calculation. This calculation suggests a ratio of low/high kinetic energy ions of 1:7. It is expected that roughly 3% of ionization will lead to the $v = 4$ and $v = 5$ levels of the $^4\Sigma\bar{g}$ state from inspection of the photoelectron spectrum. Assuming complete predissociation of this level therefore the ratio of low kinetic energy O^+ ions to O_2^+ ions should be 3%. The experimental results confirm this. On this basis the ratio of low to high kinetic energy O^+ ions should be 3:20 or 1:7. This agrees well with the figures used in the calculated fit to the observed distribution.

Frey[26] has reported the detection of O^+ ions of about 0.3 eV energy; explained by the ion-pair process:

$$O_2^+ + h\nu\ (21.22\ eV) \longrightarrow O^+(^2D^o) + O^-(^2P^o) + 0.6\ eV$$

No evidence for the occurrence of this process was found in this investigation. It is felt that the evidence for this process as published by Frey is uncertain, owing to the level of noise on the spectrum. Frey did not use mass analysis of the ions and the postulated energy release of 0.3 eV appears on the shoulder of the very high intensity O_2^+ peak. It is not uncommon in real experimental systems for peak baselines to be much wider than expected for the theoretical gaussian instrument broadening function[91] and this appears to be the case here.

Chapter 4 - Experimental Investigations of the Photoionization of some Fluorine Compounds

CHAPTER FOUR

EXPERIMENTAL INVESTIGATIONS OF THE PHOTOIONIZATION OF SOME FLUORINE COMPOUNDS

A. INTRODUCTION

The object of the experiments discussed here was to investigate the validity of the Quasi-equilibrium hypothesis for the dissociation of the ions formed from a related group of compounds. The experimental technique as developed at present lacks the mass resolution to enable the loss of a hydrogen atom from an ion to be detected except in the most favourable cases (e.g. loss of H from CH_4 or H_2O). Attention was therefore turned to a series of simple carbon-halogen compounds. Such compounds are known to undergo many fragmentation reactions upon ionization at excitation energies of 21 eV or lower; indeed in general they do not give parent peaks in their mass spectra. Sulphur hexafluoride, which has much in common with these compounds, was also studied. The photoelectron spectra of CCl_3F, CCl_2F_2, $CClF_3$ and C_2F_6 had not been reported in the literature at the time of the investigations. It was necessary therefore to record and analyse these spectra, as a knowledge of the ionic states populated in ionization is essential in interpreting the ionic fragmentations. Since this work was done an account of the spectra of CCl_3F, CCl_2F_2 and $CClF_3$ by Doucet et al. has appeared[111] supporting, in general, the results presented here. The spectrum of C_2F_6 has not been reported previously.

Figures 4.1, 4.2, 4.3 and 4.4

The Photoelectron Spectra of CCl_3F, CCl_2F_2, $CClF_3$

The 21.22 eV photoelectron spectra of the compounds are presented as they appeared on the X-Y recorder. Ionization potential rises from right to left. Figure 4.4 shows the $\tilde{D}$ band of $CClF_3$ recorded with an expanded energy scale. Two arrows on the energy scale mark the ionizing energies of neon radiation on each spectrum.

Figure 4.1

The photoelectron spectrum of trichlorofluoromethane.

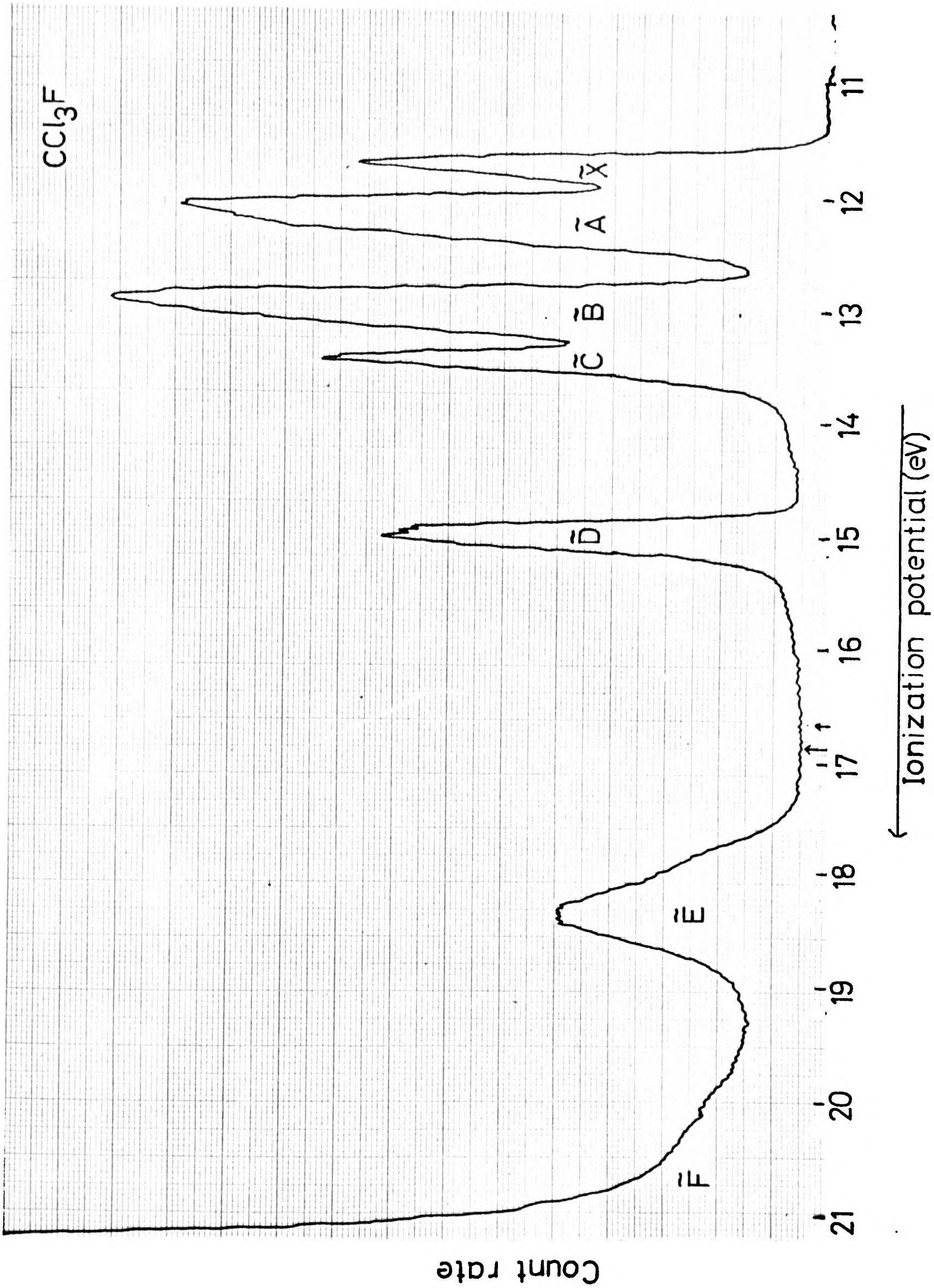

Figure 4.2

The photoelectron spectrum of dichlorodifluoromethane

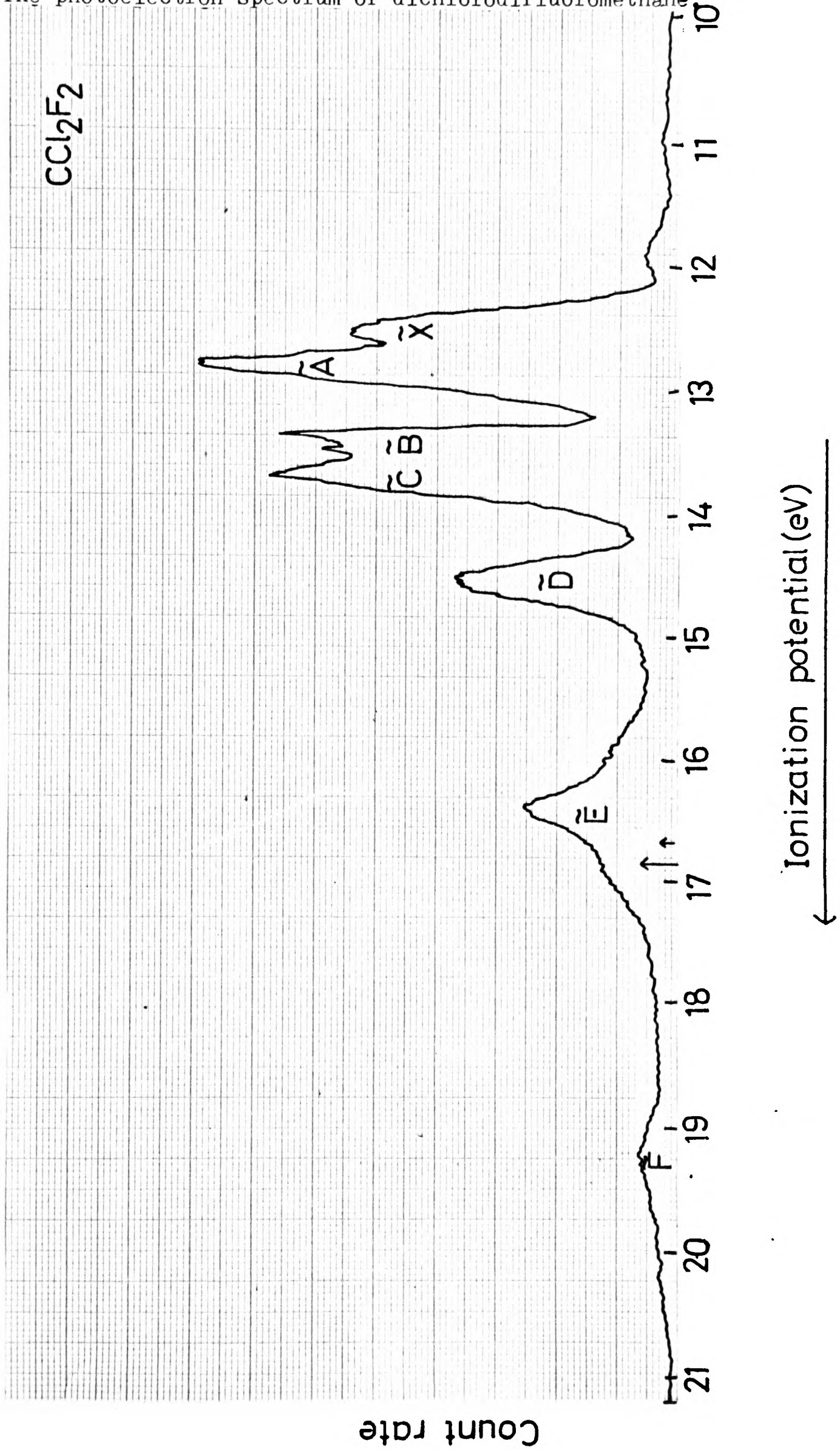

Figure 4.3

The photoelectron spectrum of chlorotrifluoromethane.

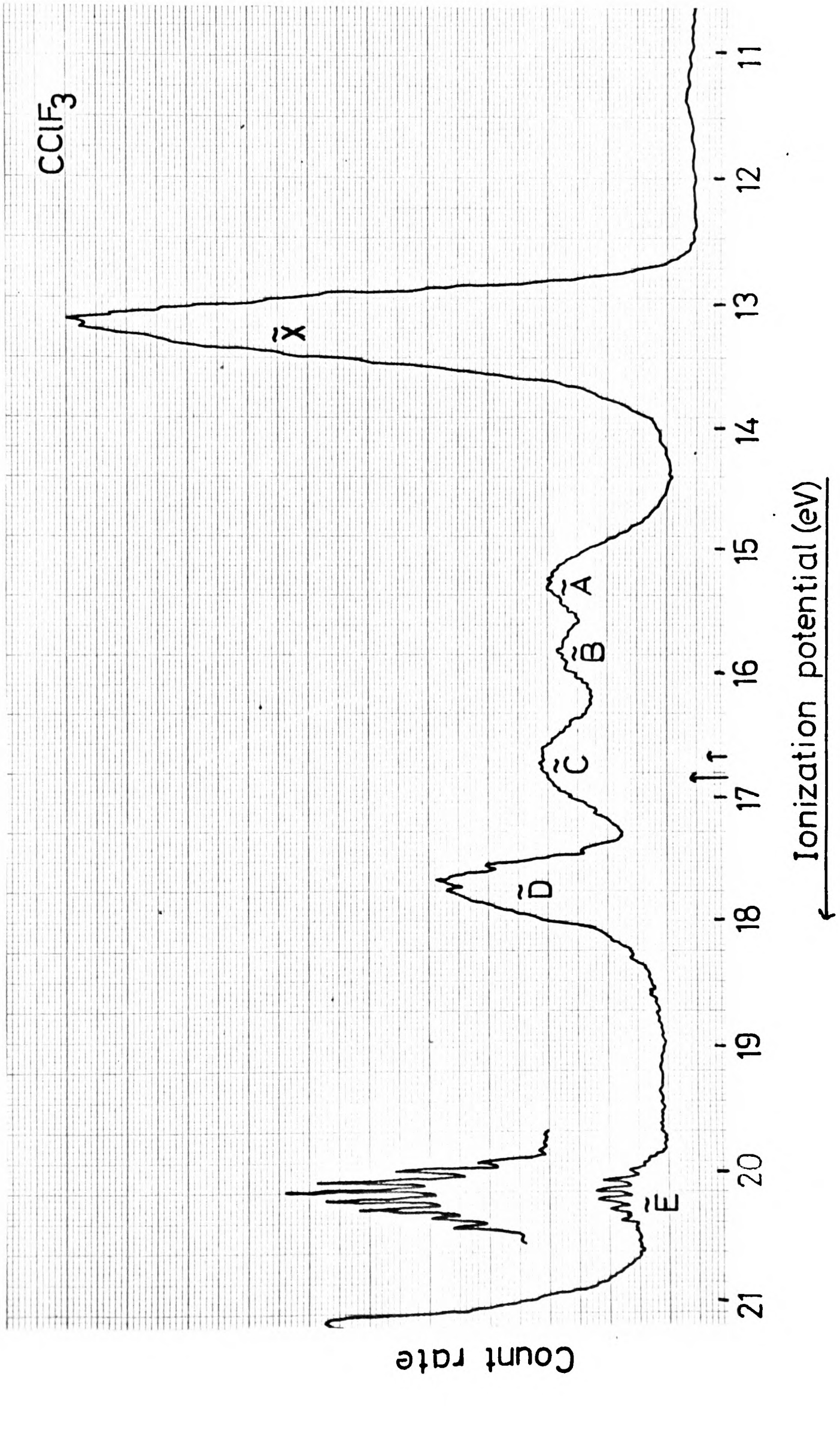

Figure 4.4

The D band of the photoelectron spectrum of chlorotrifluoromethane.

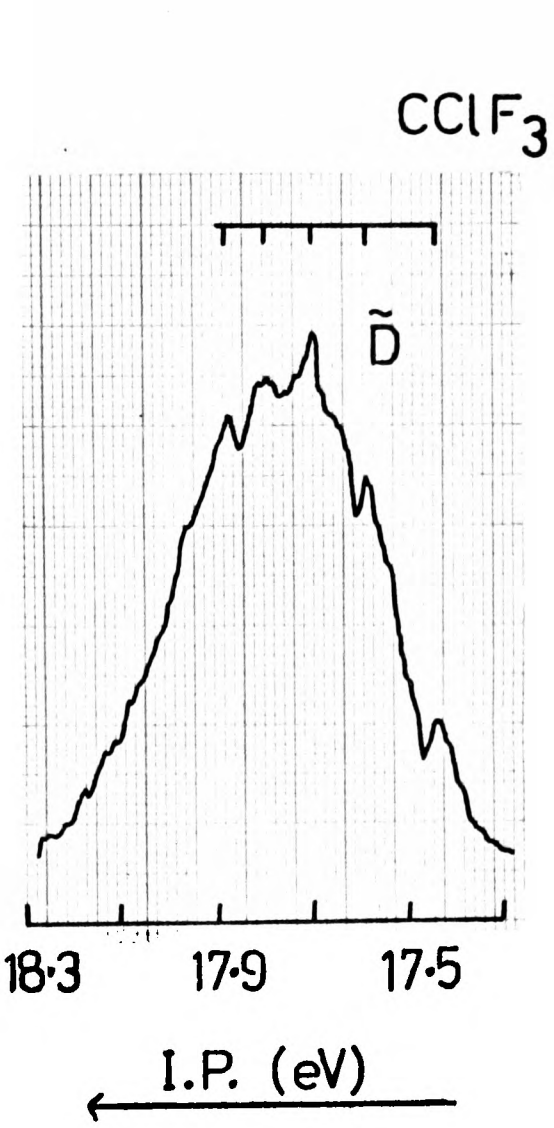

Table 4.1

Ionization potentials of CCl_3F, CCl_2F_2, $CClF_3$.

Compound	Band	Vertical I.P. (eV)	Adiabatic I.P. (eV)	Assignment
CCl_3F	$\tilde{X}$	11.83	11.6	
	$\tilde{A}$	12.24	-	
	$\tilde{B}$	13.04	12.8	a_1, a_2, e, e
	$\tilde{C}$	13.55	-	
	$\tilde{D}$	15.09	14.9	e
	$\tilde{E}$	18.4	~17.5	e
	$\tilde{F}$	?>21.2	~18.6	a_1
CCl_2F_2	$\tilde{X}$	12.35	12.1	
	$\tilde{A}$	12.67	-	
	$\tilde{B}$	13.21	13.0	a_1, a_2, b_1, b_2
	$\tilde{C}$	13.53	-	
	$\tilde{D}$	14.55	14.2	b_2
	$\tilde{E}$	16.28	15.5	a_1, a_2, b_1, b_2
	$\tilde{F}$	19.2	~18.7	b_1, a_2
$CClF_3$	$\tilde{X}$	13.17	12.7	e
	$\tilde{A}$	15.18	14.7	a_1
	$\tilde{B}$	15.7	-	a_2
	$\tilde{C}$	16.7	-	e
	$\tilde{D}$	17.6	-	e
	$\tilde{E}$	20.10	19.86?	e

B. THE PHOTOELECTRON SPECTRA OF CCl_3F, CCl_2F_2 AND $CClF_3$

The photoelectron spectra of CCl_3F, CCl_2F_2 and $CClF_3$ excited by HeI radiation are given in figures 4.1, 4.2 and 4.3. The spectra were recorded using the ion kinetic energy source configuration with wide analyzer slits. The resolution is therefore of the order of 50 meV. All the structure reported by Doucet et al.[111] was in fact seen in these spectra and in the case of $CClF_3$, additional structure on one band and another new band were observed that are not shown in Doucet's paper. Most of the bands showing structure of any kind were recorded separately at higher resolution to assign the vibrational peaks more accurately. Such a higher resolution spectrum is shown for the $\tilde{D}$ band of $CClF_3$ in figure 4.4. All spectra were additionally recorded with an acceleration applied to the electrons in order to increase the collection efficiency for electrons of low initial energy. In all cases this caused a sharp peak to appear at an apparent photoelectron energy of 0 eV. This peak seems to be due to collection of scattered electrons arising from collisions in the source. However in the case of CCl_3F, this "zero energy" band was much stronger and extended to 1.5 eV photoelectron energy, suggesting that an ionic state corresponding to an ionization energy of about 21.2 eV may well be present in the CCl_3F^+ ion. For this compound the spectrum shown is that taken with electron acceleration. The vertical and adiabatic ionization potentials found from these spectra are collected in table 4.1.

An attempt to establish the valence electron levels of these compounds and of CCl_4 and CF_4 has been made by Nevedov on the basis of X-ray emission spectra[112]. The L-spectra

of chlorine and K-spectra of chlorine, carbon and fluorine were used to construct energy levels by assuming that the peaks represented particular atomic orbital contributions to the valence shell molecular orbitals. Thus the maximum in the K-spectrum of chlorine in $CClF_3$ was associated with the $e\pi$ (lone pair) level of the molecule and the next peak in the K-spectrum was associated with a $3p\sigma$ electron of chlorine. By correlating these assignments between the various X-ray spectra a picture of the valence levels was built up. In general the levels given by Nevedov agree fairly well with the photoelectron spectra although he did not observe the four separate chlorine lone pair levels in thecompounds containing more than one chlorine atom. A weak peak in the K-spectrum of carbon in CCl_2F_2 was left unassigned; it agrees well in energy with a peak observed in the photoelectron spectrum.

B.(i) The Photoelectron Spectrum of CCl_3F

The lone pairs of chlorine in this molecule give four orbitals under C_{3v} symmetry (a_1, a_2, e and e) and four bands in approximate intensity ratio 1:2:2:1 are found at the low ionization potential end of the spectrum. Nevedov assigns the next band as a πe C-Cl bonding level, which agrees with the photoelectron assignment of chloroform. Vibrational fine structure with an interval of about 270 cm^{-1} is seen on this band. The band is narrow and the (0,0) transition strong, suggesting little change of geometry upon ionization and therefore that the ionic state is strongly bound. Turner[115] has proposed an empirical relationship between the fractional change in a molecular frequency upon ionization and the difference between adiabatic and vertical ionization potentials. For

this band the relationship would suggest a reduction of the molecular frequency by a factor of 1.1 to 1.4. The frequencies of the symmetric vibrations of the CCl_3F molecule are:-

ν_1	1070 cm^{-1}
ν_2	535 cm^{-1}
ν_3	350 cm^{-1}

Thus the vibrational structure on the band may be assigned with fair certainty to ν_3 a C-Cl stretching and C-F bending mode.

The bands at 18.4 eV and about 21 eV correspond to peaks in the X-ray emission spectra of all the constituent atoms[112] suggesting complex orbital structure: a_1 and e orbitals are expected. Intensity and band shape arguments would suggest that the 18.4 eV band is the e level which, from the X-ray results, is expected to be a predominantly fluorine lone pair orbital.

B.(ii) The Photoelectron Spectrum of CCl_2F_2

Again four chlorine lone pair molecular orbitals are expected - a_1, a_2, b_1 and b_2 under C_{2v} symmetry. These are easily assigned to the 12.35, 12.67, 13.21 and 13.53 eV bands. Structure is seen on the 13.21 eV band with a spacing of about 1000 cm^{-1} suggesting excitation of ν_1, a predominantly C-F stretching mode, which has a frequency of 1095 cm^{-1} in the neutral molecule. The next band has vibrational structure and is assigned to one of two bonding orbitals of mainly C-Cl character (a_1 and b_2). The structure is consistent with excitation of ν_3, a molecular bending mode, (the spacing is ~400 cm^{-1}). The next band clearly contains at least two overlapping contributions and quite possibly three. Two C-F bonding

orbitals are expected in this region (b_1 and a_2) as well as fluorine lone pairs (a_1, a_2, b_1 and b_2). The band at 16.28 eV is tentatively assigned to the fluorine lone pairs by analogy with CCl_3F but this is uncertain. The low ionization potential shoulder on this band may well correspond to the other C-Cl σ molecular orbital.

B.(iii) The Photoelectron Spectrum of $CClF_3$

There was some doubt about the authenticity of the band at 20.1 eV as it is weak and shows much clearer structure than any other band in this series of halogen compounds. The possibility that it could be due to an impurity was therefore investigated. Fluoroform has a band at about the same energy with similar structure but when the spectra of the two compounds, in this region, were recorded one after the other major differences appeared. The fluoroform band has a vibrational spacing of 480 cm^{-1} as compared to 630 cm^{-1} in the $CClF_3$ band and more vibrational levels are populated. The band onsets also differ; 19.86 eV for CCl_3F and 20.0 for CHF_3. A gas chromatographic study of the sample of $CClF_3$ used (carried out by Mr. J.P. Whitworth) showed only about 0.01% of CHF_3, and no other impurity was detected. The band is therefore believed to be a true band of $CClF_3$.

The lowest ionization potential will correspond to the doubly degenerate chlorine lone pair orbital (e). According to the calculations of Brundle et al.[113] for CF_3H the lone pair orbitals of fluorine combine to form a_1, a_2, e and e orbitals (as for chlorine lone pairs in CCl_3F) with a_2 having the lowest ionization potential followed by an e orbital of bonding character and an e of non-bonding character. The order of

Figure 4.5

A Correlation Diagram for the Ionization Potentials of the Series of Compounds: CCl_4, CCl_3, CCl_2F_2, $CClF_3$, CF_4

The ionization potentials of the compounds as measured by photoelectron spectroscopy are plotted and labelled according to the orbital with which they are associated. Group theoretically derived correlations of these orbitals between the different molecules are drawn in where they are known. The main bonding characteristics of the orbitals are written under each level.

Figure 4.5

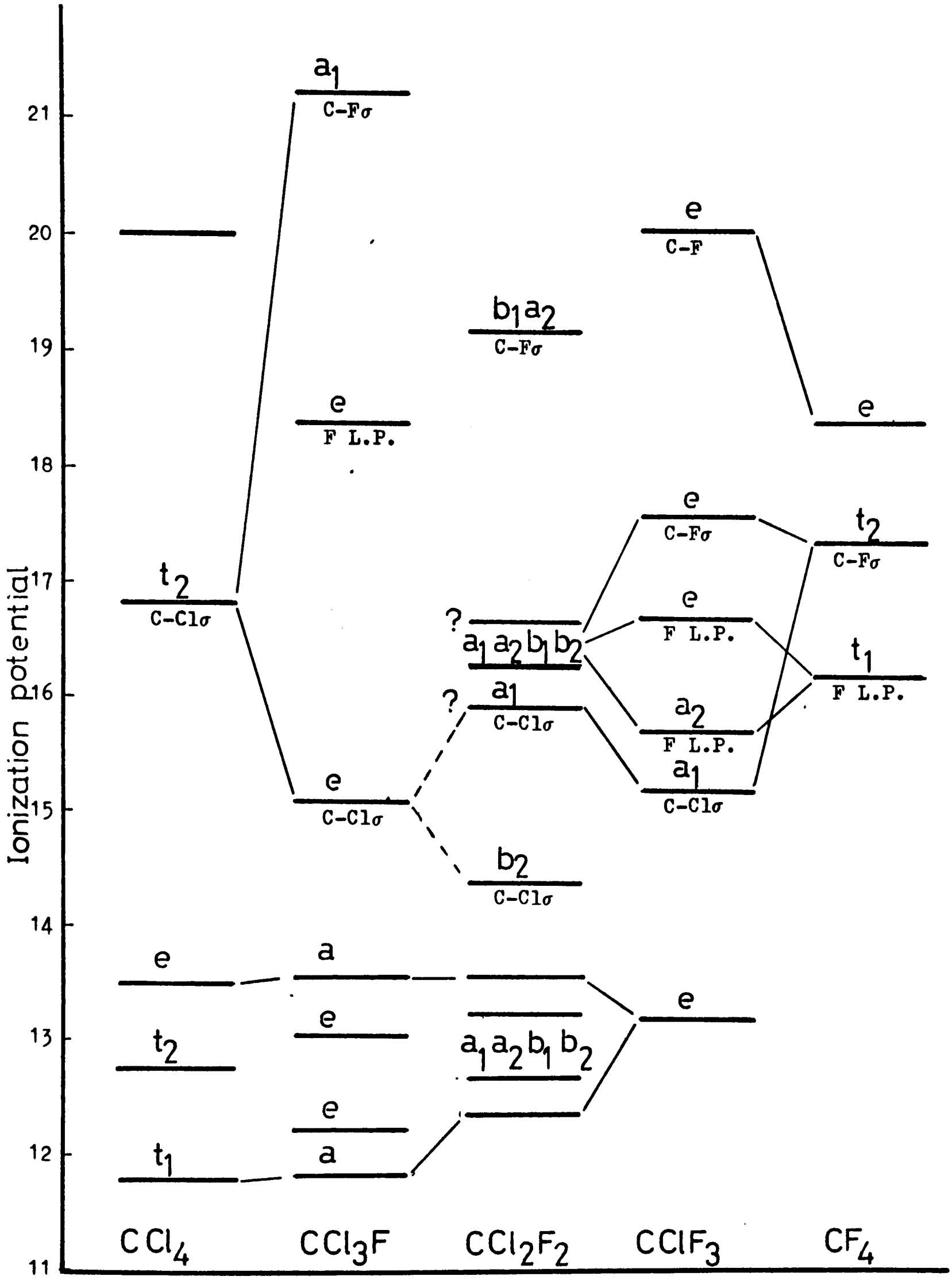
Ionization potential
21
20
19
18
17
16
15
14
13
12
11
a_1
C-Fσ
e
F L.P.
t_2
C-Clσ
e
C-Clσ
b_1a_2
C-Fσ
?
$a_1a_2b_1b_2$
?
a_1
C-Clσ
b_2
C-Clσ
e
C-F
e
e
C-Fσ
t_2
C-Fσ
e
F L.P.
t_1
F L.P.
a_2
F L.P.
a_1
C-Clσ
e
a
e
t_2
e
t_1
a
$a_1a_2b_1b_2$
e
CCl_4
CCl_3F
CCl_2F_2
$CClF_3$
CF_4

orbitals expected in CF_3Cl therefore is:-

i)	Cl lone pair	e
ii)	C-Cl bonding	a_1
iii)	F lone pair	a_2
iv)	degenerate CF_3 bonding	e

The X-ray emission spectra support this order. The band at 15.18 eV is therefore assigned to a_1 (C-Cl σ bonding). The next three bands are characteristic of - CF_3 and appear in almost the same positions in CF_3H and $CBrF_3$. These may be assigned tentatively as a_2, e and e with the position of the expected a_1 orbital uncertain. The band at 17.6 eV has structure with spacings of 960, 880, 800 and 640 cm^{-1} suggesting a very high positive anharmonicity and therefore a shallow potential curve for the ionic state. This frequency is similar to that observed in CF_4 for the 1e band[113] and assigned to the ν_1 mode of CF_4. The ν_1 frequency of CF_3Cl is 1106 cm^{-1} which is consistent with the same assignment for this band. ν_1 is a C-F stretching mode and this assignment would be consistent with ionization of a C-F bonding electron. The band at 20.1 eV shows a long progression of frequency 630 cm^{-1}. This is readily assigned to the ν_2 C-F bending mode with the frequency lower than that of the parent molecule (762 cm^{-1}) by about the amount predicted by Turner's[12] empirical relationship. This is consistent with a band corresponding to a C-F lone pair molecular orbital and this also agrees with the X-ray emission results.

A correlation diagram for the series of compounds CCl_4, CCl_3F, CCl_2F_2, $CClF_3$ and CF_4 is shown in figure 4.5. Correlations derived from the alteration of Td to C_{2V} or C_{3V}

symmetry are included in the diagram. It can be seen that the ionization potentials of the chlorine lone pair orbitals rise as the number of fluorine atoms in the molecule increases. Equally the fluorine lone pair energies tend to fall across the series.

Figures 4.6, 4.7

The Photoelectron Spectra of Hexafluoroethane

Figure 4.6 shows the spectrum of C_2F_6 obtained using helium resonance radiation. Figure 4.7 shows the spectrum obtained using neon resonance radiation in which only the $\tilde{X}$ and $\tilde{A}$ bands appear. The $\tilde{A}$ band is considerably narrower in the neon resonance spectrum despite the spread of ionizing energies (16.85 eV and 16.67 eV in 4/1 ratio). This spectrum was taken with a 5 volt acceleration on the photoelectrons before energy analysis. The ionizing energies of the neon resonance lines are marked on the helium resonance spectrum.

Figure 4.6

The photoelectron spectrum of hexafluoroethane.

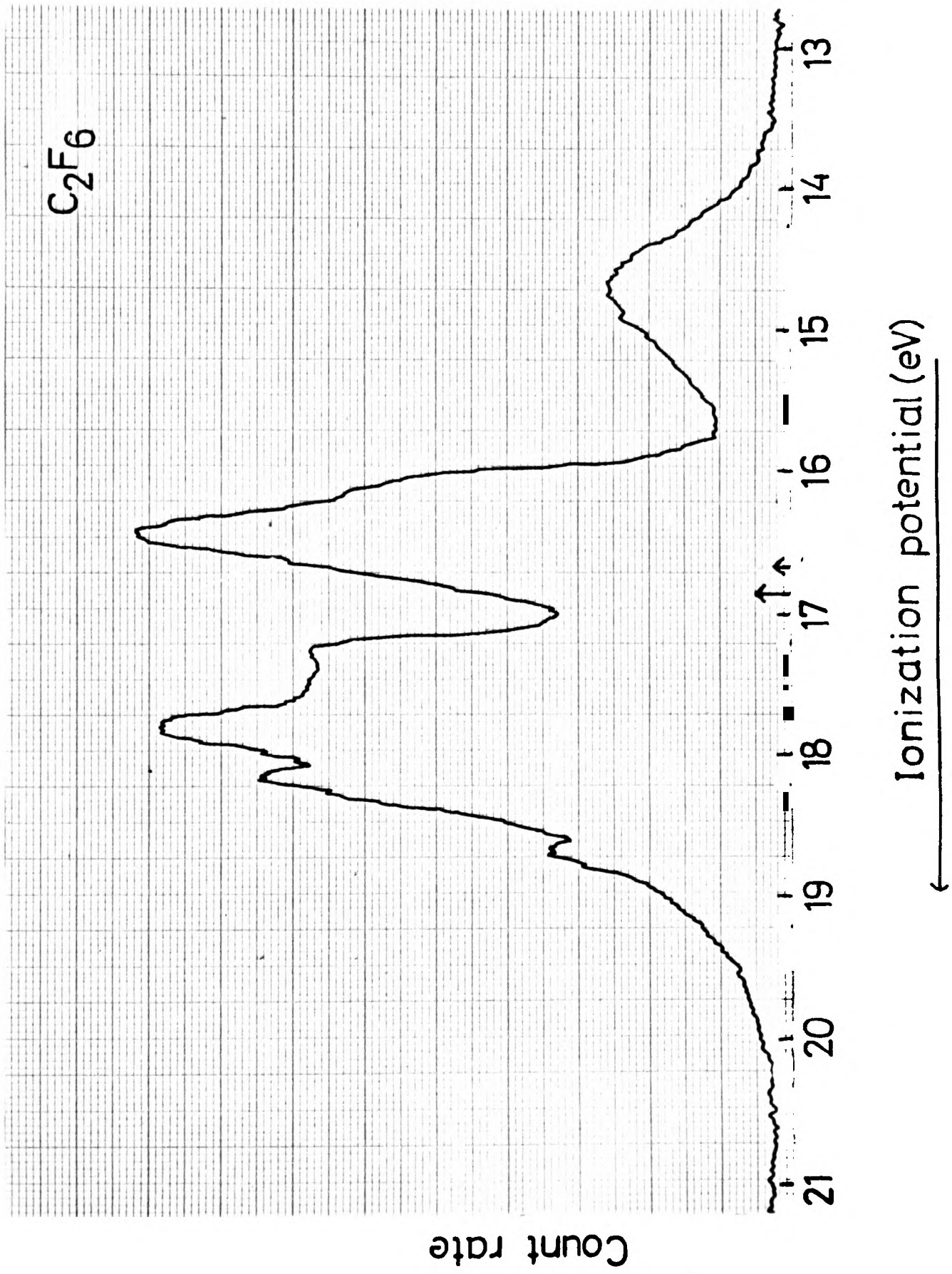

Figure 4.7

The photoelctron spectrum of hexafluoroethane taken using neon resonance radiation.

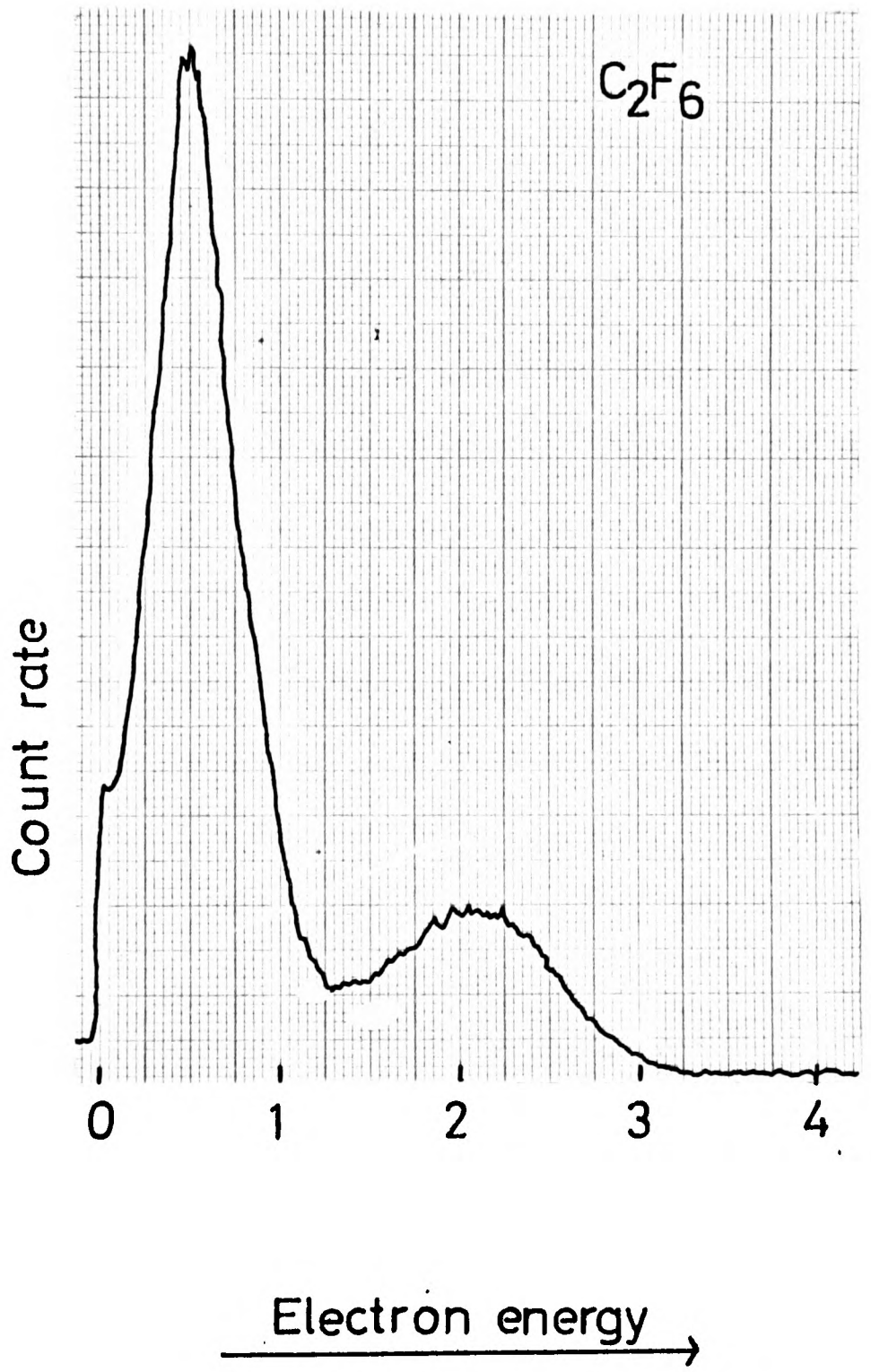

Figure 4.8a and b

The Molecular Orbitals of C_2F_6

These diagrams show the first four orbitals of C_2F_6, as computed by CNDO, in pictorial form. The main contributing atomic orbitals are drawn in each case with their size roughly in proportion to the calculated orbital coefficients. The two E type orbitals are each degenerate; the other orbital being obtained in each case by interchanging the two axes perpendicular to the C-C bond direction.

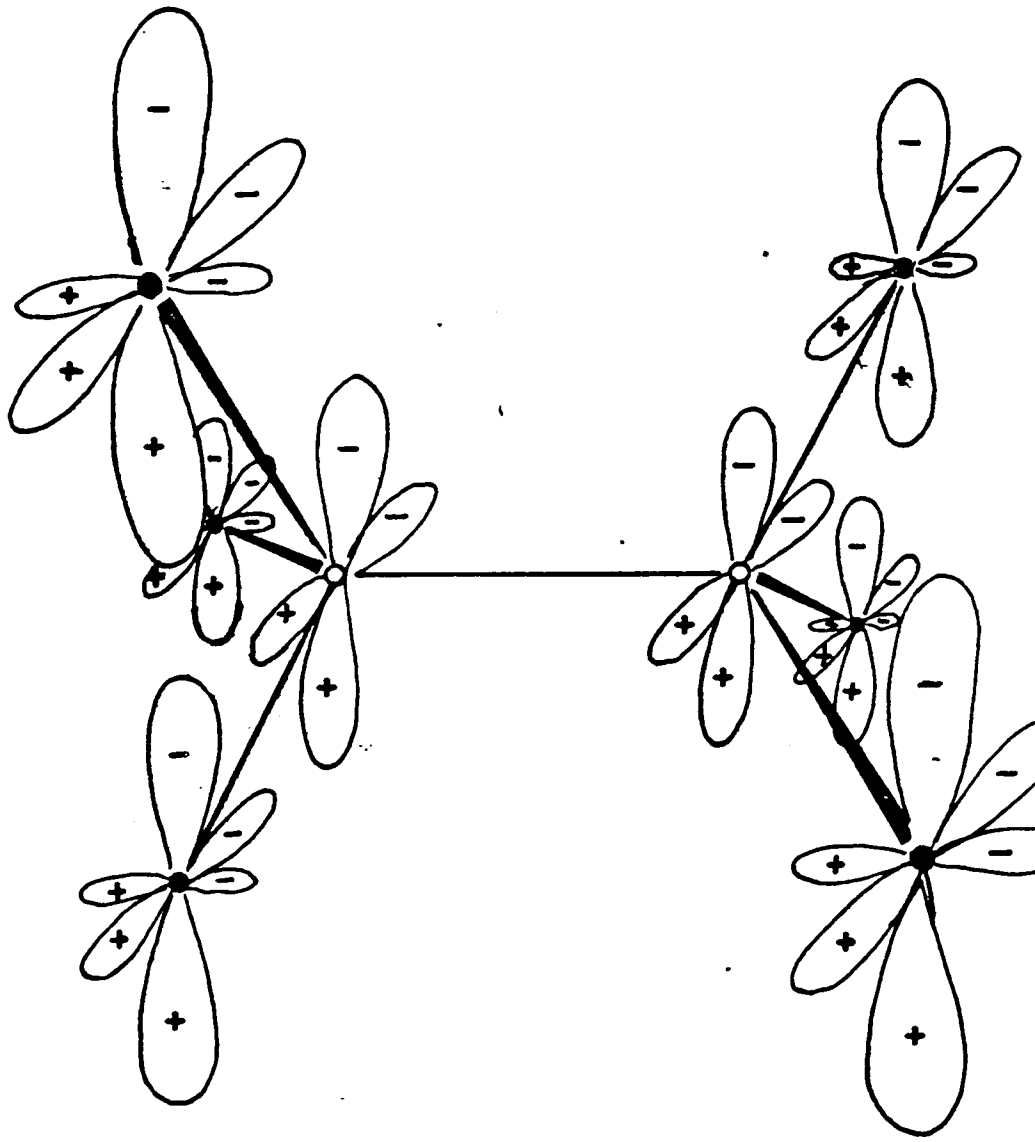

E_u

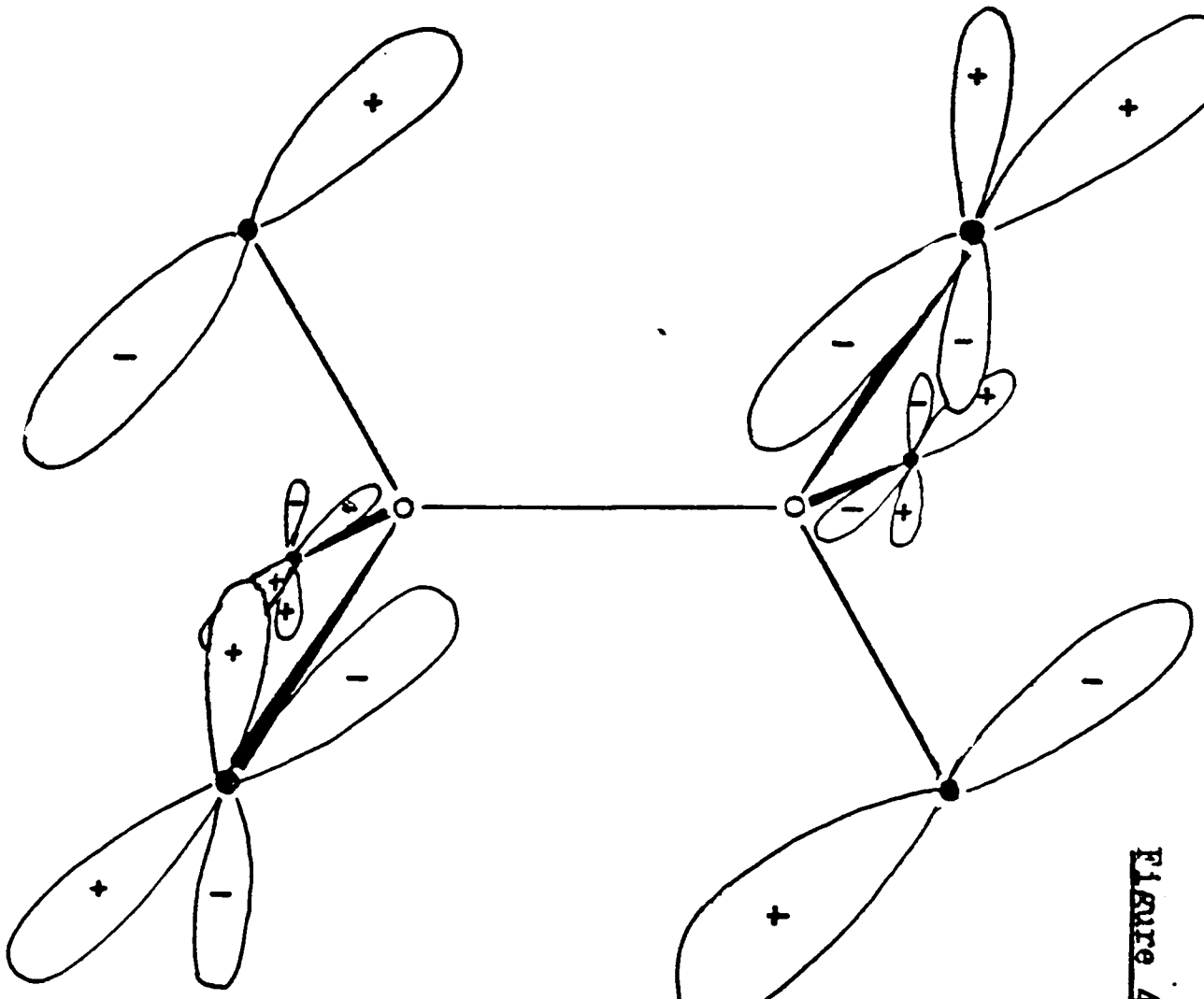

A_{2g}

Figure 4.8b

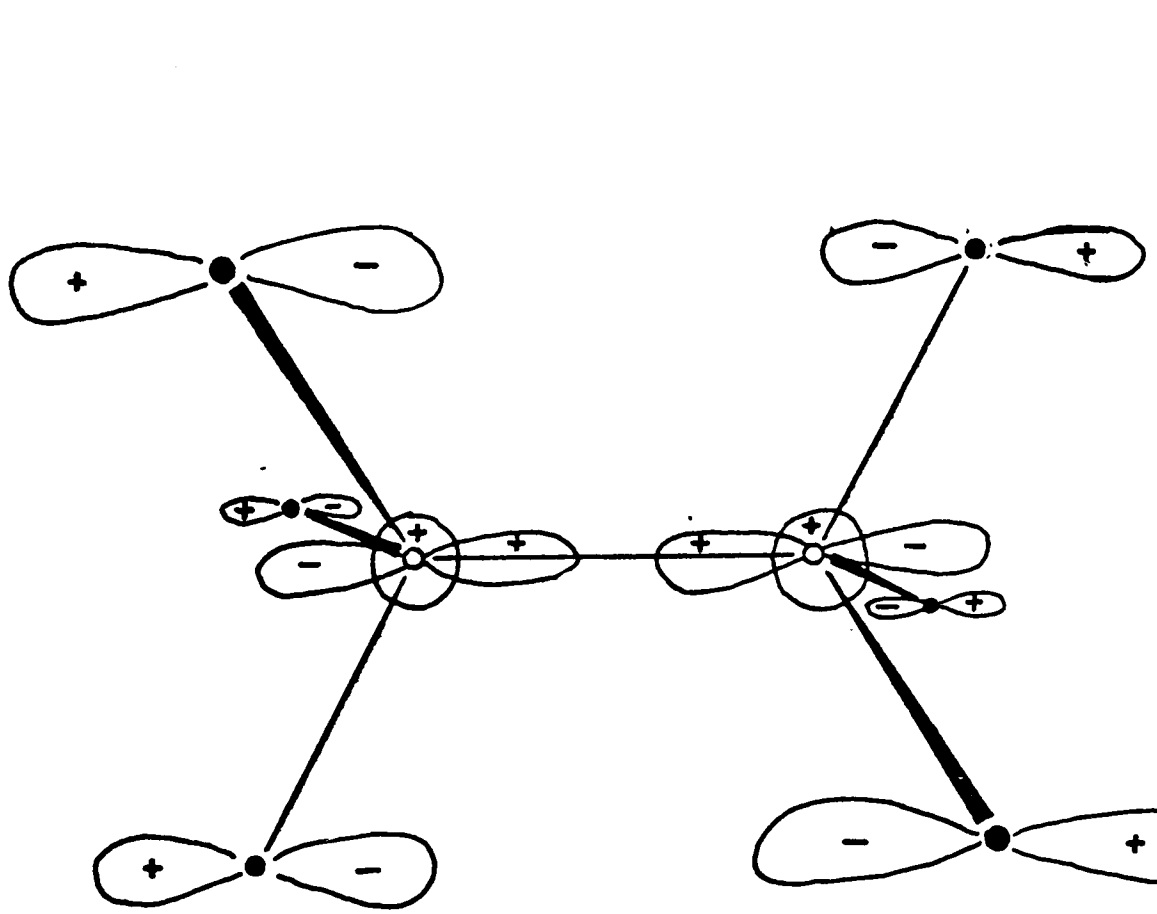

A_{1g}

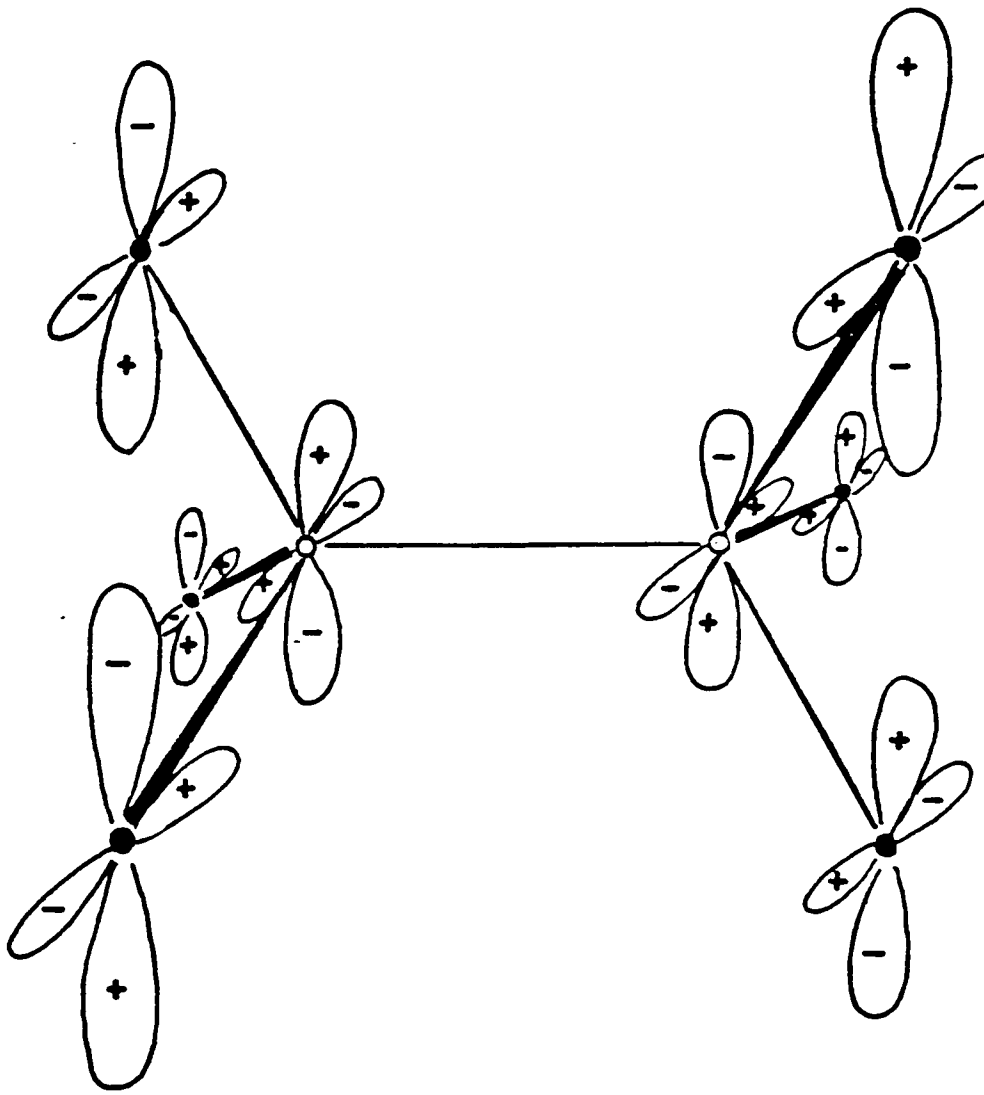

E_g

Figure 4.8a

Figure 4.9

The photoelectron spectrum of carbon tetrafluoride.

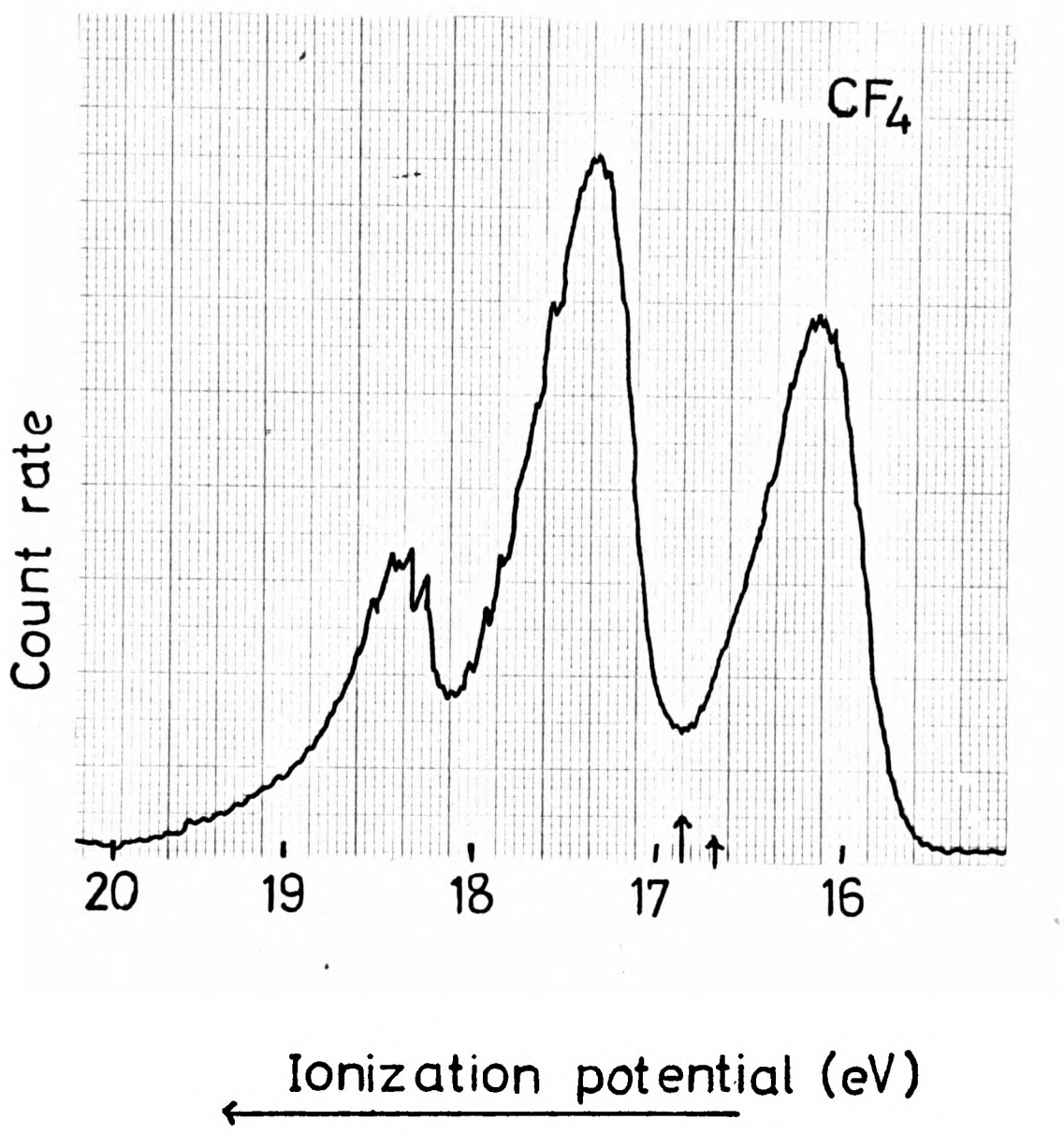

C. THE PHOTOELECTRON SPECTRUM OF C_2F_6

The observed spectrum is shown in figure 4.6. As can be seen the spectrum is diffuse and band structure rather ill defined. There are similarities to the spectrum of CF_4 (shown in figure 4.9) for which an explanation has been put forward in terms of autoionization at 21.22 eV[113]. This was suggested because the spectrum of CF_4 taken with Helium II radiation shows more distinct band structure and no "tail" at low electron energies. It is possible that a similar effect is occurring in C_2F_6 - certainly the number of zero kinetic energy electrons observed, when an electron accelerating field is applied after ionization, supports the view that a band is present at about 22 eV. When the photoelectron spectrum of C_2F_6 excited by neon resonance radiation was recorded the $\tilde{A}$ band was found to be considerably narrower than in the HeI spectrum and of a different intensity relative to the $\tilde{X}$ band. The neon resonance spectrum of C_2F_6 is shown in figure 4.7. It would be interesting to obtain a He II PE spectrum of C_2F_6 - unfortunately the lamp used at present will not produce an adequate intensity of He II radiation.

CNDO calculations were performed for C_2F_6 in the staggered (D_{3d}) and eclipsed (D_{3h}) conformations. The barrier to rotation is about 3 kcals[114] so in fact the isolated molecule is expected to be essentially of D_{3d} symmetry. C_3 symmetry is conserved during rotation of the CF_3 groups. The orbitals for the two conformations are very similar, in any case, as calculated by CNDO.

The ionization potentials measured from the PE spectrum together with CNDO energy levels are shown in table 4.2. Also

TABLE 4.2

Band	V.I.P.	A.I.P.	Assignment	Calculated		Calc.x 0.85
$\tilde{X}$	14.56	13.8	a_{1g}	16.2	Aa_{1g}	13.8
$\tilde{A}$	16.27	15.7	e_g	20.5	e_g	17.4
$\tilde{B}$	17.05	16.9	?	20.8	e_u	17.7
$\tilde{C}$	17.64		e_u ?	22.2	a_{2g}	18.9
$\tilde{D}$	17.99		?	22.3	a_{1u}	18.9
$\tilde{E}$	18.49		?	22.9	e_g	19.5
				23.0	ϵ_u	19.55
				23.3	a_{2u}	19.8

given are the calculated energy levels reduced by a factor of 0.85 as suggested by Brundle[113] to allow for the approximations inherent in the use of Koopmans' theorem. As this factor applied in the case of CF_4 rather than the previously accepted value of 0.92 it was felt that it might also apply for C_2F_6. Assignment of the bands on the basis of this calculation is not easy. However the calculation does give an idea of the type of orbitals from which ionization is occurring and a rough indication of the characteristics of the four least strongly bound orbitals is shown in figures 4.8a and 4.8b.

The a_{1g} orbital is clearly C-C sigma bonding with some attractive interaction of fluorines across the molecule. The $\tilde{X}$ band is easily assigned to this orbital on the basis of the calculation. As expected for a strongly bonding orbital a fairly broad PE band is found. The next two degenerate pairs of e orbitals are nearly of the same energy according to the calculation. The $\tilde{A}$ band could therefore represent one or both

of them. The intensity ratio of the $\tilde{X}$ and $\tilde{A}$ bands is 1:2 in the He I spectrum suggesting that $\tilde{A}$ represents one e state only. In the Neon-excited spectrum the ratio is 1:3 but not too much weight can be placed on this as the $\tilde{A}$ band is nearly resonant with Neon radiation. As mentioned earlier the band is narrower in the Neon spectrum supporting the view that it represents one (degenerate) state. The e_g orbital is C-C π antibonding, but has weak C-F σ bonding interactions and weak C-F σ antibonding interactions. The e_u orbital is C-C π bonding with C-F σ antibonding and C-F π bonding interactions. The a_{2g} orbital is essentially a fluorine "lone pair" orbital and in fact all the other orbitals in the energy range relevant to Helium I photoelectron spectroscopy have only very small computed electron density localized on the carbon atoms.

If it is assumed that the $\tilde{A}$ band represents one degenerate state only, then it may be tentatively assigned as e_g. The computed energy difference of only 0.3 eV between the e_g and e_u orbitals however makes the ordering of these levels in the PE spectrum uncertain - certainly the energy separation must be a good deal larger and the order of the orbitals could well be reversed. However independent evidence from photo-electron-photoion coincidence work supports the assignment of $\tilde{A}$ as e_g. In a coincidence study of C_2F_6 performed recently[31] it was showed that the $\tilde{A}$ band represents an isolated ionic state which fragments to give $C_2F_5^+$ and F, while the ground state of the ion dissociates to give CF_3^+. This suggests that, contrary to QET, the mode of fragmentation of this state depends upon which electron is removed. As fragmentation of ions in this upper state does not lead to rupture of the C-C bond it is suggested that it is formed by removal of an electron

from an orbital of the e_g type which is C-C antibonding and probably C-F bonding overall. Very little further can be said about the PE spectrum except that the similarity of the $\tilde{A}$ and $\tilde{C}$ bands suggests that the $\tilde{C}$ band represents the e_u state. The $\tilde{B}$, $\tilde{D}$ and $\tilde{E}$ bands will represent ionization from fluorine lone pair orbitals designated a_{2g}, a_{1u}, e_g, e_u and a_{2u}.

D. FRAGMENTATIONS OF IONS FROM SOME SIMPLE HALOGEN CONTAINING MOLECULES.

In this section the results of studies on the fragmentation of CF_4, $CClF_3$, CCl_2F_2, CCl_3F, C_2F_6 and SF_6 are presented. All these compounds were investigated after the source region of the spectrometer had been fully modified as described in chapter 2. The kinetic energy distributions of fragments formed from CF_4 and C_2F_6 were obtained using the X-Y recorder; all the others were taken using the multi-channel analyser. In some cases where the assignment of mass peaks may be uncertain photoionization mass spectra were recorded on the multichannel analyser, with the conditions of the experiment optimized for good mass resolution, in order to check the identity of the fragments which were produced. Relative abundances of fragment ions were measured by integrating the kinetic energy distributions for each ion. This procedure will not give the true relative abundances but will give a closer figure to the true one than the ratios at one kinetic energy setting. The reason that abundances measured in this way will be inaccurate is that no allowance is made for the variation of collection efficiency with energy. It is interesting therefore to note that the ratios found for fragment ions in the photoionization of SF_6 at 21.22 eV agree well with the values given by Dibeler and Walker[122] for a conventional mass spectrometric measurement. It is likely that mass spectrometers also discriminate against energetic ions. All compounds were studied using Neon I radiation as well as the Helium I line. The photoelectron spectra given in Figs. 4.1, 4.2, 4.3, 4.6, 4.9 and 4.16 all have the ionising energies of neon radiation marked on them as two arrows along the energy scale. Figure

Figure 4.10

Kinetic Energy Distributions of CF_3^+ Ions from CF_4

The distributions shown were recorded on the X-Y recorder under the following conditions:

Accelerating potential	5 volts
Source field	0.1 volt

One fifth of the accelerating field between plates 2 and 3/4.

The distributions measured using helium I (21.22 eV) and neon I (16.85 eV) radiation are shown. The Calculated kinetic energy distributions used to fit these curves are also shown.

Figure 4.10

Kinetic energy distributions of CF_3^+ ions from CF_4.

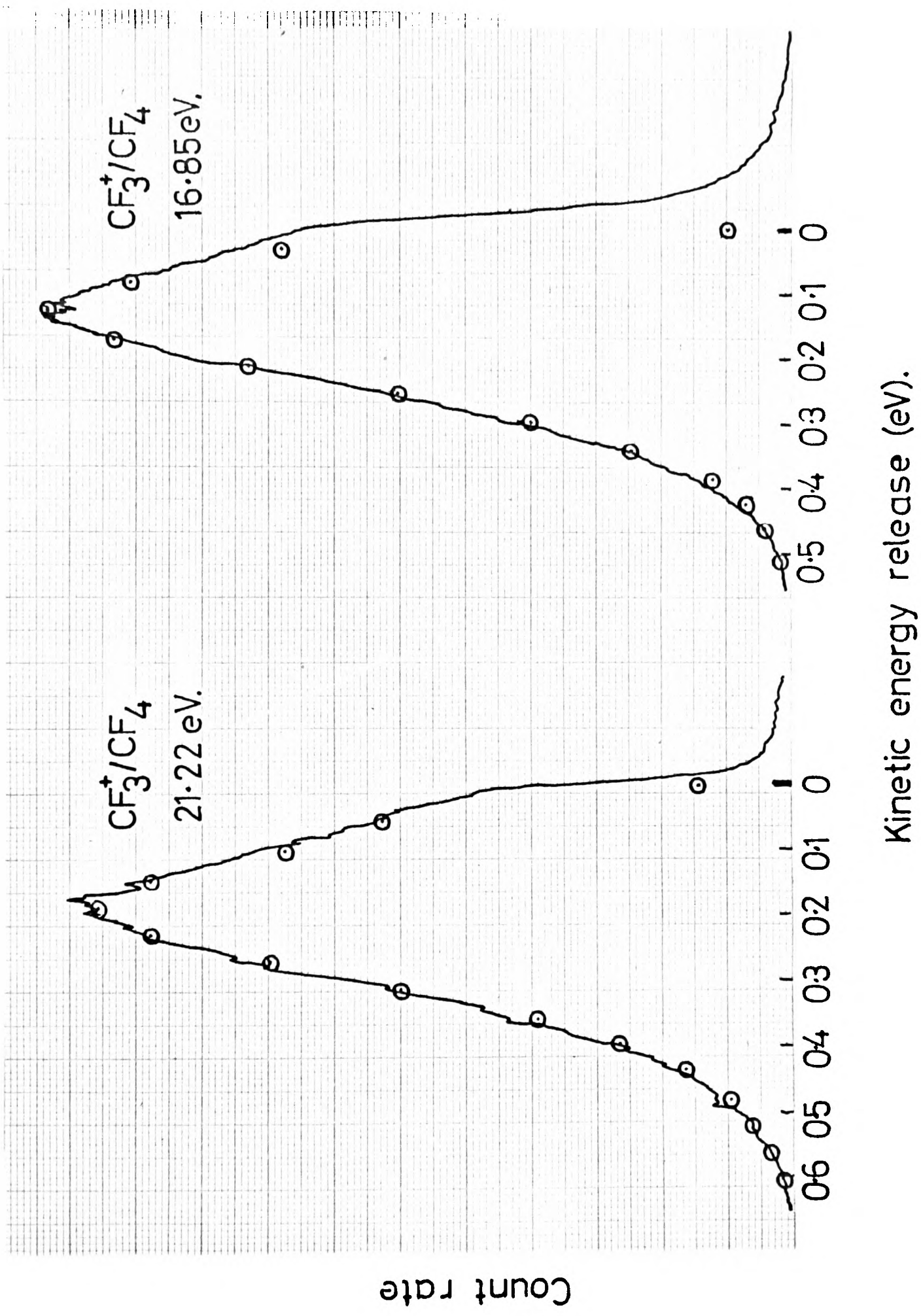

Figure 4.11

Computed CM kinetic energy releases in the fragmentation of CF_4^+.

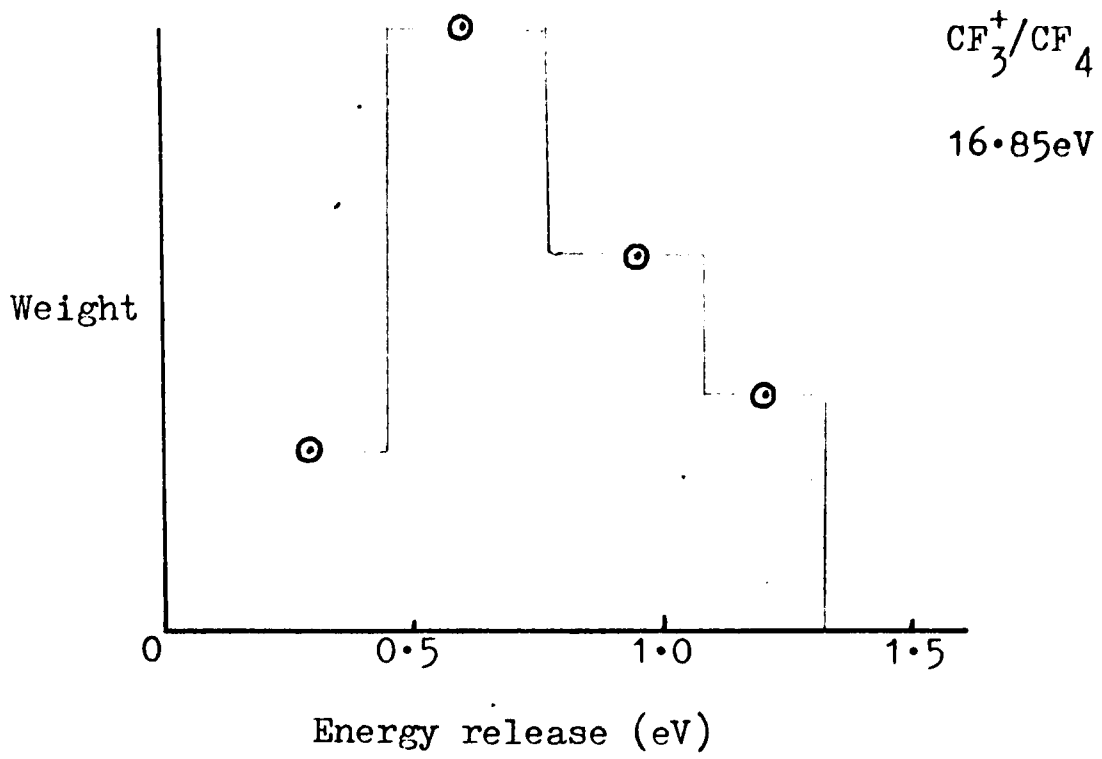

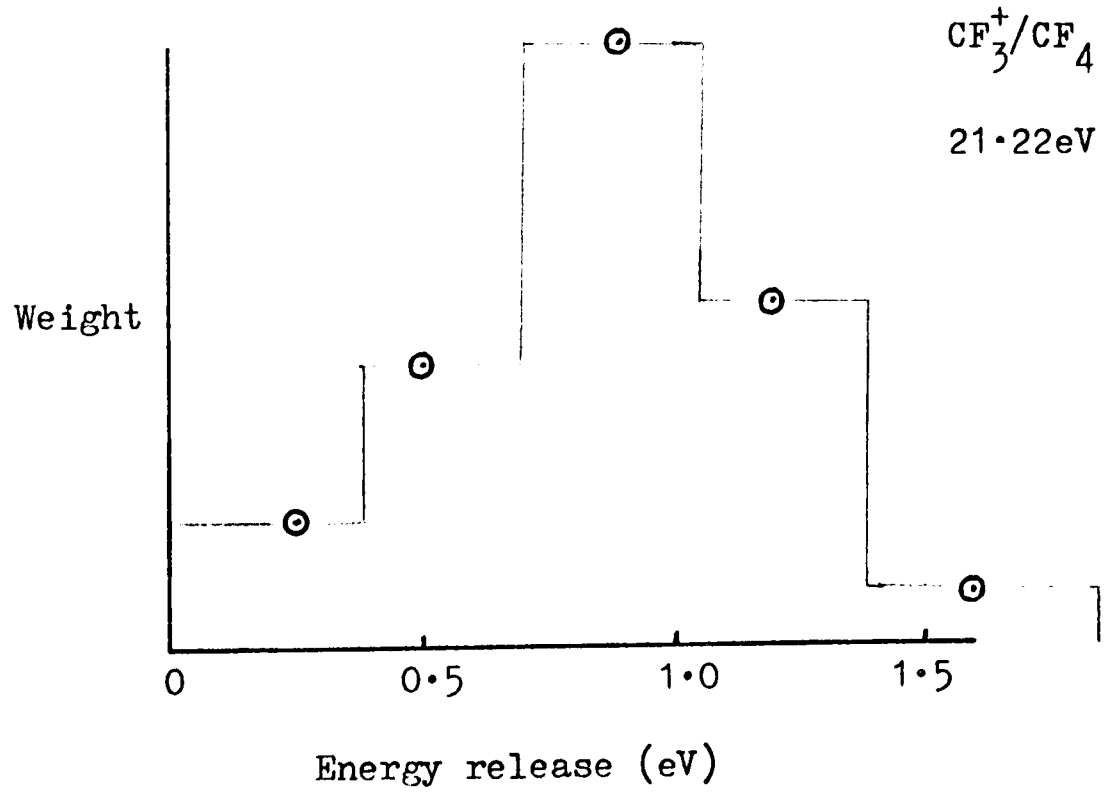

4.7 shows the photoelectron spectrum of C_2F_6 taken with neon resonance radiation.

RESULTS

(i) CF_4

The only significant fragment found in the photoionization of this compound was CF_3^+ in agreement with previous studies[123]. Taking values of ΔHf^o for CF_3[124], F and CF_4[125] reported in the literature together with the ionization potential of CF_3 derived by Walter et al.[129] the dissociation limit for the process

$$CF_4 \longrightarrow CF_3^+ + F$$

may be calculated as 14.74 eV. This is well below the onset of the lowest ionization potential band in the photoelectron spectrum (figure 4.9). The kinetic energy distributions of the CF_3^+ ion obtained using helium and neon radiation are shown in figure 4.10. Argon was used to calibrate the energy scale. These distributions were fitted well by the following sums of discrete energy releases in CM coordinates.

Helium radiation		Neon radiation	
Energy (eV)	weight	Energy (eV)	weight
0.25	0.12	0.3	0.20
0.5	0.20	0.6	0.50
0.78	0.50	0.95	0.30
1.2	0.45	1.2	0.20
1.6	0.05		

These distributions are plotted in figure 4.11 and the corresponding LAB distributions are plotted in fig. 4.10

superimposed on the experimental distributions. It can be seen from the photoelectron spectrum that neon radiation excites the ground state ionic level only. This is generally agreed to correspond to the loss of a t_1 fluorine lone pair electron[113, 139]. It seems unlikely that removal of a fluorine lone pair electron would give rise to a completely unbound ionic state. If the state is bound however it is apparent that the true adiabatic ionization potential of CF_4 must be much lower than the onset of the lowest photoelectron band. In this case dissociation of ions in this state may be occurring via a rapid vibrational predissociation process. The average excess energy available for dissociation in the $^2T_1$ state is about 1.5 eV if the calculated dissociation limit is correct. The kinetic energy releases for CF_3^+ on photoionization by neon radiation (which only populates the $^2T_1$ state) suggest that nearly half of this energy is going into translational energy of products, which is inconsistent with a statistical vibrational predissociation as usually formulated[140]. It would correspond to a value of α in Franklin's formula of about 0.05. Continuous absorbtion of UV radiation by CF_4 has been observed to occur from 15.0 eV upwards and this has been ascribed to the process

$$CF_4 \longrightarrow CF_3^+ + F^- \quad [141].$$

The calculated dissociation limit for this process is 11.1 eV (using $\Delta Hf^o(F^-)$ given in reference 125). Kisner[142] however ascribes this onset of continuous absorbtion to the appearance potential of CF_4^+, pointing out that the lack of observed CF_4^+ ions in mass spectrometry at higher ionization energies suggests that $A(CF_3^+) - I(CF_4)$ cannot be much greater than a few tenths of an electron volt. Kaufman et al.[143] have postulated a

mechanism of dissociation in which excitation to a steeply rising repulsive section of a CF_4 potential surface causes dissociation to CF_3 + F with subsequent ionization of the CF_3. They object to the concept of ionization to a steeply repulsive part of a CF_4^+ surface as their calculated dissociation limit is close to the appearance potential of CF_3^+. It seems likely that their thermochemical data are in fact in error. They calculate that the lowest two CF_4^+ states are bound. This is, however, not incompatible with complete dissociation of these states as populated by photoionization. The explanation of Kaufman et al. for the non-appearance of CF_4^+ in mass spectroscopy is clearly in error. Such an autoionizing direct dissociation as they appear to be suggesting could only occur over a narrow band of ionization energies corresponding to direct population of the CF_4 state involved.

The distribution of kinetic energy release upon ionization by helium peaks at a higher energy (about 0.8 eV) and extends to higher energies than the neon excited distribution. Higher states of the ion are therefore giving higher kinetic energy releases upon fragmentation which is consistent with the higher excess energy available. Both distributions seem to suggest a reverse activation energy of about 0.5 eV in going to products.

(ii) $\underline{CClF_3}$

The photoionization mass spectra of $CClF_3$ as determined using helium and neon resonance radiation are as follows:

Ion	He I abundance	Ne I abundance
CF^+	0.5(see below)	-
CF_2^+	0.068	-
CF_3^+	1	1
$CClF_2^+$	0.39	0.31

Small amounts of parent ion were also detected. Neon resonance radiation can populate the $\tilde{X}$, $\tilde{A}$, $\tilde{B}$ states and half of the $\tilde{C}$ state. Calculated dissociation limits for the following processes are:

$CClF_3 \longrightarrow CF_3^+ + Cl$	13.00 eV
$CClF_3 \longrightarrow CClF_2^+ + F$	14.3 eV
$CClF_3 \longrightarrow CF_2^+ + FCl$	16.56 eV
$CClF_3 \longrightarrow CF_2^+ + Cl + F$	18.5 eV
$CClF_3 \longrightarrow CF^+ + F + FCl$	19.43 eV
$CClF_3 \longrightarrow CF^+ + Cl + F_2$	20.43 eV

These values depend upon quoted values of $\Delta Hf^o(CClF_3)$[126, 127], $\Delta Hf^o(CClF_2)$[128], $\Delta Hf^o(CF_3)$[124], $\Delta Hf^o(Cl)$[125], $\Delta Hf^o(CF_2)$[130, 138], $\Delta Hf^o(FCl)$[132], $\Delta Hf^o(CF)$[137], $I(CClF_2)$[128], $I\ (CF_3)$[129], $I\ (CF_2)$[131, 138] and $I\ (CF)$[129].

The value of $I\ (CClF_2)$ is based upon the appearance potential of $CClF_2^+$ from CCl_2F_2 and consequently is probably too high an estimate. The ionization potentials of CF, CF_2 and CF_3 all appear to have been determined with a fair degree of certainty. These dissociation limits are in agreement with the observed fragmentation patterns; the calculated lower limit for production of CF_2^+ is only just below the ionizing energy of neon radiation and it is therefore not surprising that no CF_2^+ is observed on photoionization at 16.85 eV. The various fragments are now discussed individually.

Figure 4.12

Computed CM kinetic energy releases for the fragmentation of $CClF_3^+$ to give CF_3^+.

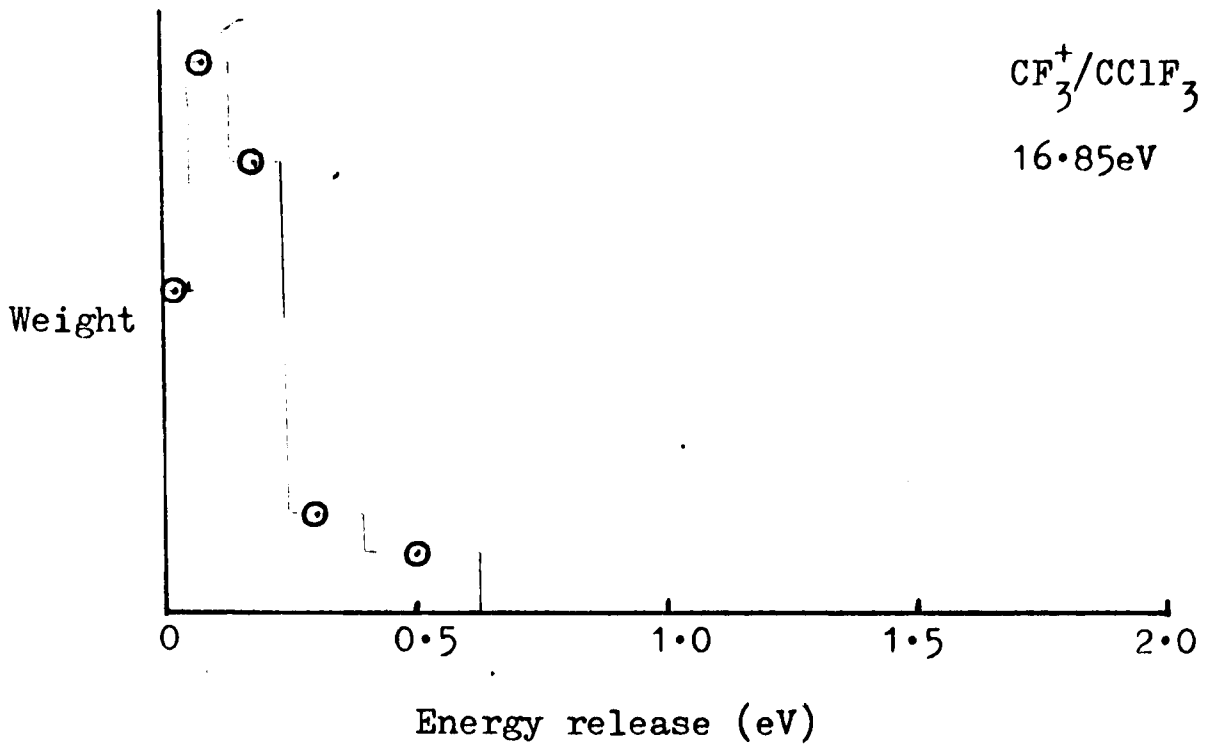

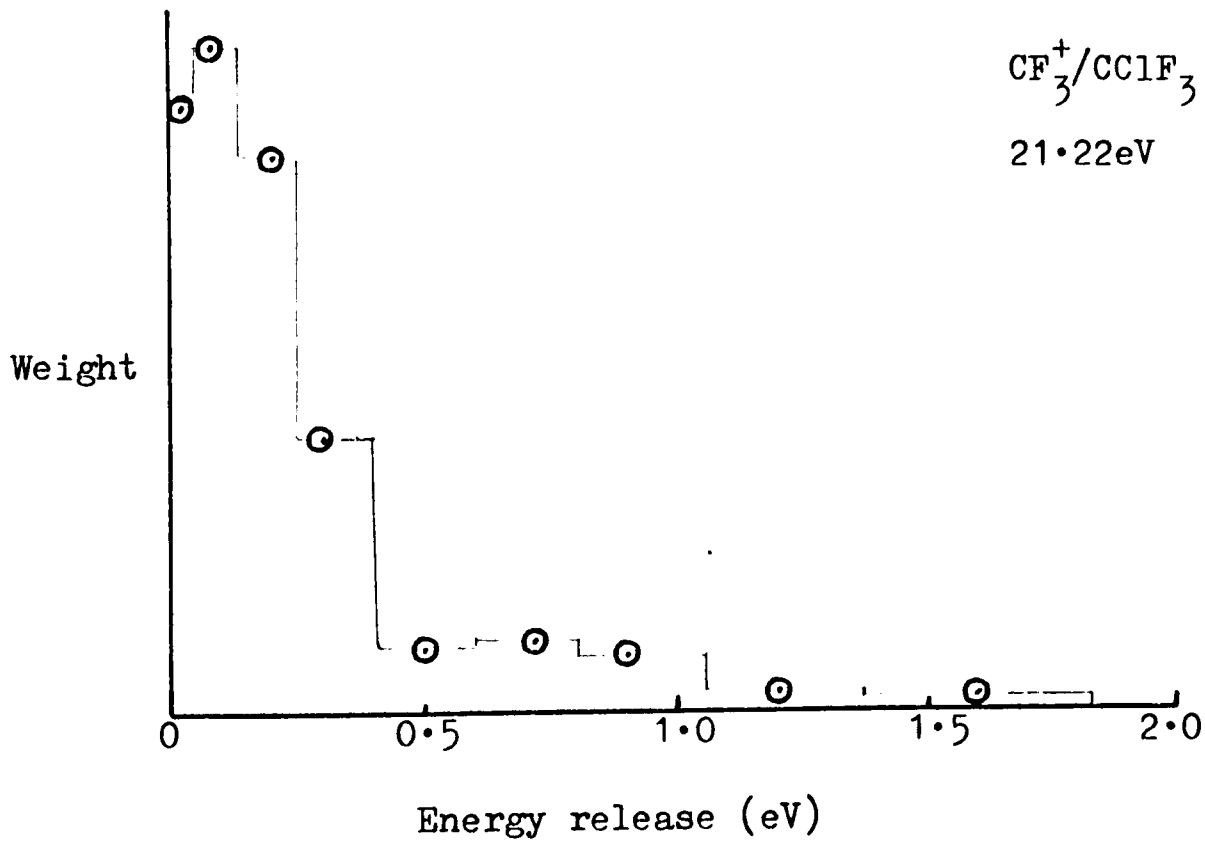

$\underline{CF_3^+}$. The computed CM energy release distributions for loss of chlorine from $CClF_3^+$ are shown in figure 4.12. With both radiation sources they peak strongly at low energies (about 0.1 eV). For He I radiation the distribution is apparently wider and a small but significant band of energy release is seen out to ~1.5 eV. It seems likely therefore that production of this ion is mainly occurring from the $\tilde{X}$ state of the ion - corresponding to loss of a chlorine lone pair electron. The calculated dissociation limit of 13.0 eV is probably too high as the onset of the lowest photoelectron band is at 12.7 eV. The proximity of the dissociation limit and the first ionization potential suggest however that virtually complete dissociation of the ionic ground state is occurring within the experimental time scale of about 10^{-6} seconds even when the excess energy available is very low. This is borne out by the experimental energy distribution. Only a very small amount of the parent ion was detected. No other dissociation limit is below the highest energy of the $\tilde{X}$ band so it may be assumed that loss of chlorine is the only process occurring from this band. It is apparent from the He I distribution of energy release that the states above 16.85 eV ($\tilde{D}$ and $\tilde{E}$) must be at least partially dissociating to give CF_3^+ with a higher energy release than that from lower states. All the bands in the PE spectrum above 16.85 eV have been associated with fluorine lone pair or F-C bonding orbitals. The high kinetic energy release for loss of a chlorine atom when these bonds are excited shows that the corresponding ionic states are probably fragmenting via internal conversion to lower states leading to vibrational predissociations involving large excess energies. (This is therefore a case where the character of the orbital from which an electron is

Figure 4.13

Computed CM energy releases for the fragmentation of $CClF_3^+$ to give $CClF_2^+$.

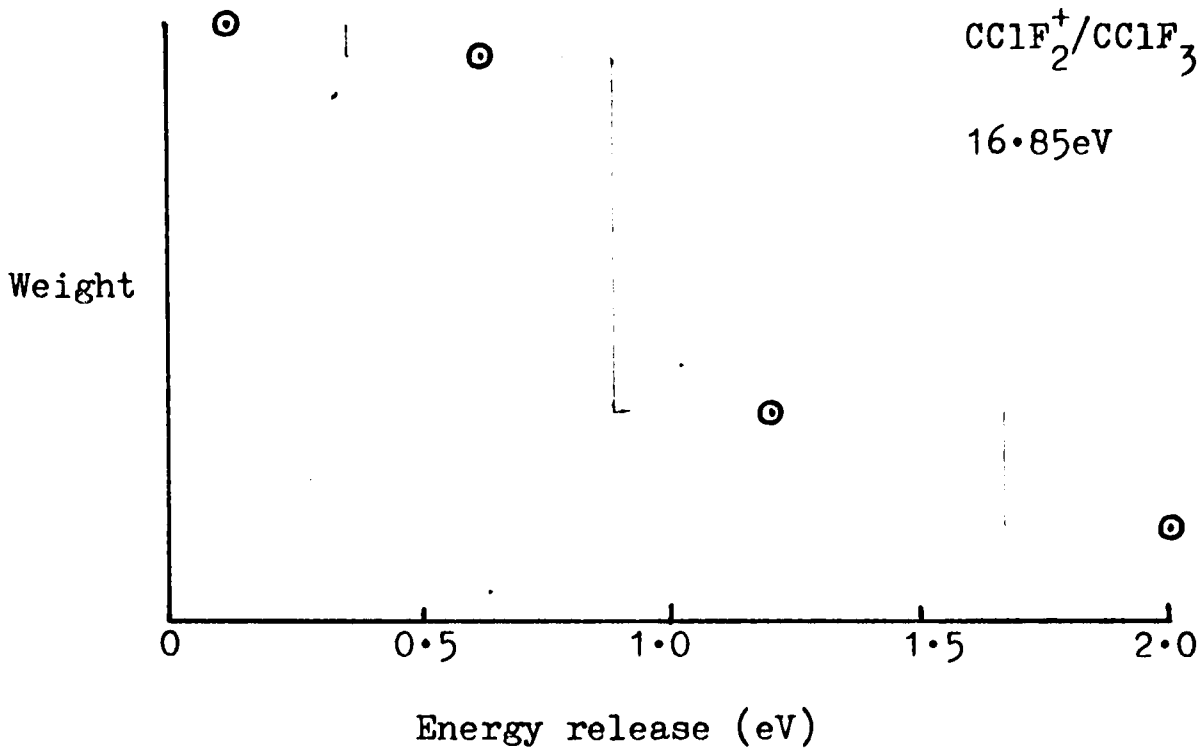

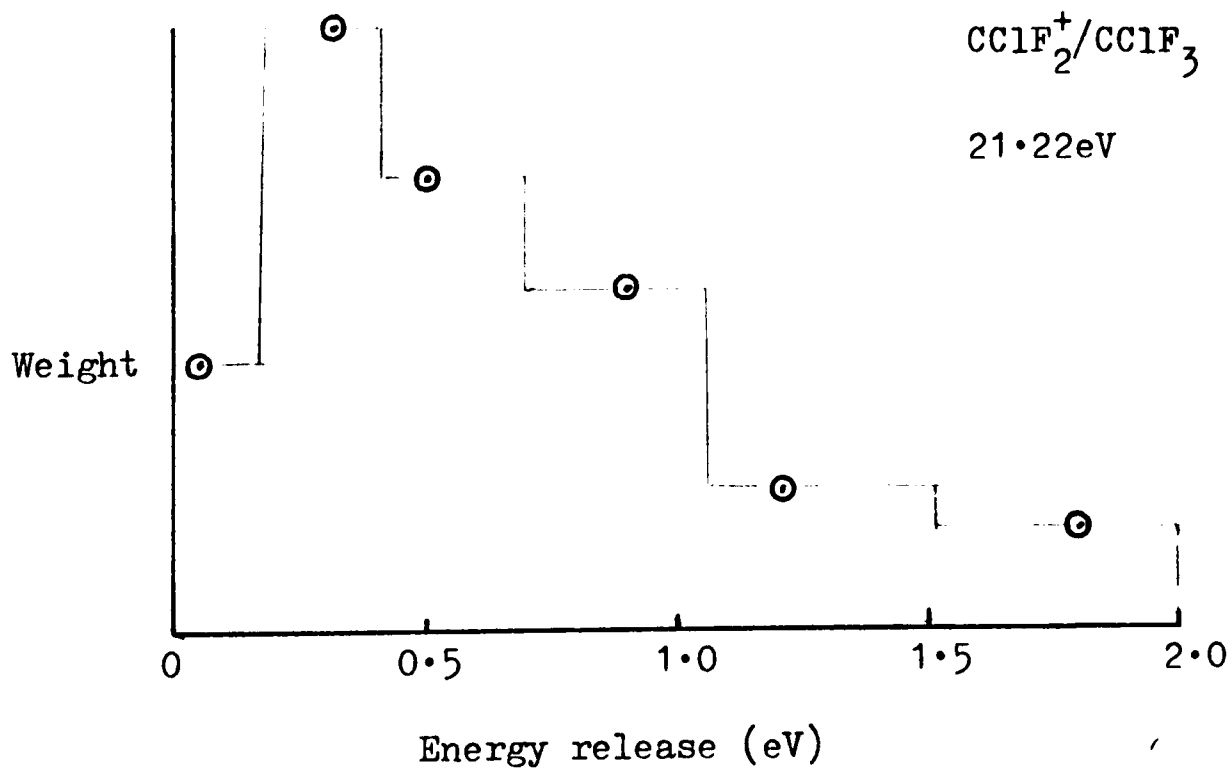

removed does not necessarily determine the fragmentation pattern.) The excess energy of the $\tilde{D}$ band relative to the lowest dissociation limit corresponding to production of CF_3^+ is at least 4.5 eV. If ions in the state corresponding to this band are dissociating via internal conversion to the ground state this would be consistent with the band of energy release at about 0.8 eV seen in the 21.22 eV energy release curve.

$\underline{CClF_2^+}$. As stated above the exact value of the dissociation limit for formation of this ion is uncertain but it probably lies between the $\tilde{X}$ and $\tilde{A}$ bands of the photoelectron spectrum. The derived kinetic energy release distributions are shown in figure 4.13. These are not inconsistent with statistical predictions of an exponential fall-off in energy release. The ratio of peak areas in the photoelectron spectrum of the $\tilde{A}$, $\tilde{B}$ and $\tilde{C}$ states to that of the $\tilde{X}$ state is about 2:3. If this is compared with the measured abundance ratio for $CClF_2^+$:CF_3^+ of 1:3 in the neon I mass spectrum it is apparent that some at least of the ions in the A, B and C states are probably dissociating via the ground state to give CF_3^+. The abundance of other ions in the HeI spectrum is very low and consequently the $\tilde{D}$ and $\tilde{E}$ states must also be giving CF_3^+ and possibly $CClF_2^+$ fragments.

$\underline{CF_2 \text{ and } CF^+}$. CF_2^+ ions could either be the product of a primary dissociation to give $CF_2^+ + FCl$, for which the dissociation limit lies just below the $\tilde{C}$ band, or could arise from a secondary dissociation of $CClF_2^+$. This latter process has a dissociation limit above the $\tilde{D}$ band so only $CClF_2^+$ ions produced from the ionization represented by the $\tilde{E}$ band could be contributing. The energy release distribution of CF_2^+ is not incompatible with this. (It may be remembered that the product

of a secondary dissociation will carry at least a proportion of its own parent ion's energy.)

The computed CM energy release distribution assuming a primary fragmentation shows a sharp peak at 0.1 eV and falls off quasi-exponentially which would fit in with the statistical models of dissociation. CF^+ was observed in the He I photoionization of $CClF_3$ but only with high kinetic energy (in a band from about 0.3 to 0.55 eV). The apparent abundance was low (about 0.5%) but in fact the number of counts due to this ion at the energies where it was observed were about the same as for CF_2^+. As there is considerable energy discrimination in the spectrometer it is felt that 0.5% is too low a value for the abundance of CF^+. It is clear that this ion must arise from the $\tilde{E}$ state of the parent ion and apparently, if the calculated dissociation limit is correct, most of the available energy for this fragmentation appears as translation of the products.

(iii) $\underline{CCl_2F_2}$

The fragmentation pattern of the ion is the most complicated of any of the compounds studied herein. In fact it is lucky that CCl_2^+ is only of vanishingly small abundance in the photoionization mass spectrum of CCl_2F_2 at 21.22 eV and 16.85 eV as it would not be possible to distinguish it clearly from $CClF_2^+$ under conditions allowing the recording of kinetic energy release spectra. The measured relative abundances of fragment ions are:

Ion	He I abundance	Ne I abundance
CF^+	?	-
CF_2^+	0.03	-
$CClF^+$	0.02	-
$CClF_2^+$	1.0	1.0
CCl_2F^+	0.18	0.15

The presence of CF^+ is uncertain and if it is formed at all it is at very low abundance. The close similarity of products from 21.22 eV and 16.85 eV photoionization is to be expected - only the high energy shoulder of the $\tilde{E}$ band and the weak $\tilde{F}$ band occur above 16.85 eV in the photoelectron spectrum. Calculated dissociation limits for processes giving these fragments are:

$CF_2Cl_2 \longrightarrow CCl_2F^+ + F$	N.A.
$CF_2Cl_2 \longrightarrow CClF_2^+ + Cl$	12.55 eV (appearance potential)*[128]
$CF_2Cl_2 \longrightarrow CCl_2^+ + F_2$	17 eV
$CF_2Cl_2 \longrightarrow CClF^+ + ClF$	5.91 eV + I (CClF)
$CF_2Cl_2 \longrightarrow CF_2^+ + Cl_2$	14.55 eV
$CF_2Cl_2 \longrightarrow CF_2 + Cl + Cl$	16.5 eV
$CF_2Cl_2 \longrightarrow CF^+ + F + Cl_2$	17.5 eV

(* This is the appearance potential upon which the value of $I(CClF_2)$ was based in the calculation of the dissociation limit for $CClF_3 \longrightarrow CClF_2^+$.)

Apart from data used in calculations of dissociation limits for $CClF_3$ literature values of $\Delta Hf^o(CF_2Cl_2)$[127], $\Delta Hf^o(CCl_2^+)$[136] and $\Delta Hf^o(CClF)$[133] were used in calculating these values. Unfortunately the values of $\Delta Hf^o(CCl_2F)$, I (CCl_2F) and I (CClF) do not appear to be known. Comparison of known

ionization potentials of CF_2, CF, CCl_2 and $CClF_2$ suggest that I (CFCl) will be somewhere in the range 9-10 eV which would place the lowest dissociation limit for production of $CClF^+$ at 15-16 eV.

$\underline{CClF_2}^+$. It is expected that the dissociation limit for production of $CClF_2^+$ will be the lowest one for the $CCl_2F_2^+$ ion even though the value for formation of CCl_2F^+ is unknown. This is because loss of chlorine would be expected to be an energetically more favourable process than loss of fluorine. Assuming this to be the case the measured appearance potential[128] of $CClF_2^+$ from CCl_2F_2 must be higher than the dissociation limit by at least 0.35 eV otherwise the low ionization potential part of the $\tilde{X}$ band of the photoelectron spectrum would be below the limit. As no parent ion is observed this cannot be the case. The measured kinetic energy release distribution of the ion peaks at low energy (0.1 eV) so it is entirely possible that the dissociation limit is only just below the ionic ground state in energy. Note that these considerations suggest that the dissociation limit for production of $CClF_2^+$ from $CClF_3$ should be at least 0.35 eV lower than quoted as the value is based upon the measured appearance potential of $CClF_2^+$ from CCl_2F_2. The CM kinetic energy release distributions for the fragmentation to give $CClF_2^+$ are essentially the same for neon and helium resonance radiation. The distribution for helium I photoionization does show a longer tail out to high energy release but this could be an experimental artefact. Thus while the neon distribution was fitted with a rather high weight energy release at 0.5 eV the helium distribution was

Figure 4.14

Computed CM energy releases for the fragmentations of $CCl_2F_2^+$ to give $CClF_2^+$ and CCl_2F^+.

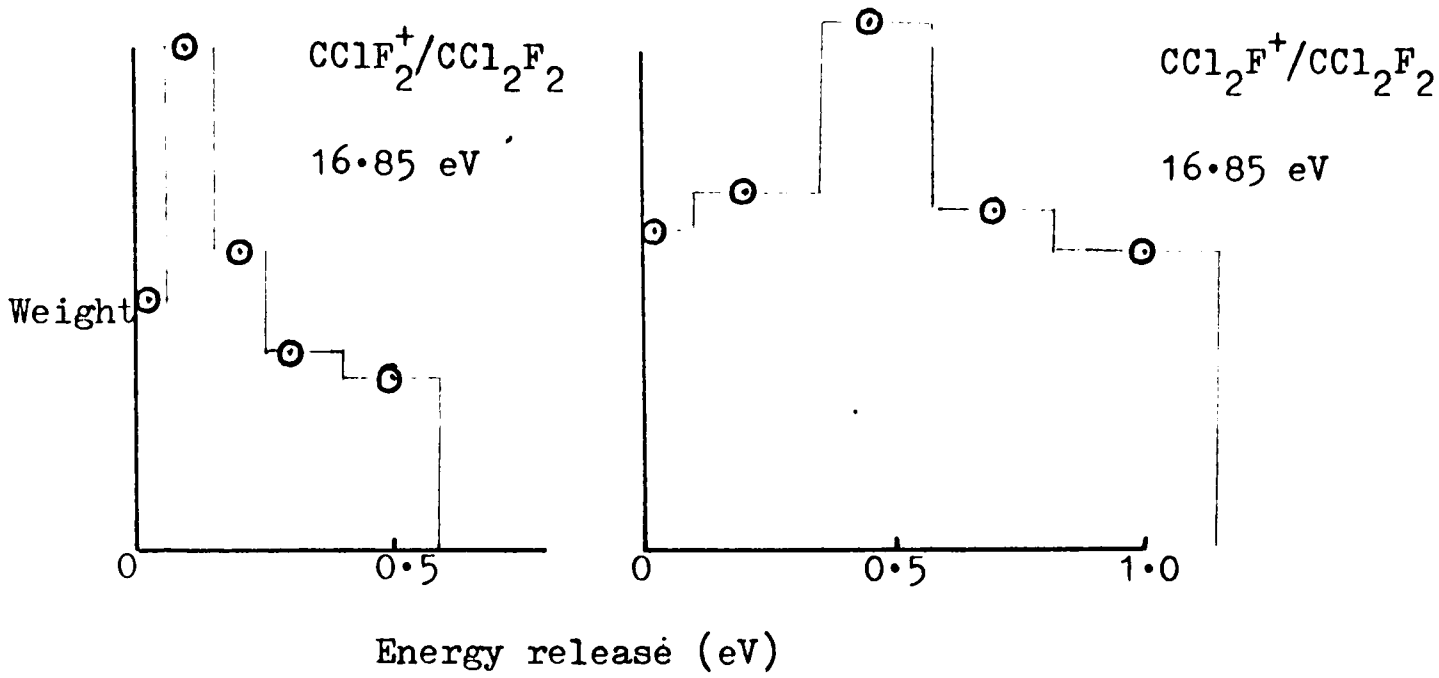

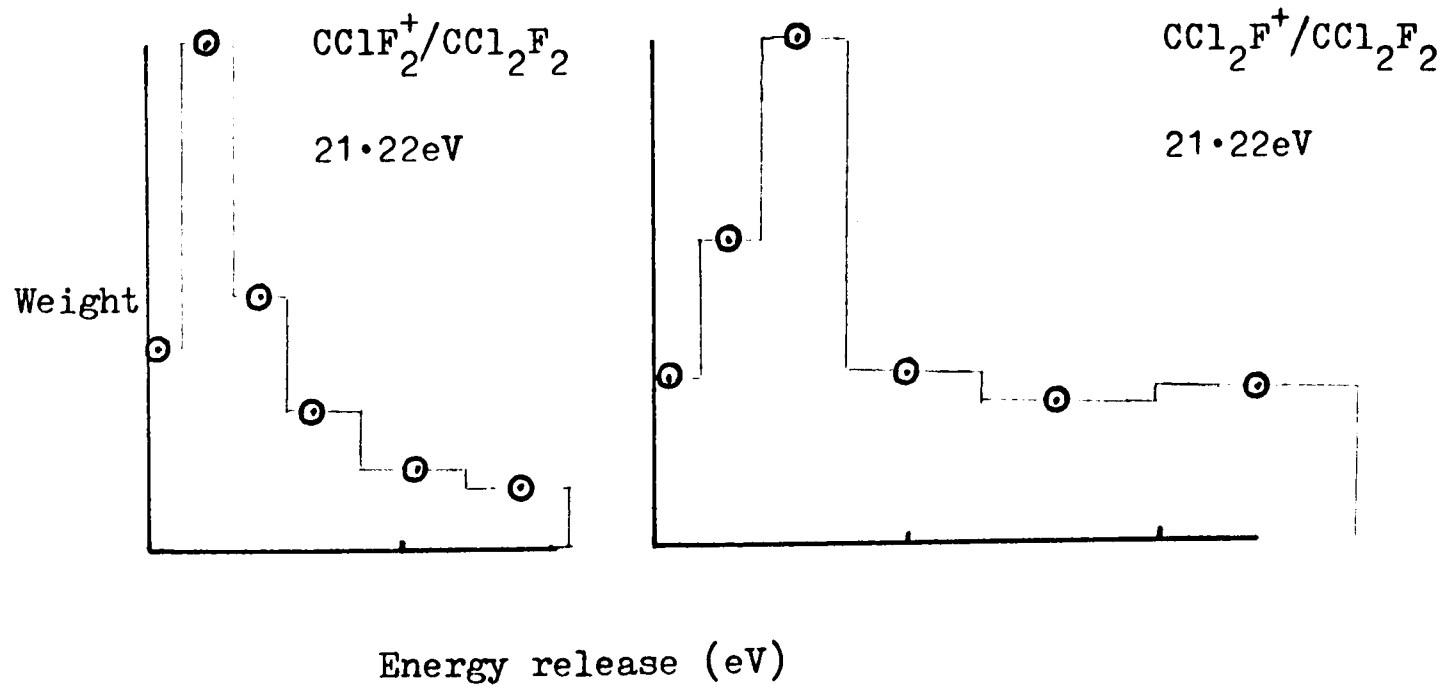

fitted with lower weight releases at 0.5 and 0.7 eV. For the unfavourable mass ratio between the fragment ion and parent ion in this case it is uncertain whether there is in fact any significant difference in the energy release distributions. Certainly the two experimental curves are very similar. The calculated CM energy release distributions that fit the experimental curves for $CClF_2^+$ are shown in figure 4.14. These show that any reverse activation energy for the fragmentation is quite low as they peak at low energy.

$\underline{CCl_2F^+}$. For this ion the results are very different. The mass ratio of fragment to parent is even less favourable than in the last case but even so it is plain from the experimental distributions that a large energy release is occurring. In fact to fit the observed experimental distributions requires a broad band of discrete CM releases of similar weightings. Agreement between the actual values used to fit the 21.22 eV and 16.85 eV distributions is less good this time so less significance can be given to the actual computed distributions which are shown in figure 4.14. In both cases significant energy release out to at least 1 eV is indicated and the distributions do not even approximate to a statistical exponential fall off. As has already been stated the position of the relevant dissociation limit cannot be fixed but it probably lies a volt or two above the ground ionic state. The minor fragments all appear only with 21.22 eV excitation despite the fact that the lower dissociation limits for production of CF_2^+ and $CFCl^+$ are probably well below 16.85 eV. This suggests that they are products of secondary reaction of highly excited

primary fragments. Only the weak $\tilde{F}$ band in the photoelectron spectrum is above the dissociation limit for formation of CF^+. It is unlikely that this would form in a primary reaction but it could represent loss of Cl_2 by CCl_2F^+. Both CF_2^+ and $CClF^+$ show kinetic energy distributions out to about 0.35 eV.

(iv) $\underline{CCl_3F}$

The relative abundances of fragments formed in the photoionization of this compound were:-

	He I	Ne I
Ion	Abundance	Abundance
CF^+	0.02	-
$CClF^+$	0.09	0.03
CCl_2^+	0.05	-
CCl_2F^+	1.0	1.0
CCl_3^+	0.04	0.05

Calculated dissociation limits are

$CCl_3F \longrightarrow CCl_3^+ + F$	12.9 eV
$CCl_3F \longrightarrow CCl_2F^+ + Cl$	N.A.
$CCl_3F \longrightarrow CCl_2^+ + FCl$	15.5 eV
$CCl_3F \longrightarrow CCl_2^+ + F + Cl$	17.7 eV
$CCl_3F \longrightarrow CClF^+ + Cl_2$	3.3 eV + I(CClF)
$CCl_3F \longrightarrow CF^+ + Cl + Cl_2$	15.88 eV

Values for $\Delta Hf^o\ CCl_3$[134], $\Delta Hf^o CCl_3F$[126], and $I(CCl_3)$[135] were again taken from the literature. Again sufficient thermodynamic data is not available for CCl_2F^+. The lower dissociation limits for formation of CF^+ and CCl_2^+ as well as that presumed for $CClF^+$ (see the previous section on CCl_2F_2) are all below 16.85 eV. Only the $CClF^+$ value (~12.5 - 13.5) is lower than the energy of the $\tilde{D}$ band in the spectrum however which is the

Figure 4.15

Computed CM energy releases for the fragmentations of CCl_3F^+ to give CCl_2F^+ and CCl_3^+.

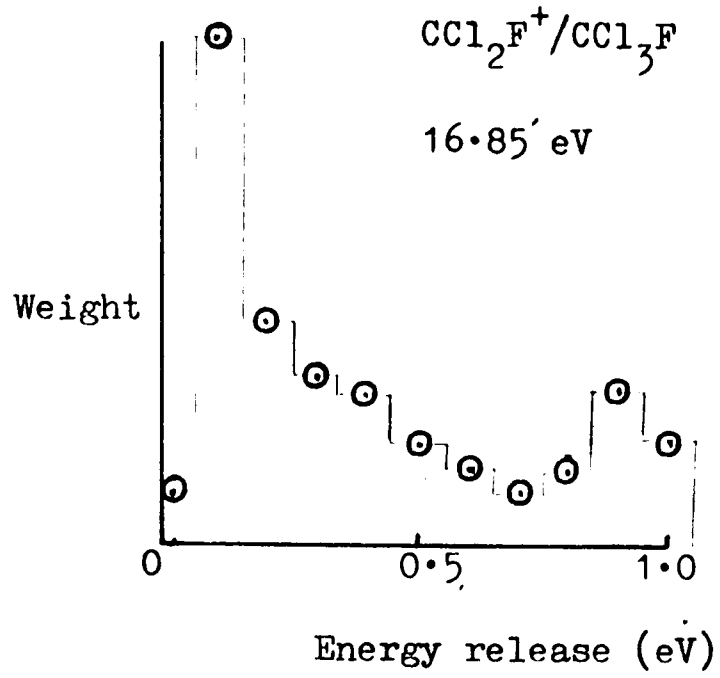

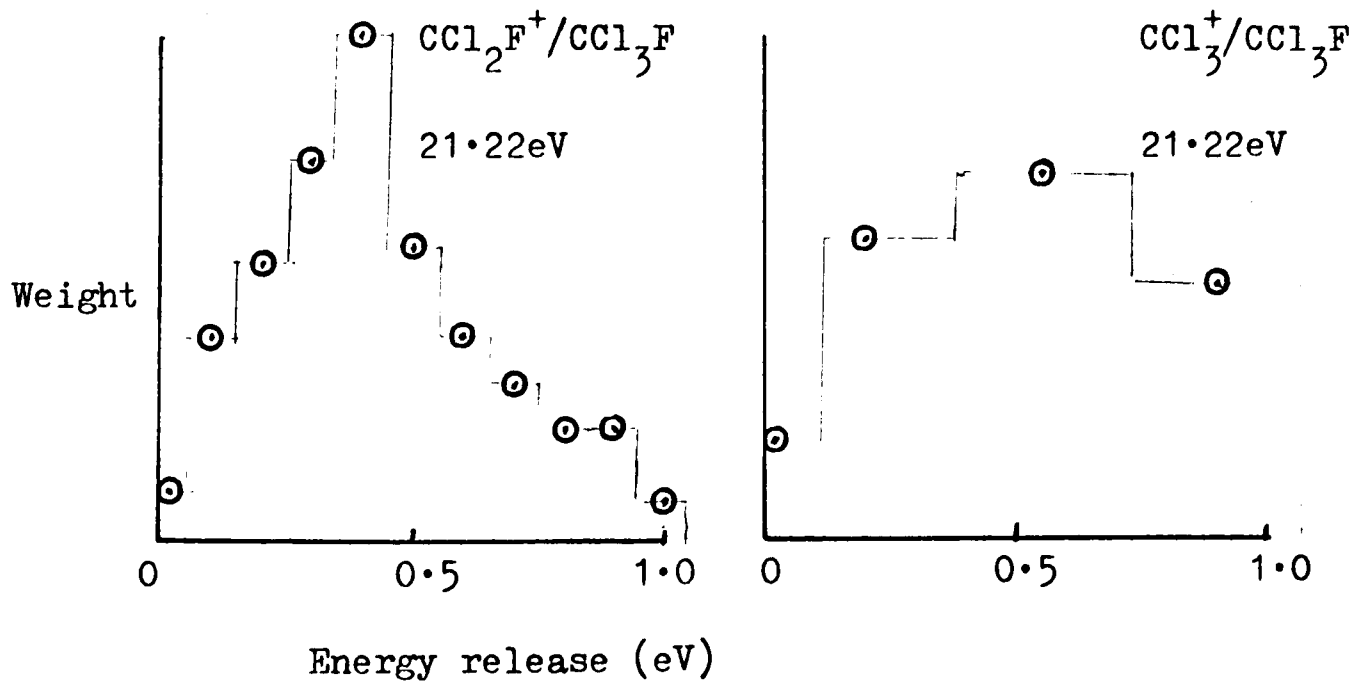

highest band excited by neon radiation. The non-occurrence of CF^+ and CCl_2^+ in the neon photoionization mass spectrum is thus readily explained. $CClF^+$ is observed with neon radiation but only very weakly.

$\underline{CCl_2F^+}$. This is presumed to be the ion associated with the lowest dissociation limit representing as it does the loss of a chlorine atom by the parent ion. As no parent ion is observed it may be inferred that the dissociation limit for production of CCl_2F^+ lies below 11.5 eV, the onset of the photoelectron spectrum. Calculated CM energy release distributions that fit the observed distribution of energy for this ion are shown in figure 4.15. There is another peak at 0.9 eV in the 16.85 eV distribution and a smaller peak in the 21.22 eV distribution at the same point. It would seem reasonable to suppose that this is due to fragmentation of ions in the state corresponding to the $\tilde{D}$ band of the photoelectron spectrum which must represent an excess energy of at least 3.5 eV over the dissociation limit corresponding to ground state CCl_2F^+. The fact that no even higher kinetic energy releases occur when higher ionic states are populated by He I radiation suggests that these states may be fragmenting to higher dissociation limits giving electronically excited products. Both distributions extend to 1 eV release with a peak at 0.1 eV for 16.85 eV excitation and a peak at 0.4 eV for 21.22 eV excitation. As this ion accounts for 85% of all fragments even with 21.22 eV excitation, it is inferred that even the highest excited ionic states (corresponding to the $\tilde{E}$ and $\tilde{F}$ bands of the PE spectrum) are mainly dissociating to give CCl_2F^+ and Cl. This fact is somewhat

surprising as the gap between ionic states is larger for this compound than any of the others mentioned so far making radiationless transitions to the ground ionic state apparently less probable. Of course the possibility of fragmentation to give CCl_2F^+ and Cl in excited electronic states with correspondingly higher dissociation limits cannot be ruled out.

$\underline{CCl_3^+}$. This ion is only seen in relatively low abundance despite the fact that the dissociation limit corresponding to its formation is between the energies of the four lowest ionic states corresponding to loss of a chlorine lone pair electron. The energy distributions for this ion are very similar for 21.22 eV and 16.85 eV excitation and show a broad release of energy similar to that observed for loss of fluorine in the other compounds. This calculated CM distribution is shown in figure 4.15.

$\underline{CCl_2^+ \text{ and } CClF^+}$. These ions both show similar CM energy distributions peaking at about 0.4 eV energy release. If they are primary fragments this is not inconsistent with the high energy difference between the dissociation limits and the lowest ionic states above them.

$\underline{CF^+}$. The LAB kinetic energy release distribution for this ion is very narrow showing the ions to have energies only of 0.1 eV and less. This is consistent with the postulate that they are formed by secondary fragmentation of a heavy primary fragment ion, probably CCl_2F^+.

(v) $\underline{C_2F_6}$

The relative abundances of fragments obtained for

photoionization of C_2F_6 were:

Ion	He I Abundance	Ne I Abundance
CF^+	0.1	-
CF_2^+	0.03	0.012
CF_3^+	1.0	0.63
$C_2F_5^+$	0.35	1.0

Calculated dissociation limits are

$C_2F_6 \longrightarrow C_2F_5^+ + F$	15.01 eV
$C_2F_6 \longrightarrow CF_2^+ + CF_3$	13.34 eV
$C_2F_6 \longrightarrow CF_2^+ + CF_4$	14.00 eV
$C_2F_6 \longrightarrow CF_2^+ + CF_3 + F$	19.56 eV
$C_2F_6 \longrightarrow CF^+ + CF_4 + F$	16.9 eV
$C_2F_6 \longrightarrow CF^+ + CF_3 + F_2$	21.22 eV

These values depend upon published values for $\Delta Hf^o\ C_2F_6$[131], $\Delta Hf^o\ C_2F_5$[131,138] and I (C_2F_5)[131,138] as well as values already quoted.

It can be seen immediately that at least part of the observed CF_2^+ intensity is the result of a direct dissociation to give $CF_2^+ + CF_4$ as only this process for formation of CF_2^+ has a dissociation limit below 16.85 eV. The fact that this process represents a considerable geometrical rearrangement presumably accounts for the low abundance of CF_2^+. The two possible secondary fragmentations that could give this ion both correspond to the dissociation limit of 19.56 eV which is higher in energy than almost all

of the measured photoelectron intensity.

Lifshitz and Long pointed out that the observed relative abundances of CF_3^+ and $C_2F_5^+$ in the mass spectrum of C_2F_6 could not be accounted for by QET[67]. They suggested that an excited state of $C_2F_5^+$ was decomposing directly and preferentially to $C_2F_5^+$ rather than to CF_3^+ via the ground state. This has since been confirmed and one of the states giving rise to $C_2F_5^+$ fragments has been characterized as that corresponding to the $\tilde{A}$ band in the photoelectron spectrum[31]. The results presented here are consistent with this finding as the observed ratio of $C_2F_5^+/CF_3^+$ at 16.85 eV is about the same as the ratio of the $\tilde{A}$ and $\tilde{X}$ band areas in the photoelectron spectrum taken with Ne I radiation (figure 4.7). The fact that CF_3^+ becomes the major product when He I radiation is used shows that even higher states of the ion do decompose to give CF_3^+. These findings are consistent with the simple hypothesis that the fragmentation observed will be determined by the bonding character of the orbital from which an electron is photoionized. Thus the lowest, A_{1g}, ionic state corresponds to the loss of a C-C sigma bonding electron (see figure 4.8a) and gives rise to C-C fission. The next, E_g, state corresponds to loss of a C-C antibonding and C-F bonding electron and C-F fission is observed from this state.

$\underline{CF_3^+}$. The energy distributions of this ion are similar for neon and helium radiation. Computed CM releases that fit the observed distributions are

21.22 eV photoionization		16.85 eV photoionization	
Energy (eV)	weight	Energy (eV)	weight
0.05	1.0	0.05	1.0
0.1	0.5	0.2	0.62
0.2	0.5	0.4	0.25
0.4	0.25		

This is rather surprising as it is known that widely spaced states of the ion are giving rise to CF_3^+ ions and whereas Neon I radiation excited only the lowest of these states, Helium I radiation will excite the higher ones as well. This is not the result that would be expected from QET. The excess energy of the higher states relative to the dissociation limit is very high and a large energy release would be expected if these were fragmenting via the ground state. It seems likely that these higher states are decomposing to a higher limit corresponding to electronically excited products.

$C_2F_5^+$. The kinetic energy distributions of this ion may be fitted by the following discrete energy releases.

16.85 eV photoionization		21.22 eV photoionization	
Energy (eV)	Weight	Energy (eV)	Weight
0.5	0.7	0.5	0.7
0.9	0.4	0.9	0.3
		1.2	0.25

The work of Simm et al. has shown that $C_2F_5^+$ is formed in the band of energies from about 15.5 - 17.5 eV. It may be inferred that the ionic states above that corresponding to the $\tilde{A}$ band in the photoelectron spectrum are giving rise to the higher energy component of the energy release at 21.22 eV. The excess energy at the peak of the $\tilde{A}$ band relative to the computed dissociation limit is about 1.5 eV and as was the case in CF_4 it is inferred that in the fragmentation of this ionic state roughly half of the energy available is going into translation. The fact that dissociation to give $C_2F_5^+$ is preferred to internal conversion to the ground state is consistent with this finding. A process with such a large kinetic energy release would be expected to be a fast one and apparently it is significantly quicker than radiationless

conversion to the ground state. The occurrence of even greater energy release upon 21.22 eV photoionization is consistent with the higher excess energies involved in the higher ionic states. The fact that above 17.5 eV production of CF_3^+ recommences suggests that a dissociation limit leading to electronically excited CF_3^+ or CF_3 lies in this region.

$\underline{CF_2^+ \text{ and } CF^+}$. It has already been stated that CF_2^+ is probably a primary fragment. The kinetic energy distribution of this ion shows a small energy release to be occurring of the order of 0.1 eV. It would appear that a slow vibrational pre-dissociation of ionic states above the dissociation limit of 14.00 eV is competing to a small extent with the process giving CF_3^+. The low probability of this process is not unexpected; a considerable rearrangement of vibrational energy can be seen to be necessary to bring about such a decomposition. The production of CF^+ has a calculated lower dissociation limit of 16.9 eV which is higher than Noutary's quoted appearance potential of 16.75 eV[146]. Very little, if any, kinetic energy release appears to occur on production of CF^+ which is perhaps more consistent with a secondary fragmentation process of $C_2F_5^+$ ions.

(vi) $\underline{SF_6}$

The abundances of observed fragment ions produced from SF_6 were

	He I	Ne I
Ion	Abundance	Abundance
SF_3^+	0.15	-
SF_4^+	0.12	-
SF_5^+	1.0	1.0

Figure 4.16

The photoelectron spectrum of sulphur hexafluoride from reference 86.

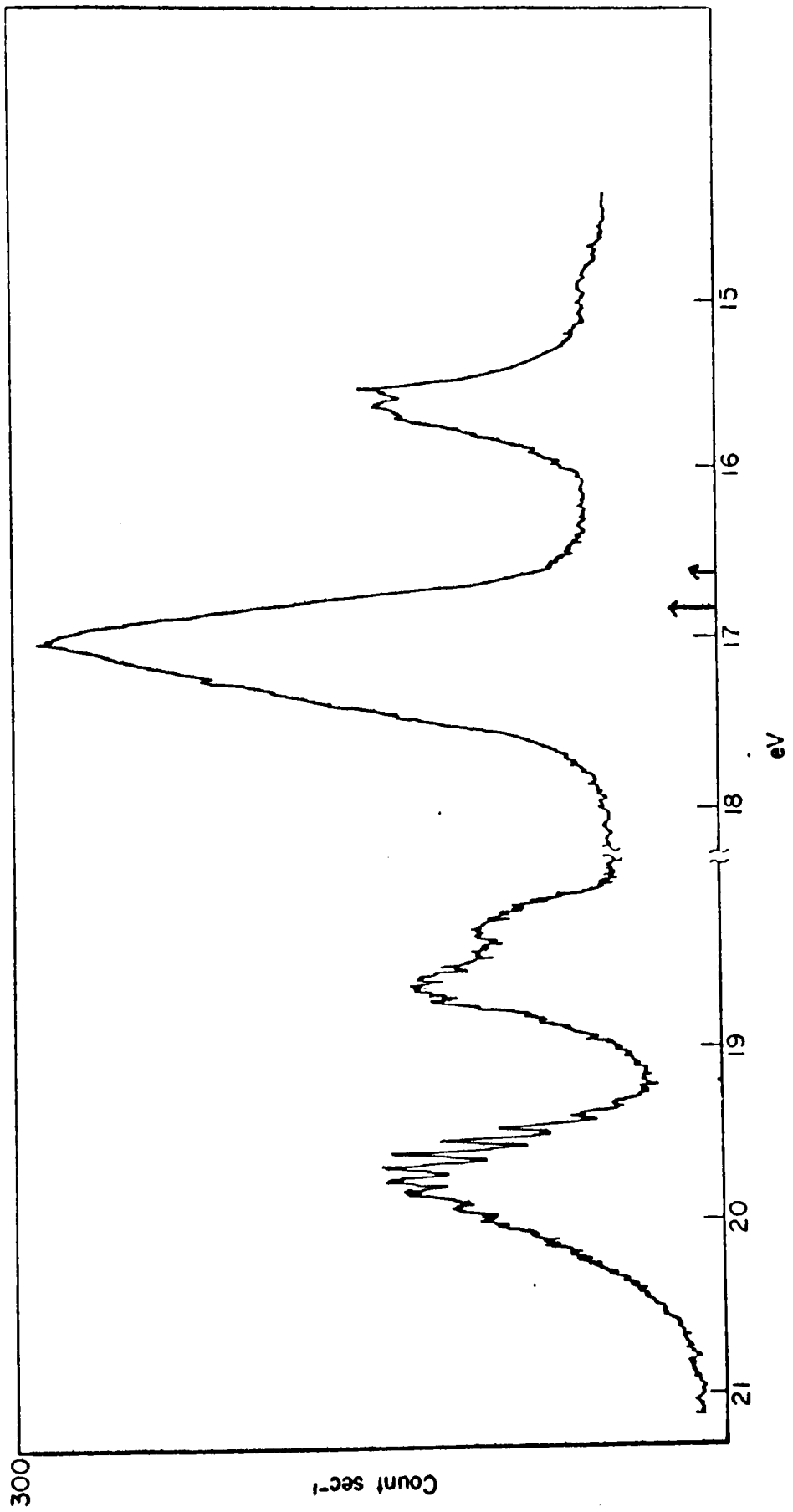

Figure 4.17

Computed CM energy releases for the fragmentation of SF_6^+ to give SF_5^+.

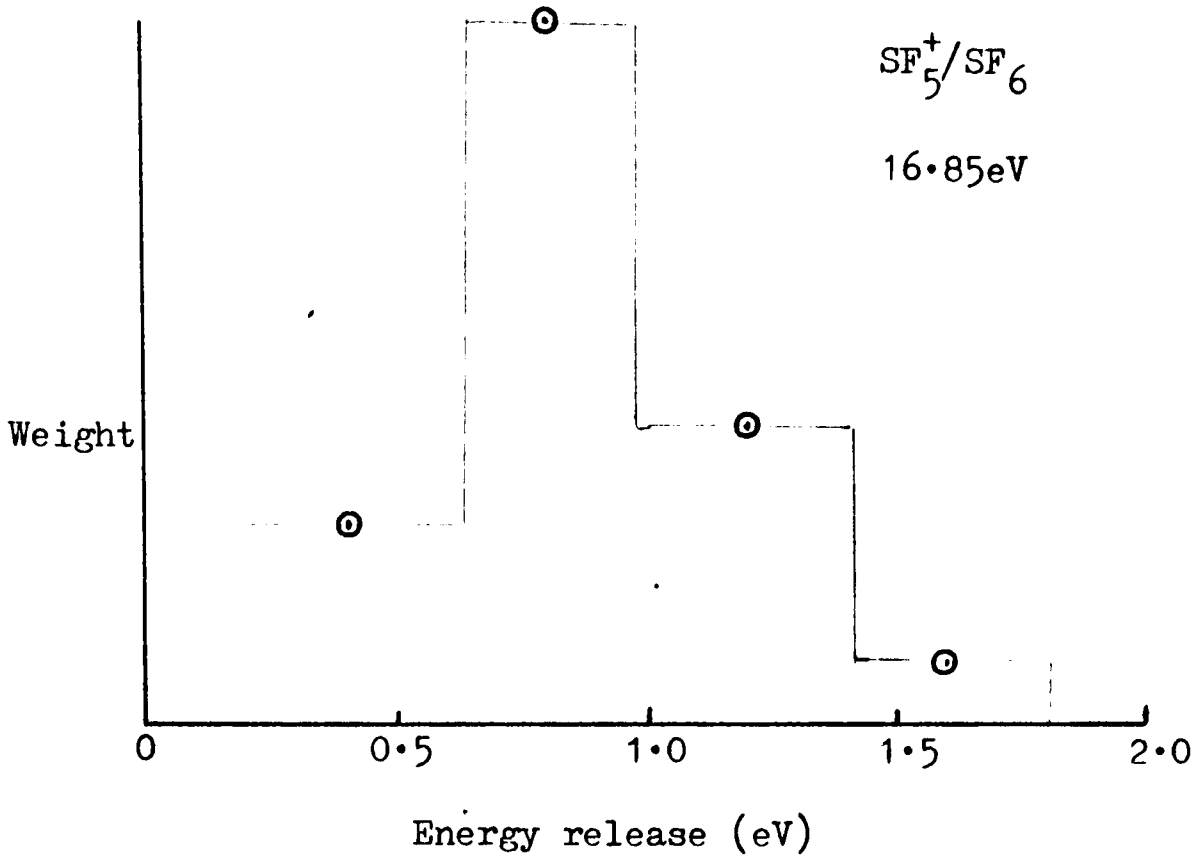

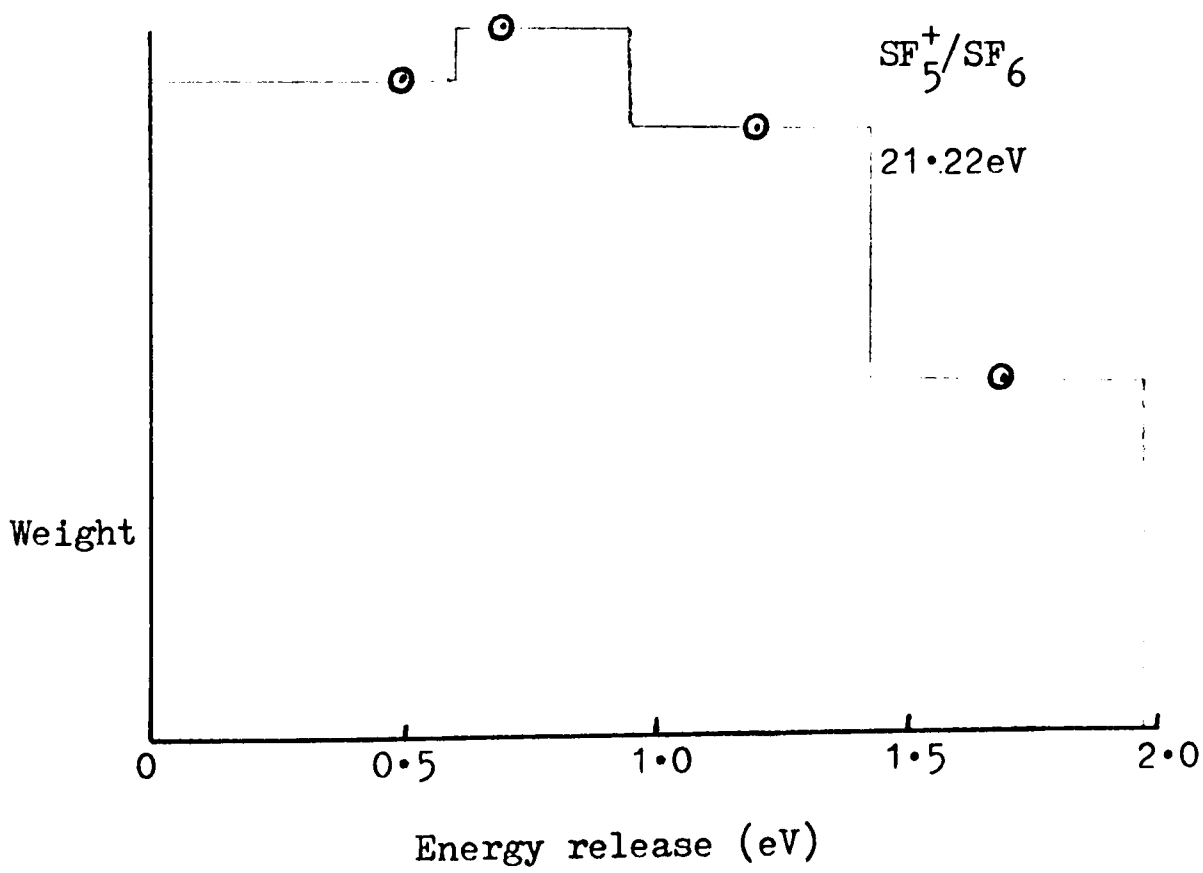

The values for 21.22 eV photoionization agree well with the published figures of Dibeler and Walker[122] who quote a ratio of $SF_6^+/SF_5^+/SF_4^+/SF_3^+$ of $3 \times 10^{-4}/1.0/0.11/0.14$. Their quoted abundance of parent ion would not be detectable on the spectrometer used in this work. The photoelectron spectrum of SF_6[86] is reproduced in figure 4.16. No useful thermodynamic data is available for calculation of dissociation limits but appearance potentials of the ions are known[147,148] and are:

SF_5^+	15.75 eV
SF_4^+	18.5 eV
SF_3^+	19.8 eV

Neon radiation will excite only the first ionic state and only SF_5^+ is observed at this energy. There is some disagreement about the assignment of the photoelectron spectrum[149,150,151]; the order of orbitals is either

$$t_{1g} > t_{1u} > e_g > t_{2u} > t_{2g}$$

or

$$t_{1u} > t_{1g} > e_g > t_{2u} > t_{2g}$$

The high intensity of the second photoelectron band is difficult to explain but may be due to autoionization at 21.22 eV[151].

$\underline{SF_5^+}$. This ion shows a very different kinetic energy distribution for 16.85 or 21.22 eV photoionization. The derived CM releases are shown in figure 4.17. The energy release of SF_5^+ ions formed from the ionic ground state appears to peak strongly at about 0.8 eV: when higher states are also populated energy releases out to 2.0 eV appear as well. These results suggest that the true dissociation limit

Figure 4.18

Computed CM energy releases for the fragmentation of SF_6^+ to give SF_4^+ and SF_3^+.

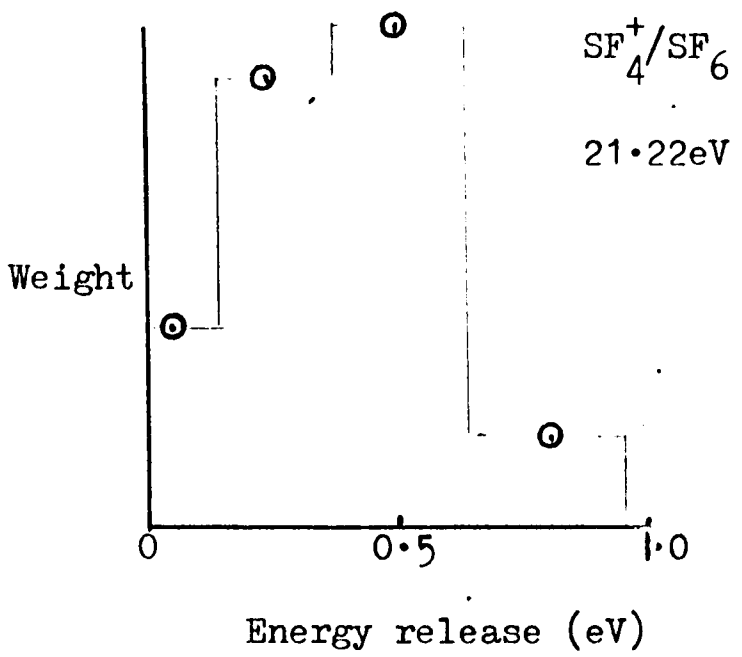

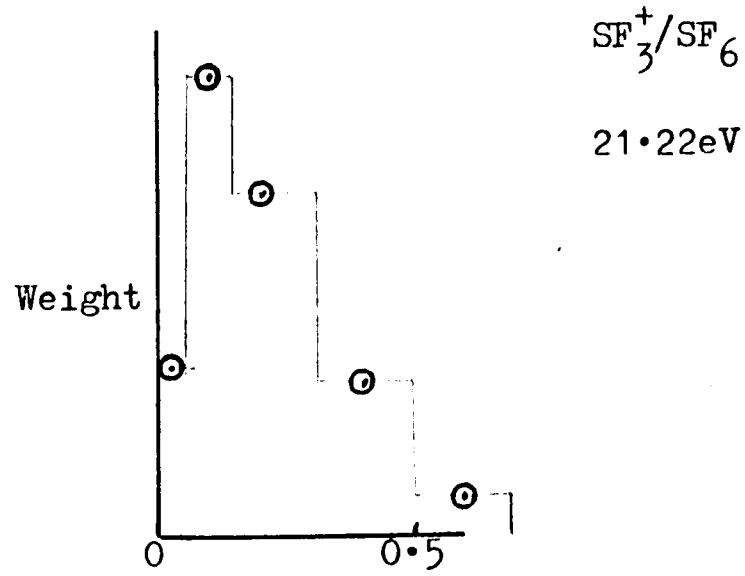

for SF_5^+ production is at least 0.8 eV below the vertical ionization potential of the first ionization band i.e. below 15 eV. The appearance potential must therefore be considerably higher than the dissociation limit. In fact it would be expected that a greater amount of excess energy in the fragmentation would go into vibrational energy of SF_5^+ but even if the vibrational energy of product SF_5^+ is the same as the translational release, as found for CF_4 and C_2F_6, the dissociation limit would be at about 14.2 eV. In view of this it seems remarkable that any parent ion is observed at all in photoionization at 21.22 eV. It seems certain that as was the case for CF_4 and C_2F_6 a large amount of excess energy is going into translational energy of products for this loss of fluorine. The larger energy releases occurring upon 21.22 eV photoionization are consistent with fragmentation to the same dissociation limit, probably via the ionic ground state.

$\underline{SF_4^+}$. The appearance potential for this ion lies at the onset of the fourth photoelectron band but as was the case for SF_5^+ this value is probably considerably above the dissociation limit. The energy distribution of these ions appears to be broad with a peak at about 0.4 eV (see figure 4.18). The relative abundances of SF_4^+ and SF_3^+ suggest that the ions in excited states above their respective appearance potentials are probably dissociating at least predominantly to the lightest ion available. If this is so the range of the excess energy available for dissociation to SF_4^+ is about 1.4 eV which would explain the broad observed energy distribution if about a third of the excess energy appears as kinetic energy.

$\underline{SF_3^+}$. The appearance potential of this ion lies in the middle of the highest ionization potential photoelectron band. If this value is accurate intensity arguments would suggest that essentially all ionization to states above the appearance potential is giving SF_3^+. This would appear to indicate that the fragmentation is a primary one. The CM energy distribution (shown in figure 4.18) has a peak at about 0.1 eV and falls off smoothly to 0.6 eV. It might appear therefore that the appearance potential is closer to the dissociation limit in this case or that more energy is appearing as vibrational energy of products. The CM kinetic energy release distribution is more compatible with statistical theories than those of the other ions formed from SF_6.

E. DISCUSSION

Some general conclusions may be drawn from the results presented here.

a) There is little evidence for any generally applicable use of the concept that the pattern of an ionic decomposition will be determined by the bonding character of the electron lost in ionization. The possible exception to this is the case of C_2F_6 where the isolated first excited ionic state loses fluorine and corresponds to the loss of a C-F bonding electron. The ground ionic states of the chlorine containing compounds all lose a chlorine atom but this is the only mode of decomposition available in any case. A better case in favour of the postulate is that of the fourth excited state of the CCl_3F^+ ion which corresponds to loss of a C-Cl bonding electron and appears to dissociate predominantly with loss of chlorine even though it lies above the dissociation limit for loss of fluorine which is a low yield process in this compound.

b) It appears that loss of a fluorine atom in these compounds is a process with a high reverse activation energy in which a large amount of the excess energy of this ion over the dissociation limit appears as kinetic energy of products. It appears therefore that where it does occur fluorine loss is a rapid process; this could explain why it competes so favourably with internal conversion to lower ionic states in C_2F_6. The effect is at a minimum in the only compound investigated containing one fluorine atom i.e CCl_3F. In the case of SF_6 it would appear that as successive fluorine atoms are lost in what appear in every case to be primary processes, the reverse activation energy appears to decrease.

Thus in the formation of SF_3^+ much less energy is released than in the formation of SF_5^+ and in the former case the distribution of energies is less broad.

c) Conversely, the loss of a chlorine atom in these compounds would appear to occur with a characteristic low peak energy release and rapid fall off of energy release at higher energies.

d) Evidence has been found for the occurrence of dissociations leading to electronically excited products. This is particularly clear with C_2F_6 and CCl_3F.

Chapter 5 - Experimental Investigation of Nitrogen Dioxide

Figure 5.1

The photoelectron spectrum of NO_2 (after Lindholm[162])

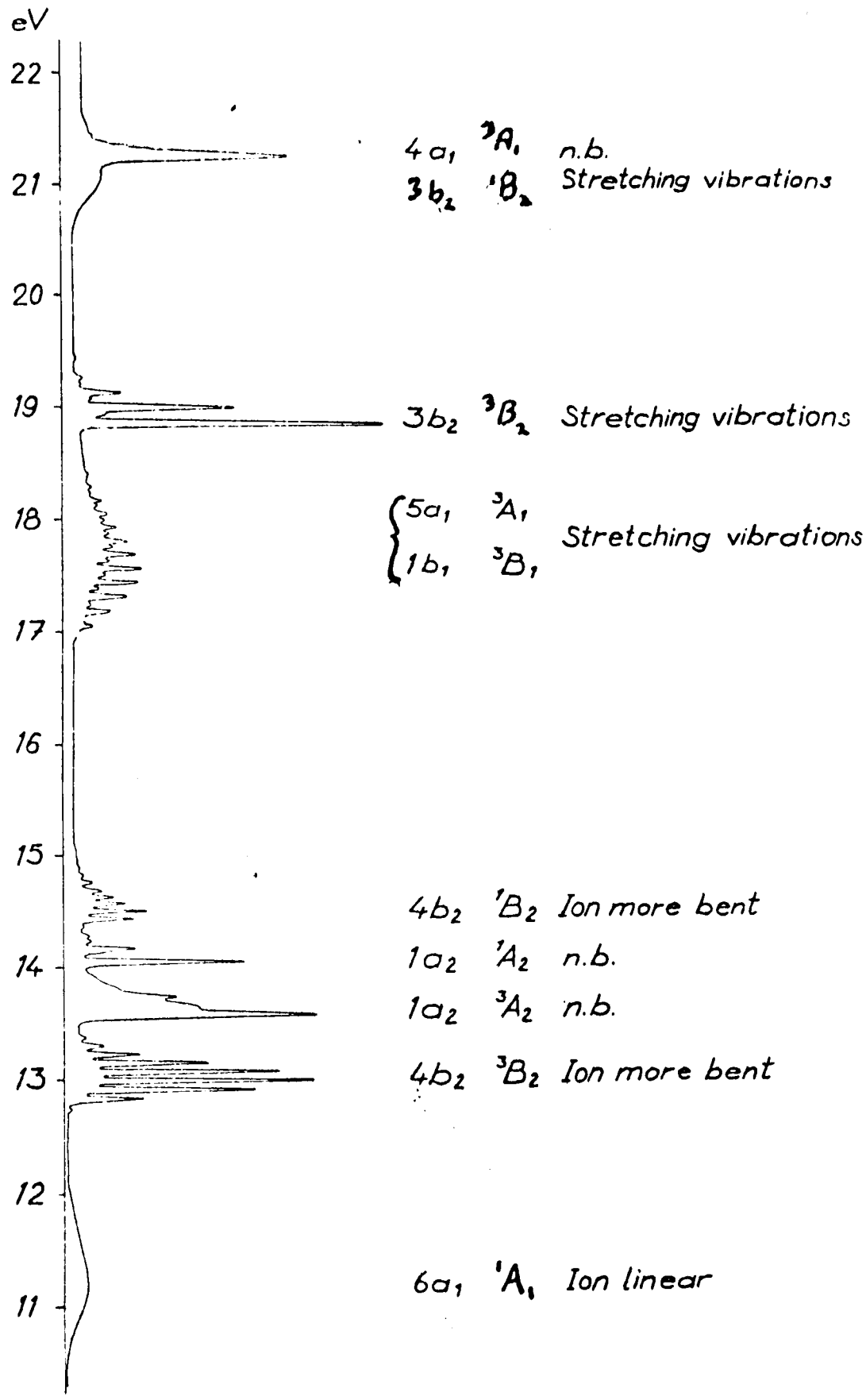

CHAPTER FIVE

THE FRAGMENTATION OF NO_2^+

The photoelectron spectrum of NO_2 has been reported and assigned[161,162] and is reproduced in figure 5.1. NO_2 is a bent triatomic (C_{2v}) molecule with a bond angle of 134^o. The corresponding ion, NO_2^+, is isoelectronic with CO_2, which is linear, and may well be expected to be linear also, at least in the ground state. It appears however that some excited ionic states may have a smaller bond angle than the parent molecule.[161]

The mass spectrum of NO_2 shows only four ions in the following relative intensities: NO_2^+, 0.37; NO^+, 1.0; O^+, 0.22 and N^+, 0.1[162]. The N^+ ion has an appearance potential of 21.2 eV according to charge exchange studies[162]. The fact that O_2^+ does not appear at all and N^+ only at 21.2 eV is interesting in the light of the calculated dissociation limits:

$$NO_2 \longrightarrow N^+ + O_2 \qquad 17.8 \text{ eV}$$

$$NO_2 \longrightarrow N + O_2^+ \qquad 16.76 \text{ eV}$$

The loss of O_2 or O_2^+ from NO_2^+ appears to have low probability even though bending vibrations of the ion are probably excited in at least some of the ionic states that are well above the lowest dissociation limits for their formation[161]. It is interesting to note that loss of O_2 rather than O + O must occur above 21.22 eV as the lowest dissociation limit for:

$$NO_2 \longrightarrow N^+ + O + O$$

is at 23 eV.

The kinetic energy distributions of O^+ and NO^+

Figure 5.2

The experimental kinetic energy distribution of NO^+ ions formed in the photoionization of NO_2 at 16·85eV.

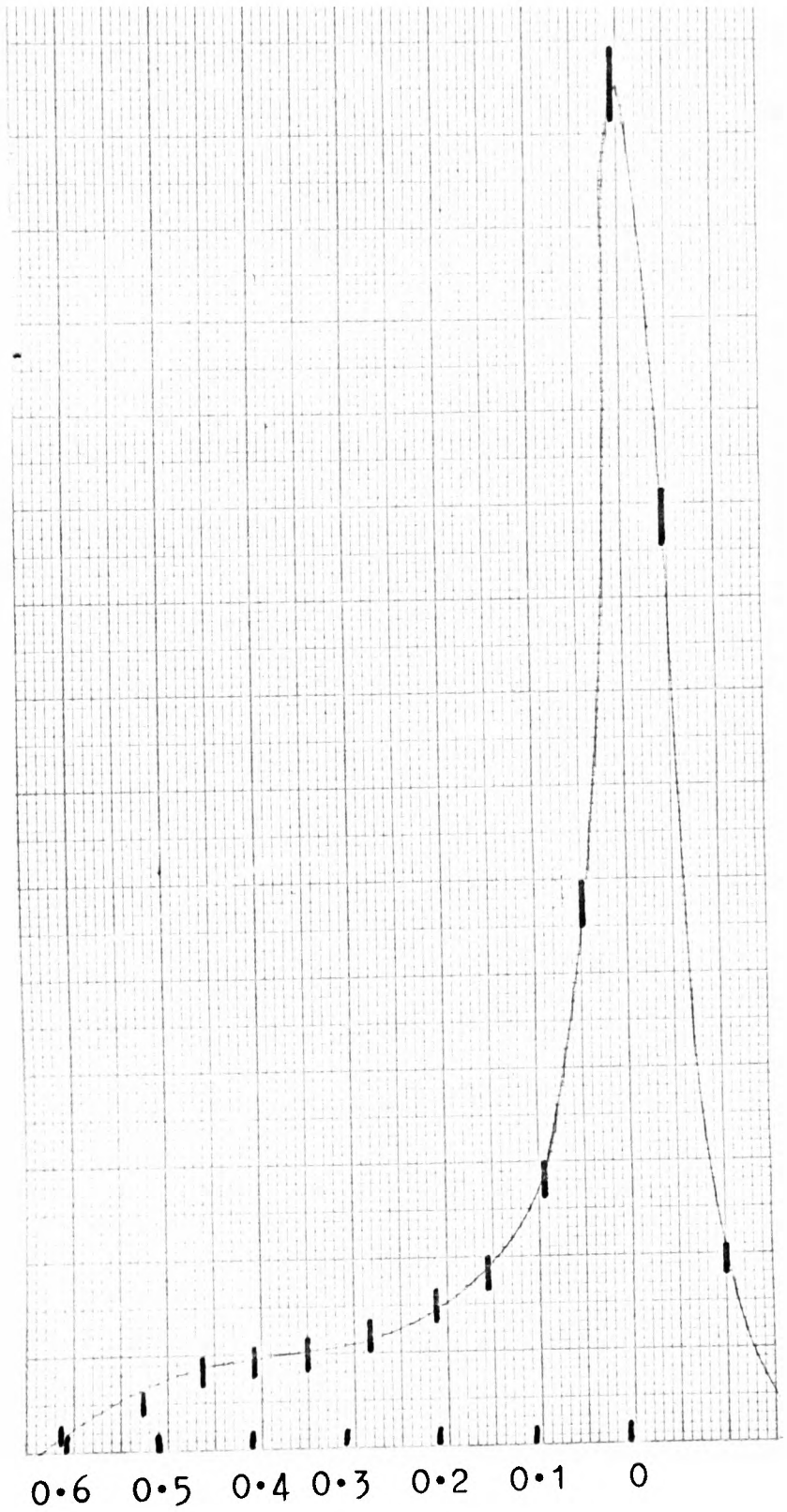

formed from NO_2^+ produced by photoionization using He I and Ne I radiation were recorded. NO_2 was prepared by mixing of NO and O_2 in 2:1 proportion. After allowing time for the reaction to occur the NO_2 was purified by freezing in a solid CO_2 bath and pumping off excess NO and/or O_2. In this way a sample was obtained that did not show any significant features due to impurities in the photoelectron spectrum.

The formation of NO^+ ions from NO_2^+

The kinetic energy distribution of the NO^+ ions produced with neon resonance radiation is shown in figure 5.2. As can be seen there is a high contribution from low energy ions and a continuous distribution of ions out to energies of 0.45 eV, corresponding to a kinetic energy release in CM of about 1.3 eV.

The ionic states which can be populated by neon resonance radiation and the ionization potentials corresponding to their formation are as follows[161]:

Ionization Potential	Ionic State	Adiabatic Ionization Potential (eV)	Vertical Ionization Potential (eV)
1st	$^1A_1$	9.75	11.23
2nd	$^3B_2$	12.85	13.01
3rd	$^3A_2$	13.6	13.6
4th	$^1A_2$	14.07	14.06
5th	$^1B_2$	14.37	14.51

The $^1A_1$ state is below all dissociation limits and hence can only give parent ions. The lowest dissociation limit for production of O^+ is at 16.8 eV which explains the non-appearance of O^+ ions with neon radiation. The measured ratio of NO^+ to

NO_2^+ ions is 0.78 but this will be an underestimate because of the influence on ion collection efficiency of the high energy release for NO^+. It is not possible to deduce whether the states above $^1A_1$ are completely predissociated as their corresponding total photoelectron intensity is about three times that of the $^1A_1$ state.

Two dissociation limits lie below 16 eV:

$$NO_2 \longrightarrow NO^+ \; ^1\Sigma^+ + O\,^1D \qquad 14.23 \text{ eV}$$

$$NO_2 \longrightarrow NO^+ \; ^1\Sigma^+ + O\,^3P \qquad 12.49 \text{ eV}$$

The $^3A_2$ and $^3B_2$ states of NO_2^+ may predissociate to the lower limit according to the selection rules[3]. Predissociations of $^1A_2$ and $^1B_2$ states to the upper limit are allowed but not to the lower limit as this is spin forbidden. It would thus seem likely that the upper vibrational levels of the $^1B_2$ state would predissociate to give $NO^+ \; ^1\Sigma^+$ and $O\,^1D$ with low energy releases in the range 0 - 0.5 eV. The $^1A_2$ state lies below this dissociation limit and there is no spin allowed fragmentation pathway open to it. It would be interesting to know whether fluorescence from this state occurs, as predicted by Lindholm[162]. He observes a metastable ion for formation of NO^+ in this energy region and this would agree with the theory that the $^1A_2$ state is predissociating slowly via a spin forbidden curve crossing. The high energy releases observed in the fragmentation may be explained by predissociation of $^3B_2$ and $^3A_2$ states of the ion to the lower dissociation limit. The excess energy of the highest vibrational level of the $^3A_2$ state above the dissociation limit is 1.34 eV. As a strong energy release distribution is observed up to this value it appears that a significant proportion of the dissociations are giving $NO^+ \; ^1\Sigma^+$ in the vibrational ground state.

Figure 5.3

The experimental kinetic energy distribution of NO^+ ions formed in the photoionization of NO_2 at 21·22eV.

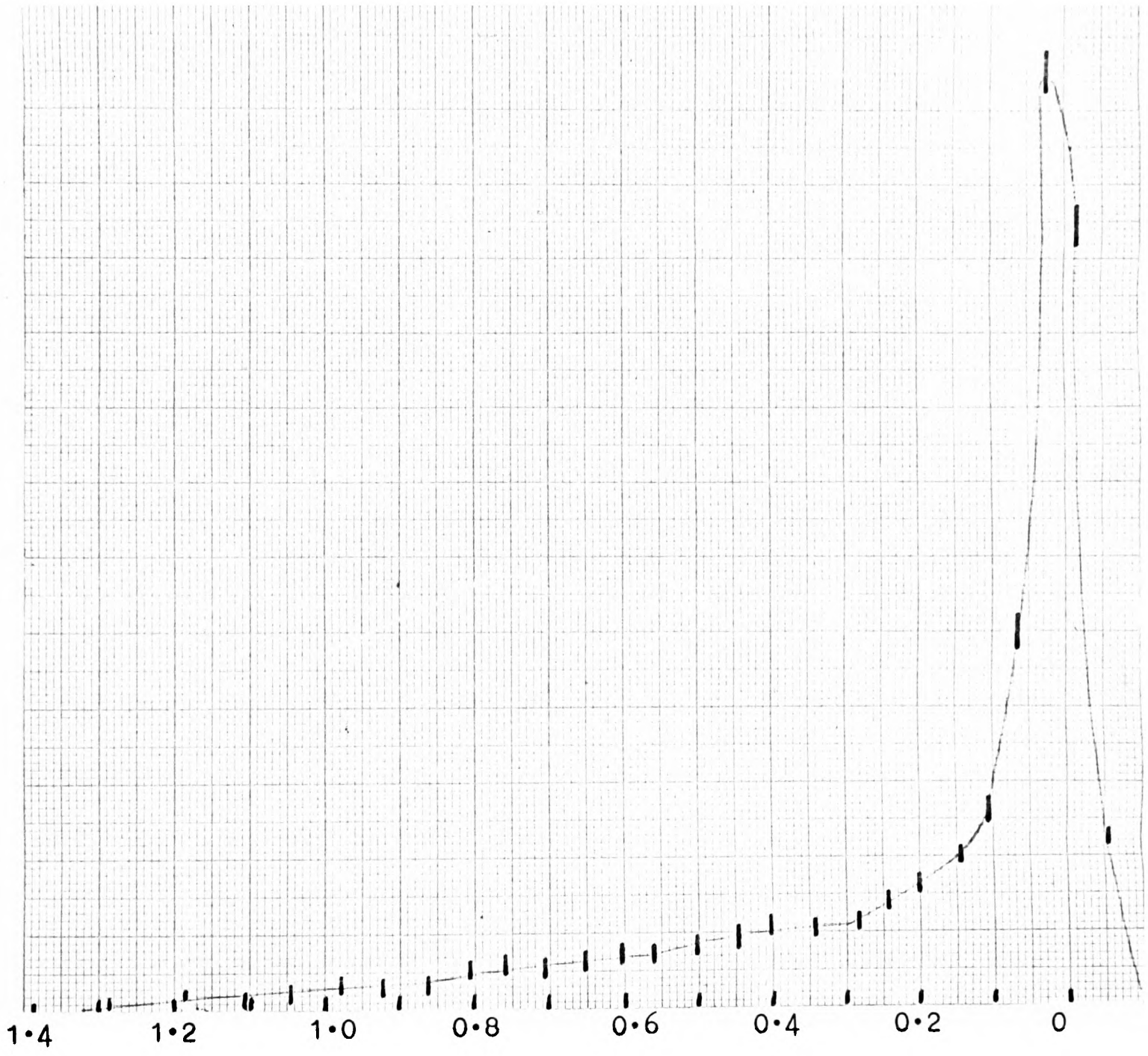

The energy distribution of NO^+ ions produced via photoionization of NO_2 with helium radiation at 21.22 eV is given in figure 5.3. There is a similarity to that for 16.85 eV photoionization but there is now significant intensity at energies beyond 0.5 eV, as far as 1.2 eV. It is apparent that kinetic energy releases in the centre of mass in excess of 3 eV are occurring. The proportion of NO^+ ions relative to NO_2^+ in the photo-ionization mass spectrum is now 2:1 and as very high energy releases are occurring, with consequent greater discrimination against NO^+, it seems probable that no parent ion is formed above 16.85 eV ion energy. Additional ionic states now populated are:

Ionization Potential	Ionic State	Adiabatic Ionization Potential (eV)	Vertical Ionization Potential (eV)
6th and 7th	$^3A_1$ $^3B_1$	16.99, 17.06	17.64, 17.45
8th	$^3B_2$	18.86	18.86
9th	$^1B_2$?	20.8	21.0 (weak)

Two more dissociation limits are now in the relevant energy region.

$$NO_2 \longrightarrow NO^+ \, ^1\Sigma^+ + O\,^1S \qquad 16.51 \text{ eV}$$

$$NO_2 \longrightarrow NO^+ \, ^3\Sigma^+ + O\,^3P \qquad 17.44 \text{ eV}$$

The lower vibrational levels of the $^3A_1$ and $^3B_1$ ionic states thus lie above only a single dissociation limit which can be reached by a spin allowed process. This is the lowest one and the $^3A_1$ and $^3B_1$ states have an average excess energy of 5 eV above this state. Thus the very high energy release in this fragmentation may be understood in terms of a predissociation of NO_2^+ ions from the $^3A_1$ and $^3B_1$ ionic states to give ground state $NO^+ \, ^1\Sigma^+$ and ground state $O\,^3P$. A large proportion of

Figure 5.4

The experimental kinetic energy distribution of O^+ ions formed in the photoionization of NO_2 at 21·22eV.

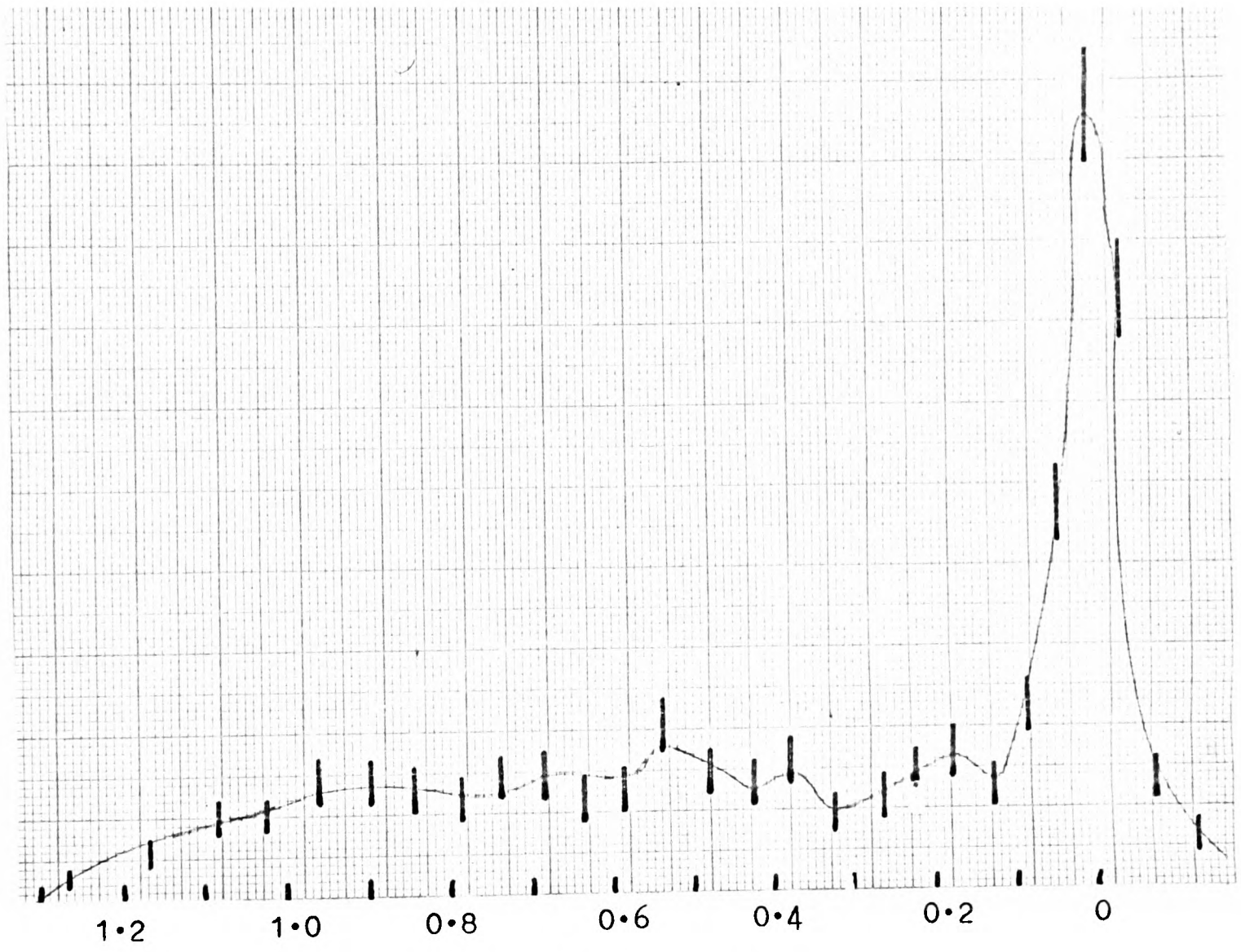

the excess energy must in this case go into vibrational excitation of the NO^+ (vibrational levels of ground state NO^+ have been observed in PES, out to at least 1.5 eV excitation[86]). The $^3B_2$ state, which is strongly populated in the photoelectron spectrum, is above the dissociation limit corresponding to formation of $NO^+ {}^3\Sigma^+ + O^3P$ to which it is allowed to predissociate. The excess energy for this process is lower (about 1.42 eV) and presumably contributes energies up to about 0.5 eV to the LAB kinetic energy release. This is in good agreement with the experimental distribution. The $^3B_2$ state is thought to be at least partly predissociated to give O^+ as also the $^3B_1$ state may well be.

The Formation of O^+ Ions from NO_2^+

O^+ ions are observed at an abundance of 10% relative to NO^+ in the photoionization of NO_2 at 21.22 eV. The observed energy distribution of these ions is shown in figure 5.4. Apart from the low energy ions this distribution appears to be made up of roughly equal contributions from energy releases of about 0.3, 0.6, 0.8, 1.1 and 1.4 eV with a release of 1.7 eV of lower weight. It would not however be wise to assign too much significance to these values as they necessarily only represent a minimum set which will fit the experimental curve. However it is worth noting that these energy values have an average spacing of 0.28 eV, and this is close to the 0.24 eV average spacing of the vibrational levels of $NO\ ^2\Pi$. It seems very possible therefore that in this case vibrational "structure" is just visible on a kinetic energy distribution. The lowest dissociation limit for formation of O^+ is

$$NO_2 \longrightarrow NO\ ^2\Pi + O^{+4}S \qquad 16.8 \text{ eV}$$

This is only a spin allowed process for triplet states of the NO_2^+ ion. The next lowest dissociation limit is:

$$NO_2 \longrightarrow NO\ ^2\Pi + O^+\ ^2D \quad - 18.6\ eV$$

which is allowed for singlet and triplet parent ionic states. Thus ions in the $^3B_1$ and $^3B_2$ states may predissociate via allowed transitions to the lower limit and the $^1B_2$ state, which is only weakly populated, may predissociate to the upper limit.

The excess energy of the v = 0 level of the $^3B_2$ state over the lower limit is 2.06 eV, whereas that of the $^3B_1$ and $^3A_1$ states is about 0.7 eV. It appears therefore from the energy released that ions in the $^3B_2$ state, at least, do predissociate to this limit. This would involve the production of NO in its second vibrational level or above, as kinetic energy release is only observed up to about 1.7 eV. The observed energy distribution of O^+ ions is entirely compatible with the formation of NO in a band of vibrational levels from v = 1 to v = 6 or 7 from NO_2^+ $^3B_2$. It is interesting to note that there is a sharp increase in the O^+ ionization efficiency curve at 18.88 eV, the energy of the $^3B_2$ band[164]. It is of course very possible that some levels of NO_2 $^3B_1$ or $^3A_1$ are also fragmenting to give O^+ + NO. This could account for the large number of low kinetic energy ions observed. Some allowed predissociations of NO_2^+ states to give O^+ and NO^+ are shown diagramatically in figure 5.5.

Figure 5.5

Allowed Predissociations of NO_2^+

Known states of the NO_2^+ ion are plotted against their potential energy in the centre of the diagram. Dissociation limits for processes yielding NO and O^+ are shown to the left and those for processes yielding NO^+ and O are shown to the right of the diagram. Lines are drawn in the diagram showing the allowed dissociation processes.

Figure 5.5

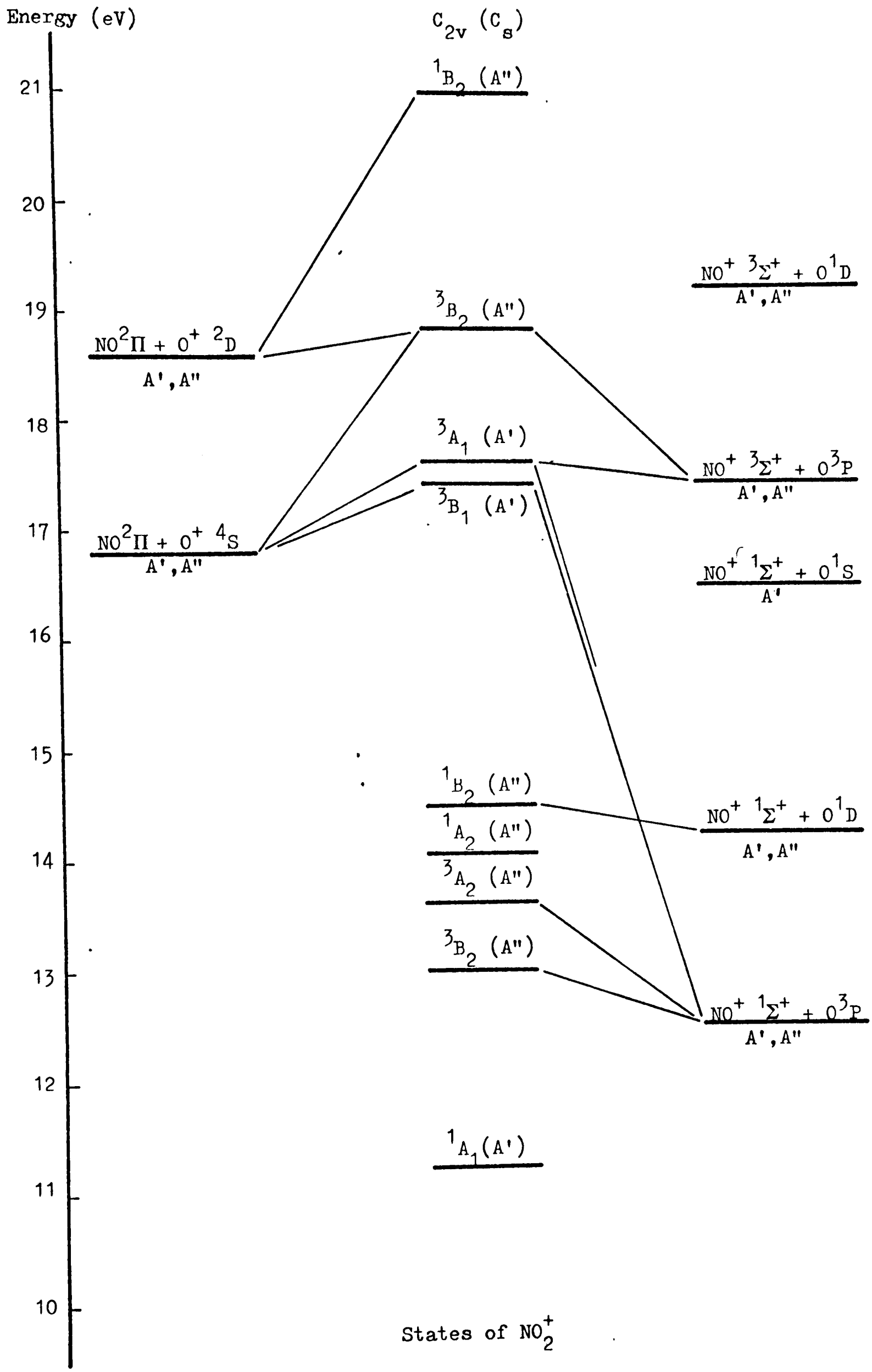

States of NO_2^+

APPENDIX A.

1) The LAB distribution function for a single valued CM kinetic energy release.

This treatment is based on that of Stanton and Monahan[104]. A derivation is also given in the D. Phil. thesis of C. Rowland .

Consider the dissociation:-

$$m_1^+ \longrightarrow m_2^+ + m_3 + E_o$$

The parent ions (m_1^+) have a thermal distribution of kinetic energies E_p, characterized by a temperature T. The distribution of kinetic energy release is $W(E_o)$.

The observed velocity, v_1, of the fragment ion is the vector sum of two components;

v_0, from thermal motion of m_1^+.

v_{01}, from the kinetic energy released.

v_1 may be considered to be a vector the tip of which lies on the surface of a sphere of radius v_{01} centred on the tip of v_0. Assuming an isotropic energy release, the probability that the angle between v_0 and v_1 lies in the range Θ to $\Theta + \delta\Theta$ is given by;

$$P(\Theta)\delta\Theta = \sin\Theta \frac{\delta\Theta}{2}$$

As $v_1^2 = v_0^2 + v_{01}^2 + 2v_0v_{01}\cos\Theta$

the distribution function $P(v_1^2)$ is;

$$P(v_1^2) = \begin{cases} \frac{1}{4v_0v_{01}} & (v_0 - v_{01})^2 \leq v_1^2 \leq (v_0 + v_{01})^2 \\ \text{otherwise } 0 \end{cases} \qquad (1)$$

(This uses the result that:

If $f(x)$ is a distribution function for x and $x = g(z)$;

the distribution function for z, $F(z)$ is given by:

$$F(z)dz = f\{g(z)\}\, g'(z)dz$$ [107])

By conservation of energy and momentum we know:

$$v_0 = \left(\frac{2E_p}{m_1}\right)^{\frac{1}{2}}$$

$$v_{01} = \left(\frac{2(m_1 - m_2)}{m_1 m_2} E_o\right)^{\frac{1}{2}}$$

The distribution function for E $(= \frac{1}{2}mv_1^2)$ is then

$$I(E) = \begin{cases} \dfrac{m_1}{4(m_2 (m_1 - m_2) E_o E_p)^{\frac{1}{2}}} & \alpha_-^2 \leq E \leq \alpha_+^2 \\ \text{otherwise } 0 \end{cases} \qquad (2)$$

$$\alpha_{\pm} = \left(\frac{m_2 E_p}{m_1}\right)^{\frac{1}{2}} \pm ((m_1 - m_2) E_o / m_1)^{\frac{1}{2}}$$

Thus for fixed values of E_o and E_p the fragment ion kinetic energy has a uniform probability distribution.

In general E_p will take the form of a distribution $f(E_p)$ and the kinetic energy release will have a distribution $W(E_o)$. The distribution function for E will be:

$$P(E) = \int_0^\infty dE_o \int_0^\infty dE_p \; W(E_o) \; f(E_p) \; I(E)$$

where $f(E_p) = \left(\dfrac{2(kT)^{\frac{2}{3}}}{\pi^{\frac{1}{2}}}\right) E_p^{\frac{1}{2}} \exp(-E_p / kT)$.

Because I (E) is not a continuous function the integration has to be divided into three parts; from zero to E_p(min); E_p(min) to E_p (max) and from E_p(max) to infinity. E_p(min) and E_p(max) are the maximum and minimum values of E_p for which I (E) is non-zero and are (from equation 2):

$$E_p(\max) = \frac{m_1 E + (m_1 - m_2)E_o + 2(m_1(m_1 - m_2)E_o E)^{\frac{1}{2}}}{m_2}$$

$$E_p(\min) = \frac{m_1 E + (m_1 - m_2)E_o - 2(m_1(m_1 - m_2)E_o E)^{\frac{1}{2}}}{m_2}$$

The part of P (E) dependant upon E_p is therefore

$$\int_{E_p(min)}^{E_p(max)} dE_p \exp(-E_p/kT)$$

$$= \frac{1}{kT} \exp-\left(\frac{m_1E + (m_1 - m_2)E_o}{m_2kT}\right) \sinh\left(\frac{2(m_1(m_1 - m_2)E_oE)^{\frac{1}{2}}}{m_2kT}\right)$$

and the complete expression is:

$$P(E) = \frac{m_1}{(\pi kT)^{\frac{1}{2}}} \int_o^\infty dE_o \frac{W(E_o)}{(m_2(m_1-m_2)E_o)^{\frac{1}{2}}} \exp-\left(\frac{m_1E+(m_1-m_2)E_o}{m_2kT}\right) \sinh\left(\frac{2(m_1(m_1-m_2)E_oE)^{\frac{1}{2}}}{m_2kT}\right) \quad (3)$$

For a delta function CM distribution integration of this gives:

$$P(E) = \frac{m_1}{(\pi kTm_2(m_1-m_2)E_o)^{\frac{1}{2}}} \exp-\left(\frac{m_1E + E_o(m_1-m_2)}{m_2kT}\right) \sinh\left(\frac{2(m_1(m_1-m_2)E_oE)^{\frac{1}{2}}}{m_2kT}\right) \quad (4)$$

Integration of the equation 3 is possible for a Maxwellian CM distribution; the result being another Maxwellian distribution function. It is not possible in general to integrate the expression for other forms of CM release function. distribution.

2) The angular acceptance function.

In the above treatment an isotropic energy release was assumed. If the energy distribution function of ions travelling in a fixed solid angle were to be measured, equation 3 would describe this distribution for an energy release function $W(E_o)$. However in a practical experiment it is likely that the solid angle within which ions are investigated will not be constant but will be some function of the actual energy of the ion.

Consider the case of an ion released at point I in fig. A.1, which represents the form of ionization region used in the experiments presented in this thesis.

figure A.1

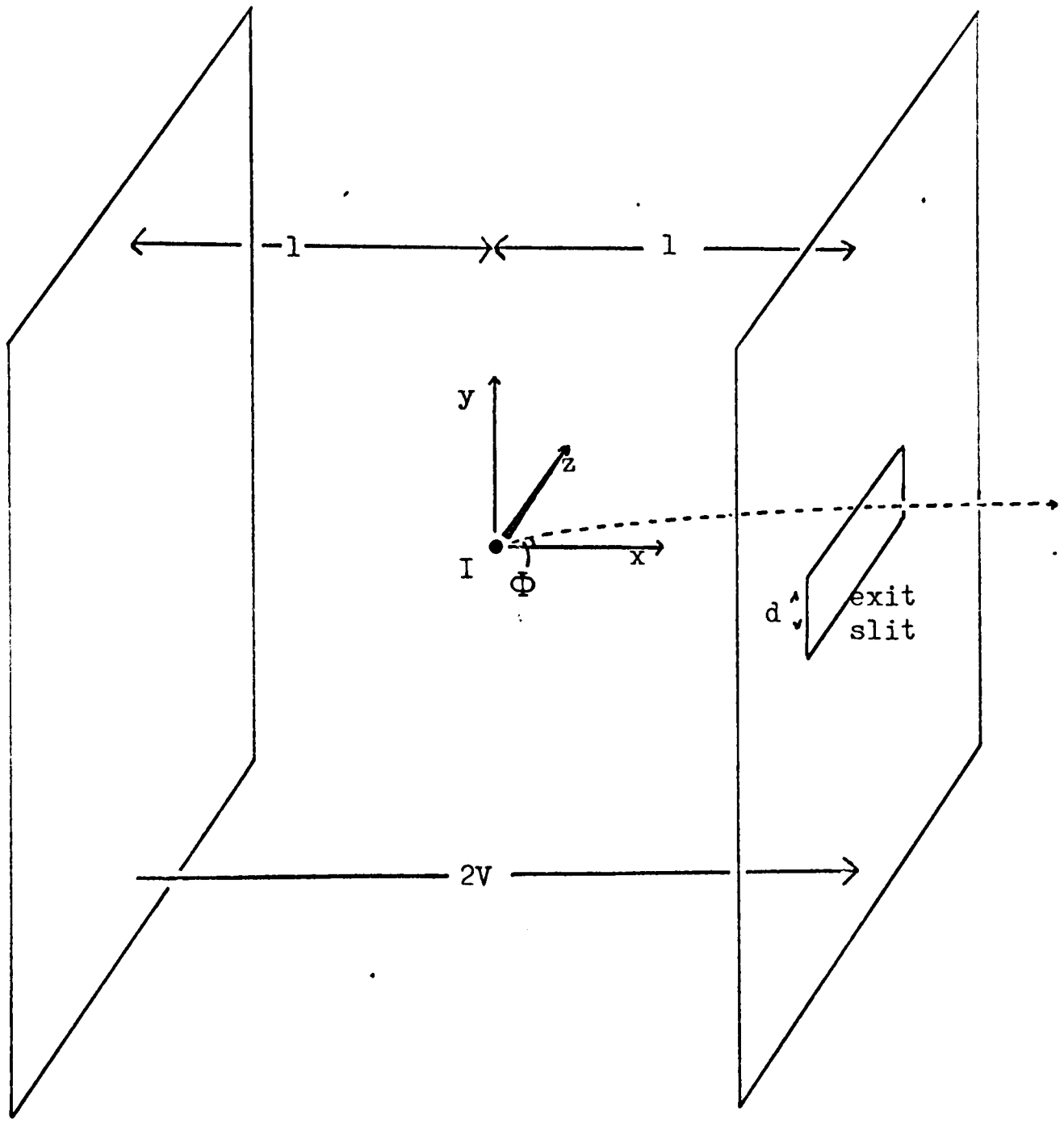

In general the ion will be emitted at an angle Φ to the slit direction x. The probability of such an ion reaching the exit slit will be a function of the angle Φ , the ion's velocity and the field between the plates.

First we consider the possibility that the motion will not be perpendicular to the z direction (the lamp axis). No accelerations are presented to the ion in this direction during the whole of its flight to the electron multiplier at the exit slit of the analyzer. Therefore the range of initial angles to the z direction that will result in collection of an ion will be a constant defined by the point of ionization and the dimensions of the slit immediatly in front of the multiplier. We can therefore confine this

discussion to the two dimensional angular acceptance function in the x,y plane.

Taking the slit half width as d; the distance between the slit and the ionization region as l and the field between slit and ionization region as V/l (see fig. A.1); for an initial velocity v:

$$v_y = v \sin\Phi$$

$$v_x = v \cos\Phi + \frac{Ve}{lm} t$$

$$= v \cos\Phi + \frac{Ve}{lm} \frac{d}{\sin\Phi} \qquad (5)$$

for an ion that just clears the slit edge.

Φ is the maximum value of the angle to the x axis.

$$v_x^2 = v^2 \cos^2\Phi + \frac{2Ve}{m} \qquad (6)$$

squaring (5)

$$v_x^2 = v^2 \cos^2\Phi + \frac{V^2e^2d^2}{l^2m^2v^2 \sin^2\Phi} + \frac{2v \cos\Phi \; Ve \; d}{l \; m \; v \sin\Phi}$$

$$\therefore \quad \dot{2} = \frac{Ved^2}{ml^2 v^2 \sin^2\Phi} + \frac{2v \cos\Phi \; d}{lv \sin\Phi}$$

hence

$$\sin^2\Phi = \frac{d^2(Vel + v^2lm \pm (m^2l^2v^4 + Vel^2mv^2 - V^2e^2d^2)^{\frac{1}{2}})}{2v^2lm\,(l^2 + d^2)} \qquad (7)$$

$\frac{1}{2}mv^2 = E$, the initial energy of the ion and for $d \ll l$

$$\sin^2\Phi = \frac{d^2(V\,l + 2E \pm (4E^2\,l^2 + 2VE\,l^2 - V^2\,d^2)^{\frac{1}{2}})}{4E\,l^3}$$

with E measured in eV.

This equation has four roots. These are Φ_{F+} and Φ_{F-} when the square root term is added and Φ_{B+} and Φ_{B-} when the square root term is subtracted . The roots are shown in fig. A.2.

figure A.2

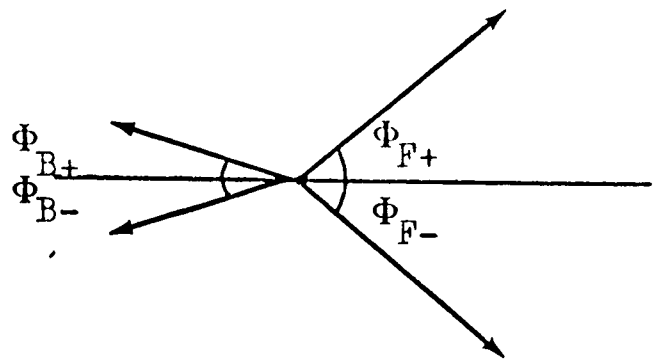

$2\Phi_F$ will represent the forward flying ion acceptance angle and $2\Phi_B$ will represent the backward flying ion acceptance angle.

For the source geometry of the spectrometer and a source voltage of 0·1volt the function becomes:

$$\sin^2\Phi = \frac{(0{\cdot}15 + 6E \pm (36E^2 + 0{\cdot}9\,E - 0{\cdot}000225)^{\frac{1}{2}})}{1200E} \qquad (8)$$

At high values of E this tends to:

$\sin^2\Phi = \frac{1}{100}$ for the forward angle and zero for the backward angle.

hence

$$\Phi_{min} = 5^{\circ}\ 44'$$

and the total acceptance angle will therefore be 11° 28'.

Equation 8 is used in the computer program LABCM5 (Appendix C) to modify energy distributions calculated using equation 4.

APPENDIX B.

1) The energy analyser.

The theory of parallel plate energy analysers has been developed by Harrower[98] and a description of a practical analyser used in photoelectron spectroscopy has been given by Eland and Danby[99].

Green and Proca[100] have reconsidered the theory of the parallel plate analyser taking into account the possibility of using entrance angles other than the 45° adopted in earlier work. This analyser was designed and built with a 45° entrance angle. It is hoped, if possible, to change the entrance angle to 30° at some later date.

Fig. B.1 shows a schematic diagram of a parallel plate analyser. For this treatment of the theory we take the earth plane to be the x, z plane, the repelling plate therefore being at $y = -d$. The source is mounted at $x = 0$, $y = +h$. The mean ray direction is taken to be at an angle $-\theta$ with the x axis.

With a retarding potential on the repelling plate one finds that an ion or electron will return to the earth plate at an x displacement of:

$\frac{2E}{V} \sin 2\theta$ where V is the electric field in volts per cm. and E is the energy of the particle in eV.

The equation of the particle path in the field free region is then:

$$x = (h + y) \cot\theta + \left(\frac{2E}{V}\right) \sin 2\theta \qquad (1)$$

Rays from the same source point (0,+h) are brought to a first order focus when $\frac{dx}{d\theta} = 0$ for y constant. Using equation 1 one finds that this applies when:

$$h + y = \frac{4E}{V} \cos 2\theta \quad \sin^2\theta$$

The foci for various values of initial energy E therefore lie on a straight line:

$$x = (h + y) \cot\theta \left(1 + \frac{1}{\cos 2\theta}\right)$$

figure B.1

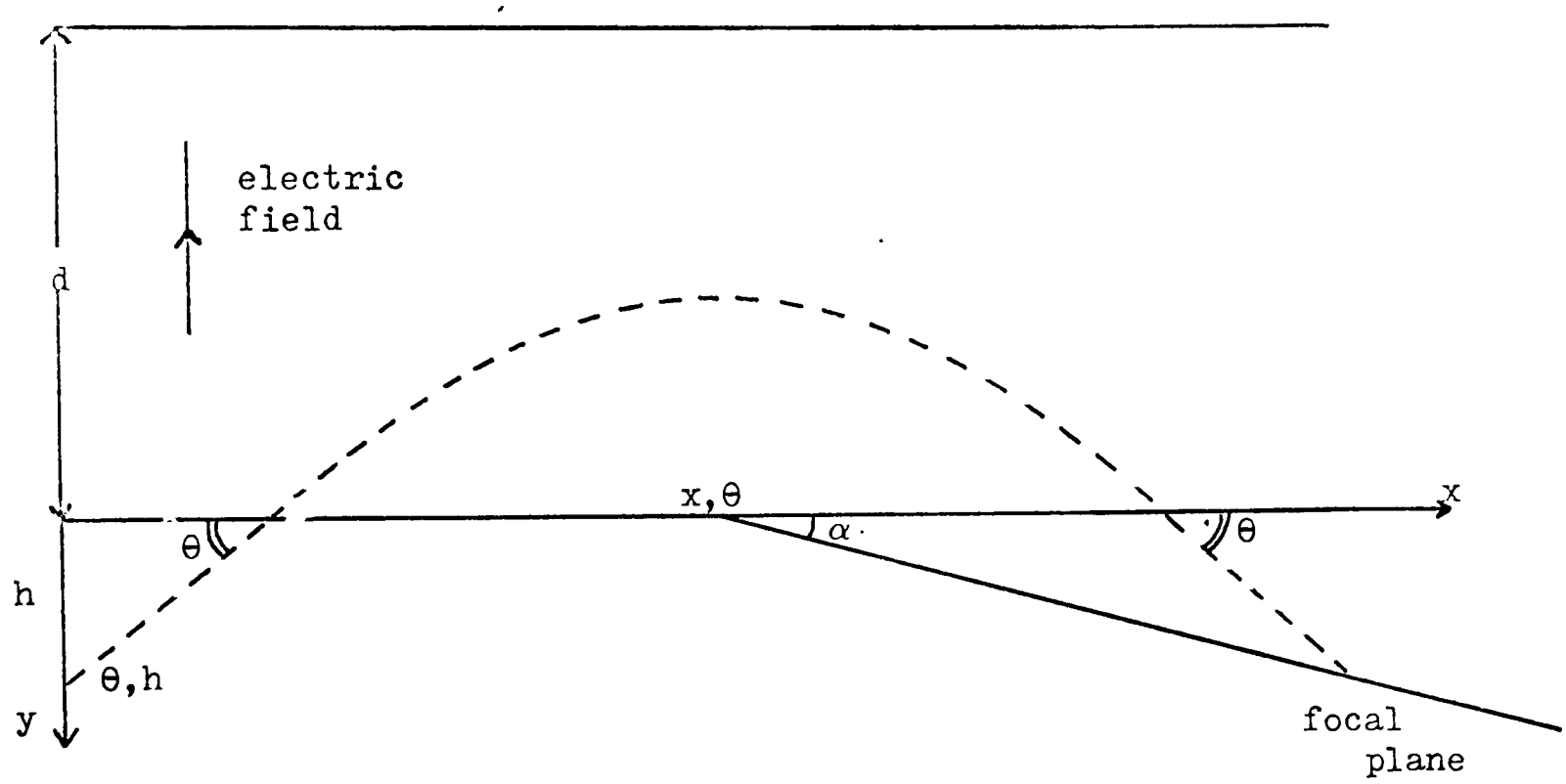

which makes an angle α to the x axis where

$$\tan \alpha = \frac{\tan \theta \ \cos 2\theta}{1 + \cos 2\theta}$$

Thus for $\theta = 45^{\circ}$ the focal line lies on the earth plane but this is only one of an infinite set of possibilities. Aberrations arise from the fact that although $\frac{dx}{d\theta}$ may be zero other terms in $\frac{d^2x}{d\theta^2}$ etc. are not.

The aberrations arising when using an extreme ray of angle $\theta + \Delta\theta$ may be calculated from the separation of the intercepts with the focal line of the mean ray and the extreme ray. If $\Delta x/x$ derived in this way is plotted against θ for small values of $\Delta\theta$ it is found that at $\theta = 30^{\circ}$ $\Delta x/x$ is very small. In fact writing the spread $\Delta x/x$ as $\Delta E/E$ one finds :

for a 30° analyser $$\frac{\Delta E}{E} \simeq 1{\cdot}6 \ (\Delta\theta)^3 \qquad (2)$$

for a 45° analyser $$\frac{\Delta E}{E} \simeq 1{\cdot}4 \ (\Delta\theta)^2 \qquad (3)$$

Obviously the 30° design would be preferable and would allow much

higher analyser acceptance angles and hence higher count rates. A resolving power of 200 is predicted for an acceptance angle of $\pm 6^{o}$.

For the 45^{o} analyser considered here a slit separation of 38cms. was chosen. For ions entering the analyser at 45^{o} the attainable resolution may be shown to be approximated by:

$$R = \frac{\text{Slit width}}{\text{baseline}}.$$

Thus for a resolving power of 500 a slit width slightly under 1mm. is required.

The slits canbe varied in width between 0 and 2·5 mm. It is desirable to place the ionization region as close as physically possible to the entrance slit. In the present machine a distance of 3·6 cm. is used. The limitation of acceptance angle due to the analyser entrance slit for a 45^{o} angle of approach is:

$$\delta\theta = \frac{s}{\sqrt{21}} \text{ radians}$$

where s isthe slit width and 1 the distance between the ionization region and the slit.

Thus for 1mm. slit width $\delta\theta$ is 1^{o} 9' which is in fact substantially less than the $\delta\theta$ value required by equation 3 for a resolving power of 500 (2^{o} 6'). It is seen therefore that the resolution of this spectrometer is not determined by the acceptance angle. The effect of angular spread of the beam in the z direction is easily shown to be negligible.

Any ions travelling at an angle ϕ to the median plane of the analyser will have a measured energy of

$$E_{obs} = E_{o} \cos\phi$$

The maximum angle of flight path for ions which can be detected at all is given by:

$$\phi = \sin^{-1}\left(\frac{\text{exit slit length}}{\text{trajectory length}}\right)$$

because there are no fields acting in the z direction.

For this analyser the trajectory is about 75 cms. in length and the length of the multiplier slit is 1cm. Thus:

$$\phi = \sin^{-1}\frac{1}{75} = 48'$$

this will cause an energy difference of:

$$\delta E_o = E_o - E_o \cos 48'$$

which is less than 0·1%

2) The spread of ion flight times in the analyser.

An ion will return to the earth plate after a time t given by:

$$t = \frac{l}{v \cos\theta} = \frac{l}{\cos\theta}\left(\frac{m}{2E}\right)^{\frac{1}{2}} \qquad (4)$$

where E is the energy of the ion.

For this analyser the equation is:

$$t = \frac{38}{\cos\theta}\left(\frac{m}{2E}\right)^{\frac{1}{2}}$$

Hence the spread of flight times for angles between θ and $\theta + \partial\theta$ is

$$\partial t = 38\left(\frac{m}{2E}\right)^{\frac{1}{2}}\left(\frac{1}{\cos(\theta + \partial\theta)} - \frac{1}{\cos\theta}\right)$$

$$= 38\left(\frac{m}{2E}\right)^{\frac{1}{2}}\left(\frac{1}{\cos\theta\cos\partial\theta - \sin\theta\sin\partial\theta} - \frac{1}{\cos\theta}\right)$$

For $\theta = 45^o$

$$\partial t = 38\left(\frac{m}{E}\right)^{\frac{1}{2}}\left(\frac{2\,\partial\theta}{1 - 2\,\partial\theta}\right) \qquad \text{for small } \partial\theta$$

Taking the typical values (argon):

m = 40 mass units

E = 5eV

$\partial\theta = 2^o$ (the angle of acceptance with the slits open)

$\partial t = 3{\cdot}8\ \mu$sec.

The broadening will be less for smaller analyser slit width settings.

```
      HO
      )
&JOB,JRC131;
&FORTRAN,LABCM5;
      GLOBAL,LABCM5,SQRT,ABS,EXP,AMAX,GRAPH2,ATAN]
      DIMENSION AT(20,100),A1(100),F(100),BT(100),E(20)
      DIMENSION S(20),W(20),CONST(20)
      COMMON AT
C     VERSION WITH FULL ANGULAR DEPENDENCE
C
C     NE IS NO. OF DISCRETE RELEASES.
C     XY IS  VALUE OF ELECTRON ENERGY AT PARENT PEAK.
C     ABCISS IS EXPANSION OF BASIC GRAPHING INTERVAL OR NUMBER
C     OF COMPUTATIONS IF KNTRL IS ZERO.
C     ORD IS ORDINATE MAXIMUM HEIGHT IN CM.
C     KNTRL SETS PROGRAM TO COMPUTE AND OUTPUT DATA IF ZERO OR TO GRAPH
C     DISTRIBUTION IF POSITIVE ; IF  GREATER THAN ONE, PARENT DIST-
C     RIBUTION IS GRAPHED AS WELL ; IF NEGATIVE PARENT ONLY IS GRAPHED
C     E(M) IS ENERGY RELEASE.
C     W(M) IS WEIGHT OF E(M).
C     ENDATA CHECKS FOR END OF DATA; A POSITIVE OR NEGATIVE VALUE GIVES
C     AN ERROR MESSAGE; ZERO CONTINUES.
C     BORD IS ORDINATE MAX. VALUE FOR PARENT DIST. AND IS ONLY
C     REQUIRED IF PARENT CALLED FOR.
C     FEED IN TAPE OF FUNCTION FIT FIRST; RESET TO 32 FOR NEW FUNCTION.
C     34 FOR CONTINUATION WITH SAME FUNCTION.
C     35 FOR NO FUNCTION.
C     36 SETS TO IGNORE ANGULAR DEPENDENCE
C     37 SETS TO CONSIDER FORWARD FLYING IONS ONLY
C     38 SETS TO USE COMPLETE ANGULAR DISTRIBUTION FUNCTION
C     DATA IN ORDER:-
C   M1 M2 IT NE XY (E(M) W(M) NE TIMES) ABCISS ORD KNTRL (BORD) ENDATA
```

CODE

```
8 L1  (loc. 33)
8 L2  (loc. 34)
8 L3  (loc. 35)
8 L4  (loc. 36)
8 L5  (loc. 37)
8 L6  (loc. 38)
L1  4 +0
5 IIF
8 Q1
L2  4 +0
5 IIF
8 Q2
L3  4 +1
5 IIF
8 Q2
L4  4 +0
5 JILL
8 ;+0
L5  4 +1
5 JILL
4 +0
5 JANE
8 ;+0
L6  4 +1
5 JILL
5 JANE
8 ;+0
JANE +0
JILL +0
IIF +0
FORTRAN
```

This section, written in assembly language, is used to set pointers defining the operation of the program. In this way computations with different forms of angular acceptance function are performed with one program. This is achieved by entering the program at absolute locations 36 - 38 before entering the program proper.

The computed curve may be compared with a function defined by a set of parameters previously derived for the function "F" by a least squares fit to an experimental curve.

Alternatively this facility may be ignored by entering the program at location 35.

```
 1 READ(1) C1,C2,C3,C4,C5,PQ,WWW,PEAK
 2 READ(1) M1,M2,IT,NE,XY
   DO 3 J=1,NE
 3 READ(1)E(J),W(J)
   READ(1)ABCISS,ORD,KNTRL
   IF(KNTRL-1)4,10,5
 4 IF(KNTRL)5,10,5
 5 READ(1)BORD
 6 IORD=ORD*4.
   IF(IORD-58)8,8,7
 7 ORD=14.5
 8 IORD=BORD*4.
   IF(IORD-58)10,10,9
 9 BORD=BORD-.25
   GO TO 8
10 READ(1)ENDATA
   IF(ENDATA)49,11,49
11 AKT=8.61705E-5*IT
   EOMAX=AMAX(E,NE)
   EOMAX=EOMAX*(M1-M2)/M1
   FRED=EOMAX*3.0+10.*AKT
12 N=ABCISS
   ABCISS=.1/ABCISS
   IF (KNTRL) 14,13,14
13 DE=1/N
   DE=DE*FRED
   I=N
   GO TO 52
14 DE  = 0.42*ABCISS
   I=FRED/DE + 1.
   IF(I-100)52,52,15
15 ABCISS=.1/ABCISS
   ABCISS=ABCISS-1
   IF(ABCISS)16,16,12
16 ABCISS=1
   FRED=FRED-.1
   GO TO 12
17 XY=XY+(.002-.05*ABCISS)
   ANGMAX=45.0/57.29578
   SUMB=0.0
   SUM=0.0
   DO 18 J=1,NE
   DOG=E(J)/AKT
   CAT=(AKT*E(J))**0.5
   CONST(J)=EXP(-DOG)/CAT
18 S(J)=2*(SQRT(M1*(M1-M2)*E(J)))/(M2*AKT)
   AM=M1/(M2*AKT)
   OZ=0.05*ABCISS
   DO 28 JA=1,I
   EN=(JA-1)*DE+OZ
   IF(JILL)23,23,19
19 IF(EN-0.7)20,23,23
20 BRA = SQRT(36.*EN*EN+.9*EN-.000225)
   ANNE= (.15 + 6.*EN + BRA)/(1200.*EN)
   ANNE=ATAN(SQRT(ANNE/(1.-ANNE)))
   IF(JANE)24,24,21
21 IF(EN-0.05)22,24,24
22 DIANA= (.15 + 6.*EN - BRA)/(1200.*EN)
   DIANA=ATAN(SQRT(DIANA/(1.-DIANA)))
   ANNE=ANNE+DIANA
   GO TO 24
23 ANNE = SYLVIA
24 IF(ANGMAX-ANNE)25,25,26
25 ANNE=ANGMAX
26 SEN=SQRT(EN)
```

This section reads in the parameters. In this version ANGMAX is defined as 45°; earlier versions of the program allowed this variable to be read in with the other parameters. (See Chapter 2.E).

Computation of kT, the energy interval and number of computations required (I).

Computation of the parts of the distribution function dependant only upon the energy released (E(J)).

Main loop: computing distributions for energy release values EN.

Angular acceptance functions.

Limitation of angle of acceptance to ANGMAX.

```
    BT(JA)=SEN*EXP(-EN/AKT)*ANNE
    BB=AM*EN
    DO 27 J=1,NE
    AA=S(J)*SEN
    BE=EXP(-AA-BB)
    AE=EXP(AA-BB)
27  AT(J,JA)=(AE-BE)*CONST(J)*ANNE
28  SUMB=SUMB+BT(JA)
    DO 29 J=1,I
29  BT(J)=BT(J)/SUMB
    IF(KNTRL)38,30,30
30  WRITE(2,57) M1,M2
    WRITE(2,58) IT
    WRITE(2,59)
    DO 31 J=1,NE
31  WRITE(2,60)E(J),W(J)
    IF(KNTRL)32,33,32
32  WRITE(2,63)ABCISS,ORD
33  WRITE(2,55)
34  DO 36 J=1,I
    A1(J)=0.0
    DO 35 JI=1,NE
35  A1(J) = A1(J) + AT(JI,J)*W(JI)
36  SUM=SUM+A1(J)
    DO 37 J=1,I
37  A1(J)=A1(J)/SUM
38  IF(IIF)39,39,50
39  XXX=XY
    DO 40 J=1,I
    YY=(XXX-PEAK)/WWW
    R=YY*YY
    R2=R*R
    U=PQ+R
    U2=PQ+R2
    F(J)=C1*EXP(-R)+C2*EXP(-R2)+C3*EXP(-ABS(YY))+C4*YY/U+C5*YY/U2
40  XXX=XXX-DE
41  IF (KNTRL) 43,44,42
42  CALL GRAPH2 (A1,F,I,DE,ORD,XY,0)
    IF(KNTRL-1) 44,2,43
43  WRITE(2,61) IT
    WRITE(2,63)ABCISS,BORD
    WRITE(2,54)
    CALL GRAPH2 (BT,BT,I,DE,BORD,XY,0)
    GO TO 2
44  DO 47 J =1, I
    IF(J-2)46,46,45
45  IF(A1(J)-0.0001)48,48,46
46  AAA=XY-(J-1)*DE
47  WRITE (2,53) AAA, A1(J)
48  WRITE(2,62)
    GO TO 2
49  WRITE(3,56)
    PAUSE
    GO TO 2
50  DO 51 J=1,I
51  F(J)=A1(J)
    GO TO 41
52  SYLVIA=.01
    SYLVIA=ATAN(SQRT(SYLVIA/(1.-SYLVIA)))
    ANNE=SYLVIA
    GO TO 17
```

In this loop the distribution values are calculated for the various energy releases (E(J)) and are placed in the matrix AT(J,JA). BT(JA) contains the parent energy distribution function.

Summation of distributions for various energy releases multiplied by their weight factors (W(JI)).

Normalization of distribution.

Computation of experimental function fit if required.

Output of the distribution numerically and graphically.

Output of parent distribution if required.

Output without graph if required.

```
   53 FORMAT(F6.3, F10.5)
   54 FORMAT(12H  E PARENT *)
   55 FORMAT(19H  E  CALC .   FIT +/)
   56 FORMAT(13HERROR IN DATA)
   57 FORMAT(29HENERGY DISTRIBUTION FOR MASS ,I4,2X,
$     21HGIVING FRAGMENT MASS ,I4,2X)
   58 FORMAT(3HAT ,I4,2X,37HDEG. K. WITH DISCRETE ENERGY RELEASES)
   59 FORMAT(/,15HENERGY   WEIGHT,/)
   60 FORMAT(F6.3,4X,F6.3)
   61 FORMAT(/,29HENERGY DISTRIBUTION OF PARENT,3H AT,I4,2X,7HDEG. K.,/
   62 FORMAT(///)
   63 FORMAT(/,9HABSCISSA ,F6.3,2X,23HVOLTS PER CM.  ORDINATE,
$     F6.2,2X,9HCMS. MAX.,/)
      END
```

```
      GLOBAL,AMAX,LABCM5]
      FUNCTION AMAX(X,NEX)
      DIMENSION X(20)
      BMAX=X(1)
      DO 2 JE=1,NEX
      IF(X(JE)-BMAX)2,2,1
    1 BMAX = X(JE)
    2 CONTINUE
      AMAX=BMAX
      RETURN
      END
```

Evaluation of the maximum value of an array X.

```
      GLOBAL,GRAPH2,LABCM5]
      SUBROUTINE GRAPH2(AAT,BBT,I,DE,AORD,XINIT,ISAME)
      DIMENSION AAT(100),BBT(100)
      AMAXZ=AAT(1)
      DO 2 J=2,I
      IF(AAT(J)-AMAXZ)2,2,1
    1 AMAXZ=AAT(J)
      MAXA=J
    2 CONTINUE
      BMAX=BBT(1)
      DO 4 J=2,I
      IF(BBT(J)-BMAX)4,4,3
    3 BMAX=BBT(J)
      MAXB=J
    4 CONTINUE
      IF(MAXA-MAXB)6,6,5
    5 AMAXZI=MAXA
      GO TO 7
    6 AMAXZI=MAXB
    7 AMAXZI=XINIT-(AMAXZI-1.)*DE
      IORD=AORD*4.
    8 IF(ISAME)12,12,9
    9 IF(AMAXZ-BMAX)10,10,11
   10 ANORM = IORD/BMAX
      BNORM=ANORM
      GO TO 13
   11 ANORM = IORD/AMAXZ
      BNORM=ANORM
      GO TO 13
   12 ANORM=IORD/AMAXZ
      BNORM=IORD/BMAX
   13 DO 16 J=1,I
      E=XINIT-(J-1)*DE
      WRITE(3,18)E,AAT(J)
      KA=AAT(J)*ANORM+0.5
      KB=BBT(J)*BNORM+0.5
```

GRAPH2 plots two independant functions on the on line teleprinter.

```
        CODE
4 +0
5 K1
4 KA
9 L1
4 KB
9 L2
4 +160
15 6148
4 KA
2 KB
7 EQUALS
9 NEG
2 +1
5 DIFF
4 KA
2 +0
5 CHA
4 +46
5 CH1
4 +43
5 CH
8 JA
EQUALS 4 KA
5 K1
10 K1
2 +0
5 DIFF
4 +170
5 CH
8 JD
NEG 5 DIFF
10 DIFF
4 KB
2 +0
5 CHA
4 +43
5 CH1
4 +46
5 CH
8 JA
L1 4 +60
15 6148
10 K1
4 KB
9 Q14
2 +0
5 DIFF
4 +43
5 CH
8 JD
L2 4 +60
15 6148
10 K1
4 KA
2 +0
5 DIFF
4 +46
5 CH
8 JD
CH +0
CHA +0
CH1 +0
K1 +0
DI1
```

```
JA 4 CHA
7 JD-3
4 +160
15 6148
10 CHA
4 CHA
9 ;-4
8 ;+2
10 K1
4 CH1
15 6148
JD 4 DIFF
7 ;+6
4 +160
15 6148
10 DIFF
4 DIFF
9 ;-4
4 CH
15 6148
FORTRAN
    14 IF(E-AMAXZI)15,16,16
    15 IF(K1-1)16,17,16
    16 CONTINUE
    17 WRITE(3,19)
    18 FORMAT(F5.3,F7.4)
    19 FORMAT(//)
       RETURN
       END
%
&FT3;
&LOAD;
&RUN;
```

This program is satisfactory for most calculations; however in some cases involving large energy releases overflow of exponentials in the calculation can occur.

Therefore a second version of this program was written capable of dealing with larger energy releases. This version differs in procedure only, and takes a good deal longer to run.

```
      HO
      )
&JOB, JRC;
&FORTRAN, CURVE;
      GLOBAL, CURVE, EXP, ABS, SQRT, FIT, VMIN, GRAPH2]
      DIMENSION X(100), F(100), E(5), VW(5), TP(11), EE(11), A1(100)
    1 READ (1) IRAND, N, PQ
      IF (N) 2, 2, 3
    2 PAUSE
    3 W=0.0
      NEVER=1
      IWSAME=0
      DO 5 M=1, N
      READ (1) X(M), F(M)
      IF (F(M)-W) 5, 5, 4
    4 W=F(M)
      J=M
    5 CONTINUE
      IF (J-3) 7, 6, 6
    6 T1=(F(J-1)-F(J-2))/(X(J-1)-X(J-2))
      T2=(F(J+2)-F(J+1))/(X(J+2)-X(J+1))
      W=((F(J+1)-F(J-2)+T1*X(J-2)-T2*X(J+1))/(T1-T2)+X(J))*0.5
    7 PEAK=W
      W=F(J)*0.4
      K=J
    8 K=K+1
      IF (F(K)-W) 9, 9, 8
    9 W=X(K)-X(J)
      W=ABS(W)
   10 WRITE(3, 66)
      READ(3)IOPT
      WRITE(3, 94)
      IF (IOPT) 13, 13, 11
(1) 11 WRITE(3, 67)
      READ(3) PQ
      WRITE(3, 68)
      READ(3) W
      WRITE(3, 69)
      READ(3) I
      IF (I) 50, 50, 12
   12 READ(3) PEAK
      WRITE(3, 94)
      GO TO 50
(2) 13 IPQ=2
      GO TO 19
(3) 14 IPQ=IPQ-1
      JIN=0
      FACT=0.8
(4) 15 WW=W*FACT
      DW=(W-WW)*0.5
   16 DO 17 J=1, 5
      VW(J)=WW+(J-1)*DW
      CALL FIT(X, F, N, PEAK, VW(J), PQ, C1, C2, C3, C4, C5, E(J), IWSAME)
   17 CONTINUE
      CALL VMIN(E, BEST, VW, L, IX)
      W=BEST
      NEVER=1
      WRITE(3, 85) W
      WRITE(3, 97) E(IX)
      IF (L) 19, 18, 19
   18 JIN=JIN+1
```

Read in number of points, then x and y values.

Estimation of value of x at peak and the parameter W (which is approximately the half-height half width)

Asks if values for parameters (W, PQ and PEAK) are to be set from on-line teleprinter and, if answer is yes, accepts the new values. Control is then transferred to the branching control of the program at statement 50.

BLOCK 1

Five values of W centered on the current value are tried in a least squares fit calculated by Subroutine FIT. Subroutine VMIN tries to fit a quadratic function to the RMS error values in order to interpolate a "best" value of W which is output on line.

```
      IF (JIN-4) 15,50,50
   19 JIM=0
(5) 20 P=PQ*.1
      PQ=PQ-(3.0*P)
   21 DO 25 J=1,5
      PQ=PQ+P
      VW(J)=PQ
      IF(NEVER)23,23,22
   22 NEVER=0
      GO TO 24
   23 IWSAME=1
   24 CALL FIT(X,F,N,PEAK,W,PQ,C1,C2,C3,C4,C5,E(J),IWSAME)
   25 CONTINUE
      JMIN=1
      ET=E(1)
      DO 27 J=2,5
      IF(E(J)-ET)26,27,27
   26 ET=E(J)
      JMIN=J
   27 CONTINUE
      IX=JMIN
      IF(JMIN-5)29,28,28
   28 BEST=VW(5)
      IF(E(5)-E(4)+.00005)32,31,31
   29 IF(JMIN-1)30,30,33
   30 BEST=VW(1)
      IF(E(1)-E(2)+.00005)32,31,31
   31 L=1
      GO TO 34
   32 L=0
      GO TO 34
   33 CALL VMIN(E,BEST,VW,L,IX)
   34 IF (L) 36,35,36
   35 PQ=BEST
      WRITE(3,86) PQ
      WRITE(3,97) E(IX)
      JIM=JIM+1
      IF(JIM-4) 20,50,50
   36 PQ=BEST
      WRITE(3,87) PQ
      WRITE(3,97) E(IX)
      IF(IPQ)37,37,14
(6) 37 FACT=0.91
      K=1
(7) 38 LCOUNT=0
      K=K+1
      FACT=FACT+(1.-FACT)*0.4
   39 WW=W*FACT
      DW=W*(1.0-FACT)*0.5
      DO 40 J=1,5
      VW(J)=WW+(J-1)*DW
      CALL FIT(X,F,N,PEAK,VW(J),PQ,C1,C2,C3,C4,C5,E(J),IWSAME)
   40 CONTINUE
      CALL VMIN(E,BEST,VW,L,IX)
      W=BEST
      NEVER=1
      WRITE(3,89) W
      WRITE(3,92)E
      IF (L) 42,41,42
   41 LCOUNT=LCOUNT+1
      FACT=FACT*0.95
```

BLOCK 2

The same set of operations carried out for parameter PQ. The flag IWSAME tells FIT that the last computation used the same value of W, allowing the subroutine to work more quickly. A maximum of four executions of these two blocks are carried out after which control returns to 50.

BLOCK 3

Again five values of W are tried - closer together. If the minimum RMS error is for the 1st or 5th values the block is executed again, otherwise control tranfers to the next block.

```
    IF(LCOUNT-2)39,39,13
(8) 42 LCOUNT=0
    43 P=.025*PQ*(1/K**2)
    44 PQ=PQ-(3.0*P)
       DO 48 J=1,5
       PQ=PQ+P
       VW(J)=PQ
       IF(NEVER)46,46,45
    45 NEVER=0
       GO TO 47
    46 IWSAME=1
    47 CALL FIT(X,F,N,PEAK,W,PQ,C1,C2,C3,C4,C5,E(J),IWSAME)
    48 CONTINUE
       CALL VMIN(E,BEST,VW,L,IX)
       PQ=BEST
       WRITE(3,90) PQ
       GO TO 49
    49 WRITE(3,92)E
    50 WRITE(3,93)
       READ(3)IGOON
       IF(IGOON)52,52,51
    51 IF(IGOON-13)53,53,52
    52 IGOON=3
    53 GO TO (11,13,14,15,20,37,38,42,54,55,56,62,63), IGOON
(9) 54 WRITE(3,75)
       READ(3)P
       WRITE(3,94)
       GO TO 44
(10) 55 WRITE(3,73)
       READ(3)DPEAK
       GOTO 57
(11) 56 DPEAK=0.01
    57 Z=W*DPEAK
       PEAK=PEAK-6.0*Z
       DO 58 J=1,11
       PEAK=PEAK+Z
       CALL FIT(X,F,N,PEAK,W,PQ,C1,C2,C3,C4,C5,EE(J),IWSAME)
       TP(J)=PEAK
    58 CONTINUE
       P=1.0
       DO 60 J=1,11
       IF (EE(J)-P) 59,60,60
    59 P=EE(J)
       K=J
    60 CONTINUE
       IF(6-K)61,62,61
    61 WRITE(3,72)EE(6),EE(K)
       PEAK=TP(K)
       WRITE(3,71)K
       WRITE(3,95)PEAK
       GO TO 50
(12) 62 PEAK=TP(6)
       WRITE (3,96) PEAK
       GO TO 50
(13) 63 CALL FIT(X,F,N,PEAK,W,PQ,C1,C2,C3,C4,C5,ER,IWSAME)
       WRITE (3,70) PEAK
       WRITE (3,76) W
       WRITE (3,77) PQ
       WRITE (3,78) C1
       WRITE (3,79) C2
       WRITE (3,80) C3
```

BLOCK 4

Similar to block 3 for PQ.

By reading a value in the range 1 - 13 from the on-line teleprinter control is transfered to various sections of the program.

Allows the interval between PQ values to be set before transfering control to block 4.

In this block 11 values of PEAK are tried centering on the current value. The value giving minimum RMS error is selected and control returned to 50.

Computation and output of final result.

```
      WRITE (3,81) C4
      WRITE (3,82) C5
      DX=(X(N)-X(1))/(N-1)
      DO 65 M=1,N
      X(M+1)=X(M)+DX
      Y=(X(M)-PEAK)/W
      R=Y*Y
      V=PQ+R
      V2=PQ+R*R
      B=R*R
      F=C1*EXP(-R)+C2*EXP(-B)+C3*EXP(-ABS(Y))+C4*Y/(V)+C5*Y/(V2)
      A1(M)=F
      IF(IRAND)65,65,64
   64 F(M)=A1(M)
   65 CONTINUE
      WRITE(3,83) ER
      WRITE (3,84)
      CALL GRAPH2 (A1,F,N,DX,12.,X(1),1)
      WRITE(2,88)C1,C2,C3,C4
      WRITE(2,88)C5,PQ,W,PEAK
      GOTO 1
C
C
   66 FORMAT(/7HOPTION=)
   67 FORMAT(/3HPQ=)
   68 FORMAT(/2HW=)
   69 FORMAT(/5HPEAK?)
   70 FORMAT (///3X,11HBEST VALUES//5HPEAK=,F14.8)
   71 FORMAT(/2HK=,I3)
   72 FORMAT(/19HERROR IMPROVED FROM,F12.8,3H TO,F12.8/)
   73 FORMAT(6HDPEAK=)
   74 FORMAT(/2HL=)
   75 FORMAT(/2HP=)
   76 FORMAT (/2HW=,F14.8)
   77 FORMAT (/3HPQ=,F14.8)
   78 FORMAT (///18HCOEFF OF EXP(-X2)=,F14.8)
   79 FORMAT (/18HCOEFF OF EXP(-X4)=,F14.8)
   80 FORMAT (/19HCOEFF OF EXP(-IXI)=,F14.8)
   81 FORMAT (/20HCOEFF OF X/(PQ+X2) =,F14.8)
   82 FORMAT (/20HCOEFF OF X/(PQ+X4) =,F14.8)
   83 FORMAT(//11H RMS ERROR=,F14.8///)
   84 FORMAT(19H   X    FIT +   EXPT ./)
   85 FORMAT(3HW= ,E12.5)
   86 FORMAT(3HPQ=,E12.5)
   87 FORMAT(/3HPQ=,E12.5)
   88 FORMAT(4E20.12,2H  )
   89 FORMAT(3HW= ,E15.7)
   90 FORMAT(3HPQ=,E15.7)
   91 FORMAT(/3HPQ=,E15.7)
   92 FORMAT(/5HE(J)=,5F12.8/)
   93 FORMAT(/5HGOON=)
   94 FORMAT(//)
   95 FORMAT(/5HPEAK=,E15.7)
   96 FORMAT(/23HPEAK UNCHANGED; VALUE:-,E15.7/)
   97 FORMAT(Z,8X,E15.7)
      END
```

```
      GLOBAL,FIT,ABS,EXP,SQRT,CURVE]
      SUBROUTINE FIT(DX,DF,N,PEAK,W,PQ,C1,C2,C3,C4,C5,E,IWSAME)
      DIMENSION DX(100),DF(100),S(100),ZF(100),EF(100),TF(100)
      IF(IWSAME)1,1,2
    1 D1A=0.0
      D6A=0.0
      D6B=0.0
      D6C=0.0
      D2A=0.0
      D2B=0.0
      D3A=0.0
      D3B=0.0
      D3C=0.0
    2 D4A=0.0
      D4B=0.0
      D4C=0.0
      D4D=0.0
      D5A=0.0
      D5B=0.0
      D5C=0.0
      D5D=0.0
      D6D=0.0
      D5E=0.0
      D6E=0.0
      DO 5 M=1,N
      X=DX(M)
      F=DF(M)
      X=(X-PEAK)/W
      TT=X*X
      S(M)=X
      A=ABS(X)
      Y=TT
      ZZ=Y*Y
      IF(IWSAME)3,3,4
    3 ZF(M)=EXP(-A)
      EF(M)=EXP(-ZZ)
      TF(M)=EXP(-Y)
      D3C=D3C+ZF(M)*ZF(M)
      D6C=D6C-ZF(M)*F
      D6B=D6B-F*EF(M)
      D3B=D3B+EF(M)*ZF(M)
      D2B=D2B+EF(M)*EF(M)
      D6A=D6A-F*TF(M)
      D3A=D3A+TF(M)*ZF(M)
      D2A=D2A+TF(M)*EF(M)
      D1A=D1A+TF(M)*TF(M)
    4 R=X/(PQ+TT)
      R3=X/(PQ+ZZ)
      D6D=D6D-F*R
      D4D=D4D+R*R
      D5D=D5D+R*R3
      D5E=D5E+R3*R3
      D6E=D6E-F*R3
      D4C=D4C+ZF(M)*R
      D5C=D5C+ZF(M)*R3
      D5B=D5B+R3*EF(M)
      D4B=D4B+R*EF(M)
      D5A=D5A+R3*TF(M)
      D4A=D4A+R*TF(M)
    5 CONTINUE
```

FIT calculates coefficients for a least squares fit of the function:

$$y = C1\ \exp{-x^2} + C2\ \exp{-x^4} + C3\ \exp|x| + C4\ \frac{x}{PQ+x^2} + C5\ \frac{x}{PQ+x^4}$$

to the experimental points and the RMS error of the fit. W is a parameter defining the expansion of x values such that;

$$X(\text{function}) = \frac{X(\text{real})-PEAK.}{W}$$

```
      Z=-D2A/D1A
      C2B=D2B+Z*D2A
      C3B=D3B+Z*D3A
      C4B=D4B+Z*D4A
      C5B=D5B+Z*D5A
      C6B=D6B+Z*D6A
      Z=-D3A/D1A
      C2C=D3B+Z*D2A
      C3C=D3C+Z*D3A
      C4C=D4C+Z*D4A
      C5C=D5C+Z*D5A
      C6C=D6C+Z*D6A
      Z=-D4A/D1A
      C2D=D4B+Z*D2A
      C3D=D4C+Z*D3A
      C4D=D4D+Z*D4A
      C5D=D5D+Z*D5A
      C6D=D6D+Z*D6A
      Z=-D5A/D1A
      C2E=D5B+Z*D2A
      C3E=D5C+Z*D3A
      C4E=D5D+Z*D4A
      C5E=D5E+Z*D5A
      C6E=D6E+Z*D6A
      Z=-C2C/C2B
      C3C=C3C+Z*C3B
      C4C=C4C+Z*C4B
      C5C=C5C+Z*C5B
      C6C=C6C+Z*C6B
      Z=-C2D/C2B
      C3D=C3D+Z*C3B
      C4D=C4D+Z*C4B
      C5D=C5D+Z*C5B
      C6D=C6D+Z*C6B
      Z=-C2E/C2B
      C3E=C3E+Z*C3B
      C4E=C4E+Z*C4B
      C5E=C5E+Z*C5B
      C6E=C6E+Z*C6B
      Z=-C3D/C3C
      C4D=C4D+Z*C4C
      C5D=C5D+Z*C5C
      C6D=C6D+Z*C6C
      Z=-C3E/C3C
      C4E=C4E+Z*C4C
      C5E=C5E+Z*C5C
      C6E=C6E+Z*C6C
      C5=(C6E*C4D-C6D*C4E)/(C5D*C4E-C4D*C5E)
      C4=-(C6E+C5E*C5)/C4E
      C3=-(C6C+C5C*C5+C4C*C4)/C3C
      C2=-(C6B+C5B*C5+C4B*C4+C3B*C3)/C2B
      C1=-(D6A+D5A*C5+D4A*C4+D3A*C3+D2A*C2)/D1A
      E=0.0
      DO  6  M=1,N
      X=S(M)
      R=X*X
      OB=R*R
      F=C1*EXP(-R)+C2*EXP(-OB)+C3*EXP(-ABS(X))+C4*X/(PQ+R)+C5*X/(PQ+OB
      G=F-DF(M)
      E=E+G*G
    6 CONTINUE
      E=SQRT(E/N)
      IWSAME=0
      RETURN
      END
```

```
  GLOBAL,VMIN,CURVE]
  SUBROUTINE VMIN(E,BEST,VW,L,JMIN)
  DIMENSION E(5),VW(5)
  JMIN=1
  ET=E(1)
  DO 2 J=2,5
  IF(E(J)-ET)1,2,2
1 ET=E(J)
  JMIN=J
2 CONTINUE
  IF (JMIN-5) 4,3,3
3 BEST=VW(5)
  IF(E(5)-E(4)+.000002)7,6,6
4 IF (JMIN-1) 5,5,8
5 BEST=VW(1)
  IF(E(1)-E(2)+.000002)7,6,6
6 L=1
  GOTO 14
7 L=0
  GOTO 14
8 L=1
  S4=0.0
  S3=0.0
  S2=0.0
  S1=0.0
  SF2=0.0
  SF1=0.0
  SF=0.0
  DO 9 N=1,5
  Y=E(N)
  X=VW(N)
  Z=X*X
  S1=S1+X
  S2=S2+Z
  S3=S3+X*Z
  S4=S4+Z*Z
  SF1=SF1+X*Y
  SF=SF+Y
  SF2=SF2+Z*Y
9 CONTINUE
  Z=-S2/S1
  A2=S2*Z+S3
  A3=SF1*Z+SF2
  A1=S3*Z+S4
  Z=-S2*0.2
  B1=S2*Z+S4
  B2=S1*Z+S3
  B3=SF*Z+SF2
  B=(A3*B1-A1*B3)/(B1*A2-A1*B2)
  A=(B3-B2*B)/B1
  BEST=-B*0.5/A
  IF(BEST-VW(1))11,11,10
10 IF(BEST-VW(5))15,15,11
11 JMIN=1
  ET=E(1)
  DO 13 J=2,5
  IF(E(J)-ET)12,13,13
12 JMIN=J
  ET=E(J)
13 CONTINUE
  BEST=VW(JMIN)
```

VMIN calculates a quadratic fit of the five error values in array E and returns the corresponding VW values in BEST.

```
   14 RETURN
   15 WRITE(3,16)
      RETURN
   16 FORMAT(Z,1H>)
      END
%
&FT3;
&LOAD;
&LIBRARY,0,GRAPH2;
&RUN;
```

This program is used to fit experimental distributions obtained at discrete energy intervals to a smooth function and also to find as accurately as possible the energy value at the peak of the distribution.

Various tests of the program were performed to ensure that it did not distort the true distribution. In one such test 31 points were read off an actual distribution plotted by the X -,Y plotter and various randomly chosen sets of these points were independantly processed using the program.

The results were as follows:-

Run	Number of points	Peak value (eV)	RMS error of fit (peak value 1.0)
1	11	0·601	0·009
2	10	0.578	0·013
3	10	0.588	0·011
4	10	0·574	0·007
5	11	0.594	0·018
6	16	0·592	0·020
7	31	0·593	0·023

It was found that the peak values deteriorated as fewer points were used; about 10 points being the threshold for this distribution. In all cases where 11 or more points were used a peak value within 5meV of the correct one was obtained and for all 31 points a very good value was obtained.

The print out of run 1 is reproduced below to illustrate the action of the program. The test is deliberately more stringent than the fitting of actual experimental points. For actual experimental fits more than 11 points are used and these are more evenly spread than were the points used in the test; in particular the set of points used for runs 4 and 5 were very unevenly spaced and had large gaps between the points in the region of the peak.

Output of CURVE, run 1 (Q denotes an interrogation by the program)

```
Q OPTION=0

                                        RMS errors
   PQ=  0.12000?+01                  0.3253871?-01
   PQ=  0.14400?+01                  0.3235676?-01
   PQ=  0.17280?+01                  0.3218947?-01
   PQ=  0.20736?+01                  0.3203381?-01

 Q GOON=3 >                  3 transfers control to block 1.
   W=   0.13066?+00                  0.3045433?-01
   PQ=  0.24883?+01                  0.3033894?-01
   PQ=  0.29860?+01                  0.3020411?-01
   PQ=  0.35832?+01                  0.3006643?-01
   PQ=  0.42998?+01                  0.2992669?-01

Q  GOON=11                   11 tries 11 values of PEAK each varying by 1% of W.

   ERROR IMPROVED FROM  0.02992671 TO  0.02373719

   K=  11                    K is the number of the PEAK value giving min. RMS error.

   PEAK=   0.5805238?+00

 Q GOON=10                   10 tries 11 values of PEAK each varying by DPEAK*W.
 Q DPEAK=.025

   ERROR IMPROVED FROM  0.02373718 TO  0.02031905

   K=   9

   PEAK=   0.5903235?+00

Q  GOON=7 >                  to block 3.
   W=    0.1381279?+00

   E(J)=   0.02457319  0.02220992  0.02031905  0.01969765  0.02056969

   PQ=   0.4297667?+01

   E(J)=   0.01968943  0.01969024  0.01969105  0.01969186  0.01969267

Q  GOON=9                    to block 4 with PQ varied by an amount P

 Q P=1.2

   PQ=   0.1897667?+01

   E(J)=   0.01718752  0.01864976  0.01968943  0.02050130  0.02117157
```

```
Q  GOON=9
Q  P=.6

   PQ=   0.6976673?+00
   E(J)=   0.01516660   0.01619455   0.01718752   0.01799096   0.01864976

Q  GOON=6 >                to block 3.
   W=    0.1383619?+00
   E(J)=   0.01621816   0.01542562   0.01516660   0.01542481   0.01606263
   PQ=   0.6889464?+00
   E(J)=   0.01515807   0.01516323   0.01516847   0.01517379   0.01517920

Q  GOON=9
Q  P=.2

   >
   PQ=   0.6194022?+00
   E(J)=   0.01554613   0.01505418   0.01515807   0.01545664   0.01581627

Q  GOON=11
   ERROR IMPROVED FROM   0.01508871 TO   0.01271747

   K=   9
   PEAK=   0.5944744?+00

Q  GOON=7
   W=    0.1428448?+00
   E(J)=   0.01458142   0.01353310   0.01271747   0.01220215   0.01202651
   >
   W=    0.1439404?+00
   E(J)=   0.01597750   0.01315291   0.01202651   0.01292211   0.01459504
   PQ=   0.6190925?+00
   E(J)=   0.01206229   0.01206277   0.01206326   0.01206375   0.01206424

Q  GOON=11
```

```
ERROR IMPROVED FROM  0.01206227 TO  0.01085406

K= 11

PEAK=  0.6016714?+00

Q GOON=6 >
W=   0.1493449?+00

E(J)=  0.01662019  0.01342682  0.01085406  0.00963032  0.01006526

PQ=  0.6113538?+00

E(J)=  0.00959849  0.00961165  0.00962495  0.00963839  0.00965198

Q GOON=13            print out results.


   BEST VALUES

PEAK=     0.60167143

W=     0.14934487

PQ=     0.61135383

COEFF OF EXP(-X2)=    -1.01430984

COEFF OF EXP(-X4)=     0.46079836

COEFF OF EXP(-IXI)=     1.23491792

COEFF OF X/(PQ+X2) =    -0.10307674

COEFF OF X/(PQ+X4) =    -0.03280761

 RMS ERROR=     0.00959849


  X    FIT +   EXPT .

 .050 0.0581 0.0581       *
 .135 0.0863 0.0863          *
 .220 0.1332 0.1332             *
 .305 0.1988 0.1988                *
 .390 0.2371 0.2371                   *
 .475 0.3997 0.3997                                *
 .560 0.5105 0.5105
 .645 0.3907 0.3907                                *
 .730 0.2154 0.2154                      *
 .815 0.1060 0.1060             *
 .900 0.1001 0.1001              *
```

Abbreviations used in Reference List

I.J.M.S.I.P	International Journal of Mass Spectrometry and Ion Physics.
J. C. P.	The Journal of Chemical Physics.
J. P. C	The Journal of Physical Chemistry

REFERENCES

1. Auger J. Phys. Radium 6, 205.
2. Shenstone Phys. Rev. 38, 783.
3. Kronig Z. Physik. 50, 347.
4. Marr "Photoionization Processes in Gases" 1967 Ac. Press.
5. Herzberg "Mol. Spectra and Mol. Structure" I; "Spectra of Diatomic Molecules." Van Nostrand; Princeton, N.J.
6. Cook, Metzger and Ogawa. J. Chem. Phys. 44, 2935 (1966).
7. Reid I.J.M.S.I.P. 6, 1.
8. Siegbahn "ESCA". North-Holland, Amsterdam (1969).
9. Turner and Al-Joboury J.C.P. 37, 3007 (1962).
10. Chilton Part II Thesis, Oxford (1970).
11. Bethe and Salpeter "The Quantum Mechanics of One and Two Electron Atoms" Acad. Press, N.Y. 1957.
12. Wannberg et al. J. Phys. E. Sci. Instr. 7, 149 (1974).
13. Price Mol. Spectr. Rept. Conf. London 1967, 221.
14. Collin and Natalis I.J.M.S.I.P. 2, 231.
    Natalis and Collin Chem. Phys. Lett. 2, 414.
15. Smith Phil. Trans. Roy. Soc. London A268, 169 (1970).
16. Lorquet and Cadet I.J.M.S.I.P. 7, 245 (1971).
17. Cairns et al. Phil. Trans. Roy. Soc. London A268, 163 (1970).
18. Busch and Wilson J.C.P. 56, 3626 (1972).
    Mitchell and Simons Disc. Far. Soc. 44, 208.
    Simons and Tasker Mol. Phys. 26, 1267.
19. Rosenstock, Wallenstein, Wahrhaftig and Eyring Proc. Natl. Acad. Sci. U.S. 38, 667 (1952).

20. Marcus and Rice J. Phys. & Colloid. Chem. 55, 894 (1951).
Marcus J.C.P. 20, 359 (1952).

21. Beynon and Cooks Research/Development 22, 26 (1971).

22. Washburn and Berry Phys. Rev. 70, 559.
Oberghaus and Taubert Angew. Chem. 63, 287.

23. Rowland et al. I.J.M.S.I.P. 2, 457.

24. Andlauer and Ottinger Z.N. 27A, 293, and J.C.P. 55, 1471 (1971).

25. Crellin Part II Thesis; Oxford 1972.

26. Frey Diplomarbeit; Frieburg 1973.

27. Dibeler and Reese J. Res. Nat. Bur. Stand. A68, 409.

28. Dibeler et al. J.C.P. 44, 1271.

29. Eland I.J.M.S.I.P. 8, 143 (1972).

30. Brehm and von Puttkamer Z.N. 25A, 1062 (1970).

31. Simm et al. J. Chem. Soc. Chem. Comm. 1973, 833.

32. Eland I.J.M.S.I.P. 12, 389.

33. Brehm et al. Ibid. 12, 197.

34. Brehm et al. Ibid. 12, 213.

35. Cant Part II Thesis, Oxford 1973.
Cant, Eland and Danby J.C.S. Faraday II - in press.

36. Gilmore J. Quant. Spectr. Rad. Transf. 5, 369.

37. Sathe "Mass Spec. A NATO Adv. Study Inst." R.I. Reed, ed., Acad. Press, 129.

38. Wahrhaftig Ibid. 137.

39. Wahrhaftig M.T.P. Internat. Rev. of Sci. Mass Spec. ed. MacColl, Butterworths.

40. Rosenstock and Krauss "Mass Spec. of Org. Ions" ed. McLafferty, Acad. Press, N.Y.

41. Rosenstock and Krauss "Adv. Mass Spec." 2, 251.

42. Vestal "Fund. Proc. Rad. Chem." Ch. 2, p.59, ed. Ausloos.

43. Rosenstock "Adv. Mass Spec." 4, 523.

44. Chupka and Kaminsky J.C.P. 35, 1991.

45. Hoare et al. J.C.P. 52, 113.

Hoare Ibid. 52, 5695, and 54, 3048 (a correction).

46. Eyring J.C.P. 3, 107 (1935).

47. Rabinovitch et al. J.C.P. 38, 2466 amd 41, 1883.

48. Haarhoff Mol. Phys. 7, 101.

49. Thiele J.C.P. 39, 3258.

50. Vestal et al. J.C.P. 37, 1276.

51. Tou and Wahrhaftig J.P.C. 72, 3034.

Hoare and Pal Mol. Phys. 20, 695.

Lin Mol. Phys. 20, 953.

52. Forst and Prasil J.C.P. 51, 3006.

53. Forst and Prasil J.C.P. 53, 3065.

54. Klots J.P.C. 75, 1526.

55. Klots Z.N. 27A, 553.

56. Klots Chem. Phys. Lett. 10, 422.

57. Ottinger Z.N. 20A, 1232.

Hills, Vestal et al. J.C.P. 54, 3834.

58. Levine J.C.P. 44, 2046.

59. Rynbrandt and Rabinovitch J.C.P. 54, 2275.

60. LeRoy J.C.P. 53, 846.

Haney and Franklin J.C.P. 48, 4093.

61. Rosenstock et al. I.J.M.S.I.P. 11, 309.

62. Jortner, Rice et al. Adv. Photochem. 7, 149 (1969).

63. Dixon and Jortner J. Chem. Phys. 48, 715 (1968).

64. Vestal and Lerner "Fundamental Studies Relating to the Radiation Chemistry of Small Molecules" Aerospace Res. Lab. Rept. 67-0114 (1967) see also ref. 42.

65. Beynon et al. I.J.M.S.I.P. 8, 341.

66. von Koch Arkiv. Fysik. 28, 529.

67. Lifshitz and Long J.P.C. 69, 3746.

68. Friedman et al. J.C.P. 30, 1605.

69. Mies and Krauss J.C.P. 45, 4455.

70. Fano Phys. Rev. 124, 1866.

71. Light J.C.P. 40, 3221 and 42, 3281 and Disc. Far. Soc. 44, 14 (1967).

72. Knewstubb I.J.M.S.I.P. 6, 229.

73. Knewstubb Ibid. 6, 217.

74. Gilbert et al. J.C.P. 52, 5718.

75. Rynbrandt and Rabinovitch J.P.C. 75, 2164.

76. Lindholm et al. I.J.M.S.I.P. 3, 385; 6, 161, 177, 191, 203; 8, 85, 101, 215, 229.

77. Lorquet et al. Org. Mass Spec. 8, 387.

78. Leclerc and Lorquet J.P.C. 71, 787.

79. Fischer and Kollmar Theor. Chim. Acta 13, 213.

80. Hirota et al. J.P.C. 74, 410 and Z. Physik. Chim. 67, 244.

81. Dewar Mol. "Orbital Theory of Org. Chem" McGraw Hill (1969).

82. McLafferty Interpretation of Mass Spec. Benjamin N.Y. (1966)

83. Bentley and Johnstone Adv. Phys. Org. Chem. 8, 151 (1971).

84. Bommer and Biemann Ann. Rev. Phys. Chem. 16, 481.

85. Tomboulain et al. Phys. Rev. 102, 1423 (1956) and J. Appl. Phys. 29, 804 (1958).

Guyon Adv Mass Spec. 6 403 (1974)

86. Turner Molecular Photoelectron Spectroscopy Wiley - Interscience.

87. Baker et al. I.J.M.S.I.P. 1, 443.

88. Turner and Price in "Molecular Spectroscopy", London Inst. of Petroleum (1968).

89. Klemperer Rept. Prog. Phys. 28, 77 (1965).

90. Turner Adv. Mass Spec. 4, 755 (1968).

91. Steckelmacher J. Phys. E. Sci. Instr. 6, 1061 (1973).

92. Simpson Rec. Sci. Instr. 35, 1698 (1961).

93. Frost et al. Proc. Roy. Soc. A296, 568.

94. Forst Z. Angew. Phys. 20, 265 (1965) and 10, 546 (1958).

95. Zeeman et al. Rev. Sci. Instr. 42, 485.

96. Golden and Zecca Rev. Sci. Instr. 42, 210.

97. Yarnold and Bolton J. Sci. Instr. 26, 38.

98. Harrower Rev. Sci. Instr. 26, 850.

99. Eland and Danby J. Sci. Instr. Ser. 2 1, 406 (1968).

100. Green and Proca Rev. Sci. Instr. 41, 1409.

101. Schmitz et al. J. Phys. E. Sci. Instr. 5, 64.

102. Zashkvara et al. Soviet Phys. Tech. Phys. 5, 2033.

103. Allen et al. I.J.M.S.I.P. 8, 81.

104. Rowland D. Phil. Thesis Oxford 1969.

Stanton and Monahan J.C.P. 41, 3964.

105. Holland Part II Thesis, Oxford 1971.

106. Simm Personal Communication.

107. Lamb "Statistical Methods and Formulae" E.U.P. London, 1967.

108. Samson "Techniques of Vacuum U.V. Spectroscopy" Wiley, N.Y. (1967).

109. Koopmans Physica 1, 104 (1933).

110. Kuyatt and Simpson Rev. Sci. Instr. 43, 1030 (1972).

111. Doucet et al. J.C.P. 58, 3708 (1973).

112. Nefedov Zh. Strukt. Khim. 12, 521 translated in Journal Struct. Chem. 12, 476.

113. Brundle and Robin J.C.P. 53, 2196.

114. Mardashev et al. Acta Chim. (Budapest) 65, 1 (1970).

115. Turner Phil. Trans. Roy. Soc. London A268, 7 (1970).

116. Fuchs Personal Communication.

117. Gilmore J. Quant. Spectr. Rad. Transfer 5, 369.

118. Turner and May J.C.P. 45, 471 (1966).

119. Doolittle et al. J.C.P. 49, 5108.

120. Moore Natl. Bur. Stand. (U.S.) Circ. No. 467 (1949).

121. Frost et al. Proc. Roy. Soc. London A296, 566 (1967).

122. Dibeler and Walker J.C.P. 44, 4405 (1966).

123. Dibeler et al. J. Res. Nat. Bur. Stand. A 57, 113.

124. Coomber and Whittle Trans. Farad. Soc. 63, 1394.

125. Johnson "Some Thermodynamic Aspects of Inorganic Chemistry" Cambridge University Press (1968).

126. Baibuz et al. Tr. Gos. inst. Prikle Khim. 49, 84.

127. Kolesov et al. Zh. Fiz. Khim. 37, 720.

128. Leyland et al. Trans. Farad. Soc. 66, 898.

129. Walter et al. J.C.P. 51, 3531.

130. Zmbov et al. J. Am. Chem. Soc. 90, 5090.

131. Franklin et al. "Ionization Potentials, Appearance Potentials, and Heats of Formation of Gaseous Positive Ions" N.S.R.D.S. - NBS - 26, 1969.

132. Rossini (ed) et al. "Selected Values of Chemical Thermodynamic Properties" N.B.S. 1952.

133. Syrvatha et al. Zh. Org. Khim. 7, 9.

134. Martins and Huybrechts J.C.P. 43, 1845.

135. Kisner "Tables of Ionization Potentials" U.S.A.E. Comm. rep. TID 6142 (1960)

136. Shapiro and Lossing J.P.C. 72, 1552.

137. Farber et al. Trans. Farad. Soc. 65, 3202.

138. Marcotte and Tiernan J.C.P. 54, 3385.

139. Green et al. Phil. Trans. Roy. Soc. A268, 111 (1970).

140. Wang et al. J.C.P. 58, 5417.

141. Zobeler and Duncan J. Am. Chem. Soc. 77, 2611.

142. Kisner J. Am. Chem. Soc. 287, 922 (1965).

143. Kaufman et al. Int. J. Quant. Chem. 4, 391 (1971).

144. Haney and Franklin J.C.P. 48, 4093.

145. Simm et al. I.J.M.S.I.P. 14, 285.

146. Noutary J. Res. Nat. Bur. Stand. A72, 479.

147. Delwiche Dynamic Mass Spectrometry vol. 1, ed. Price, p.71 (1970).

148. Dibeler et al. J. Res. Nat. Bur. Stand. 40, 25 (1948).

149. Potts et al. Phil Trans. A 268, 59.

150. Siegbahn et al. "ESCA Applied to Free Molecules" (North-Holland, Amsterdam 1969) p.94.

151. Decock et al. Farad. Discuss. Chem. Soc. 54, 84.

152. Chupka J.C.P. 30, 191 (1959).

153. Beynon et al. I.J.M.S.I.P. 2, 291 (1969).

154. Hickling and Jennings Org. Mass. Spec. 3, 1499 (1970).

155. Klots J.C.P. 41, 117.

156. Klots J.C.P. 58, 5364.

157. Franklin J.C.P. 48, 4093.

158. Spotz et al. J.C.P. 51, 5142.

159. Jones et al. J.C.P. 57, 3207.

160. Safron et al. Chem. Phys. Lett. 12, 564.

161. Brundle et al. J.C.P. 53, 705.

162. Lindholm and Sahlström I.J.M.S.I.P. 4, 465.

163. Herzberg "The Electronic Spectra of Polyatomic Molecules" Van Nostrand, N.Y. (1950).

164. Dibeler et al. J. Res. Nat. Bur. Stand. 71A, 371.

ABSTRACT OF A THESIS ENTITLED

STUDIES IN PHOTOIONIZATION

SUBMITTED FOR THE DEGREE OF

DOCTOR OF PHILOSOPHY

IN THE

UNIVERSITY OF OXFORD

BY

J. R. CRELLIN, WORCESTER COLLEGE

ABSTRACT

This thesis is concerned with a study of the fragmentations of some small ions produced by photoionization. The study of unimolecular reactions of this kind is of fundamental interest, providing a much clearer insight into the processes occurring than do conventional kinetic studies where results are complicated by collisions between molecules. Such studies are also of interest in connection with the mechanisms and energetics of the ion dissociation processes responsible for the fragmentation patterns in mass spectroscopy.

A general discussion is given of the processes occurring within a molecule after the absorbtion of a photon, with specific reference to the study of the energy distribution of the electrons produced in photoionization and the energetics of the fragmentation of the residual photoions. Direct and statistical theories of dissociation are considered; in particular the well established Quasi Equilibrium Theory (QET). This theory assumes that the rate of dissociation of an ion is slow relative to the rate of internal energy equilibration and describes each fragmentation pathway as a motion along a separable 'reaction coordinate'. This theory is in many ways similar to the statistical theories of unimolecular reactions. It is difficult to devise a direct and unambiguous test of the extent to which the QET is obeyed in particular cases.

The release of kinetic energy in ion dissociations was first noted in relation to mass spectral appearance energies - partly accounting for the so called 'kinetic shift' of appearance energies from their thermodynamic limits. A

major aim of the work presented here was to relate this release of kinetic energy to the mechanism of fragmentation.

A discussion of experimental techniques is introduced by a general consideration of the types of photon source and energy analyzer which may be used. The experimental work was carried out with an analyzer built originally as a photoelectron spectrometer (with a view to various possible avenues of development). For ion kinetic energy measurements various modifications were found to be necessary, particularly to achieve satisfactory mass resolution of the various ionic fragments from their time of flight through the instrument. Initial experiments were made by pulsing the photon source but extensive investigations and modifications led to a new technique in which the ions were continuously produced and their admission to the energy analyzer was pulsed. Electronic equipment was developed to allow the recording of the data on a multi-channel analyzer. Eventually a reasonable mass resolving power was obtained and the kinetic energy resolution for ions improved to approximately 15 meV.

Much consideration was given to the interpretation of the ion energy distribution data obtained. A detailed investigation of the fragmentation of the O_2^+ ion was employed to test these methods as this dissociation is fairly well understood from spectroscopic information. Equations were developed to enable the observed energy distributions to be related to the kinetic energy releases occurring in centre of mass coordinates and computer programs written to handle the data. For the O_2^+ ion it was found that the observed shape of the O^+ fragment energy distribution could be completely accounted for on the basis of the known potential energy curves

for the O_2^+ ion.

An experimental study was then made of a group of fluorine compounds; for some of these the investigations required an initial study of their photoelectron spectra in order to obtain information about the excited states of the ions. For CCl_3F, CCl_2F_2 and $CClF_3$ the photoelectron spectra and their assignments are in broad agreement with results published elsewhere after this work was completed. In the case of $CClF_3$ a band not reported elsewhere was observed. The photoelectron spectrum of C_2F_6 was also obtained; it does not appear to have been previously reported. The energy distribution of fragment ions produced in the photoionization of all these compounds as well as those of CF_4 and SF_6 were recorded and analyzed using both the helium and neon resonance lines (21.22 eV and 16.85 eV respectively).

Little evidence was found to support the idea that the pattern of ionic decomposition is necessarily determined by the bonding character of the electron lost in ionization. A high reverse activation energy appears to apply to processes in which fluroine is lost from these molecules. The loss of a chlorine atom however seems to be a less rapid process with little kinetic energy release.

In an investigation of the fragmentation of NO_2^+ the ions NO^+, O^+ and N^+ were observed. Consideration of the predissociations of the various states of NO_2^+ showed that dissociation from the $^1A_2$ state of the ion could only be via a spin-forbidden process. High kinetic energy releases were observed in many cases, reflecting the large excess energies possessed by the ions over their dissociation limits. In general the experimental energy distributions were shown to

be consistent with the excess energies involved. In the case of the O^+ fragment there appears to be structure in the distribution of energy release which may reflect the vibrational levels of the parent molecule ion.